Switching/Interpolating LPV Control based on Youla-Kucera Parameterization : application to Autonomous Vehicles

Hussam Atoui

THÈSE

Pour obtenir le grade de

DOCTEUR DE L'UNIVERSITÉ GRENOBLE ALPES

École doctorale : EEATS - Electronique, Electrotechnique, Automatique, Traitement du Signal (EEATS)
Spécialité : Automatique - Productique
Unité de recherche : Grenoble Images Parole Signal Automatique

Synthèse/Interpolation de Régulateurs LPV Basé sur Paramétrisation de Youla-Kucera : Application aux Véhicules Autonomes

Switching/Interpolating LPV Control based on Youla-Kucera Parameterization: Application to Autonomous Vehicles

Présentée par :

Hussam ATOUI

Direction de thèse :

Olivier SENAME Université Grenoble Alpes	Directeur de thèse
John Jairo MARTINEZ MOLINA Université Grenoble Alpes	Co-directeur de thèse
Vicente MILANES Renault	Co-directeur de thèse

Rapporteurs :

Bei LU
PROFESSEUR, Shanghai Jiao Tong University
Fawzi NASHASHIBI
DIRECTEUR DE RECHERCHE, INRIA CENTRE DE PARIS

Thèse soutenue publiquement le **20 octobre 2022**, devant le jury composé de :

Olivier SENAME PROFESSEUR DES UNIVERSITES, Grenoble INP	Directeur de thèse
Bei LU PROFESSEUR, Shanghai Jiao Tong University	Rapporteure
Fawzi NASHASHIBI DIRECTEUR DE RECHERCHE, INRIA CENTRE DE PARIS	Rapporteur
Vicente MILANES INGENIEUR HDR, Renault Espana SA	Co-directeur de thèse
Thierry Marie GUERRA PROFESSEUR DES UNIVERSITES, Université Polytechnique Hauts-de-France	Président
Christophe BERENGUER PROFESSEUR DES UNIVERSITES, Grenoble INP	Examinateur

Invités :

John-Jairo MARTINEZ-MOLINA
PROFESSEUR DES UNIVERSITES, Grenoble INP

"Robustness is not needed only for automatic systems. People always need to adapt their lives, as fast as possible, when disturbed by life uncertainties"

Hussam ATOUI

Acknowledgements

This PhD thesis is a result of a hard work, passion, and overnights to get it done on time. But I wasn't alone, God and the spirit of my family and friends were the mainstay for me to keep giving until the end.

I thank God always and forever for every little success that I have achieved in this thesis. With every drop from people, blessings were raining on me from every side.

Secondly, I would like to thank my parents, who supported me in every circumstance, and in every failure. If it wasn't for their steadfastness in my moments of failure, this work would not be as what you are reading now. I thank my sister Rawan for being there and I hope to read her PhD thesis one day. In mentioning my family, I will never forget to mention my sister and childhood friend Riham, I hope you are proud of me among your friends in heaven...

My supervisors: Olivier Sename, Vicente Milanes, and John Martinez, thank you very much for giving me your attention for 3 years. I'm really lucky to have you, and I'm so glad I had supervisors like you. You gave me the opportunity to learn from your expertise and integrate in your projects. The theoretical results, the experiments, and the list of publications wouldn't be achieved without your regular support.

Special thanks to my manager Eric, and to all my friends and colleagues in Renault. Especially Imane, David, Nievsabel, Dimitris, Francisco, Mathieu, Arun, and Antoine. I would like to mention also my colleagues and students in Gipsa-lab: Ariel, Marcelo, Gian-Marco, Wissam, Hassan, Mohamad, Ana, and Zaman for all our fruitful discussions.

Last but not least, I want to express my sincere gratitude to Alexandre for his time and support to obtain our main experimental results that improved a lot the quality of the following work.

Contents

List of Figures

List of Tables

Chapter 1

Introduction

This thesis is developed within the framework of the PhD CIFRE (from french: Convention Industrielle de Formation par la Recherche) from November 2019 till October 2022. Research work has been accomplished between the SAFE team (which was previously Robust and Linear Systems team (SLR)) at the Gipsa-Lab laboratory at Grenoble-Alpes University for research in robust control, in collaboration with Renault research centre (from french: Technocentre).

Since the first foot-step in the world of automotive, huge number of scientists, engineers and researchers were attracted to this basic field of land transportation. During the 20th century, this field was subjected to many changes and developments especially in the autonomous domain. Intelligent and autonomous vehicles are at the heart of the societal concerns of future transportation. These cars, equipped with numerous sensors and actuators, will enhance road safety, streamline traffic, make transportation more accessible to people with disabilities, and participate in the development of new modes of transportation.

The way an automated vehicle behaves, takes a vital role in rating its acceptability. It is important as much as it is general since there exist infinite ways to travel a vehicle from point A to point B. Specifically, the performance evaluation of any vehicle is done by testing it in critical situations, i.e. how much it is able to deal with critical lane changes, collision avoidance, instability, sensor failure, autonomous starting mode, low speed precision, driver emergency, high slipping motions, high oscillations, aggressive maneuvers, etc. For each automated system in the vehicle, a controller is responsible to provide stability and performance for its motion.

In that context, the field of switching or multi-mode control architecture has been opened to solve variant tasks and achieve different driving performances. Such an architecture is resulted from a combination between several controllers to achieve an interpolated performance. The main problem arises when the transition between such control algorithms occurs, leading to undesirable instability responses. To cope with such difficult situations, this PhD is focused on complex dynamic environment that will lead to advanced control structures, enabling multi-controller transitions while taking into account sensors failures or traffic circumstances. The motivation of the thesis, objectives, manuscript organization, and its main contributions are presented below.

1.1 Motivation

Nowadays, systems are getting more and more complex leading to control algorithms able to consider online varying objectives for performance and safety. The field of autonomous systems, in particular autonomous vehicles, is indicative of such an evolution. Indeed, their driving capabilities have been recently improved for highly, and even fully, autonomous driving thanks to advanced control theory. A

fully autonomous car needs to perform several tasks including longitudinal control, lateral control, chassis control, etc.

It is known that the lateral dynamics of an autonomous vehicle varies significantly with respect to its longitudinal speed. Specifically, at low speeds, the lateral dynamics become harder to be controlled (due to approaching system singularity), whereas at high speeds, robustness and system stability decrease. On the other hand, even at nominal speeds, the lateral control aims to achieve various objectives such as lane tracking, lane changing, obstacle avoidance, etc. Consequently, various performances are required accordingly for different traffic situations that faces the vehicle. However, it is difficult to design a single controller covering the full speed range and achieving multiple objectives. This work focuses on developing advanced switching/interpolating control structures that can guarantee several control objectives over the full speed-range.

In the literature, various techniques have been proposed to obtain parameter-varying switching/interpolating control structures. In this thesis, Linear Parameter-Varying (LPV) control approaches and Youla-Kucera (YK) parameterization are introduced to formulate different LPV-YK interpolating/switching control schemes, guaranteeing stable transition under arbitrary switching.

1.2 Objectives

The main objective of this PhD work is to design a general control configuration able to maintain different vehicle performances covering the low and high speed vehicle dynamics. In addition, it can handle different situations including lane-keeping, lane-changing, obstacle avoidance, etc.

Generally speaking, the focus is on obtaining interpolating/switching control algorithms running in a real experimental research platform validating the efficiency of the proposed solutions in a real traffic conditions. The main achievements of this study are summarized below:

- Review of the state-of-the-art on the field of switching and interpolation of LPV controllers, and its use in different control applications.
- Define and compare the design and implementation of the main LPV approaches (polytopic, gridding, and LFT), with experimental validation on autonomous vehicles. Advantages and disadvantages of each approach are presented also.
- Propose new LPV-YK switching/interpolating control structures to improve the closed-loop performance and the stability during the switching instants.
- Implement the proposed LPV-YK controllers on lateral control of autonomous vehicles, in simulation and experimental environments, showing the performance improvement.
- The improvement caused by the LPV-YK control approaches on the vehicle lateral performance is shown by either: 1) Adapting the closed-loop specification regarding the performed lateral task; or 2) Maintaining a constant closed-loop specification over the full speed range by switching between consecutive parameter subsets.

1.3 Manuscript Organization

This PhD manuscript is organized in different eight chapters. A brief summary of each of the next chapters is represented below:

- **Chapter 2, Toward Switching / Interpolating LPV Control: A Review:**
  This chapter corresponds to a state-of-the-art review that was carried out on the switching/interpolation of Linear Parameter-Varying (LPV) control approaches. These concepts have been used to develop theoretical tools solving many control problems ranging from closed-loop stabilization, robust control, gain-scheduling control, switching control to interpolating control. Recent works are collected and classified providing the latest advances with main applications in different control fields. A final discussion is presented viewing the time evolution of the described switching LPV techniques and classifies them with respect to their applications.

- **Chapter 3, Autonomous Vehicles Architecture:**
  A historical background of Renault projects on automated vehicles is first presented in this chapter. Then, the architecture of the vehicle platform that has been used in our experiments is detailed. The vehicle modelling with the steering actuator dynamics are formulated. In addition, a brief literature review is shown on the lateral control which has been mainly tackled in this thesis.

- **Chapter 4, Application of LPV approaches to Vehicle Lateral Control:**
  This chapter presents the simulation and experimental implementation of the polytopic, grid-based and LFT LPV approaches to solve the lateral control problem on an electric Renault ZOE vehicle. A comparative analysis is shown among the three LPV approaches to the autonomous vehicle lateral control. The design of the three approaches from a theoretical point of view as well as their application on a real vehicle are presented, including a comparative analysis.

- **Chapter 5, Advanced LPV-YK Control Structures: Theoretical Proofs:**
  Four switching/interpolating control architectures based on LPV and Youla-Kucera (YK) parameterization are proposed in this chapter, aiming to achieve robust and adaptive closed-loop specifications (rising time, steady-state error, etc.). An LPV-YK control architecture incorporates multiple LPV or LTI controllers which can switch/interpolate between them with ensuring stability. It can be used to interpolate between different control performances aiming to achieve different closed-loop specifications, or to switch over partitioned parameter subsets when dealing with systems having large parameter variations.

- **Chapter 6, Application of the LPV-YK Structures on Vehicle Lateral Control:**
  This chapter uses the LPV-YK control structures, presented in the previous chapter, to improve the vehicle tracking performance over a large speed range. The performance of the vehicle lateral control is shown to be improved by either adapting the closed-loop specification regarding the performed lateral task, or by maintaining a constant closed-loop specification over the full speed range by switching between consecutive parameter subsets. The chapter first presents, for each approach, the implementation architecture with its designing steps, then, simulation and experimental results are presented to validate the efficiency of the proposed LPV-YK control structures.

- **Chapter 7, About The Interpolation Logic of LPV-YK Control: An Example Using Reinforcement Learning:**
  An RL-based LPV-YK interpolation scheme is proposed in this chapter, aiming to achieve an optimal performance with guaranteeing closed-loop quadratic stability. First, it is shown how the interpolating signals affect the closed-loop specifications by analyzing the closed-loop step responses. Then, the RL model is trained and simulated using our Renault's simulation environment. Simulation results are presented to validate the efficiency of the RL-based interpolation logic.
- **Chapter 8, Discussion:**
  This chapter includes conclusions and most important remarks, with respect to the problems addressed in the current PhD manuscript. In addition, future research perspectives that could be derived from the results of this PhD work are mentioned.

1.4 Contributions

The main contributions in this thesis concern the LPV and YK control concepts with their implementation on the lateral control of autonomous vehicles, including:

1.4.1 Comparison of LPV approaches concerning modelling, control design, and experimental implementation on vehicle lateral control

1. Quasi-LPV models are structured using the three LPV approaches from the nonlinear bicycle model that vary with respect to the longitudinal velocity.
2. To limit the control input effort and to achieve the noise/disturbance rejection performance, LPV/$\mathcal{H}_\infty$ problems are solved using a set of LMIs.
3. The design and experimental validation of grid-based and LFT approaches is carried out for the first time on the lateral control of autonomous vehicles.
4. Input reference is adjusted as a function of the speed and lateral error, modifying the look-ahead parameter accordingly to deal with large lateral errors (lane changing) and the small ones (lane tracking).
5. Simulation and experimental results (on a Renault ZOE vehicle) are shown to compare the performance of the controllers concerning tracking, actuator limitations and noise/disturbance rejection.

1.4.2 Novel LPV-YK control structures design with stability proofs

Four LPV-YK control structures are proposed. The closed-loop stability of each approach is analyzed and proved.

1. The first two structures are designed to maintain several control objectives over the full speed-range. Such structures are considered to be more efficient than the LPV switching control systems since: 1) There is no limitation on the switching/interpolating signals; 2) The interpolated LPV controllers are predefined and designed separately without requiring any common condition or re-design; and 3) The generalized LPV-YK interpolation scheme is defined and proved to achieve closed-loop quadratic stability with smooth assumptions and LMI conditions. More details on both structures are shown below:

- **Interpolation of polytopic-based LPV controllers:** It is used to interpolate between already designed LPV controllers, knowing that all the interpolated LPV controllers should quadratically stabilize the LPV model for any parameter variations.
- **Interpolation of YK-based LPV controllers:** This structure uses the LTI-YK parameterization to first design multiple quadratically stabilizing LPV controllers. Then interpolates between these YK-based LPV controllers providing a whole closed-loop quadratic stability.

2. The other two LPV-YK control structures are grid-based and partitioned polytopic-based LPV-YK. Their main objective is to switch smoothly between local YK-based LPV controllers, each is designed to be suitable over a certain parameter subregion. Their interest is to decrease the control design conservatism and limitations compared to the standard LPV control approaches, and improving the closed-loop performance. For more details:

   - **Switching of partitioned YK-based LPV controllers:** It is designed aiming to solve the conservatism of the quadratic stability problem due to overbounding (in convex regions), large number of varying parameters, and their large range of variations. A YK-based LPV controller is designed in each parameter subset, and the switching appears at the intersection boundary between each two consecutive subsets.
   - **Switching of grid-based LPV controllers:** This structure is formulated to switch between multiple grid-based LPV controllers, each is designed to be useful over its subset. Each parameter subset is gridded and the local LPV controllers are required to be exponentially stabilizing.

1.4.3 Implementation of the proposed LPV-YK controllers on lateral control

1. The implementation steps of each LPV-YK control structure are detailed and some of them are simulated using our Renault simulator.

2. For the first time, the LPV-YK control structures are implemented and experimentally validated on a real Renault ZOE vehicle. Experimental tests on the vehicle lateral control enhance the stability of the closed-loop system, and show the different performances achieved by the vehicle.

1.4.4 Propose an RL-based LPV-YK interpolation scheme

An RL-based LPV-YK interpolation scheme is proposed aiming to achieve an optimal performance with guaranteeing closed-loop quadratic stability. Specifically:

1. Analyze how the interpolating signals affect the closed-loop specifications using step response analysis.

2. The RL model is trained and simulated using the Renault simulator for successive lane changes at different vehicle speeds.

1.5 Publications

The scientific contributions derived as a result of the developed research work are listed below:

1.5.1 Journals

Title: Interpolation of Multi-LPV Control Systems Based on Youla-Kucera Parameterization
Authors: H. Atoui, O. Sename, V. Milanes, J. Martinez
Journal: Automatica
Status: Published by Elsevier. **Volume: 134**
Reference: *Hussam Atoui, Olivier Sename, Vicente Milanes, John J. Martinez, Interpolation of multi-LPV control systems based on Youla–Kucera parameterization, Automatica, Volume 134, 2021, 109963, ISSN 0005-1098.*

Title: LPV-Based Autonomous Vehicle Lateral Controllers: A Comparative Analysis
Authors: H. Atoui, O. Sename, V. Milanes, J. Martinez
Journal: IEEE Transactions on Intelligent Transportation Systems
Status: Published by IEEE. **Volume: 23** . **Pages: 13570 - 13581** .
Reference: *H. Atoui, O. Sename, V. Milanés and J. J. Martinez, "LPV-Based Autonomous Vehicle Lateral Controllers: A Comparative Analysis," in IEEE Transactions on Intelligent Transportation Systems, vol. 23, no. 8, pp. 13570-13581, Aug. 2022.*

Title: Toward Switching / Interpolating LPV Control: A Review
Authors: H. Atoui, O. Sename, V. Milanes, J. Martinez
Journal: Annual Reviews in Control
Status: Published by Elsevier.
Reference: *Hussam Atoui, Olivier Sename, Vicente Milanes, John-Jairo Martinez, Toward switching/interpolating LPV control: A review, Annual Reviews in Control, 2022, ISSN 1367-5788.*

Title: Multi-Variable and Multi-Objective Gain-Scheduled Control Based on Youla-Kucera Parameterization: Application to Autonomous Vehicles
Authors: H. Atoui, O. Sename, V. Milanes, J. Martinez
Journal: International Journal of Robust and Nonlinear Control
Status: Submitted and under review

Title: Advanced LPV-YK Control Design with Experimental Validation on Autonomous Vehicles
Authors: H. Atoui, O. Sename, V. Milanes, J. Martinez
Journal: Automatica
Status: Submitted and under review

1.5.2 Conferences

Title: Design And Experimental Validation Of A Lateral LPV Control Of Autonomous Vehicles
Authors: H. Atoui, V. Milanes, O. Sename, J. Martinez
Conference: 2020 IEEE 23rd International Conference on Intelligent Transportation Systems (ITSC)
Place: Rhodes, Greece. **Date:** September 20 - 23

Title: Real-Time Look-Ahead Distance Optimization for Smooth and Robust Steering Control of Autonomous Vehicles
Authors: H. Atoui, O. Sename, V. Milanes, J. Martinez
Conference: 2021 29th Mediterranean Conference on Control and Automation
Place: Puglia, Italy. **Date:** June 22 - 25

Title: Intelligent Control Switching for Autonomous Vehicles based on Reinforcement Learning
Authors: H. Atoui, O. Sename, V. Milanes, J. Martinez
Conference: 2022 33rd IEEE Intelligent Vehicles (IV) Symposium
Place: Aachen, Germany. **Date:** June 5 - 9

Title: Smooth Switching of Multi-LPV Control Systems Based on Youla-Kucera Parameterization
Authors: H. Atoui, O. Sename, V. Milanes, J. Martinez
Conference: 2022 5th IFAC Workshop on Linear Parameter Varying Systems (LPVS)
Place: Montreal, Canada. **Date:** September 27 - 30

Title: Design and experimental Validation of an $\mathcal{H}_\infty$ Adaptive Cruise Control for a Scaled Car
Authors: W. Sayssouk, H. Atoui, A. Medero, O. Sename
Conference: 2021 10th International Conference on Mechatronics and Control Engineering (ICMCE 2021)
Place: Lisbon, Portugal. **Date:** July 26 - 28

1.5.3 Patents

Because of the CIFRE opportunity at Renault, I had the opportunity to collaborate in several projects, leading to different patents submissions. Below includes a list of my cooperation within my working time at Renault.

Title: Procédé de supervision du fonctionnement d'un véhicule automobile.
Authors: H. Atoui, V. Milanes, O. Sename, J. Martinez
Status: Accepted by Renault SAS.
Year: 2021

Title: Méthode de supervision pour le contrôle d'un véhicule automobile autonome.
Authors: H. Atoui, I. Mahtout, V. Milanes, O. Sename, J. Martinez
Status: Accepted by Renault SAS.
Year: 2020

Title: Méthode de contrôle pour contrôler le déplacement d'un véhicule automobile autonome.
Authors: H. Atoui, I. Mahtout, V. Milanes, O. Sename, J. Martinez
Status: Accepted by Renault SAS.
Year: 2020

Title: Dispositif et procédé d'évaluation d'un système d'aide à la conduite pour véhicule automobile, le système d'aide à la conduite mettant en oeuvre un réseau neuronal.
Authors: N. Fernandez, H. Atoui
Status: Accepted by Renault SAS.
Year: 2021

Title: Méthode d'aide à la conduite d'un véhicule automobile autonome sur une route.
Authors: V. Milanes, I. Mahtout, D. Gonzalez, H. Atoui
Status: Accepted by Renault SAS.
Year: 2020

Chapter 2

Toward Switching / Interpolating LPV Control: A Review

This chapter corresponds to a state-of-the-art review that has been carried out on the switching/interpolation of Linear Parameter-Varying (LPV) control approaches. These concepts have been used to develop theoretical tools solving many control problems ranging from closed-loop stabilization, robust control, gain-scheduling control, switching control to interpolating control. This chapter collects the recent works and classifies them providing the latest advances with main applications in different control fields. A final discussion presents the time evolution of the described LPV techniques and classifies them with respect to their applications.

This chapter presents the literature review shown in:

- *Toward Switching/Interpolating LPV Control: A Review*, see [1].

The rest of the chapter is organized as follows: Section 2.1 presents the fundamentals of the LPV modelling, control, and its applications. In Section 2.2, LPV-switched systems are represented including the switching methods: hysteresis and Average Dwell-Time (ADT). To solve the aggressive transient switching, the smooth LPV switching technique is explained in Section 2.3. Section 2.4 introduces the LPV control interpolation based on bumpless transfer. The fundamental of Youla-Kucera (YK) parameterization is depicted in Section 2.5 including some of its applications. In Section 2.6, the LPV-YK control interpolation is presented with its new applications in different domains. Finally, the concerned LPV switching/interpolating approaches as represented in a timeline with application classification in the last section.

2.1 LPV Systems

Since 1970s, robust control research field started [2]. From a practical point of view, linearization at different operating points was deeply investigated in the literature [3]. Linear systems are of several types such as Linear Time-Invariant (LTI), Linear Time-Varying (LTV), and Linear Parameter-Varying (LPV) systems. These systems can be formulated as LPV system which can be considered the most generalized form. LPV concept surged as a control technique that can use LTI synthesis tools to control a nonlinear model. The studies tended to improve robustness in addition to the optimal performance which can handle parameter variations in the plant model.

Consider the following LPV system:

$$G(\rho): \begin{cases} \dot{x}(t) = A(\rho)x(t) + B_1(\rho)w(t) + B_2(\rho)u(t) \\ z(t) = C_1(\rho)x(t) + D_{11}(\rho)w(t) + D_{12}(\rho)u(t) \\ y(t) = C_2(\rho)x(t) + D_{21}(\rho)w(t) + D_{22}(\rho)u(t) \end{cases} \tag{2.1}$$

where $x(t) \in \mathbb{R}^{n_x}$, $y(t) \in \mathbb{R}^p$, $u(t) \in \mathbb{R}^m$, $z(t) \in \mathbb{R}^{n_z}$ are the state, output, input, controlled output vectors respectively. $w(t)$ contains the exogenous inputs, and $\rho \in \mathbb{R}^{n_p}$ is a vector of n_p measurable varying parameters that belongs to $\mathcal{P}$. $\mathcal{P}$ is the parameter space which can be represented by the below set:

$$\mathcal{P} := \{\rho(.) := [\rho_1 \dots \rho_{n_p}]^T \in \mathbb{R}^{n_p} \text{ and } \rho_i \in [\underline{\rho}_i, \overline{\rho}_i] \forall i = 1, ..., n_p\}$$

It can be shown that according to the following cases of ρ, different types of systems can be achieved:

- ρ=constant, the system is Linear Time-Invariant (LTI).
- $\rho = \rho(t)$, where the variation of ρ with respect to time is known explicitly, the system is Linear Time-Varying (LTV).
- $\rho = \rho(x(t))$, the system is called quasi-Linear Parameter Varying (Quasi-LPV) system.
- $\rho = \rho(t)$, which is an external parameter, the system is Linear Parameter-Varying (LPV).

Notice that if the model parameters can be measured online, a gain-scheduling between LTI controllers, designed at different operating points, can be used [4]. Otherwise, the unmeasurable parameters are considered as model uncertainties in the control design to reduce their effects on the closed-loop performance [5].

For time-varying systems, it may not be possible to find a single Linear Time-Invariant (LTI) controller that can perform well for all operating conditions. Therefore, the Linear Parameter-Varying (LPV) control concept has been successfully developed to achieve a stable gain-scheduling [6], self-scheduling [7] or interpolation [8] between LTI systems synthesized at different operating points. The importance of the LPV approach to control general nonlinear systems comes from the fact that the system can be written in the form of a quasi-LPV, where the parameter can vary as a function of states, inputs or outputs and not just considered as exogenous inputs [9]. [10] and [11] present successful application example of LPV/robust techniques to different domains. In the last decades, research studies have developed multivariable control systems using gain-scheduling techniques, see for instance the pioneering works [12], [13]. Gain-scheduling control is used when a plant changes significantly among different operating conditions; which is actually the case in many real applications, see [14] and references therein.

2.1.1 LPV/$\mathcal{H}_\infty$ Control Design

LPV/$\mathcal{H}_\infty$ controllers have been widely used for different objectives: noise rejection, parameter uncertainties, significant parameter variations, vibration control, tracking control, etc. This section defines the design of an LPV/$\mathcal{H}_\infty$ controller based on Linear Matrix Inequality (LMI) satisfying the closed-loop stability. The robust $\mathcal{H}_\infty$ control approach is usually used to design an LPV control. The main objective of the $\mathcal{H}_\infty$ control is to minimize the $\mathcal{L}_2$ induced gain from the external input w to the controlled output z. This is achieved by solving the following $\mathcal{L}_2$ induced minimization problem:

$$\|z\|_2 \leq \gamma_\infty \|w\|_2$$

and $\gamma_\infty > 0$, to be minimized, represents how much the demanded performance is achieved. If $\gamma_\infty < 1$, the demanded performance is totally achieved by the controller.

Among the three approaches, each controller is designed by solving its corresponding LMI-based optimisation problem. For each approach, the complexity of LPV controller existence conditions is determined in terms of the size of LMIs and the number of decision variables.

Consider a generalized plant $P(\rho)$ as follows:

$$P(\rho) = \begin{cases} \dot{x}(t) = A_p(\rho)x(t) + B_1(\rho)w(t) + B_2(\rho)u(t) \\ z(t) = C_1(\rho)x(t) + D_{11}(\rho)w(t) + D_{12}(\rho)u(t) \\ y(t) = C_2(\rho)x(t) + D_{21}(\rho)w(t) + D_{22}(\rho)u(t) \end{cases} \tag{2.2}$$

$$\longrightarrow \left[\begin{array}{c} \dot{x} \\ \hline z \\ y \end{array}\right] = \left[\begin{array}{c|cc} A_p(\rho) & B_1(\rho) & B_2(\rho) \\ \hline C_1(\rho) & D_{11}(\rho) & D_{12}(\rho) \\ C_2(\rho) & D_{21}(\rho) & D_{22}(\rho) \end{array}\right] \left[\begin{array}{c} x \\ \hline w \\ u \end{array}\right] \tag{2.3}$$

The LMI-based LPV/$\mathcal{H}_\infty$ control design in Appendix A shows infinite optimization problem due to the infinite possibilities of values of the scheduling parameters. Usually, the formulation of an LPV control problem requires to solve an infinite number of Linear Matrix Inequalities (LMIs) due to the parameter space. Methods have been proposed to reduce the problem to a finite set of LMIs: polytopic [7], [15], grid-based [16], and Linear Fractional Transformation (LFT) [6] approaches that have been discussed in the literature. An informative review on the three approaches is drawn in [14]. Currently, there exists a commercial LPV toolbox [17] for use in MATLAB that focuses on model reduction and gridding-based LPV control.

The synthesis of an LPV control can be formulated as an LMI optimization problem using a single Lyapunov function, either quadratic [12] or parameter-dependent [18]. Early synthesis methods have been limited to slow parameter variations [19], however, methods have been proposed over the years allowing arbitrarily fast parameter variations [7]–[20]. Moreover, it has been shown how incorporating bounds on the parameters' rate of variation can reduce control design conservatism, see for instance, [5] and [21]. A recent significant survey on LPV control approaches for suspension systems is shown in [22].

2.1.2 Polytopic Approach

The polytopic approach is the most popular among the LPV control approaches [14]. In many fields, engineers are interested in applying the gain-scheduling method based on optimized designs at different operating points. However, the application of this approach is limited to only a few scheduling parameters. This is due to the exponential growth of the vertices with the number of parameters. In many applications, it is unnecessary to consider the full hyperbox spanned by all combinations of extrema of the scheduling parameter values, as some portions are physically inadmissible. It may then be possible to find tighter convex sets that require fewer vertices.

Overbounding of the parameter set is considered as a main cause of conservatism. The operating region of the underlying LPV model is defined by a convex polytope containing the parameter trajectories. This convex parameter region may include vertices that are not attained by the real plant, resulting in conservatism. The reason is that the construction of the polytope is based on the assumption that all parameters vary independently, whereas they could be related to each other by inherent couplings. For example, the known bicycle model describing the lateral dynamics of an autonomous vehicle is parameterized by the scheduling parameters "v_x" and "$1/v_x$" [23] (being v_x the longitudinal speed). Such a situation might cause

unstable models at the vertices of the polytope. In addition, the parameters could be physically correlated with each other, such that some combinations of extreme values of the parameters do not occur in real operation. For example, an LPV model describing the vertical flight dynamics of an aeroplane might be parameterized by the external scheduling signals (i.e., parameters) "speed" and "altitude." But usually, the maximum speed is not reached for minimum altitude and vice versa [24].

Several solutions have been investigated in the literature to find a reduced convex parameter region. Several solutions has been investigated in the recent survey [25]. [26] suggests to construct convex polyhedrons along given parameter trajectories, and solve the control design problem using affine parameter-dependent LMIs. Unfortunately, these methods often result in a huge number of vertices or nonconvex parameter sets and thus in increased computational burden. Scheduling Dimension Reduction (SDR) approach based on principal component analysis is proposed in [24], [27], [28] which changes the coordinate basis. This method could be used to reduce the parameter set based on experimental data [24], and yields the benefit of tailoring a control design to specific trajectories. Gridding the signal range can also be done [27],[28], to obtain a more comprehensive approximate representation without experimental data, which is especially useful if the plant is unstable. The multiconvexity approach has been proposed, extended to polynomial parameter-dependent LMIs (PLMIs), and relaxed by incorporating slack variables in [29]. Other approaches are convex approximations and so-called difference convex representations [30]. In [31], a Deep Neural Network (DNN) approach is used to develop the SDR methods and achieve higher model accuracy under scheduling dimension reduction. In [32] and [33], authors develop an LPV switching controller and prove its stability when switching among the overlapped subsets of a polytopic parameter region.

Another reason, which makes the polytopic LPV synthesis conservative, is that it requires a constant Lyapunov function to ensure quadratic stability, which increases the problem conservatism. For more illustration, consider a closed-loop LPV system $CL(\rho)$, where ρ belongs to a polytopic parameter region $\mathcal{P}$. Then, the closed-loop quadratic stability is achieved according to the following theorem.

Theorem 1. *Define $A_{cl}(\rho)$ as the state matrix of the closed-loop system $CL(\rho)$. The closed-loop quadratic stability is achieved for every $\rho \in \mathcal{P}$, and for any parameter variation $\dot{\rho}$, if there exists a constant, positive definite Lyapunov matrix P satisfying condition (2.4).*

$$PA_{cl}(\rho) + A_{cl}^{T}(\rho)P < 0 \tag{2.4}$$

Later, a solution has been proposed in the literature to design LPV controllers based on parameter-varying Lyapunov function [18].

2.1.3 Grid-based Approach

The grid-based approach is based on the definition of a mesh on the parameter region. A grid-based LPV system is formulated using a linear or nonlinear interpolation between the corresponding LTI systems at the gridded operating points. It is known that a higher density of gridded points is required for better interpolation performance. An advantage of this technique is that it is applicable for any LPV plants with general parameter-dependency, requiring neither polytopic nor LFT representations. Moreover, model elements like lookup tables can be introduced in the design, since gridding is not restricted to convex regions. Consequently, the Lyapunov variable can be parameterized by general parameter dependency [18].

The implementation of the controller is computationally inexpensive, but may require large amounts of memory, to store the local controllers. The implementation scheme may consider an interpolation or a switching between local controllers. In general, this approach is limited to a few scheduling signals because of the exponential increase in grid points, hence memory requirements or interpolation complexity. Note, however, that if observer-based synthesis is performed, parameter-dependent state-feedback matrices of both observer and controller can be computed online each by a single matrix inversion without the need to store multiple controllers in memory [34], [35], [36].

Consider a closed-loop LPV system $CL(\rho)$, where ρ belongs to a gridded parameter region $\mathcal{P}$. Then, the closed-loop exponential stability is achieved according to the following theorem.

Theorem 2. *Define $A_{cl}(\rho)$ as the state matrix of the closed-loop system $CL(\rho)$. The closed-loop exponential stability is achieved for every $\rho \in \mathcal{P}$, and for a bounded parameter variation $\dot{\rho} \in [\underline{\nu}, \overline{\nu}]$, if there exists a positive definite, parameter-dependent Lyapunov matrix $P(\rho)$ satisfying condition (2.5).*

$$\dot{P}(\rho) + P(\rho)A_{cl}(\rho) + A_{cl}^{T}(\rho)P(\rho) < 0 \tag{2.5}$$

2.1.4 LFT Approach

An LPV-LFT system is formulated as a Linear Fractional Representation (LFR) containing the nominal LTI system and the model uncertainties block (see [6] for more illustration). LFT control synthesis using D-scalings is presented in [6] and [37], which is then refined to D/G-scalings in [38], [39], and [40]. The underlying theory to LFT LPV controller synthesis essentially relies on the S-procedure [41], and its variants and extensions, most notably the so-called full-block S-procedure (FBSP), [42], [43]. A general unifying approach to both LFT and grid-based LPV synthesis was presented in [20]. Historical surveys of the S-procedure can be found in [44] and [45]. The S-procedure was also used early on for robust/LPV analysis problems, already extending to less conservative results using parameter-dependent Lyapunov functions [46], [47]. It was much later, that LFT LPV synthesis was extended to parameter-dependent Lyapunov functions [21], while the basic idea was first presented in [48]. A general framework for the synthesis of uncertain dynamical systems described by standard linear fractional representations, and robust gain-scheduling controllers by convex optimization techniques has been investigated in [49].

2.1.5 LPV Control Applications

The three LPV control approaches have been widely used and experimentally validated in different applications. Knowing that most of the real systems are accurately modeled as nonlinear, the LPV approaches have been chosen to simplify the control design problems providing both stability and multi-objective performance. Such an advantage has encouraged researchers and engineers to apply the LPV control approaches on real systems such as aircrafts, aero-engines, vehicles, and different electronic and mechatronic systems. Recently, the three LPV approaches have been compared and experimentally validated on a real automated vehicle in [23].

Polytopic Approach:

Since the polytopic controller has been considered to be the simplest to design and implement, plenty of works have investigated its application to several kinds of systems. Active Magnetic Bearing (AMB) system has been modelled and controlled using the polytopic approach in [50],[51],[52], [53], [54], [55], [56]. The polytopic approach has been mainly chosen due to its high robustness in dealing with input disturbances and parameter uncertainties.

An example of a more complex LPV model can be a three degrees-of-freedom (3-DOF) robotic manipulator that is introduced in [57]. A polytopic controller that is scheduled affinely on 16 different scheduling parameters has been designed and simulated in MATLAB on an accurate nonlinear model. In [57], [58], [59], [60], [61], [62], [63], [64], [65], the design complexity of the robotic manipulators, due to its high number of scheduling parameters, has been tackled by employing different methods such as a principle component analysis-based reduction of parameter set.

Additionally, the polytopic controller has been widely used in different kinds of applications, including engine control [66], [67], [68], miscellaneous mechatronic systems [69], [70], [71], [72], [73], [74], [75], [76], [77], [78], vehicle motion control [79], [80], [11], [81],[82], academic test benches [83], [84], [85], [86], [87], noise cancelling headsets and vibration control test benches, [88], [89], [90], [91], aerospace flight control [92], aero-engine systems [93] temperautre control [94], and computer sciences [95].

Grid-based Approach:

The grid-based approach has been raised since the pioneering works [16] and [5] and the experimental results in flight control shown in [96], with interesting results. This approach has been mainly used for systems that have shown high conservatism when using the polytopic approach, in particular, aircraft motion control [97] and [98]. The grid-based approach has been used also in vehicle control for: 1) Automated lane guidance [99]; 2) Automated driving via visual feedback [79]; 3) Longitudinal and lateral tracking controls [100]; 4) Brake control [101]; 5) Electric steering system [102]; and 6) Car engine control [103].

Moreover, several applications are introduced in the literature using the gridding approach including AMB [104], robotics [105], [106], engine control [107], [108], [109], wind turbine [110], and the control of a control moment gyroscope [111], [112], and aero-engine control [113].

LFT Approach:

LFT LPV synthesis with full-block multipliers has been successfully applied in [114], validating simulation results shown in [115]. Even though the LFT controllers have not been widely used compared to the polytopic and the gridding approaches, experimental results with industrial relevance were published between 2001 and 2014. These include CD players [116], [117], induction motors [118], [119], engine control [120], [121], [122], and a wafer stage [123]. In addition, it is worth mentioning that the LFT approach has been experimentally validated on lateral control of autonomous vehicles [124].

Like the polytopic and gridding approaches, the LFT control synthesis has been tested on the AMB system [125], [126], flight control [127],[128], and aero-engine [129]. It has been widely used in the field of active noise cancellation headsets and

vibration control [6] that is also followed by [130], [131], [132], [133], [134]. In [135], a diesel engine controller has been designed using the LFT approach.

2.1.6 LPV complexity

The application of LPV techniques on robotic manipulators has been always chosen to validate methods aiming to solve the high LPV complexities with large number of scheduling parameters [27], [57], [136], [137]. Moreover, negative examples of applied LPV controllers that do not show an increase in performance are given in [75], [76]. [75] compares the LPV technique against a classical gain-scheduled PI control approach, which consists in designing LTI controllers for several operating points and then applying an interpolation strategy. In [76], a comparison is shown between an LPV control with a classical gain-scheduling approach and constant non-scheduled LTI controllers. The performance increase obtained by the LPV controller is considered insignificant. In both works, possible reasons are stated in the conservatism due to parameter-independent Lyapunov functions, which is not a restriction when classical gain-scheduling is applied [75].

Nowadays, systems are getting more and more complex leading to control algorithms able to consider online varying objectives for performance and safety. For instance, the field of autonomous systems, in particular autonomous vehicles, is indicative of such an evolution. Indeed, their driving capabilities have been recently improved for highly, and even fully, autonomous driving thanks to advanced control theory. A fully autonomous car needs to perform several tasks including longitudinal control, lateral control, chassis control, etc. Moreover, the lateral dynamics of an autonomous vehicle varies significantly with respect to its longitudinal speed [138], [139]. Specifically, at low speeds, the lateral dynamics becomes harder to be controlled (due to approaching system singularity), whereas at high speeds, robustness and system stability decrease [140]. On the other hand, even at nominal speeds, the lateral control aims to achieve various objectives such as lane tracking, lane changing, obstacle avoidance, etc. Consequently, various performances are required accordingly for different traffic situations that faces the vehicle. However, it is difficult to design a single controller covering the full speed range and achieving multiple objectives. As shown below, some solutions have been investigated in the literature to design LPV switched/interpolated control systems.

2.2 Switching LPV Systems

Describing system dynamics over a large scheduling parameter region by a single LPV model would lead to significant modeling errors, and hence inevitably degrades the closed-loop system performance [141]. In addition, it could be very conservative to design a single LPV controller that aims to shape the closed-loop performance over a certain operating condition, or according to critical/fault situations.

Fig. 2.1 shows a parameter region $\mathcal{P}$ divided into multiple subregions, so that $\mathcal{P} = \bigcup_{i\in[1,4]} \mathcal{P}_i$. The i^{th} subregion is denoted by $\mathcal{P}_i(\rho)$ $(i \in Z_N = \{1, 2, \ldots, N\})$. The sub-systems for adjacent subregions are to be switched according to different laws, including scheduling-parameter-dependent laws, state-dependent laws or external switching signals. In 2004, Lu and Wu [142] have proposed a switching LPV control design based on multiple parameter-dependent Lyapunov functions, each suitable for a specific parameter subregion, the switching allowing to achieve better

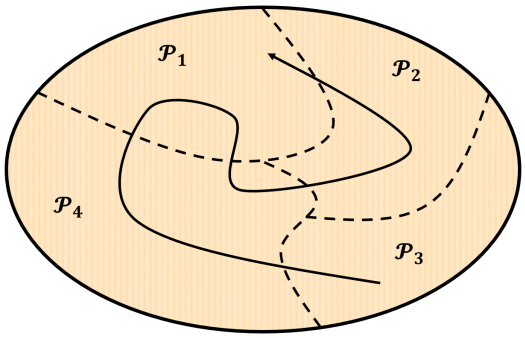

FIGURE 2.1: Multiple parameter subregions

performance. The switching stability has been studied for hysteresis switching and switching with average dwell-time strategies [142].

Later, several research studies have been focused on relaxing the LPV switching stability constraints [143], [144], [145], [146], [147], [148], [149], [150]. It is worth mentioning that, in the literature, it has been often proposed to design the multiple LPV controllers in the same form and order. Even though the local LPV controllers can have different order and form, however switching stability conditions will be difficult to derive. The assumption of same-order controllers has been always taken into consideration to primarily simplify the stability issue and controller synthesis.

The switching LPV controllers are usually designed offline, and their switching logic is determined in terms of scheduling parameter region division. The switching stability is often proved by non-increasing Lyapunov functions in the switching sequence. In [142], hysteresis switching and average-dwell-time switching strategies have been introduced, and different control synthesis conditions have been proved for each strategy. In addition, the minimum switching strategy has been reported in [151]. These switching strategies impose constraints on Lyapunov matrices or switching signals on switching surfaces and achieve guaranteed switching stability. The switching strategies are illustrated more in the next section.

2.2.1 Switching strategies

Switching systems can be seen as a hybrid system of the continuous-time system and discrete-time switching signal. The neighboring controllers to be switched are always assumed to be in the same form and order to simplify the stability problem and controller synthesis complexity. It is noted that this dissertation also follows this assumption. In the literature, there are many studies about the switching strategies and switching stability conditions, in particular, for linear systems [152], [148], [153]. These switching strategies have been extended to switching LPV systems [154], [142]. In this section, the state-of-art research about switching LPV system and control will be covered, then popular switching strategies and associated switching stability conditions of LPV systems will be given. Consider the closed-loop autonomous LPV system without external inputs in (2.6) for analysis of switching stability,

$$CL_i(\rho) : \{\dot{x}(t) = A_{cl,i}(\rho)x(t) \tag{2.6}$$

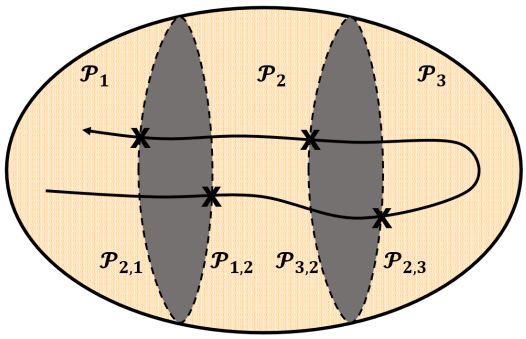

FIGURE 2.2: Hysteresis switching

Hysteresis Switching

Hysteresis switching requires to have an overlapped subregion between any two neighboring subregions. Referring to Figure 2.2, when ρ crosses the switching surface $\mathcal{P}_{1,2}$, the sub-system $CL_1(\rho)$ is switched to $CL_2(\rho)$, and when ρ crosses the switching surface $\mathcal{P}_{2,1}$, $CL_2(\rho)$ is switched back to $CL_1(\rho)$. Direct Lyapunov method is often used to prove the switching stability. Since the multiple controllers are designed on subregions, it is supposed that there is a family of positive definite Lyapunov matrices $P_i(\rho)$ dependent on the scheduling parameter ρ. Then parameter-dependent Lyapunov functions are formulated as quadratic functions as

$$V_i(x,\rho) = x^T P_i(\rho) x, \quad \forall i \tag{2.7}$$

where i represents the local active controller on the i^{th} subregion $\mathcal{P}_i$, and its corresponding Lyapunov matrix $P_i(\rho)$ is used in formulating the Lyapunov function. The switching stability can be achieved by non-increasing Lyapunov functions during each switching event [142]. The non-increasing condition is proved to be a sufficient condition but not a necessary condition. In literature, there are proven results to relax this conservative result, in which the multiple Lyapunov functions may increase its value during a time interval, only if the increment is bounded by certain kinds of continuous functions. Interested readers are recommended to the reference [155], [156]. Consider a switching event on a surface $\mathcal{P}_{i,j}$ from i^{th} subregion to j^{th} subregion, if the hysteresis switching is used, the sufficient condition of globally exponentially stability of switching system is given by the following Theorem.

Theorem 3. *Consider the closed-loop LPV system in (2.6), if there exists a family of parameter-dependent Lyapunov matrices satisfying condition (2.8), then the closed-loop exponential stability is achieved within local subsystems $CL_i(\rho)$ with $(\rho, \dot{\rho}) \in \mathcal{P}_i \times \mathcal{V}$. Moreover, if condition (2.9) is satisfied on the switching surface, then global exponential stability is achieved on entire scheduling parameter region $(\rho, \dot{\rho}) \in \mathcal{P} \times \mathcal{V}$.*

$$\dot{P}_i(\rho) + P_i(\rho) A_{cl,i}(\rho) + A_{cl,i}^T(\rho) P_i(\rho) < 0 \tag{2.8}$$

$$P_i(\rho) \geq P_j(\rho), \quad \rho \in \mathcal{P}_{i,j}, i, j \in N_J, i \neq j \tag{2.9}$$

Proof is illustrated in [142].

Average-Dwell-Time (ADT) switching

The Average-Dwell-Time (ADT) switching strategy enforces the "slow-switching" property of switching signals so that the closed-loop system achieves global stability

under the switching sequence. By ADT switching strategy, only a limited number of switches are allowed within a finite time interval [142], [157], [152]. [158], [159], [160], [161]

We assume that switching signal $\sigma(t)$ renders $N_\sigma(T,t)$, the number of switching events within the time interval $[t,T]$. If there exist two positive numbers N_0 and τ_a such that

$$N_\sigma(T,t) \leq N_0 + \frac{T-t}{\tau_a}, \quad \forall T \geq t \geq 0 \tag{2.10}$$

where N_0 is the chatter bound to avoid chattering phenomenon, then a sufficient condition for ADT switching stability is given in the next Theorem.

Theorem 4. *Given positive scalar λ_0 and μ, if there exists a family of parameter-dependent Lyapunov matrices $P_i(\rho)$ satisfying condition (2.11) on each subregion $(\theta,\dot{\theta}) \in \mathcal{P}_i \times \mathcal{V}$ and condition (2.12) on switching surface, then the exponentially stability is achieved by switching signal with average dwell time $\tau_a > \frac{ln\mu}{\lambda_0}$ within the entire scheduling parameter region $(\theta,\dot{\theta}) \in \mathcal{P} \times \mathcal{V}$.*

$$\dot{P}_j(\rho) + \lambda_0 \dot{P}_j(\rho) + P_j(\rho)A_{cl,j}(\rho) + A_{cl,j}^T(\rho)P_j(\rho) < 0 \tag{2.11}$$

$$\frac{1}{\mu}P_j(\rho) \geq P_i(\rho) \geq \mu P_j(\rho), \quad \rho \in \mathcal{P}_{i,j}, i,j \in N_J, i \neq j \tag{2.12}$$

The proof is illustrated in [148], [152].

2.2.2 Applications

Since 2004, the switched LPV control has augmented the use of the LPV control approaches achieving better performance and lower conservatism. They have been simulated and experimentally validated in several applications, mainly in aircraft flight control [162], [163], [164], [165], [166], [167], [168], [169], [170], [171], [172], [173], and aero-engine control [174], [175], [176], [177], [178], [179], [180], [181], [182], [183], [184], [185], [186]. In addition, [187], [149], [188], [188], [149] apply the switched-LPV control on the Exhaust Gar Re-circulation (EGR) system.

In mechatronics, the LPV-switched controller has been designed for different systems such as quadrotors [189], [190], vehicle lateral dynamics [191], robotic manipulators [192], suspension control [193], [194], microsatellite [195]. In addition to other applications as AMB [142], [196], [197], wind turbine [198], [199], hard disk drives [200], flexible ball-screw drives [201], mass-spring-damper [202],[203], glucose [204], [205], [206], and academic simulation [207].

2.3 Smooth LPV switching

It has been shown in [142] that the switched LPV controllers may not provide a smooth transient response during switching, when aggressive performance is obtained at switching instants. Such a case may lead to mechanical damage, decrease material lifetime, or signal saturation which is out of real application objectives. Following this work, challenges have been raised to smooth the control response during switching, and to relax the limitations on the switching signals. Several research studies have been involved in solving the switching smoothness.

The leading cause of un-smooth switching control response is due to the sudden change of control variables during switching events. The ultimate reason is that

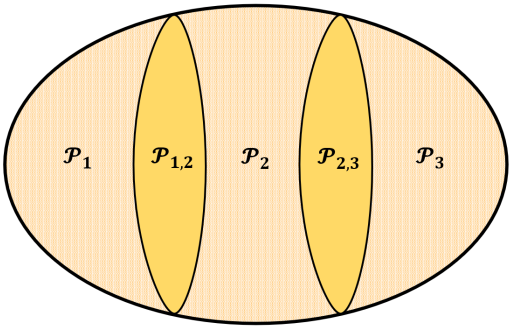

FIGURE 2.3: Smooth LPV switching

un-smooth switching LPV control optimizes closed-loop system performance over each subregion, nevertheless switching smoothness between adjacent controllers is not considered. The system performance optimization over each subregion, but ignoring switching often leads to high-gain controllers with jumped controller gains. This can be easily validated by checking the control gain difference between two neighboring subregions over the switching surface.

The smooth switching LPV controller aims to minimize the gap between controller gains and achieves smooth switching, whereas the conventional LPV controller only considers the switching stability but not the switching smoothness. To this purpose, a new small subregion is considered between each two consecutive subregions which plays the role of smooth switching. Fig. 2.3 shows the developed partitioning expressed in the smooth LPV switching where:

$$\begin{aligned} \mathcal{P}_i &:= \{\rho \in \mathbb{R} : \underline{\rho}^{(i)} < \rho < \overline{\rho}^{(i)}\}, i \in Z_N \\ \mathcal{P}_{i,i+1} &:= \{\rho \in \mathbb{R} : \overline{\rho}^{(i)} < \rho < \underline{\rho}^{(i+1)}\}, i \in Z_{N-1} \end{aligned} \tag{2.13}$$

Consequently, the smooth switching LPV controller can be described as:

$$K(\rho) = \begin{cases} K_i(\rho), & \text{if } \rho \in \mathcal{P}_i,\ i \in Z_N \\ K_{i,i+1}(\rho), & \text{if } \rho \in \mathcal{P}_{i,i+1},\ i \in Z_{N-1} \end{cases} \tag{2.14}$$

Here, the controller K_j is interpreted as a local LPV controller, to which the LPV controller K is switched when the parameter ρ lies in the sub-interval $\mathcal{P}_i$. On the other hand, the controller $K_{i,i+1}$ plays a role in smoothly switching between two local LPV controllers K_i and K_{i+1} while the parameter ρ is in a transitional sub-interval $\mathcal{P}_{i,i+1}$.

2.3.1 Smooth LPV switching control design

In this section, an example of the requirements demanded to design a smooth LPV switching control is introduced, the conditions are illustrated more in [208].

For a given LPV plant in (2.1), with $\rho \in \mathcal{P}$, $\dot{\rho} \in \mathcal{V}$ ($\mathcal{V} := \{\, \nu \in \mathbb{R} : \underline{\nu} \leq \nu \leq \overline{\nu} \,\}$), and the subintervals in (2.13), the objective is to design an LPV controller with the switching rule in (2.14) that satisfies the following requirements for any trajectory $\rho(.)$ with $\rho(t) \in \mathcal{P}$ and $\dot{\rho}(t) \in \mathcal{V}$ for all $t \geq 0$.

1. The closed-loop system containing the plant $G(\rho)$ and the switching LPV controller $K(\rho)$ (2.14) is exponentially stable.

2. For zero initial condition, the L_2-gain of the closed-loop system from the external input w to to the controlled output z is bounded by a specified value $\gamma > 0$.

3. The controllers switch continuously and smoothly between K_i and $K_{i,i+1}$, as well as between $K_{i,i+1}$ and K_{i+1}, i.e., for $i \in Z_{N-1}$, and for $m = 0, 1, \ldots, M$ for a specified integer $M \geq 0$,

$$\begin{cases} \frac{d^m}{dt^m} K_i(\rho(t)) = \frac{d^m}{dt^m} K_{i,i+1}(\rho(t)), & \text{at } \rho(t) = \overline{\rho}^{(i)}, \\ \frac{d^m}{dt^m} K_{i+1}(\rho(t)) = \frac{d^m}{dt^m} K_{i,i+1}(\rho(t)), & \text{at } \rho(t) = \underline{\rho}^{(i+1)} \end{cases} \tag{2.15}$$

4. The rate of change of the controller matrix is bounded by a specified value $\eta > 0$ in the transitional subintervals, i.e.,

$$\left\| \frac{d}{dt} K(\rho(t)) \right\| < \eta, \tag{2.16}$$

for any $\rho \in \mathcal{P}_{i,i+1}$, $i \in Z_{N-1}$, and any $\dot{\rho} \in \mathcal{V}$. Here, $\|.\|$ denotes the l_2-induced matrix norm, i.e., the largest singular value of a matrix.

An iterative descent algorithm has been introduced in [208] to solve a series of convex optimization problems by fixing a part of optimization variables. This method is used to find a feasible solution numerically for a non-convex optimization problem. The problem has been also augmented to two dimensional parameter regions.

In [209], two smooth switching techniques, simultaneous design and sequential design, have been illustrated. These two approaches are discussed briefly as follows:

- **Simultaneous design approach** : All the switching controllers are designed at the same time to formulate a convex optimization problem [210]. Using the norm of deviation of controller parameters between two consecutive switching surfaces, a numerically tractable smoothness index is introduced into the cost function. The minimization of this smoothness index helps in reducing significantly the sharp changes in control states and outputs, but at the cost of degraded $\mathcal{H}_2$ and $\mathcal{H}_\infty$ system performance. This means that there exists a trade-off relationship between switching smoothness and system performance. Thus, a tunable weighting coefficient is introduced in the cost function to balance the system performance and switching smoothness. This weighting coefficient is tuned until finding an optimal trade-off which provides smooth-switching LPV controller with acceptable system performance. In the simultaneous design approach, the control synthesis conditions depend on the adjacent subregions due to the switching stability condition. Consequently, a higher-dimensional optimization problem, with a higher amount of LMI constraints, decision variables, online computational load, and memory requirement are obtained when increasing the number of subregions [211], [14]. As a result, the simultaneous design would be practically infeasible for high-order systems with many divided subregions.

- **Sequential design approach**: This approach is proposed in [212], [213] to reduce the computational complexity found in the previous approach. Over each subregion, PLMIs for $\mathcal{H}_\infty$ are used to synthesize switching LPV controllers separately. While for each overlapped subregion, the Lyapunov matrix

is formulated by convexly combining Parameter-Dependent Lyapunov Matrix (PDLM) on adjacent subregions. In addition, this method guarantees that the overlapped subregion has intermediate performance between its neighboring subregions. An individual LPV controller is designed for each subregion in sequential order, instead of synthesizing all controllers simultaneously. By iteratively solving the reduced-dimensional optimization problem for each subregion, switching controllers with guaranteed $\mathcal{H}_\infty$ performance on all subregions and overlapped subregions can be obtained.

Moreover, other methods have been proposed in the literature for switching smoothness. In [32] and [33], the authors develop an LPV switching controller and prove its stability when switching among the overlapped subsets of a polytopic parameter region. More recently, [214] proposes a more developed smooth LPV switching control design. On the other hand, it is worth noticing that such algorithms have increased the complexity and the design constraints of the local controllers to achieve their objectives. These methods rely heavily on iterative computations to solve multi-objective convex or non-convex problems. In addition, the introduced smoothness index lacks physical meaning, and the smoothness constraints on controller matrices are selected through trial and error.

2.3.2 Applications

The additional smoothness to the transient response of the LPV switched controllers has encourages more researchers and engineers to implement it on simulated and real environments. The concerned applications include aircraft flight control [211], [215], [216], [217], [218], [219], [220], [221], [222], [161], aero-engine control [223], [224], [225], wind turbine [226], missile control [227], flexible ball-screw [228], and TORA (Translational Oscillator with Rotational Actuator) systems [229], [230].

In addition to the smooth switching approaches, an extensive research on bumpless transfer-based switching controllers has been investigated. The following section illustrates briefly the bumpless transfer method and its applications.

2.4 LPV Control Interpolation Based on Bumpless Transfer

A bumpless transfer aims to improve the transient switching behavior for a switched system. In order to reduce switching bumps, a bump constraint method has been contributed to realize bumpless transfer. The main objective is to study the switching bumps problem by modifying the original controllers, while the switching design is neglected. A description of most popular strategies for bumpless transfer can been found in [231], [232], [233] and [234]. One of the first schemes is proposed by Hanus for nonlinear plants [235]. The idea consists in pre-setting the off-line controller state for reducing the transient behavior at the switching time. Turner and Walker have generalized the results of Hanus for controllers which are not bi-proper [236], [237]. For instance, a bumpless transfer of switching controllers is proposed in [238] followed by some developments in [239] and [240].

A bumpless transfer method can be used also to overcome the problem of switching jumps in a scheduled robust model predictive control approach [241]. A scheduled robust model predictive controller implements a set of local robust model predictive controllers based on an on-line switching strategy. This method could enlarge the domain of attraction efficiently but the transient response might be hampered by spikes appearing at the moment of switching between adjacent local controllers. The algorithms based on bumpless transfer could enhance the transient response by implementing some intermediate controllers augmented to the main control scheme to solve the problem without needing more computation.

Figure 2.4 represents a bumpless-transfer switching between the pre-designed off-line controllers controller$_1$ and controller$_2$ using two on-line controllers $\bar{Q}^1$ and $\bar{Q}^2$. Let us define the signal

$$\bar{z}_e^i(k) = \alpha^i(k) - e(k), \tag{2.17}$$

which represents the difference between the i^{th} off-line controller input $\alpha^i(k) \in \mathbb{R}^m$ and the on-line controller input $e(k) = r(k) - y(k)$, where $r(k) \in \mathbb{R}^m$ is the reference; and the signal

$$\bar{z}_u^i(k) = u^i(k) - u(k), \tag{2.18}$$

that represents the difference between the i^{th} off-line controller output $u^i(k)$ and the on-line controller output $u(k)$, for any $i \in \mathcal{I}$ and for all $k \in \mathbb{Z}^+$. The idea in [237] is to minimize the following LQ criterion:

$$\bar{J}^i = \bar{\phi}^i(\bar{T}_f^i) + \frac{1}{2}\sum_{k=t_i}^{\bar{T}_f^i-1}[\bar{z}_u^{i^T}(k)\bar{W}_u^i\bar{z}_u^i(k) + \bar{z}_e^{i^T}(k)\bar{W}_e^i\bar{z}_e^i(k)], \tag{2.19}$$

where

$$\bar{\phi}^i(\bar{T}_f^i) = \frac{1}{2}\bar{z}_u^{i^T}(\bar{T}_f^i)\bar{X}^i\bar{z}_u^i(\bar{T}_f^i),$$

$\bar{W}_e^i = W_e^{iT} > 0$ and $\bar{W}_u^i = W_u^{iT} > 0$ are the weighting matrices. t_i is the switching time to the sybsystem corresponding to the mode $i \in \mathcal{I}$, $\bar{T}_f^i$ is the terminal time and $\bar{X}^i = \bar{X}^{i^T}$ is a terminal weighting matrix $\forall i \in \mathcal{I}$. Since reference signals are not known a priori, an extension to an infinite horizon is required for practical implementation. This leads to a constant feedback matrix $\bar{Q}^i$ that adds a condition on the i^{th} off-line controller to achieve the desired transient behavior at the switching instant (Fig. 2.4).

In particular,

$$\alpha^i(k) = \bar{Q}^i\begin{bmatrix} x_c(k) \\ u(k) \\ e(k) \end{bmatrix}, \tag{2.20}$$

with

$$\bar{Q}^i = (I_m - \Gamma^i B_c^{i^T}\Pi^i B_c^i)^{-1}\Gamma^i\begin{bmatrix} (D_c^{i^T}\bar{W}_u^i C_c^i + B_c^{i^T}\Pi^i A_c^i)^T \\ -(D_c^{i^T}\bar{W}_u^i + B_c^{i^T}(I_p - M^i)^{-1}U^i)^T \\ -(\bar{W}_e^i + B_c^{i^T}(I_p - M^i)^{-1}E^i)^T \end{bmatrix}^T$$

More details can be found in [242].

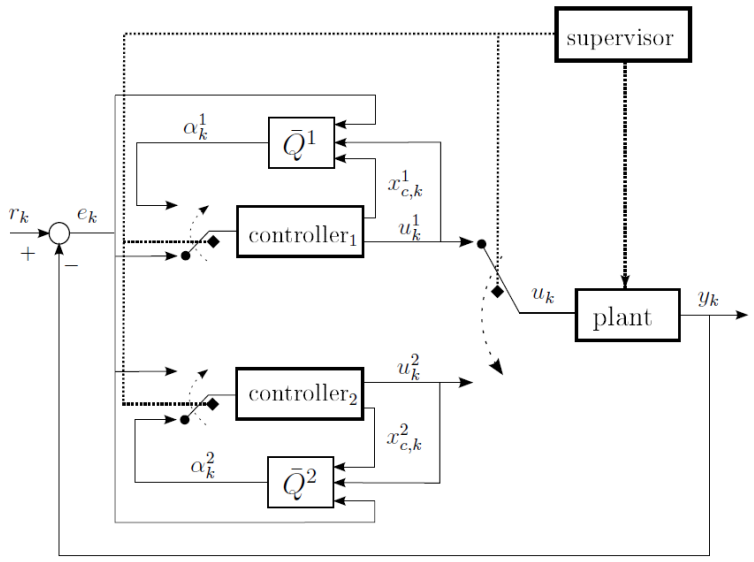

FIGURE 2.4: Bumpless Transfer with $\mathcal{I} = \{1, 2\}$ [242]

LQ bumpless transfer has been one of most celebrated bumpless transfer methods on industrial MIMO applications [243], [244]. This success is due to different factors: the existence of several reliable numerical solvers for Riccati equations, the excellent convergence properties of LQ based feedback controllers, and the fact that no plant knowledge is needed. Nevertheless, the extension to an infinite horizon assumes that the tracking error e and the control signal u are constant. This approximation is effective only if these signals vary slowly enough, with reference to the system dynamics. Another drawback is concerned with the fact that this strategy guarantees the closed loop stability only around a specific operating point. In general, it is assumed that the closedloop stability of the whole process is maintained, if both on-line and off-line control loops are stable. This assumption is justified only if the operating point is subject to "slow" variations.

2.4.1 Applications

Several research studies have concerned the application of the LPV bumpless-transfer approach to AMB [245], aircraft flight control [246], [247], [248], aero-engine control [249], [250], [251], [252], [253], [254], [255], [256], and wind turbine [257]. In addition, it has been implemented on inverted pendulum [258], water-tank level control [241], academic examples [259], [260], [261], and on electronic systems [262], [263].

2.5 YK Parameterization

Recently, a new smooth LPV switching technology is proposed based on Youla-Kucera (YK) parameterization [264]. Compared with the literature [142], the novelty of this method is to introduce a parameter overlap division method to improve the smoothness of switching. The flexibility and freedom of the switching controller are increased, and the transient response disturbance during the switching is suppressed. The next section introduces a general review on YK parameterization.

The fundamentals of YK parameterization started in 1970s, developed by Youla [265], [266] and Kucera [267]. The interest behind YK concept is to parameterize a

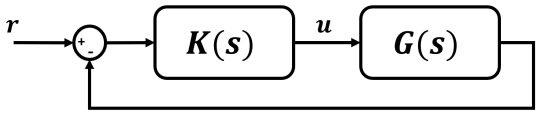

FIGURE 2.5: Negative feedback loop

set of linear stabilizing controllers $K(Q)$ for a given LTI plant in a feedback control loop (see Fig. 2.5). Each one is parameterized by its corresponding YK dynamical parameter $Q(s)$ [268]. The stability is guaranteed depending on the parameter $Q(s)$. Similarly, the dual YK parameterization provides all the linear plants stabilized by a given controller. The class of all the plants stabilized by a controller depends on the transfer function called dual YK dynamical parameter $S(s)$, so $G(S)$. This parameter could represent any plant variations. Hence, this useful way of parameterizing either plants, controllers or both is employed to solve many control issues.

According to the control objectives, three main configurations can be targeted:

- **Controller parameterization:** allows stable controller reconfiguration when some change occurs. It is also widely used in disturbance and noise rejection control. A number of successful applications can be found in the last two decades, being the most used approach in different control fields [269].
- **Plant parameterization:** is employed to solve the problem of closed-loop identification. Some successful implementation can be found in Plug & Play control where the dynamics of new sensors or actuators are identified on real-time without system disconnection [268].
- **Simultaneous control and plant parameterization:** provides a new control structure that changes according to new identified dynamics on the plant. This principle is mainly used in fault tolerant control and adaptive control [270].

The current review mainly focuses on the controller parameterization part. Consider a SISO LTI plant $G(s)$ connected to a controller $K(s)$ in a stable feedback structure (see Fig. 2.5 for details). The closed-loop transfer function is obtained as:

$$CL(s) = \frac{G(s)K(s)}{1 + G(s)K(s)} \tag{2.21}$$

Moreover, let's define a transfer function $Q(s)$ from the reference r to the control input u, then:

$$Q(s) = \frac{K(s)}{1 + G(s)K(s)} \tag{2.22}$$

Thus, if $G(s)$ and $Q(s)$ are known, the controller $K(s)$ can be expressed as:

$$K(s) = \frac{Q(s)}{1 - G(s)Q(s)} \tag{2.23}$$

From (2.22), it is shown that if $K(s)$ stabilizes $G(s)$, then $Q(s)$ is stable and proper. Equivalently, if $Q(s)$ is stable and proper, then $K(s)$ given by (2.23) stabilizes $G(s)$.

In addition, reformulating the closed-loop expression to be written in terms of $Q(s)$, the closed-loop transfer function is affine with respect to $Q(s)$ expressed as:

$$CL(s) = Q(s)G(s) \tag{2.24}$$

From this point, the concept of a controller parameterized by a YK transfer function $Q(s)$ is opened. Then, a set of stabilizing controllers can be parameterized in terms of all stable and proper functions $Q(s)$ for any LTI plant $G(s)$. The LTI-YK parameter $Q(s)$ is designed using the doubly coprime factorisation [271], [272].

YK parameterisation uses the doubly coprime factorisation concepts to reduce the algebraic complexity of Q computation [271],[272]. Let an LTI controller K stabilizes the LTI plant G, then they can be factorized (from left and right) as a product of a stable transfer function matrix and a transfer function matrix with a stable inverse as shown below:

2.5.1 Doubly Coprime Factorisation

YK parameterisation uses the doubly coprime factorisation concepts to reduce the algebraic complexity of Q computation [271],[272]. Let an LTI controller K stabilizes the LTI plant G, then they can be factorized (from left and right) as a product of a stable transfer function matrix and a transfer function matrix with a stable inverse as shown below:

$$\begin{aligned} G &= NM^{-1} = \tilde{M}^{-1}\tilde{N} \\ K &= UV^{-1} = \tilde{V}^{-1}\tilde{U} \quad \forall j \end{aligned} \tag{2.25}$$

Lemma 1. *If the coprime factors M, N, $\tilde{M}$, $\tilde{N}$, U, V, $\tilde{U}$, $\tilde{V} \in \mathcal{RH}_\infty$ (stable and proper), and they satisfy the following Bezout Identity:*

$$\begin{aligned} \begin{bmatrix} \tilde{V} & -\tilde{U} \\ -\tilde{N} & \tilde{M} \end{bmatrix} \begin{bmatrix} M & U \\ N & V \end{bmatrix} &= \begin{bmatrix} M & U \\ N & V \end{bmatrix} \begin{bmatrix} \tilde{V} & -\tilde{U} \\ -\tilde{N} & \tilde{M} \end{bmatrix} \\ &= \begin{bmatrix} I & 0 \\ 0 & I \end{bmatrix} \end{aligned} \tag{2.26}$$

then, all the factorized LTI controller K stabilize G (proof in [269]).

2.5.2 LTI-Q Parameterisation

Consider the LTI-YK parameter Q as a transfer function which characterizes the dynamic mapping of a controller K that stabilizes the plant G.

Lemma 2. *Assume an LTI plant $G = NM^{-1}$ stabilized by the LTI controller $K = UV^{-1}$, with M and N are coprime and $\in \mathcal{RH}_\infty$, U and V are coprime and $\in \mathcal{RH}_\infty$. Then the set of all stabilizing controllers $\tilde{K}$, for G, as a function of a stable filter YK parameter Q with appropriate dimensions is defined as:*

$$\begin{aligned} \tilde{K} = \tilde{K}(Q) &= (U + MQ)(V + NQ)^{-1} \\ &= (\tilde{V} + Q\tilde{N})^{-1}(\tilde{U} + Q\tilde{M}) \end{aligned} \tag{2.27}$$

where $Q \in \mathcal{RH}_\infty$ by construction[269].

Control reconfiguration is important to improve system performance, especially for multi-variable and multi-objective systems. Such complex systems may require some specifications which is difficult to handle using a single controller, such as desired bandwidth, time response, or robustness against modeling errors. an $\mathcal{H}_\infty$ multi-objective controller can hold several specifications in a single controller, however, it is known to be conservative when complexity increases. In addition to the previously mentioned switching methods: 1) Gain-scheduled approach [37]; Ad-hoc technique [13]; and 2) Bumpless transfer [273], YK parameterization has been

also used for switching objective, where a set of linear stabilizing controllers can be mapped onto a Q-based controller [274].

On the other hand, YK parameterization for switching/interpolating controllers has shown several advantages: 1) It allows stable interpolation between unstable controllers [275]; 2) Interpolated controllers can be designed and tuned separately using different techniques ($\mathcal{H}_\infty$, LQR, PID, ...) [269]; 3) It facilitates adding new parts to an existing system online as Plug&Play control theory [276]; and 4) The closed-loop stability is guaranteed under arbitrary continuous/discontinuous interpolating signals between different stabilizing controllers without requiring a common Lyapunov function [274]. In 80s, the first application of YK-based control parameterization has been performed [277]. Specifically, two controllers K_1 and K_2 have been designed satisfying reference tracking and disturbance rejection respectively. Both controllers have been parameterized with respect their corresponding YK parameters Q_1 and Q_2 respectively.

2.5.3 Applications

A significant literature review on YK work including applications can be found in [278]. The YK parameterization has been successfully used in several domains. A Q-based YK controller has been applied on the roll angle of an aircraft to compensate the well-known trade-off between performance and robustness [274]. Another work has formulated a YK-based switching architecture to switch between a high performance controller when the measured angle is not noisy, to a robust controller when there are model uncertainties and external disturbances [279]. In [280], two classes, Irrigation systems and Hypersonic vehicles have been controlled based on YK parameterization. Both classes are formulated by hyperbolic partial differential equations. The YK controller switches between different LTI controllers to regulate time-domain specifications (i.e. peak value of control signal, overshoot). Thanks to YK parameterization, [281] and [282] were able to introduce new components to the control control loop without affecting system stability. The controller reconfiguration is implemented on a livestock stable climate system, where a new temperature measurement come out during system operation and a new controller is added to the existent control loop.

In [283], the YK concept has been proposed for a steam boiler to switch between two controllers with different objectives; the first aims to regulate the water level within min and max bounds, and the second control objective is to keep the feed water flow steady. In addition, noise/vibration control domains have investigated the YK controllers to attenuate noises and disturbances [284]. Moreover, it has been also applied for different applications requiring high control precision and noise sensitivity such as: wafer scanning in semiconductors [285], data storage systems (reading/writing) [286], [287], [288], mechatronics [289], active suspension systems [290], [291] and biochemistry [292] where the regulation problem is to maximize the biomass productivity in the fed-batch fermentation of a specie of yeasts and the cell growth is an undesirable consequence and considered as an unstable disturbance. An application on steamboiler is represented in [283].

Moreover, YK control schemes have been successfully used for Intelligent Transportation Systems (ITS) in the last years. A steering control of autonomous vehicles considering two LTI controllers designed separately (one for lane-changing and one for lane-tracking) [293]. The YK control scheme of both controllers has shown interesting performance for small and large lateral errors. Moreover, [294], [295] have

experimentally validated the YK control structure by switching between Cooperative Adaptive Cruise Control system (CACC) and ACC when the communication between vehicles fails.

2.6 LPV-YK Parameterization

Consider an LPV plant $G(\rho)$ (2.1), with ρ is a scheduling parameter within a predefined range $\rho \in [\underline{\rho}, \overline{\rho}]$, is formulated using either polytopic or grid-based approach. Let $K(\rho)$ be an LPV controller designed to stabilize $G(\rho)$ over the whole parameter region. Then, at each vertex or grid point ρ_i, the local LTI controller K_i is known to stabilize the local plant G_i. Using YK parameterization, it is possible to parameterize each local LTI controller K_i by a corresponding local LTI-YK parameter Q_i, obtaining a parameterized LTI-YK local controller $\tilde{K}_i$. The interpolation or gain-scheduling between the obtained $\tilde{K}_i$ ($i \in [1, N]$) achieves a gain-scheduling LPV-YK control scheme $\tilde{K}(\rho)$ satisfying:

1. Stability of the closed-loop including LPV system under fast changes of the varying parameter ρ.
2. Recovering the local controllers K_i in the operating points.

In [296], conceptions of doubly coprime factorisation and Youla parameterization of LTI systems have been extended to LPV systems with respect to quadratic stability using a state-space expression:

2.6.1 LPV Doubly Coprime Factorization

YK parameterization uses the doubly coprime factorization concepts to reduce the algebraic complexity of Q-computation. Assume an LPV controller $K(\rho)$ stabilizes the LPV plant $G(\rho)$, then they can be factorized (from left and right) as a product of a stable transfer function matrix and a transfer function matrix with a stable inverse as shown below:

$$\begin{aligned} G(\rho) &= N(\rho)M^{-1}(\rho) = \tilde{M}^{-1}(\rho)\tilde{N}(\rho) \\ K(\rho) &= U(\rho)V^{-1}(\rho) = \tilde{V}^{-1}(\rho)\tilde{U}(\rho) \end{aligned} \tag{2.28}$$

Lemma 3. *If the coprime factors $M(\rho)$, $N(\rho)$, $\tilde{M}(\rho)$, $\tilde{N}(\rho)$, $U(\rho)$, $V(\rho)$, $\tilde{U}(\rho)$, $\tilde{V}(\rho)$ are stable and proper, and they satisfy the following Bezout Identity:*

$$\begin{aligned} \begin{bmatrix} \tilde{V}(\rho) & -\tilde{U}(\rho) \\ -\tilde{N}(\rho) & \tilde{M}(\rho) \end{bmatrix} \begin{bmatrix} M(\rho) & U(\rho) \\ N(\rho) & V(\rho) \end{bmatrix} &= \begin{bmatrix} M(\rho) & U(\rho) \\ N(\rho) & V(\rho) \end{bmatrix} \begin{bmatrix} \tilde{V}(\rho) & -\tilde{U}(\rho) \\ -\tilde{N}(\rho) & \tilde{M}(\rho) \end{bmatrix} \\ &= \begin{bmatrix} I & 0 \\ 0 & I \end{bmatrix} \end{aligned} \tag{2.29}$$

then, the factorized LPV controller $K(\rho)$ stabilizes $G(\rho)$ [296].

2.6.2 LPV-Q Parameterization

Consider the LPV-YK parameter $Q(\rho)$ that maps its corresponding LPV controller $K(\rho)$ to a parameterized Q-based LPV-YK controller $\tilde{K}(\rho)$. Then, the following Lemma is proved to be satisfied [278].

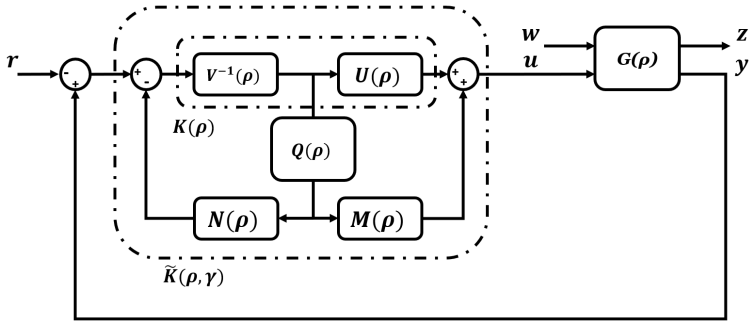

FIGURE 2.6: Parameterized LPV-YK control scheme

Lemma 4. *Assume an LPV plant $G(\rho) = N(\rho)M^{-1}(\rho)$, and an LPV controller $K(\rho) = U(\rho)V^{-1}(\rho)$ that has been designed to stabilize $G(\rho)$ for every $\rho \in \mathcal{P}$. $M(\rho)$ and $N(\rho)$ are coprime, stable, and proper, $U(\rho)$ and $V(\rho)$ are coprime, stable, and proper. Then, it is possible to obtain a family of LPV controllers $\tilde{K}(\rho)$ formulated as (Fig. 2.6):*

$$\begin{aligned}\tilde{K}(\rho) &= (U(\rho) + M(\rho)Q(\rho))(V(\rho) + N(\rho)Q(\rho))^{-1} \\ &= (\tilde{V}(\rho) + Q(\rho)\tilde{N}(\rho))^{-1}(\tilde{U}(\rho) + Q(\rho)\tilde{M}(\rho))\end{aligned} \tag{2.30}$$

where $Q(\rho)$ is designed to be quadratically stable (see [296] for details).

In addition, [296] has designed an observer-based state-feedback LPV controller based on Youla parameterization. It has been proved that any quadratically stabilizing LPV controller can be parameterized based on YK concept, providing the closed-loop quadratic stability.

On the other hand, some works have proposed the YK concept to design a polytopic gain-scheduling controller with lower conservatism than the standard LPV design. [297] proposes a YK-based gain-scheduled controller by interpolating LTI controllers designed separately at the different vertices of a polytopic parameter region. The interpolation is performed as a function of the varying parameters of the LPV model. Closed-loop quadratic stability and performance are guaranteed at intermediate interpolation points of the convex domain. However, the proposed interpolation is preferably used when the system often remains at the designed operating points with rarely transitions from one to another. As a conclusion, the polytopic LPV controllers could perform better in fast parameter changes where a uniform performance is obtained in the designed convex region.

In [298], a YK configuration is proposed to improve the performance of a polytopic LPV control. It introduces an LPV system which switches between a minimum-phase and nonminimum-phase dynamics as a function of the parameter variations. An LPV controller based on the polytopic approach is designed as a nominal controller in the full parameter region. Then, two different LTI controllers ($\mathcal{H}_\infty$ and PID) are designed separately at certain operating conditions (one in minimum-phase region and another in nonminimum-phase region). These LTI controllers are then interpolated with the nominal LPV controller using an LTI-YK configuration. In [299], a fixed pole-assignment application is introduced using an LPV YK-based method to preserve the closed-loop poles at the same location by interpolating between different controllers regardless the variations in the LPV system. Therefore, a unique performance is obtained along the variation of the parameters while keeping stability.

Recently, [300] proposes a YK-based interpolation scheme between two LPV controllers, designed separately, to achieve a multi-objective control system. Each LPV controller is designed over a convex domain with a common Lyapunov function (following the approach in [12]), to quadratically stabilize the plant model. However, this approach may be conservative since it requires all the local LPV controllers to be designed based on standard polytopic-based LPV approach.

2.6.3 Applications

LPV-YK control schemes have not been widely used in applications yet. However, some works have implemented them with remarkable results. In [296], an LPV model of mass-spring-damper system (with a varying stiffness) is controlled using quadratically stabilizing LPV-YK controller. Another application has been performaed on a MIMO LPV system of a quadruple tank [298]. The objective is to control the water height in four tanks using two valves; the plant changes from minimum phase to a non minimum-phase with respect to the operating points (valves values). Two LTI-YK controllers are designed; one corresponding to a PID controller designed in the minimum phase operating point, and another $\mathcal{H}_\infty$ controller in the non-minimum phase operating point. These two controllers are parameterized on two significant operating points with respect to a polytopic LPV controller. The overall interpolation control scheme shows optimal performance in both operating conditions.

In [299] the LPV Q-based controller is used in fixed pole assignment application, the Q-based controller switches among different controllers to place the closed-loop poles always at the same location independently of the varying parameter. Thus, the LPV closed-loop system achieves the same performance in the range of the varying parameter without loosing stability. A YK based feedback controller rejecting bounded disturbances is extended to cover LPV systems using LMI computation toolbox in [301].

To validate the smoothness of the LPV-YK control structure compared to the previous approaches, it has been implemented on the known AMB system in [264], [302], [303], [304], [305], [306], [307], and aircraft flight control [308], [309]. Different applications have been also concerned including wind turbine [310], hydro-active gas bearings [311], damping control [312], and several academic examples [313], [314], [315], [316], [317].

2.7 Discussion

This chapter has reviewed the evolution of the smooth LPV switching/interpolating control starting from the basic gain-scheduled LPV control, switched-LPV control, smooth LPV switching control, bumpless-transfer-based LPV switching, and the most recent LPV-YK interpolating control. From the beginning of 90s till the current year, different kinds of applications have been controlled based on them. The timeline of LPV switching/interpolating concepts is presented in Fig. 2.7, where the column represents the time evolution and the row shows the studied switching and interpolating LPV controls.

2.7.1 Time evolution of the theoretical contributions

In 90s, the LPV control approaches have been proposed referring to the known works: polytopic [7], grid-based [18], and LFT [6]. The LMI approaches have been

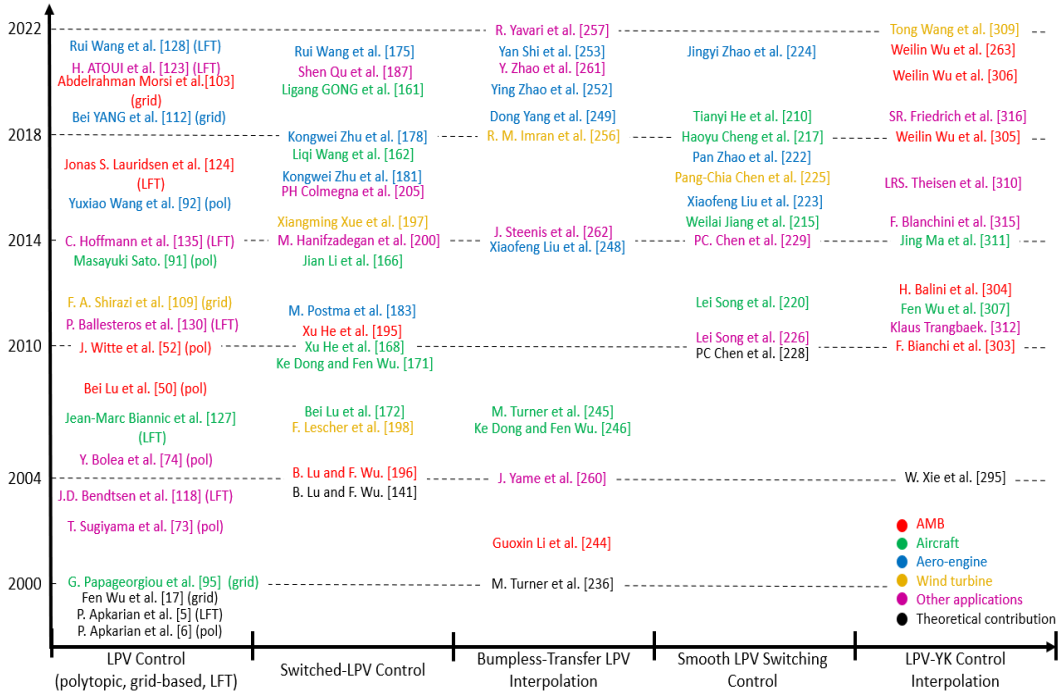

FIGURE 2.7: Timeline of known applications using LPV switching/interpolating approaches

used to achieve either quadratic stability over convex parameter region (using constant Lyapunov function), or exponential stability over gridded parameter region (using parameter-dependent Lyapunov function). It is worth mentioning that the LPV approaches have shown lower closed-loop performance, than a local LTI one, and conservatism in some applications having large parameter regions, large number of parameters, or significant dynamic uncertainty. Since 2000, researchers have been involved in solving the conservatism problem using switching/interpolating concepts.

In [237], the first step to design a gain-scheduled LPV control based on bumpless-transfer has been raised. The advantage of bumpless-transfer is to reduce the difference of the control input just before and just after switching. [142] has proposed a switched-LPV control design using multiple parameter-dependent Lyapunov functions. It shows good performance over each parameter sub-region, however, an unsmooth performance appears at the transient switching. Later, switching smoothness conditions have been added to the LMI optimization problem [229]. These three LPV switching approaches have increased the design complexity and stability studies. A parameterization approach has been also used to design a gain-scheduling LPV controller in [296]. It shows several advantages compared to the previous ones including lower design complexity, closed-loop stability can be proved easier, smooth switching, and most important that the local controllers can be designed separately with different state dimensions.

The importance of LPV control approaches, switched-LPV control, bumpless-transfer LPV interpolating, smooth-LPV switching, and LPV-YK control interpolation is shown regarding their implementation to several applications mainly Active Magnetic Bearing (AMB), aircraft motion, aero-engine, wind turbine, and others. Fig. 2.7 presents the applications with different colors and their time evolution.

2.7.2 LPV control

Several applications of the LPV control approaches are shown in the first column of the timeline in Fig. 2.7. Researchers have been interested in applying them to nonlinear models, by reformulating them to LPV models. For instance, the AMB system is nonlinear with respect to the rotor speed, which has been considered as a parameter varying. AMB systems are known to be highly nonlinear, multi-variable and inherently unstable systems. The nonlinearity is described in the relationship between the electro-magnetic force, current and length of the air gap. Moreover, The system (vibrational) dynamics depend on the rotational speed due to gyroscopic and electro-magnetic coupling. The AMB has been controlled using the three LPV approaches: polytopic [51], [52], grid-based [104], and LFT [125]. Moreover, the aircraft speed and altitude have been chosen as varying parameters for aircraft motion control. In 2000, it has been first applied using the gridding approach [96], then using the LFT approach in 2006 [247], and the polytopic in 2013 [92].

In 2012, the grid-based approach has been applied on wind turbine control [110]. The nonlinearity in the wind turbine model is due to the aerodynamic interaction of the wind and the rotor blades. Therefore, the LPV model is formulated considering the rotor speed, absolute wind speed, and pitch angle variables as varying parameters. Since 2016, the three LPV approaches have been implemented on aero-engine control using the polytopic in 2016 [93], the grid-based in 2019 [113], and most recently in 2021 the LFT [129]. The high pressure rotor speed is chosen as a varying parameter that changes over time. Furthermore, other domains have been interested in LPV control including electro-hydraulic servo system (2002) [74], induction motor (2003) [119], canal control (2005) [75], active-noise cancellation (2011) [91], mechanical systems (2014) [136], and real experiment on autonomous driving (2020) [124].

2.7.3 Switching LPV control

The second column of the timeline concerns the switched-LPV control applications. As already mentioned, this approach has been contributed by Fen Wu in 2004 [142] to decrease the conservatism of the LPV control design using multiple parameter-dependent Lyapunov function. The application on the AMB system in [197] and [196] shows the performance improvement over the parameter subregions. Moreover, this approach has been widely used for aircraft flight motion between 2006 and 2020 in [173], [171], [169], [167], [163], and [162]. Similarly, it has been implemented on aero-engine control such as in [184] (2012), [182] (2016), [179] (2018), [176] (2021). In addition to wind turbine control [199], [198], and other domains like flexible ball-screw drives [201], glucose control in type 1 diabetes [206], and engine Exhaust Gas Recirculation (EGR) [188].

2.7.4 Bumpless-Transfer LPV control Interpolation

Some applications on bumpless-transfer LPV interpolation are shown in the third column of the timeline. In 2002, an implementation on the AMB is shown [245]. Later in 2006, two works have proposed the bumpless-transfer approach for aircraft flight control [247], [246]. Recently, bumpless-transfer LPV interpolation has been widely implemented on the aero-engine control starting from 2014 [249], then 2019 [250], then 2020 [253], and the newest in 2021 [254]. Others applications are mentioned including electronics [263], inverted pendulum [258], and academic examples [261], [259].

2.7.5 Smooth LPV switching control

In the fourth column of the timeline, the applications on smooth LPV switching control are represented. This approach has been mostly applied on aircraft motion control since 2012 [221], and later in 2015 [222], 2018 [218], and the last one in 2019 [211]. In 2016 and 2017, [224] and [223] have proposed the smooth LPV switching control for aero-engine control. Moreover, it has been implemented on different applications such as wind turbine [226] (2016), missile control [227] (2010), and TORA [230] (2014).

2.7.6 LPV-YK control Interpolation

The last column in the timeline shows the applications on the LPV-YK control interpolation. This approach has not been yet applied to aero-engine control. However, it has been widely used for AMB in [304] (2010), [305] (2012), [306] (2018), [307] (2020), and recently in [264] (2021). It has been also implemented on aircraft control [308] (2012), [309] (2014), and wind turbine [310] (2022). In addition to different applications including hydroactive gas bearings [311], flexible-link robot [317], and academic examples [313], [316].

Table 2.1 lists the main advantages and disadvantages of each studied switching/interpolating approach.

TABLE 2.1: Overview of discussed approaches

Switching/Interpolating approach	Advantages	Disadvantages
LPV control	Simple and fast design conditions	High conservatism for large number of parameters and large ranges
Switching LPV control	Decreased conservatism and providing better performance at each parameter subset	Aggressive transient response at switching instants
Bumpless-Transfer LPV control Interpolation	Continuity of the control input is ensured at switching instants	Local controllers are blended to guarantee closed-loop and switching stability
Smooth LPV switching control	Smoothness can be guaranteed from the design by a matrix norm	Complex design conditions including the design of the switching signals for switching stability
LPV-YK control Interpolation	Controllers are designed separately, new parts can be added to an existing system online, no constraints on the switching signals	Transient response is directly affected by the designed YK parameter

Chapter 3

Autonomous Vehicles Architecture

3.1 Introduction

First, it is worth noting that the work in this thesis is not starting from scratch but it is a long work that has been carried out in the research department at Renault for developing an autonomous driving architecture. Fig. 3.1 shows the projects timeline achieved by Renault since 2013 to the present time. The main general objective of these projects was to offer a taxi pool for people transportation to their work, home or a Mall. Before the beginning of this thesis work, Renault has already developed several autonomous driving prototypes such as: PAMU (in 2013), KAIROS (in 2014), TRAJAM (in 2015), SYMBIOZ (in 2017), and ROUEN Autonomous Lab (in 2018). The current thesis has been done by the time of the running projects TORNADO and SAM Saclay. The prototype of TORNADO has been used for the experimental validation of the work presented here.

Even if we focus on the control part, it is worthy to review the full autonomous driving architecture to understand the input/output connections of our work by describing the connected modules.

The current chapter presents the architecture of the vehicle platform that has been used in our experiments. In addition a brief literature review is shown on the lateral control system which has been mainly tackled in this thesis. The field of autonomous vehicles has been expanding rapidly in the last decade, in order to meet road safety and environmental objectives. Most of the definitions and details that we present here are issued from [318], the readers that would like to have more details can refer to it.

To validate the contributions raised by this thesis, a RENAULT ZOE robotized car has been used. The following Section 3.2 presents the Autonomous Vehicle (AV) architecture including its subsystems perception, map service, localization, world model, decision-making, navigation, supervisor, and control. In addition, a brief review on vehicle control is depicted in Section 3.3. Section 3.4 discusses the main parts in the AV architecture that are tackled and concerned in the later chapters.

3.2 Experimental Platform Description

This section presents the test vehicle concerning the scientific and technical development especially from perception, navigation and control point of view. The platform is a fully robotized Renault ZOE car (see Fig. 3.2) that has been prepared for Renault project available for the use in the Rambouillet Territory in France [318].

Autonomous driving is computationally demanding and requires integrating different functions such as perception, map service and localization, world model, decision-making, navigation, and vehicle control into a unified system achieving intelligent behavior. The interaction and organization of these functional components

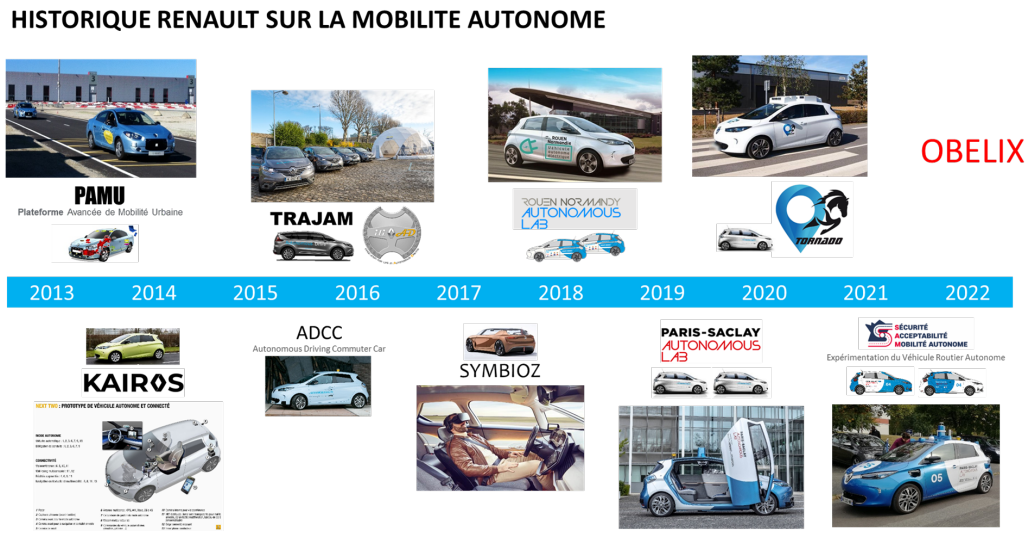

FIGURE 3.1: Renault's History on Autonomous Vehicles

FIGURE 3.2: Renault ZOE automated vehicle

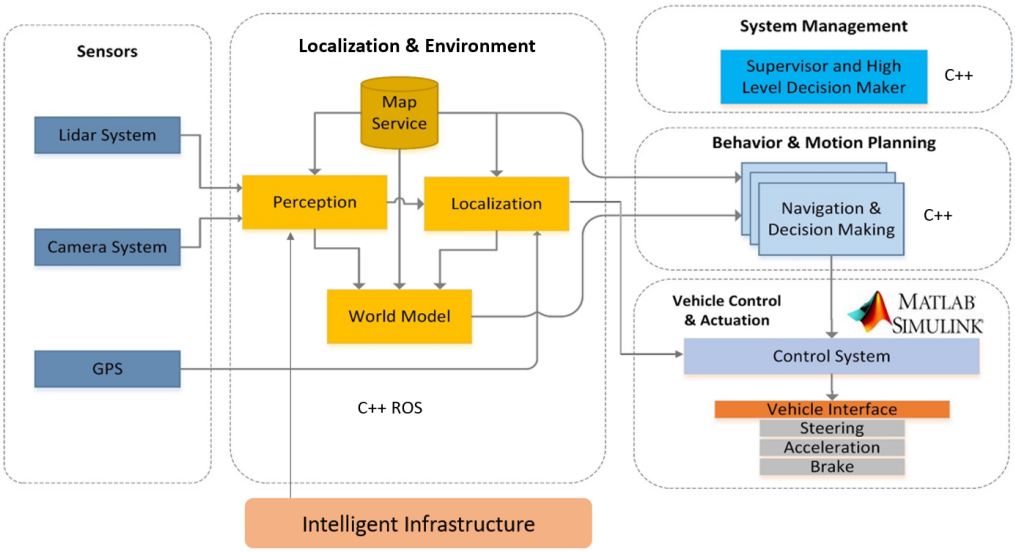

FIGURE 3.3: Functional components of the automated ZOE

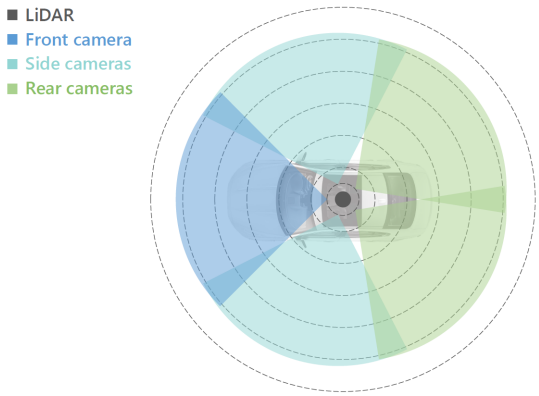

FIGURE 3.4: Sensor setup in the automated ZOE Vehicle [318]

FIGURE 3.5: Pipeline for 3D object detection. Objects are detected in the images from the cameras. Later, LiDAR data is included to infer the geometrical properties of the objects. Finally, all the detections are merged, and a tracking stage adds temporal consistency across consecutive frames [318]

play a vital role on the robustness and reliability of the vehicle operation. FIGURE 3.3 represents the connections and interactions of the components of the vehicle. Notice that the next sections are easily identified in FIGURE 3.3.

3.2.1 Perception

The automated car is equipped by five evenly distributed cameras and a 32-layer LiDAR located in the center of the roof rack, providing a 360° field of view as shown in Fig. 3.4, see [319] for more details. Through a low-level fusion, the sensors information is fused to provide obstacle detection, classification, 3D box estimation, and tracking. Briefly speaking, the perception system uses a robust state-of-the-art framework and feeds the vision-based detections to a 3D box estimation method that makes use of LiDAR information to know their size and location. Then, the tracking algorithm exploits this spatial reasoning to add time consistency and enhance the reliability of the final detections, refer to Fig. 3.5.

Vision-based detection and classification

Computer vision approaches are used to take advantage of the feature-rich appearance information delivered by the cameras. Notice that thanks to the multi-camera setup, the system can identify agents in the entire range of interest, without blind spots. To improve the data fusion between images and LiDAR data, detections with a pixel-wise semantic mask is chosen, knowing that accurate extrinsic calibration is available.

At the end, a set of 2D bounding boxes with information about the category (e.g., car, pedestrian, bus etc.) is provided as an output. Each one contains a pixel-wise

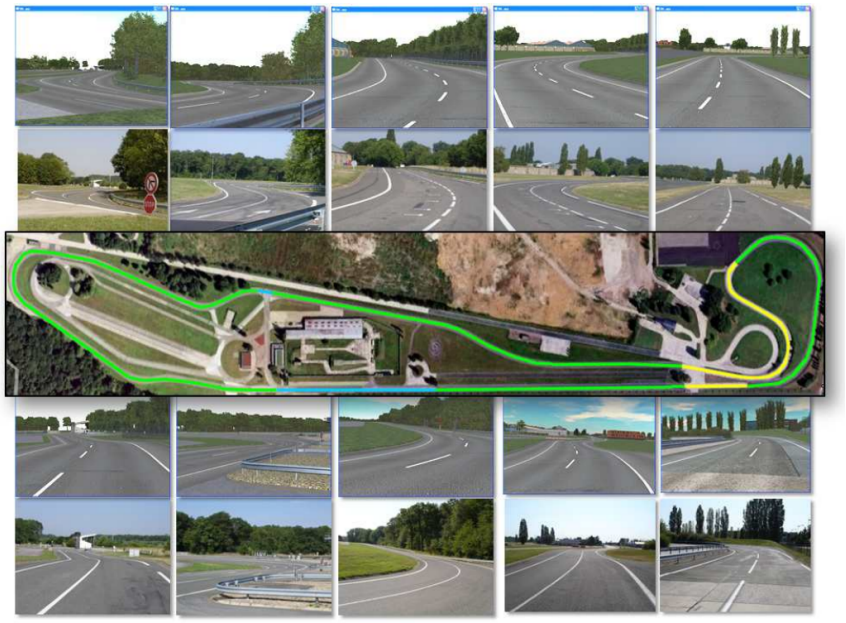

FIGURE 3.6: *Satory* private test track

mask that defines the contour of the object. Note that each camera gives a different set of detections.

3D box estimation

The LiDAR scanners is known to be highly accurate in measuring distances. So, it is used here to obtain geometrical information about the previously identified objects. A frustum PointNet approach [320] is used to recover the geometrical structure behind the raw LiDAR representation of the obstacle. This approach provides the size, location, and orientation of each obstacle using LiDAR information, and taking into consideration the missing parts due to occlusions or perspective.

This stage outcomes positioned cuboids representing the real geometry and distance from the ego-vehicle to every obstacle.

Tracking

The main objective of this stage is to add consistency to the 3D detections that have been expressed in the same frame. It is composed of three steps: 1) Movement estimation based on an Unscented Kalman Filter [321] for different pedestrians and vehicles movement models; 2) Ego-vehicle movement compensation, due to its displacement, is important to correct the misalignments on the subsequent detections. This is achieved using the GPS/INS system available in the vehicle; and 3) Data association aiming to correlate the detection in the current cycle with the set of already tracked agents, adding new instances whenever it is necessary.

3.2.2 Map Service

The map database is a High Definition Map that has been created specially for a certain experimentation. It represents the road network and includes topological, geometrical and semantic information. It is mainly composed of details about the interactions existing between roads at a lane level. The center and the boundaries

of each lane is also found in the stored map with centimeter accuracy. In addition, information such as speed limit, marking types, and driving directions are also associated with each lane as attributes. Moreover, different information are included in the map service such as: 1) Intersection type, shapes or priority order; and 2) Traffic lights location and association to lanes. All these information are compiled as a geographical database within the vehicle. For the experimental tests in this thesis, the private test track in *Satory* is used, see FIGURE 3.6

3.2.3 Localization

The Localization component is responsible for centralizing the ego vehicle within the available map information. It provides position, heading, velocity and timing information, together with integrity information. To achieve its objective, it receives information from the perception, map service, and the GPS. The accuracy of localization is improved by performing map matching with landmarks detected. For instance, the localization system identifies detected lane markings with the corresponding lane markings found in the map database. After this identification, it corrects absolute pose estimation so that relative position of detected landmarks correspond with absolute position of lane markings in the map. Consequently, the system upgrades its covariance matrix. In order to prevent localization leaps, these corrections can be smoothed, preserving both requirements on absolute and relative accuracy. Finally, the output localization information includes position, heading, velocity and timing information, together with integrity information.

3.2.4 World Model

The main objective of the World Model component is to understand the situation of the ego-vehicle with its surrounding by combining the information from the perception and the map service. Since the perception system does not consider context information while providing the surrounding situation, it is important to associate it with the map service to better understand the current scene. The map service is used to:

- Find the global path to transport from the departure location A to the final destination B.
- Assist the navigation system module to generate a real time local trajectory while operating in autonomous mode.
- Provide context in which the vehicle navigates.

The World Model component is composed of four modules: Contextualization, Interaction, Intention, and Coherence module. For more illustration:

- Contextualization Module: The perceived objects from the perception system are matched with the map to identify their position with respect to the road and to enrich them with semantic information. For instance, it labels the perceived objects (received from the perception system) as *pertinent* or *not pertinent*. The objects are labelled as *pertinent*, such as pedestrians, if they can be located within the navigable space. On the other hand, the vehicles and other obstacles are considered as *not pertinent* when they are not located on the navigable space of the ego vehicle. In addition, it can deal with traffic lights detected using Vehicle to Infrastructure (V2I) communication since the perception system in our platform does not return traffic lights information.

- Interaction Module: It identifies the maneuvers that the ego vehicle is allowed to perform and determines the perceived objects with which it would interact. This process is performed with respect to the context in which the ego vehicle navigates and applicable traffic laws that are stored in a map database.
- Intention Module: It estimates the intention of the road users with respect to the other entities with which they may interact. For this purpose, it uses the state of the entities provided by the contextualization module and the data from the interaction module. While the interaction module identifies the possible entities that might interact with each other, the intention module estimates the behaviors that those entities are likely adopting.
- Coherence module: It computes whether any conflicting intentions are present.

3.2.5 Decision-Making

After a global route plan has been found, the autonomous vehicle must be able to navigate the selected route and interact with other traffic participants according to driving conventions and rules of the road. Given a sequence of road segments specifying the selected route, the Decision-Making system is responsible for selecting an appropriate driving behavior at any point of time based on the perceived behavior of other traffic participants, road conditions, and signals from infrastructure. To obtain a comfort and safe vehicle behaviour, the driving plan is modified to the expected interaction between the ego vehicle and the detected obstacles. The decision is taken according to several criteria: 1) the relative position of the obstacle: same lane as ego vehicle, opposite lane, partially on ego lane, side walk; 2) obstacle direction: moving along and backward or forward, moving perpendicular and to or away from the driving plan; and 3) obstacle type: pedestrian, vehicle.

For example, when the vehicle is reaching the stop line before an intersection, the decision-making system will command the vehicle to come to a slow down, observe the behavior of other vehicles, bikes, and pedestrians at the intersection, and let the vehicle proceed once it is its turn to go. The maneuver associated with each perceived obstacle is created in an expert system manner. So, the computational complexity is kept low and a deterministic behaviour is obtained. Every maneuver adds constraints on the longitudinal (slow down, follow, stop) and lateral (avoid) dimensions which are taken into account in the local trajectory planning process.

3.2.6 Navigation

After the driving behavior is decided, which could be cruise-in-lane, change-lane, or turn-right, a path or trajectory that can be tracked by the low-level feedback controller is constructed. The main role of the Navigation system is to generate the local trajectory of the ego vehicle in real time. The resulting trajectory should be dynamically feasible for the ego vehicle, comfortable for the passengers, and avoid collisions with the existing obstacles. The trajectory generation data includes the geometric description of the desired path, lateral error tolerance and associated speed profile. This process can be described in three stages:

- Space definition: The high definition vector map provides a geometric description of each lane which is used to create lateral boundaries (i.e., a driving corridor) limits to the vehicle. According to the closest obstacle, a longitudinal boundary is set so that the decision system chooses a stop maneuver. Spatio-temporal footprint of each obstacle combined with an avoidance maneuver is

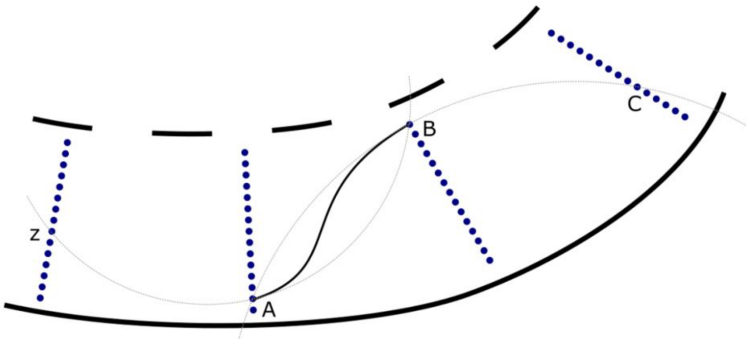

FIGURE 3.7: Sampling of driving space with vertices (blue dots) arranged in layers. An example of a circle spline that connects second and third layer is shown in solid black. Continuity with first and fourth layer are shown in dotted black lines. [318]

computed based on estimated position and speed. The available driving space is therefore reduced according to the set of perceived obstacles.

- Path optimization: It aims to optimize the driving space in the short term horizon. The driving space is discretized into a set of vertices along regularly spaced. These vertices are then used to construct the path by connected splines as shown in Fig. 3.7. A second order geometric continuity [322] is applied to compute a convenient optimized path after splines combination.

- Speed profile: After constructing the geometric path, a speed profile is associated to the optimal path considering road geometry and vehicle dynamic constrains (i.e. maximum allowed speed or desired lateral acceleration in turns). Additional constraints such as pedestrian lines, approaching intersections, and obstacle avoidance are considered to modify the speed profile. The final trajectory including the path and speed profile is then sent to the control system as a set of way-points with information about vehicle position, heading, speed, acceleration and road curvature within a speed-based horizon.

3.2.7 Supervisor in System Management

The purpose of the Supervisor system is to monitor and control the components to ensure the safety and robustness of the operational components and to facilitate the integration, deployment, and for graceful degradation of software components. It selects the discrete behavior of the components, that is, to determine which continuous behavior each of the functional components must have at each moment of time.

The supervisor maintains different operational modes (e.g. autonomous/manual mode) and sends signals to the operational components to switch their states accordingly. Its main functions are as follows:

1. Safely deploys the software components and brings the system to the safe operational state.

2. Interacts with the driver to start or stop the autonomous mode.

3. Monitors the states of all the operational components.

4. Identifies the problems in the components and switches to alternative modes of operation to keep the system under safe state and to request the driver to take back the control.

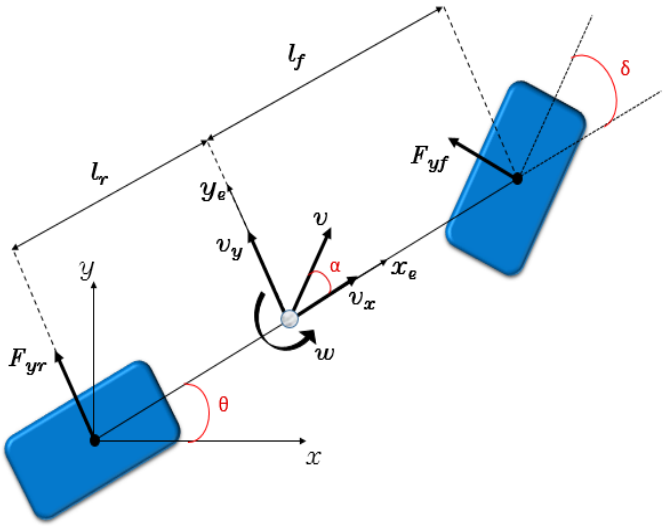

FIGURE 3.8: Vehicle Bicycle Model

5. Facilitates the integration and maintenance of the overall system.

3.2.8 Vehicle Model

The main dynamics which are usually considered in the vehicle model are the longitudinal, lateral and vertical dynamics [138], [139]. Thus, simplified models are taken at the beginning such as the bicycle model (two-wheels model), without considering the suspension system (see FIGURE 3.8). Notice that the vehicle model contains two types, the kinematic model and the dynamic model. The kinematic model assumes that the tire-slip of the vehicle with the ground is null. It is derived geometrically where no forces and tire-slips are considered, as if it is a point-object. This kind of models is mainly used at low speed systems such as mobile-robots as well as for the vehicles in automatic parking tasks. Moreover, kinematic model is very useful for motion planning (reference tracking or path-following) [323]. Considering the tire-slips in the model is vital for high speed vehicles. Thus, the dynamic model is used to introduce the side-slip angle with the applied forces from the vehicle and on it. This model can better use the vehicle's capabilities for executing aggressive maneuvers that will be significant in planning motions with high accelerations and jerks.

This section represents the kinematic and dynamic models of both longitudinal and lateral vehicle motions that have been briefly derived and verified in [138] and [139].

Kinematic Model

As mentioned before, the kinematic model is derived geometrically as a point-object. Thus, observing the marked center of gravity in FIGURE 3.8, the longitudinal and the lateral vehicle motions in the global reference can be computed as:

$$\begin{cases} \dot{x} = v\cos\theta \\ \dot{y} = v\sin\theta \\ \dot{\theta} = w \end{cases} \tag{3.1}$$

where

- x and y are the cartesian coordinates of the vehicle's center of gravity in the global frame (x,y). (m)
- θ represents the rotation of the vehicle with respect to the $x-axis$ and called the yaw angle. (rad)
- w is the yaw rate that represents the rotation rate of the vehicle. (rad/s)

Since the equations in (3.1) are derived in the global frame, the following rotation matrix is used to write them in terms of the vehicle's frame as follows:

$$\begin{bmatrix} x_e \\ y_e \\ \theta_e \end{bmatrix} = \begin{bmatrix} \cos\theta & \sin\theta & 0 \\ -\sin\theta & \cos\theta & 0 \\ 0 & 0 & 1 \end{bmatrix} \begin{bmatrix} x_d - x \\ y_d - y \\ \theta_d - \theta \end{bmatrix} \tag{3.2}$$

where

- x_d, y_d and θ_d are the coordinates of the reference to be tracked.
- x_e, y_e and θ_e represent the longitudinal, lateral and rotational errors of the vehicle with respect to the demanded trajectory.

From (3.2), the kinematic-error model differential equations are derived to obtain:

$$\begin{cases} \dot{x}_e = w y_e + v_{ref}\cos\theta_e - v_x \\ \dot{y}_e = -w x_e + v_{ref}\sin\theta_e \\ \dot{\theta}_e = w_{ref} - w \end{cases} \tag{3.3}$$

where v_{ref} and w_{ref} are the longitudinal and rotational velocity references in the vehicle's frame. Derivations can be found in [324].

Dynamic Model

The dynamic model is derived using physical concepts, the side-slip angle α will be considered from now on. Applying Newton's 2^{nd} law to the vehicle's longitudinal and lateral motions we get:

$$\begin{cases} \dot{v}_x = \frac{-F_{yf}\sin\delta - \mu m g}{m} + w v_y + a \\ \dot{v}_y = \frac{F_{yf}\cos\delta + F_{yr}}{m} - w v_x \\ \dot{w} = \frac{F_{yf} l_f \cos\delta - F_{yr} l_r}{I} \end{cases} \tag{3.4}$$

where

- v_x, v_y and w are the body frame velocities, i.e. longitudinal, lateral and rotational velocities in the vehicle's frame.
- δ and a are the control inputs, steering angle and longitudinal acceleration respectively.
- F_{yf} and F_{yr} are the lateral forces applied on the front and rear tires respectively.
- I, m, l_f and l_r are the vehicle's inertia, mass and the distance from the center of gravity to the front and rear wheel axes respectively.
- μ and g are the friction coefficient and the gravity acceleration constant respectively.

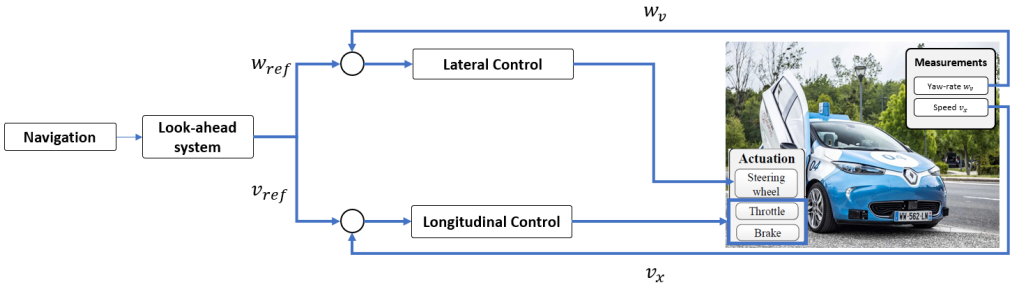

FIGURE 3.9: Control system architecture

F_{yf} and F_{yr} can be modelled using Pacejka's tire model [138] as follows:

$$\begin{aligned} F_{yf} &= c_3 \sin(c_2 \tan^{-1}(c_1 \alpha_f)), \quad \alpha_f = \delta - \tan^{-1}(\tfrac{v_y}{v_x} - \tfrac{l_f w}{v_x}) \\ F_{yr} &= c_3 \sin(c_2 \tan^{-1}(c_1 \alpha_r)), \quad \alpha_r = -\tan^{-1}(\tfrac{v_y}{v_x} - \tfrac{l_r w}{v_x}) \end{aligned} \tag{3.5}$$

where c_1, c_2 and c_3 are constants.

It is worth mentioning that the above tire model shows a nonlinear-dependency of F_{yf} and F_{yr} with respect to α. Notice that the objective of this thesis, related to the internal project at RENAULT, concerns the passenger vehicles (or daily vehicles) which constrains the lateral acceleration, and consequently small slipping angle α. Thus, assuming small α, one can linearize it resulting the following relation:

$$\begin{aligned} F_{yf} &= C_f(\delta - \tfrac{v_y}{v_x} - \tfrac{l_f w}{v_x}) \\ F_{yr} &= C_r(-\tfrac{v_y}{v_x} + \tfrac{l_r w}{v_x}) \end{aligned} \tag{3.6}$$

where C_f and C_r represent the tires' stiffness of the front and rear wheels.

Steering Actuator Model

The dynamics of the steering actuator affects significantly the vehicle dynamics, leading to model uncertainties in the vehicle model. Thus, the steering actuator model is identified at the nominal longitudinal speed $v_x = 12\ m/s$ as an LTI model. A second order transfer function has been obtained in the following form:

$$G_{act} = \frac{k}{s^2 + 2\zeta w_n s + w_n^2} e^{-T_d s} \tag{3.7}$$

where k, ζ, w_n, and T_d are the static gain, the damping, the natural frequency and the time delay, respectively. The second order Padé approximation is chosen for the time delay. Consequently, the time delay term is then represented as:

$$e^{-T_d s} = \frac{1 - \frac{T_d s}{2} + \frac{(T_d s)^2}{12}}{1 + \frac{T_d s}{2} + \frac{(T_d s)^2}{12}} \tag{3.8}$$

3.2.9 Control System

The first functionality of the Control system is to ensure stability when switching from manual to autonomous mode and vice-versa. During autonomous mode:

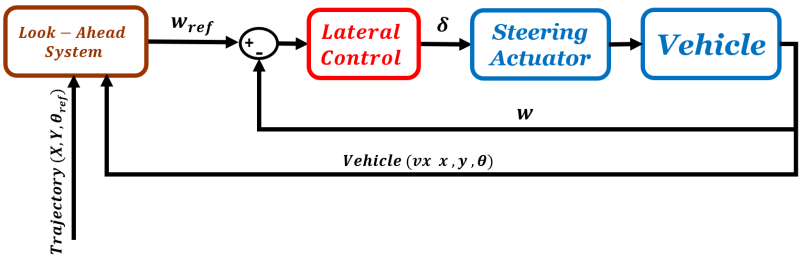

FIGURE 3.10: Lateral control closed-loop scheme

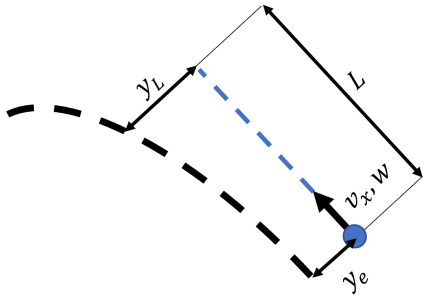

FIGURE 3.11: Lateral control based on look-ahead concept

1. It monitors a set of vehicle accessories such as lights, wipers, horn and warning light.
2. It observes continuously the health state of the surrounding systems and inner modules, and executes specific fail-safe policies or emergency actions triggered using vehicle safety devices (emergency stop button, override key, etc.).
3. It receives the vehicle localization and the planned trajectory to achieve accurate, safe, and comfort tracking.

The general control architecture is shown in FIGURE 3.9 including the longitudinal and lateral controllers.A dSPACE MicroAutoboxII (MABx) is used to embed the control algorithms using MATLAB/Simulink turning at 100 Hz. The MABx is connected to the vehicle via a CAN network. On-board sensors provide the system with information such as vehicle localization, speed, longitudinal acceleration, yaw rate, etc. The maximum capacity (100 Hz) is used for the communication with the steering, throttle, and brake actuators.

Longitudinal Control

A low-level, longitudinal controller is designed to control the throttle and brake actuators according to the speed reference received from the navigation system. Since the speed reference could include discontinuities which can affect the stability and performance of the low-level control. A high-level longitudinal controller is designed achieving high robustness and tracking capabilities. This is obtained using a Linear Parameter-Varying (LPV) control concept, considering the rate of the speed reference as a scheduling parameter.

Lateral Control

The lateral control is responsible to control the steering actuator aiming to track the required path maneuvers. To maintain human steering behavior, the look-ahead

concept is used by measuring the lateral displacements from the reference trajectory at a distance in front of the vehicle. Such concept mainly uses the GPS, where a high integrity navigation system of an automated vehicle, based on the fusion between the Inertial Measurement Unit (IMU) and the GPS, is developed and implemented. This allows to predict the future lateral error and try to minimize it smoothly as the human driver does.

The used scheme for the lateral control, as shown in Fig. 3.10, consists of:

1. A feedforward term which concerns the reference trajectory by considering the road curvature and vehicle speed (see Fig. 3.11). The road curvature is estimated at a target point chosen in front by a look-ahead distance in order to predict the future lateral displacement.

2. A feedback compensator which activates the steering actuator to minimize the current vehicle errors and correct its lateral and heading positions..

The lateral controller, applied to the automated ZOE, is designed using the LPV concept, having the vehicle longitudinal speed as the scheduling parameter. It can be designed using any control concept (pole-placement, PID, $\mathcal{H}_\infty$, ...). The aim is to track the yaw rate reference w_{ref} and respecting the actuator limitations.

The Look-Ahead System (LAS) block represented in Fig. 3.10 aims to generate a coherent yaw-rate reference w_{ref}. The LAS uses the current vehicle situation measured by the sensors and the information from the navigation system. The main role of LAS is to improve the lane-tracking accuracy and driving comfort at the same time. w_{ref} can be approximated as:

$$w_{ref} = \frac{2v_x y_L}{L^2} \tag{3.9}$$

where y_L is the predicted lateral error at the look-ahead distance L (see Fig. 3.11).

3.3 Related works on vehicle control

Vehicle automation was leveled from 0 to 5 according to the SAE J3016 standard. In this standard, levels were distributed as follows: Level 0, where the human driver has the full responsibility of all driving actions. Level 1 contains basic driving assistance like adaptive cruise control (ACC), anti-lock braking systems and electronic stability control [139]. Level 2 is more assisted than level 1, by considering advanced assistance such as hazard-minimizing lateral/longitudinal control, e.g., [325], or emergency braking, see e.g., [326], [327]. At level 3, the system is fully automatic in driving with environment monitoring under specific conditions. However the human driver is still able to take control when the driving actions are out of autonomous system's operational circumstance. Level 4 represents the vehicle with full automation as in the previous level but in addition to safe control of the vehicle in in case that the operator fails to control the intervention request. Finally, level 5 performs all the driving situations as fully autonomous, i.e. the vehicle moves without a driver. Autonomous driving aims to avoid accidents, reduce fuel consumption, improve traffic flow. It also provides passenger comfort in critical situations and make it possible to car travelling for everyone regardless of their abilities or conditions.

Several studies in the literature have focused on the path tracking performance of the vehicle, their references differ by taking either online or offline motion plan.

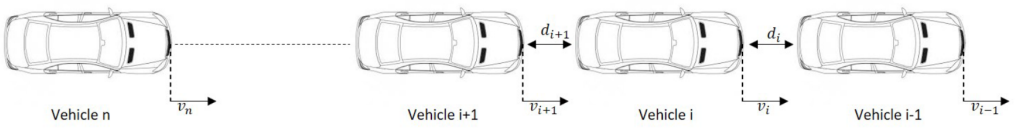

FIGURE 3.12: Adaptive Cruise Control (ACC) scheme

The topic of motion planning is taking a wide range of interest discussing different strategies to design a plan feasible to the vehicle dynamics (see [323]).

Different vehicular models (linear or not) can be considered for control design objectives. For example, in [323], the authors neglect the dynamics of the vehicle for path-planning design. In [328], an LTI model is used including the dynamics of the vehicle, whereas in [82] and [329], the authors prefer to use a Linear Parameter Varying (LPV) bicycle model to track normal and racing car references, respectively. However, in the field of heavy vehicles, the vertical dynamics cannot be neglected, as observed in [330]. In [100], a more complete model, considering kinematic and dynamic equations, rewritten in the LPV form, is proposed. In addition to increasing accuracy, the LPV approach allows the use of linear-like control design tools. In [331] and [82], the authors design a cascaded control scheme for the kinematic and the dynamic controls. This strategy adds some limitations and constraints into the control design.

Vehicle control methodologies that include the vehicle, the path, and the driver are currently being developed at several research centers and automotive suppliers. The importance of the used control strategy lies in its simplicity and the achieved performance. The main objective in [100] is to track an offline trajectory safely by minimizing the external disturbances and noises (from the driver, sensors, etc.), and dealing with uncertainties due to some neglected (or unmodeled) dynamics or fixed parameters. Referring to these demanded performances, robust control is a suitable technique to achieve their goal where it is able to deal with model uncertainties and disturbance rejection, see [332]. In [82], the authors use the LMI-based LPV-LQR/$\mathcal{H}_2$ cascaded controllers with an LPV UIO observer to estimate the road friction force and achieve less tracking error. The controller is computed offline using the polytopic approach. Moreover, in [329], the authors apply the LPV-MPC approach, for a racing car, where the controller is computed online with reducing the computational cost.

3.3.1 Longitudinal control

Longitudinal control has been studied considering energy efficiency, fuel consumption and traveling time. For instance, Adaptive Cruise Control (ACC) strategies have been contributed for automated car-following. Recent results have proposed new spacing policies and new control architecture to decrease the time gap between vehicles, while ensuring the string stability [333]. Concerning the cruise control performances, the speed control algorithm [334] has been augmented to enhance road stability and safety of the vehicle, see [335]. In addition, the look-ahead cruise control has been improved using a parameter-dependent model describing the traffic flow in terms of the velocity trajectory design. Hence, the design of a longitudinal control strategy becomes challenging.

ACC systems adjusts vehicle speed and provides a specified distance to the preceding vehicle by automatically controlling the throttle and brake actuators [336]. ACC with the Stop&Go system offered by the Advanced Driver Assistance System

(ADAS), makes driving easier and less stressful. Different control approaches have been proposed for ACC. The Model Predictive Control (MPC) is largely and commonly used, where a high level controller is proposed based on MPC approaches, taking into consideration the driver longitudinal ride comfort, driver permissible tracking range, and rear-end safety [337]. In [338], a Fractional-Order Control (FOC) approach has been presented to design a feed-forward structure for ACC to enhance the car-following while ensuring the robustness/stability. A fuzzy longitudinal control is studied in [339] to control the throttle and braking pedals, this control approach is using (IF...THEN) conditions based on experience and experimental results. [340] introduces the Cooperative Adaptive Cruise Control (CACC), it is known as the extension of the ACC by enabling the wireless communication between vehicles (V2V) to control the time gap. An LPV control has been used to deal with the variations of the time headway while ensuring the convergence of the spacing errors towards zero and the attenuation of any disturbance propagating along the platoon.

3.3.2 Lateral control

Vehicle lateral control is a vital problem to achieve an on-road automated movement. It is important as much as it is critical where it concerns lane-keeping, lane-changing, obstacle avoidance, autonomous parking, etc. Most of the path-tracking methods in practice encounter challenges when high accuracy and robustness are required [341]. The first role of the lateral control is to keep the vehicle within the boundaries of a lane, which is performed by adjusting the steering actuator to minimize the lateral error between the vehicle position and a target point in the generated reference. The question comes on how to choose the target point. If the target point is chosen to be the closest point (in the reference) to the vehicle, the actuator may not be able to minimize the corresponding lateral error in case of high speeds, high curvature changes, etc. This is due to delays in the used sensors and actuators. Then, a look-ahead approach is raised to predict the future lateral error at a chosen look-ahead distance. Look-ahead systems use sensors as machine vision, radar, and LiDAR, to measure the lateral displacement in front of the vehicle.

Lateral control for overtaking or obstacle avoidance maneuvers has been also tackled in the literature. This concept took a part of the studies concerning the steering rate and the forward distance to be covered by ensuring safety with respect to the vehicles around. Fuzzy logic control [342] and different optimization techniques, as in [343],[344], and [345], were used to maintain better scenarios for lane change and collision avoidance.

3.3.3 Look-ahead based lateral control

In 90s, the control concepts based on look-ahead systems have been raised. These concepts have been developed to mainly improve the efficiency and performance of the longitudinal and lateral vehicle controls. [346] proposes a new approach to improve the vehicle trajectory prediction for the Adaptive Cruise Control (ACC) system. It concludes that the higher look-ahead distance, the greater the prediction errors. Moreover, the look-ahead approach is also used to optimize traffic flow, minimize trip time [347], decrease fuel consumption and provide safety for heavy-duty vehicles [348], [349], [350].

On the other hand, look-ahead systems are used for lateral objectives as shown in the pioneering works [351], [352]. In [353] and [354], the authors have recognized that the closed-loop stability is sensitive to the variation of speed. Specifically, when

the vehicle speed increases, the closed-loop zeros and poles move toward the imaginary axis leading to poor damping of the poles. Increasing the look-ahead distance moves the zeros closer to the real axis, improving the damping of the closed-loop poles. As a result, the choice of a proper look-ahead distance is important for stability and performance of the closed-loop system. Practically, as much as the look-ahead distance decreases, the vehicle will lose farer information which leads to periodic oscillations due to actuators and sensors delays. On the other hand, when the look-ahead distance increases, the vehicle may not be able to deal with near obstacles or maneuvers. The relation has been analyzed between the look-ahead distance and the longitudinal velocity, the road curvature and the processing delay of the vision. In [355], the authors introduce an equation which calculates the look-ahead distance as a function of vehicle specifications and longitudinal speed taking into account the distance between the vehicle and a bumper. [356] proposes a dynamic look-ahead distance $L(s)$ which varies with respect to speed. The aim was to obtain the lateral acceleration independent of the longitudinal speed which makes the design of the steering control much easier.

One of the most used schemes for the lateral control consists of:

1. A feedforward term which generates the desired yaw rate at a varying look-ahead distance with respect to the vehicle's speed.

2. A feedback compensator that minimizes the current vehicle yaw rate error to reduce the lateral error.

In [357], the steering rate is defined to be proportional to both heading and lateral errors, adapting look-ahead distance accordingly to vehicle speed. Thus, a Linear Time-Invariant (LTI) controller is designed for a fixed look-ahead distance and speed. Each one of those obtained LTI controllers has a different performance to be used in a certain situation. [293] uses this approach to design a switching LTI controller based on Youla-Kucera (YK) parameterization. Two LTI controllers are designed separately having the same speed but different look-ahead distance parameter d; the first one with $d = 30m$ for managing larger lateral errors smoothly, and the second with $d = 15m$ to provide fast tracking capabilities. When the absolute lateral error increases from 0.6 to $3m$, the controller switches its performance from the second to the first. A recent approach has been proposed in [23], solving the same problem but by adapting the look-ahead distance within the generated yaw rate reference in terms of the absolute lateral error, and using a single robust LPV controller.

Recently, several studies aim to find the best tuning of the look-ahead distance L with respect to the vehicle speed v_x. The studies in [358], [359] and [360] propose to tune L from numerical analysis. [357] estimates L manually by analyzing the closed-loop poles with respect to speed, look-ahead distance, and lateral control feedback gains. In [361], the authors indicate three look-ahead distances (L_1, L_2, L_3) at a fixed speed. Then, a feedback lateral control uses vehicle lateral deviations at the indicated look-ahead points to improve the performance of the vehicle at different road curvatures. In [362], the look-ahead distance is formulated as a linear function of speed by choosing a suitable look-ahead time as a slope, with lower and upper bounds. The same methodology is also introduced in [363] and [364]. [365] and [366] propose a simplified adaptive method that tunes the look-ahead distance from the commanded speed instead of the measured one to improve a path prediction process. The tuning method parameters are obtained from a number of different experiences. Other works employ the fuzzy logic approach to tune the look-ahead

distance [367], [368]. They consider the road curvature and the current vehicle lateral error for the selection of the look-ahead distance.

As an overall, the look-ahead distance may be determined based on at least one of the following: vehicle speed, rotating speed, steering acceleration, steering angle, heading angle, lane curvature, current lateral error, predicted lateral error, distance to lane boundary, vehicle rotating performance, obstacle location. Tuning the look-ahead distance based only on the vehicle speed is not sufficient, since it could face some critical situations as large lateral errors for example. Recently, [369] proposes a method to find, in real-time, an optimal look-ahead distance according to the vehicle speed and steering acceleration, and taking into consideration the vehicle heading error. This improves the vehicle performance when subjected to high noises at high-ways, and to large lateral errors that may occur at the autonomous mode initialization or sudden lane-changes.

3.4 Discussion

The current thesis focuses on the Control system, mainly the look-ahead based lateral control of autonomous vehicles. A general control architecture is formulated based on LPV and YK parameterization aiming to switch/interpolate between multiple controllers. Its objective is to maintain different lateral motion capabilities, at low and high speeds. The thesis contributions are validated using simulations and real-time implementations:

- **Simulation environment:** The simulations are employed by a Renault simulator considering the electric Renault ZOE vehicle, developed in MATLAB / Simulink, and including nonlinear vehicle and tire models. They are performed in discrete-time domain with a sampling time $Ts = 10ms$.
- **Real-time experiment:** The vehicle in FIGURE 3.2 is used for the performed experiments. This automated vehicle is adapted for lateral and longitudinal controls by computer-controlled steering and pedal actuators. Vehicle speed and the global coordinates are measurable using GPS and IMU. The vehicle is employed using a dSPACE MicroAutoBox. The tests are done in the private closed track *Satory* shown in FIGURE 3.6.

Chapter 4

Application of LPV Approaches to Vehicle Lateral Control

4.1 Introduction

This chapter presents, the real implementation of the polytopic, grid-based and LFT LPV approaches to solve the lateral control problem on an electric Renault ZOE vehicle. A comparative analysis is shown among the three LPV approaches to the autonomous vehicle lateral control. The design of the three approaches from a theoretical point of view as well as their application on a real vehicle are presented, including a comparative analysis.

Specifically, comparison is carried out attending to the following criteria:

1. Designing procedure which is discussed in a theoretical point of view.
2. Controller performance when dealing with different situations (noise, disturbance, large lateral errors, low and high speeds, etc...). This is achieved by analysing the lateral errors (to ensure safety) and the control input efforts (to ensure comfortability and actuator limitation) from the simulation and real implementation results.
3. Implementation complexities when applying them on real applications and their effects on the computational costs.

The main contribution of this chapter is to develop, experimentally validate and compare three distinct LPV controllers which can deal, comfortably, with both lane change and lane tracking problems of a daily passenger vehicle. This can be summarized as follows:

- Quasi-LPV models are structured for the three approaches from the nonlinear bicycle model that vary with respect to the longitudinal velocity.
- To limit the control input effort and to achieve the noise/disturbance rejection performance, LPV/$\mathcal{H}_\infty$ problems are solved using a set of LMIs.
- The design and experimental validation of grid-based and Linear Fractional Transformation (LFT) approaches is carried out for the first time on the lateral control of autonomous vehicles.
- Input reference is adjusted as a function of the speed and lateral error, modifying the look-ahead parameter accordingly to deal with large lateral errors (lane changing) and the small ones (lane tracking).

- Simulation and experimental results (on a Renault ZOE vehicle) are shown to compare the performance of the controllers concerning tracking, actuator limitations and noise/disturbance rejection.

The simulation and experimental results shown in this chapter have been presented in:

- *LPV-Based Autonomous Vehicle Lateral Controllers: A Comparative Analysis, published in IEEE Transactions on Intelligent Transportation Systems (T-ITS)*, refer to [23].

This chapter is organized as follows: In Section 4.2, a brief theoretical explanation on how LPV structures are formulated for the different approaches. The used control scheme of a full speed-range controller is represented in Section 4.3. Also, the optimization problems of the LPV/$\mathcal{H}_\infty$ control synthesis are discussed. Section 4.4 presents the implementation control scheme achieving multiple tasks (lane change and path tracking). Then, simulation results obtained by the designed controllers and the limitations of each approach are analysed. In section 4.5, experimental validation is demonstrated to ensure the reliability of the comparison done. Section 4.6 summarizes the comparison in general concerning all the chosen criteria, and some comments are introduced. Finally, section 4.7 collects some conclusions and remarks.

4.2 Model Formulation

The lateral vehicle dynamics is modelled using the well-known bicycle model [138], [139]. Next subsections describe the plant model and the design of each LPV model.

4.2.1 Lateral Bicycle Model

In [138] and [139], the nonlinear lateral bicycle model is derived as:

$$\begin{cases} \dot{v}_y = \frac{F_{yf}\cos\delta + F_{yr}}{m} - w v_x \\ \dot{w} = \frac{F_{yf} l_f \cos\delta - F_{yr} l_r}{I}, \end{cases} \tag{4.1}$$

where v_x, v_y and w are the longitudinal, lateral and rotational velocities in the vehicle's frame, respectively. δ is the control input, the steering front angle of the front tire. I, m, l_f and l_r are the vehicle's inertia, mass and the distance from the center of gravity to the front and rear wheel axes respectively. F_{yf} and F_{yr} are the lateral forces applied to the front and rear tires, respectively.

Considering small side-slip angles and constraint lateral acceleration ($\leq 5m/s^2$). Then, the lateral forces can be approximated as follows:

$$\begin{aligned} F_{yf} &= C_f(\delta - \tfrac{v_y}{v_x} + \tfrac{l_f w}{v_x}), \\ F_{yr} &= C_r(-\tfrac{v_y}{v_x} + \tfrac{l_r w}{v_x}), \end{aligned} \tag{4.2}$$

where C_f and C_r are the stiffness of the front and rear wheel-tires respectively. Notice that the linear bicycle model with constraint lateral acceleration has been stated as a good approximation of the nonlinear model [370]. Then this model could be sufficient for daily passenger vehicles.

4.2.2 LPV Model Structures

After choosing $\rho(t) = v_x \in \mathbb{R}^{n_\rho}$ as a varying parameter, and assuming small steering front angles ($\sin(\delta) \approx \delta$), and small slip angles, the LPV state-space representation is written as:

$$G(\rho) \begin{cases} \dot{x}(t) = A(\rho)x(t) + Bu(t) \\ y(t) = Cx(t) + Du(t) \end{cases} \tag{4.3}$$

where:

$$x(t) = \begin{bmatrix} v_y \\ w \end{bmatrix} \in \mathbb{R}^{n_x},\ u(t) = \delta,\ ,y(t) = w,\ B = \begin{bmatrix} \frac{1}{m}C_f \\ \frac{1}{I}C_f l_f \end{bmatrix},$$

$$A(\rho) = \begin{bmatrix} -\frac{C_r+C_f}{mv_x} & -\frac{l_f C_f - l_r C_r}{mv_x} - v_x \\ -\frac{l_f C_f - l_r C_r}{Iv_x} & -\frac{l_f^2 C_f + l_r^2 C_r}{Iv_x} \end{bmatrix}. \tag{4.4}$$

The parameter-dependency of the LPV model differs from one approach to another. Specifically, the control synthesis of the polytopic approach requires an affine parameter-dependency. However, the gridding approach does not require such assumption. Finally, the LFT model is defined to be a lower or upper Linear Fractional Representation (LFR) between a known LTI model and a varying-parameter block. The following discussion shows how each approach is formulated.

Polytopic Model

The polytopic model is defined in a convex hull bounded by the parameters extremums (see Fig. 4.1). It is formulated as a convex combination between the vertices of the polytope. Two conditions must be satisfied: 1) the input and output matrices should be independent of the varying parameters, this is usually solved by pre-filtering the input or output; and 2) the model must be affine with respect to the varying parameters. So, (4.4) is written as:

$$A_{pol}(\rho) = \begin{bmatrix} -\frac{C_r+C_f}{m}\rho_2 & -\frac{C_f l_f - C_r l_r}{m}\rho_2 - \rho_1 \\ -\frac{C_f l_f - l_r C_r}{I}\rho_2 & -\frac{C_f l_f^2 + l_r^2 C_r}{I}\rho_2 \end{bmatrix}, \tag{4.5}$$

where ρ_1 and ρ_2 are v_x and $\frac{1}{v_x}$ respectively. Figure 4.1 shows the polytope formed by the extremums of the two parameters. Notice that the parameter vector is represented as a convex combination between the 4 vertices, where $\rho = \sum_{i=1}^{2^{n_p}} \mu_i \omega_i$ and $\sum_{i=1}^{2^{n_p}} \mu_i = 1,\ \mu_i \geq 0\ \forall i$ being

$$\begin{aligned} \omega_1 &= (\underline{\rho_1}, \underline{\rho_2}), & \mu_1 &= \frac{|\overline{\rho_1} - \rho_1|}{|\overline{\rho_1} - \underline{\rho_1}|} \times \frac{|\overline{\rho_2} - \rho_2|}{|\overline{\rho_2} - \underline{\rho_2}|} \\ \omega_2 &= (\underline{\rho_1}, \overline{\rho_2}), & \mu_2 &= \frac{|\overline{\rho_1} - \rho_1|}{|\overline{\rho_1} - \underline{\rho_1}|} \times \frac{|\rho_2 - \underline{\rho_2}|}{|\overline{\rho_2} - \underline{\rho_2}|} \\ \omega_3 &= (\overline{\rho_1}, \underline{\rho_2}), & \mu_3 &= \frac{|\rho_1 - \underline{\rho_1}|}{|\overline{\rho_1} - \underline{\rho_1}|} \times \frac{|\overline{\rho_2} - \rho_2|}{|\overline{\rho_2} - \underline{\rho_2}|} \\ \omega_4 &= (\overline{\rho_1}, \overline{\rho_2}), & \mu_4 &= \frac{|\rho_1 - \underline{\rho_1}|}{|\overline{\rho_1} - \underline{\rho_1}|} \times \frac{|\rho_2 - \underline{\rho_2}|}{|\overline{\rho_2} - \underline{\rho_2}|} \end{aligned} \tag{4.6}$$

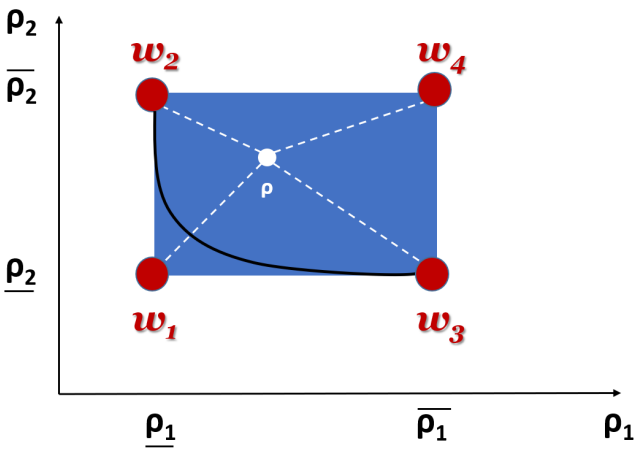

FIGURE 4.1: The polytope

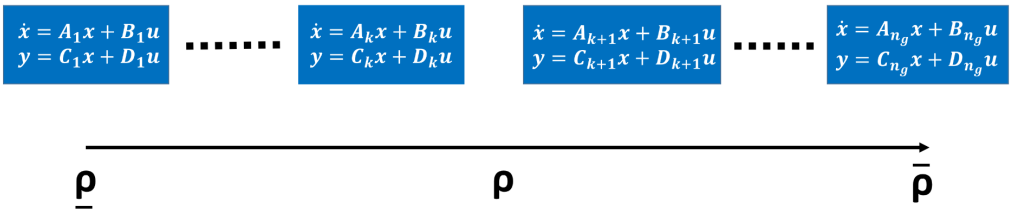

FIGURE 4.2: The gridded matrices

The LPV model is then written as a convex combination of the LTI systems obtained at the vertices of the polytope:

$$\left[\begin{array}{c|c} A_{pol}(\rho) & B_{pol} \\ \hline C_{pol} & D_{pol} \end{array}\right] = \sum_{i=1}^{2^{n_p}} \mu_i(\rho) \left[\begin{array}{c|c} A(\omega_i) & B \\ \hline C & D \end{array}\right] \tag{4.7}$$

where $n_p = 2$ is the number of the varying parameters.

Grid-based Model

The grid-based LPV model is a model interpolated over a set of LTI models that are linearized at different operating points. This approach can be considered when the parameter dependency of the model is nonlinear (without model reformulation) [14], [16]. So, the only needed parameter here is $\rho = v_x$. The varying parameter is gridded to a chosen number of n_g grid points as shown in Fig. 4.2.

The gridding approach uses any kind of interpolation (linear or nonlinear) between the gridded models to compute the LPV model. Suppose that, at an instant, the longitudinal velocity $\rho \in [\rho_k, \rho_{k+1}]\ m/s$, the linear interpolation of the state-space matrices:

$$\left[\begin{array}{c|c} A_{grid}(\rho) & B_{grid}(\rho) \\ \hline C_{grid}(\rho) & D_{grid}(\rho) \end{array}\right] = \sum_{i=k}^{k+1} \alpha_i(\rho) \left[\begin{array}{c|c} A_i & B_i \\ \hline C_i & D_i \end{array}\right], \tag{4.8}$$

where,

$$\alpha_k = \frac{\rho_{k+1}-\rho}{\rho_{k+1}-\rho_k} \quad and \quad \alpha_{k+1} = \frac{\rho-\rho_k}{\rho_{k+1}-\rho_k} \tag{4.9}$$

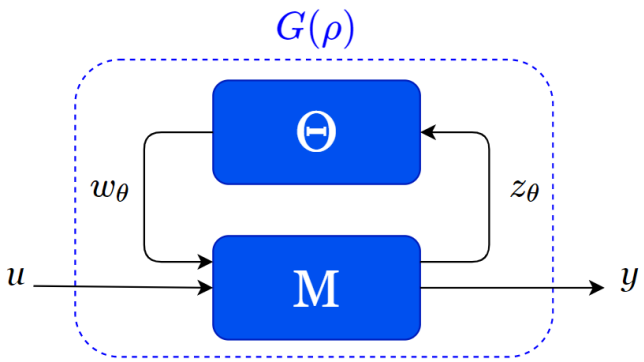

FIGURE 4.3: Linear fractional representation of a parameter-varying system

LFT model

The LFT approach defines the model as the upper LFR between a known LTI model and a parameter block as shown in Fig. 4.3 [6]. At each instant, the parameters in the block Θ are updated being the input of the LTI model M. In general, the upper LFT interconnection of the shown model is written as:

$$\begin{bmatrix} \dot{x} \\ z_\theta \\ y \end{bmatrix} = \begin{bmatrix} A & B_\theta & B \\ C_\theta & D_{\theta\theta} & D_{\theta 1} \\ C & D_{1\theta} & D \end{bmatrix} \begin{bmatrix} x \\ w_\theta \\ u \end{bmatrix} \tag{4.10}$$

$$w_\theta = \Theta z_\theta$$

where Θ is the time-varying operator block introduced as:

$$\Theta = blockdiag(\theta_1 I_{r_1}, ..., \theta_k I_{r_k}) \tag{4.11}$$

being $r_i > 1$ which presents the number of occurrences of the varying-parameter θ_i. Notice that θ_i can be normalized to be always $\in [-1, 1]$, which makes M represents the nominal model when $\theta_i = 0 \; \forall i$.

Let us consider the system model (4.3), considering the parameter v_x varying as:

$$v_x = v_{x_0} + a\theta \tag{4.12}$$

where $v_{x_0} = \frac{v_{x_{min}} + v_{x_{max}}}{2}$ represents the nominal value of v_x, and $a = \frac{v_{x_{max}} - v_{x_{min}}}{2}$ represents the rate of variation when θ varies in [-1,1]. Then, (4.3) can be rewritten under the LFT form (4.10) where:

$$A = \begin{bmatrix} -\frac{C_r+C_f}{mv_{x_0}} & -\frac{l_fC_f-l_rC_r}{mv_{x_0}} - v_{x_0} \\ -\frac{l_fC_f-l_rC_r}{Iv_{x_0}} & -\frac{l_f^2C_f+l_r^2C_r}{Iv_{x_0}} \end{bmatrix}$$

$$B_\theta = \begin{bmatrix} -\frac{a}{v_{x_0}} & 0 & -\frac{a^2}{v_{x_0}} & 0 \\ 0 & 0 & 0 & -\frac{a}{v_{x_0}} \end{bmatrix}$$

$$C_\theta = \begin{bmatrix} -\frac{C_r+C_f}{mv_{x_0}} & -\frac{l_fC_f-l_rC_r}{mv_{x_0}} + v_{x_0} \\ 0 & 1 \\ 0 & 0 \\ -\frac{l_fC_f-l_rC_r}{Iv_{x_0}} & -\frac{l_f^2C_f+l_r^2C_r}{Iv_{x_0}} \end{bmatrix} \tag{4.13}$$

$$D_{\theta\theta} = \begin{bmatrix} -\frac{a}{v_{x_0}} & 0 & -\frac{a^2}{v_{x_0}} & 0 \\ 0 & 0 & 0 & 0 \\ 0 & 1 & 0 & 0 \\ 0 & 0 & 0 & -\frac{a}{v_{x_0}} \end{bmatrix}$$

$$D_{\theta 1} = 0_{4\times 1}, D_{1\theta} = 0_{1\times 4}, \Theta = \theta \times I_4$$

And finally, the state-space matrices of $G(\rho)$ are scheduled as:

$$\begin{aligned} A_{LFT}(\rho) &= A + B_\theta \Delta_\theta C_\theta \\ B_{LFT}(\rho) &= B + B_\theta \Delta_\theta D_{\theta 1} \\ C_{LFT}(\rho) &= C + D_{1\theta} \Delta_\theta C_\theta \\ D_{LFT}(\rho) &= D + D_{1\theta} \Delta_\theta D_{\theta 1} \\ \Delta_\theta &= \Theta(I - D_{\theta\theta}\Theta)^{-1} \end{aligned} \tag{4.14}$$

It is worth noting that, in the LFT approach, the LPV model is converted as in Fig. 4.3 in a single LTI model feeded by a parameter dependent input. It differs from the polytopic and grid-based approach where a set of LTI models is handled.

4.3 LPV/$\mathcal{H}_\infty$ Control Design

Fig 4.4 presents the control design scheme where an LTI actuator model G_{act} (first order transfer function + input delay) is added to the bicycle model dynamics (δ_c is the controller output). Note that the input delay is described as a first order transfer function, so as a result, G_{act} is a second order transfer function. Considering this structure, the controller $K(\rho)$ (in Fig. 4.4) is designed for the three approaches using LPV/$\mathcal{H}_\infty$ concept. Notice that w_{ref} represents the yaw rate reference.

Control performance criteria in $\mathcal{H}_\infty$ control theory are given by frequency domain functions (check Appendix B). Two weighting functions W_e and W_u are used to achieve tracking and actuator limitations performances respectively. The objective is to achieve both performances with a trade-off between minimizing the lateral error and ensuring the driving comfort. Notice that the steering speed $\dot{\delta}$ could be related to the driving comfort since it reflects how fast the front wheels are acting (e.g. at high values of $\dot{\delta}$), and how noisy they appear (when $\dot{\delta}$ oscillates around zero at high frequencies). We know that when $\dot{\delta}$ increases, the lateral acceleration increases, and

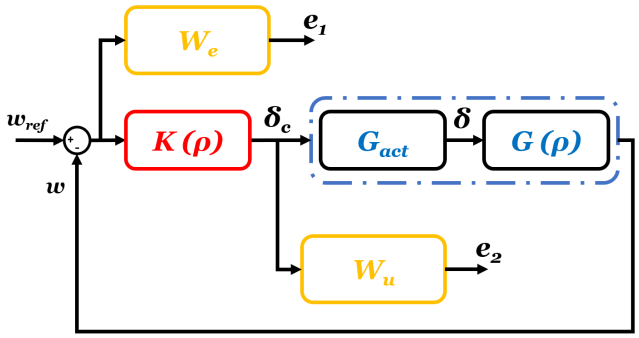

FIGURE 4.4: Control design scheme

consequently more aggressive actions are achieved. Moreover, a highly frequent oscillation of the steering speed around zero leads to noises in the front wheels, which encounters uncomfortable driving. As a result, W_u is designed in a way to achieve low steering speeds with noise rejection.

4.3.1 Tracking specification (W_e)

The weighting transfer function is chosen as:

$$W_e(s) = \frac{\frac{s}{M_s} + w_b}{s + w_b \epsilon} \tag{4.15}$$

where the parameters M_s, w_b and ϵ are tuned as follows:

- $M_s = 2$, to ensure robustness at any frequency.
- $w_b \geq 10$, to choose the speed of rising time-response.
- $\epsilon \leq 10^{-4}$, to represent the steady-state tracking error.

4.3.2 Specification on the control input limitations (W_u)

A filter is used to minimize the effort of the steering actuator control δ_c. This filter is designed as:

$$W_u(s) = \frac{s + \frac{w_{b_u}}{M_u}}{\epsilon_u s + w_{b_u}} \tag{4.16}$$

The parameters M_u, w_{b_u} and ϵ_u are adopted as:

- M_u represents the limitations on the maximum allowed effort of the actuators.
- w_{b_u}, is related to the actuator bandwidth.
- $\epsilon_u \leq 10^{-2}$, is concerned with the noise rejection from the control inputs at high frequencies.

4.3.3 Generalized Plant

Using the plant model and the weighting functions, Fig. 4.4 is converted to build a general control configuration as in Fig. 4.5a. The generalized plant $P(\rho)$ is structured to consider the chosen weights in addition to the LPV model ($G(\rho) \times G_{act}$). Thus the state vector of $P(\rho)$ is $x_P = \begin{bmatrix} x & x_{act} & x_{W_e} & x_{W_u} \end{bmatrix}^T$, and the controlled output

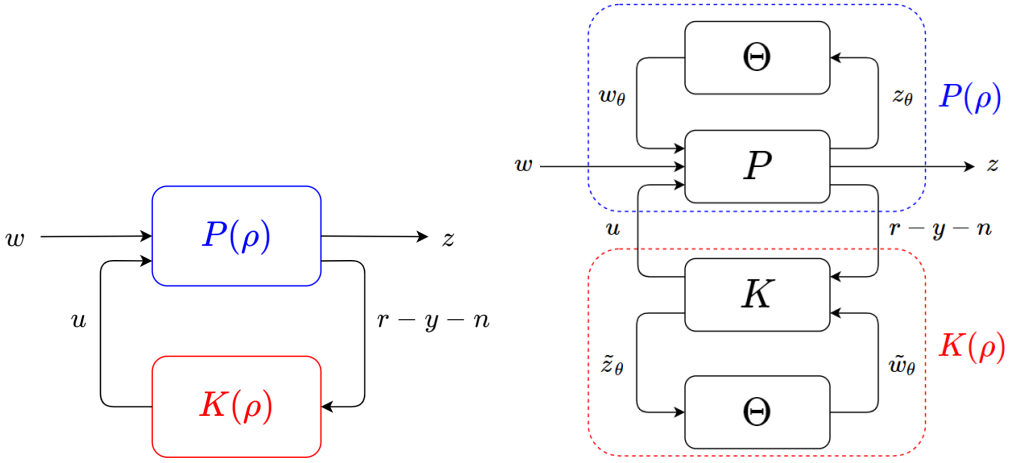

(A) General control configuration (B) LFT general control configuration

$z = \begin{bmatrix} e_1 & e_2 \end{bmatrix}^T$ represents the objective function to be optimized when designing the controller. $w = \begin{bmatrix} r & d & n \end{bmatrix}^T$ is the exogenous input, where r, d and n are the desired reference, input disturbance and the measurable noises respectively.

For the polytopic and the gridding approaches, the state-space representation of $P(\rho)$ (see Fig. 4.5a) has the form:

$$\begin{bmatrix} \dot{x}_P \\ e_1 \\ e_2 \\ r-y-n \end{bmatrix} = \left[\begin{array}{c|cccc} A_P(\rho) & B_1 & B_2 & B_3 & B_4 \\ \hline 0 & W_e & 0 & -W_e & -W_e G(\rho) \\ 0 & 0 & 0 & 0 & W_u \\ 0 & 1 & 0 & -1 & -G(\rho) \end{array}\right] \begin{bmatrix} x_P \\ \begin{bmatrix} r \\ d \\ n \end{bmatrix} \\ u \end{bmatrix}. \tag{4.17}$$

In the polytopic approach, there exist four generalized plants, each one is related to a corresponding vertex of the polytope. However, a set of n_g P_i's are formulated along the gridded points for the gridding approach.

Fig. 4.5b shows the generalized plant $P(\rho)$ as an upper LFR between a parameter-invariant P and the parameter block Θ for designing an LPV/LFT controller. Using this approach, P is then structured as:

$$\begin{bmatrix} \dot{x}_P \\ z_\theta \\ e_1 \\ e_2 \\ r-y-n \end{bmatrix} = \left[\begin{array}{c|cccccc} A_P & B_\Theta & B_1 & B_2 & B_3 & B_4 \\ \hline C_\theta & D_{\theta\theta} & D_{\theta 1} & D_{\theta 2} & D_{\theta 3} & D_{\theta 4} \\ 0 & 0 & W_e & 0 & -W_e & -W_e G(\rho) \\ 0 & 0 & 0 & 0 & 0 & W_u \\ 0 & 0 & 1 & 0 & -1 & -G(\rho) \end{array}\right] \begin{bmatrix} x_P \\ w_\Theta \\ \begin{bmatrix} r \\ d \\ n \end{bmatrix} \\ u \end{bmatrix}. \tag{4.18}$$

4.3.4 LPV/$\mathcal{H}_\infty$ Control Synthesis

For the rest of the paper, the longitudinal speed is considered to be bounded as:

$$v_x \in [3, 30]\ m/s \tag{4.19}$$

The main objective of the $\mathcal{H}_\infty$ control is to minimize the $\mathcal{L}_2$ induced gain from the external input w to the controlled output $z = \begin{bmatrix} e_1 & e_2 \end{bmatrix}^T$. This is achieved by solving

the following $\mathcal{L}_2$ induced minimization problem:

$$\|z\|_2 \leq \gamma_\infty \|w\|_2$$

and $\gamma_\infty > 0$, to be minimized, represents how much the demanded performance is achieved. If $\gamma_\infty < 1$, the demanded performance is totally achieved by the controller. Among the three approaches, each controller is designed by solving its corresponding LMI-based optimisation problem. A complete overview of the synthesis and implementation complexity of LPV approaches can be found in [371]. For each approach, the complexity of LPV controller existence conditions is determined in terms of the size of LMIs and the number of decision variables. Note that the obtained controller $K(\rho)$ is an *LPV Dynamic Output Feedback Controller*.

Polytopic Approach

Fig. 4.1 shows that the polytopic approach is considering the parameters v_x and $\frac{1}{v_x}$ as two independent parameters. However, they depend on each other as a function of the black curve (i.e. $y = 1/x$). Since the polytope is a very large set compared to the real parameter variation rule (and mainly due to w_4), this may lead to conservatism when solving the optimisation problem on the 4 vertices. Thus, a solution to this problem is drawn in [372], where the number of vertices is reduced from 2^{n_p} to $n_p + 1$. So, the polytope in Fig. 4.1 can be reduced to $\mathcal{C}_\mathcal{O}\{w_1, w_2, w_3\}$, and then, the coefficients $\mu_i's$ will be:

$$\mu_1 = 1 - (\mu_2 + \mu_3), \quad \mu_2 = \frac{|\underline{\rho_2} - \rho_2|}{|\overline{\rho_2} - \underline{\rho_2}|}, \quad \mu_3 = \frac{|\underline{\rho_1} - \rho_1|}{|\overline{\rho_1} - \underline{\rho_1}|} \tag{4.20}$$

In the polytopic approach, the problem is solved in the framework of quadratic stability of the closed-loop system. This is obtained by solving a set of LMIs at the vertices of the polytope with a constant Lyapunov function [7]. The existence conditions of this approach show the number of LMIs to grow by $\mathcal{O}(2^{n_p})$. Also, the number of decision variables is computed to be $n_x(n_x + 1)$ [371]. As a result, a controller K_i is obtained at each vertex and $K(\rho)$ is computed as (in the case of non-reduced polytope and $\forall\rho$ inside the polytope of Fig. 4.1):

$$\left[\begin{array}{c|c} A_K(\rho) & B_K(\rho) \\ \hline C_K(\rho) & D_K(\rho) \end{array}\right] = \sum_{i=1}^{2^{n_p}} \mu_i(\rho) \left[\begin{array}{c|c} A_{K_i} & B_{K_i} \\ \hline C_{K_i} & D_{K_i} \end{array}\right] \tag{4.21}$$

Grid-based Approach

Grid-based approach formulates the problem in the context of robust stability [373] by using a parameter-dependent Lyapunov function along the gridded axis [16]. Notice that a basis function is chosen to write the Lyapunov function in terms of the varying parameters. An example on the lateral vehicle control problem, the Lyapunov function $X(\rho)$ is chosen to be linearly dependent (order 1) on the varying parameter $\rho = v_x$:

$$X(\rho) = X_0 + \rho X_1, \tag{4.22}$$

where X_0 and X_1 are unknown constant matrices to be computed from the LMIs. From this point of view, one can see an advantage in the optimisation problem of this approach where it reduces the conservatism of the polytopic approach. Notice that the LMIs include the absolute maximum rate-change of the parameter. Studying the existence conditions of this control approach, the number of LMIs grows

with $\mathcal{O}(n_g^{n_\rho})$. To determine the number of decision variables, let us assume that the parameter-dependent Lyapunov matrix is parameterized as:

$$X(\rho) = X_0 + \sum_{i=q}^{s} a_i(\rho) X_i, \tag{4.23}$$

then the number of decision variables is $\frac{1}{2} n_x (n_x + 1)(n_\rho^X + +1)$, where $n_\rho^X = s - q + 1$. For more details, the LMIs are derived in *Theorem 4.3.1* in [16]. As a result, a set of controllers is obtained where each one corresponds to a frozen value in the gridded axis of the parameter. When $\rho \in [\rho_k, \rho_{k+1}]$, the controller $K(\rho)$ can be linearly interpolated as [14]:

$$\left[\begin{array}{c|c} A_K(\rho) & B_K(\rho) \\ \hline C_K(\rho) & D_K(\rho) \end{array}\right] = \sum_{i=k}^{k+1} \alpha_i(\rho) \left[\begin{array}{c|c} A_{K_i} & B_{K_i} \\ \hline C_{K_i} & D_{K_i} \end{array}\right], \tag{4.24}$$

where,

$$\alpha_k = \frac{\rho_{k+1} - \rho}{\rho_{k+1} - \rho_k} \quad and \quad \alpha_{k+1} = \frac{\rho - \rho_k}{\rho_{k+1} - \rho_k} \tag{4.25}$$

LFT Approach

The LPV/LFT controller synthesis mainly relies on the $\mathcal{S}$-procedure [41]. The solution of the LMI-based optimization problem is detailed in [6], where continuous and discrete-time LMI problems are discussed. The LMI size is typically smaller than that in the polytopic approach since there is no anymore a set of LMIs to be solved for a set of parameter values (see Fig. 2 in [14] for more details). However, a trade-off is found where the number of decision variables of LFT is much bigger than the polytopic approach when n_ρ increases ($n_x(n_x + 1) + 2n_\Theta(2n_\Theta + 1)$ where $\Theta \in \mathbb{R}^{n_\Theta \times n_\Theta}$). Control synthesis is formulated in two steps: 1) A quadruple (R, S, L_3, J_3) is found - by solving 2 LMIs - to ensure the solvability of the control problem (check *Theorem 5.1* in [6]); and 2) The gain-scheduling controller is then computed using the quadruple and solving another LMI with one decision variable containing the controller matrices (*Algorithm 6.1* in [6]). Then, the designed controller is written in the form of a lower LFR $F_l(K, \Theta)$, and obtained as follows:

$$K(\rho) = F_l(K, \Theta) = K_{11} + K_{12}\Theta(I - K_{22}\Theta)^{-1}K_{21} \tag{4.26}$$

being $K(\rho)$ defined as:

$$\begin{bmatrix} u \\ \tilde{z}_\theta \end{bmatrix} = \left[\begin{array}{c|c} K_{11} & K_{12} \\ \hline K_{21} & K_{22} \end{array}\right] \begin{bmatrix} r - y - n \\ \tilde{w}_\theta \end{bmatrix} \tag{4.27}$$

where K_{11}, K_{12}, K_{21} and K_{22} are obtained from the LMI's. Thus, the state-space matrices of $K(\rho)$ are computed as:

$$\begin{array}{c} A_K(\rho) = A_K + B_{K_\theta}\Delta_\theta C_{K_\theta} \\ B_K(\rho) = B_K + B_{K_\theta}\Delta_\theta D_{K_{\theta 1}} \\ C_K(\rho) = C_K + D_{K_{1\theta}}\Delta_\theta C_{K_\theta} \\ D_K(\rho) = D_K + D_{K_{1\theta}}\Delta_\theta D_{K_{\theta 1}} \\ \Delta_\theta = \Theta(I - D_{K_{\theta\theta}}\Theta)^{-1} \end{array} \tag{4.28}$$

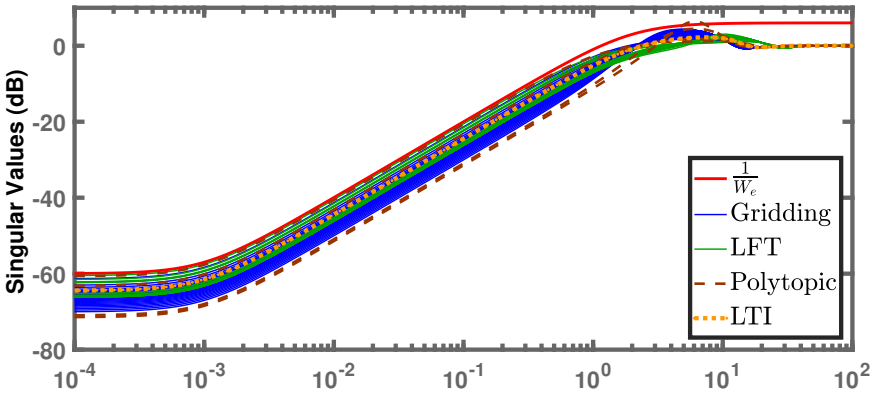

FIGURE 4.6: Sensitivity Functions $S = \frac{w_{ref} - w}{w_{ref}}$

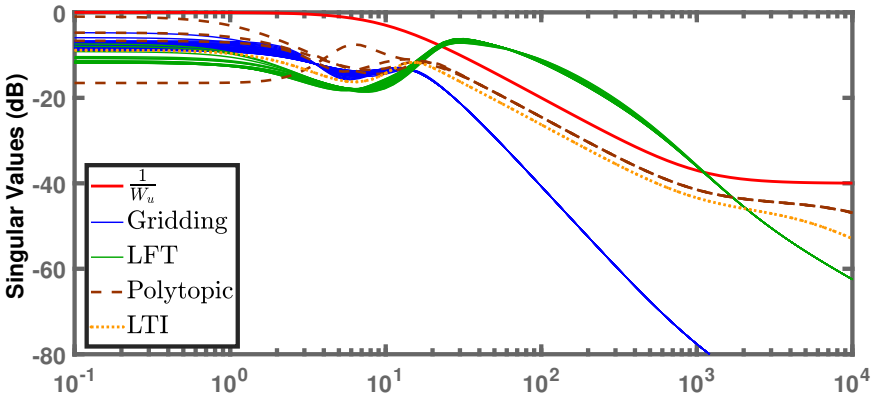

FIGURE 4.7: Sensitivity Functions $KS = \frac{\delta}{w_{ref}}$

4.3.5 Frequency Domain Analysis

This subsection analyses the designed controllers in frequency-domain in order to check if the requirements are satisfied by the controllers. This is achieved using several sensitivity functions compared to the weights designed previously. Additionally, an LTI controller designed at the fixed-nominal speed v_x=14 m/s is added to the analysis to show the benefits of using parameter-varying approaches.

To observe the tracking performance, the error sensitivity function S is drawn as shown in Fig. 4.6. Sensitivity functions of the tracking error to the reference are drawn with the required performance $\frac{1}{W_e}$. Notice that each of the LPV approaches has several sensitivity functions where each one is referred to a corresponding value of speed (in gridding and LFT approaches) or a corresponding vertex (in polytopic approach). At low frequencies, all the controllers achieve the demanded steady-state tracking error. Also, all the controllers are respecting the requirements at high frequencies related to robust margin ($\max_{\forall w} \left\| \frac{r-y}{r} \right\| < 6\ dB$).

On the other hand, the analysis of the control input is carried out to evaluate the sensitivity to the noise. To do so, the control sensitivity function KS of each controller is computed. Fig. 4.7 shows the sensitivity functions of the control input δ with respect to the reference, and the requirements on the actuator limitations $\frac{1}{W_u}$. It is shown that all the controllers are respecting the demanded limitations with a small exceeding in the bandwidth of the LFT approach. One can appreciate how the gridding approach shows the best noise rejection at high frequencies compared to the others.

4.4 Simulation Results

The simulations are employed by a Renault simulator considering the electric Renault ZOE vehicle, developed in MATLAB/Simulink, and considering nonlinear vehicle and tire models. The simulations are performed in discrete-time domain with a sampling time $T_s = 10\ ms$. The proposed control strategies are implemented in simulation following the scheme in Fig. 4.8. The look-ahead system block is added to perform smoothly both lane-keeping and lane-changing (i.e. small and large lateral errors respectively). It modifies the yaw rate reference when having large lateral errors (initial error in autonomous starting mode, sudden lane-changes, etc.). Since the desired curvature is inversely proportional to the look-ahead distance [357], a smooth or aggressive steering can be obtained by changing the look-ahead distance. Specifically, as much as the lateral error y_e increases, the look-ahead distance d is increased linearly as a function of the lateral error as follows:

$$d(v_x, ye) = sat(\frac{d_{nom}(v_x)}{2} \times (1 + abs(y_e)), [d_{nom}(v_x), d_{max}]) \tag{4.29}$$

where $d_{nom}(v_x)$ is the nominal look-ahead distance tuned at each speed v_x for small lateral errors ($y_e \leq 0.6m$), d_{max} is the maximum saturation of look-ahead distance chosen when $y_e \geq 3m$. d_{max} is chosen depending on the facing situation where it should ensure that the vehicle is not losing forward information (we choose it here as $d_{max} = 40m$).

As discussed in subsection 4.3.4, the LPV approaches have different ways of implementation and interpolation. Each one differs with respect to its complexity and time consuming, which makes it worthy to see how they can be simplified and what will be the effects of such simplifications. Due to the limited number of real tests

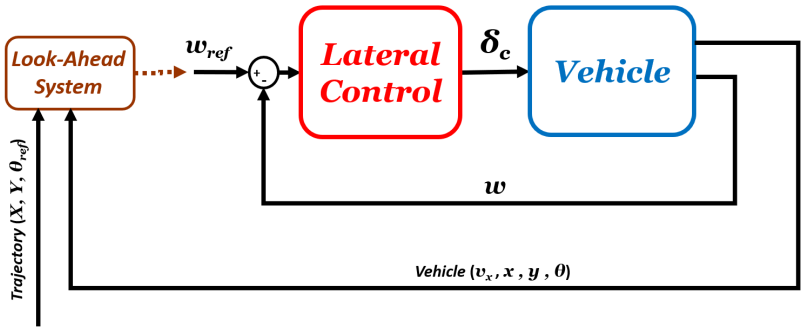

FIGURE 4.8: Control implementation scheme

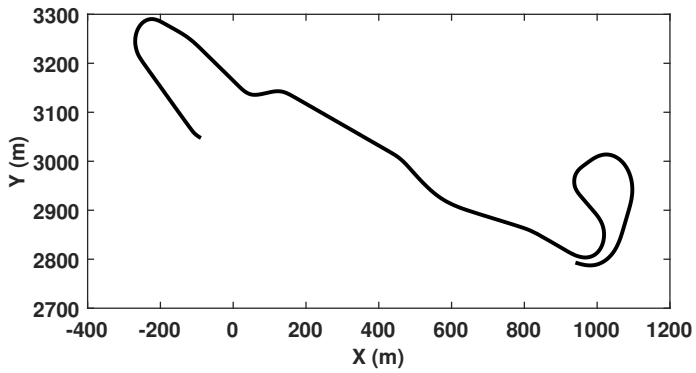

FIGURE 4.9: Reference Trajectory

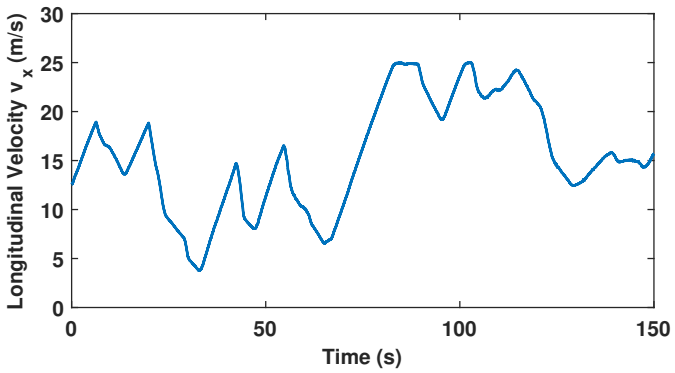

FIGURE 4.10: Speed profile measured from a real test (m/s)

which can be done, this section discusses different ways of implementations for each approach separately and their impact on the system performance. The trajectory in Fig. 4.9 is used to test the lateral control performance. Vehicle speed input is recovered from a real test (see Fig. 4.10). Some critical situations were chosen to show the functionality of the look-ahead system and to compare the response of the different designed controllers, where:

- a large lateral error is presented at the initialization time,
- the reference positioning system (X,Y) is recovered from a real test with noises.
- the rate of the varying parameter v_x is increased to be large enough at some times ($t \in [70, 80]s$),
- a high speed $v_x = 25\ m/s$ is reached at time $t = 80s$,
- two successive aggressive maneuvers (with high lateral acceleration greater than 5 m/s^2) at high speed (around 23 m/s) are carried out between $t = 105s$ and $t = 115s$.

4.4.1 LPV Approaches Limitations

This subsection describes the main limitations of each approach from the implementation point of view.

Polytopic Approach

As mentioned in paragraph 4.3.4, the polytope is reduced to decrease its problem conservatism. Thus, to analyse the benefit of this reduction, two polytopic LPV controllers (one with four vertices and the other with three vertices) are designed. Both of them are simulated separately and the results of the obtained lateral errors and steering input angles are represented in Fig. 4.11 and 4.12.

Table 4.1, Fig. 4.11 and 4.12 show that both controllers achieve approximately the same lateral error and steering performance. This result is due to the fact that the bicycle model is not highly nonlinear in terms of the speed v_x. Moreover, Fig. 4.11 and 4.12 show that the initial lateral error is minimized smoothly, thanks to the look-ahead system which adapts the look-ahead distance as the lateral error increases (see Fig. 4.13). Notice that the look-ahead distance is no more adapted for $t > 6s$, i.e. $d = d_{nom}(v_x)\ \forall t > 6s$ except when lateral error exceeds $0.6m$.

Finally, Table 4.1 shows the lateral error RMS for both polytopic controllers. One can appreciate the benefits of reducing the polytope, especially when having varying-parameters that depend on each other.

TABLE 4.1: RMS of the lateral error using the polytopic approaches

	4-Vertices Polytope	Reduced Polytope
RMS	0.98	1.01

Gridding Approach

The gridding approach reduces the problem of conservatism by using a parameter-varying Lyapunov function. Gridded controllers are often interpolated either linearly or nonlinearly to obtain the current-state controller. The benefit of this interpolation is that even if the parameter goes out of its extremum bounds that was

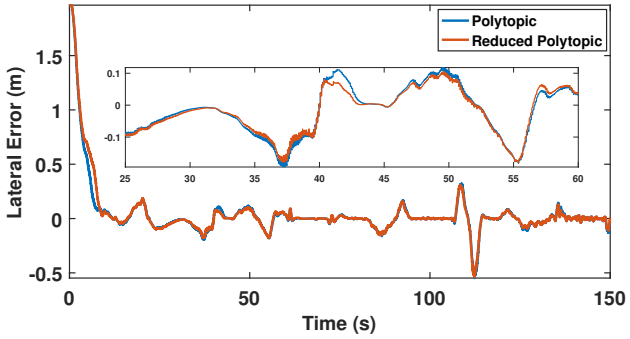

FIGURE 4.11: Lateral error using the polytopic approaches (m)

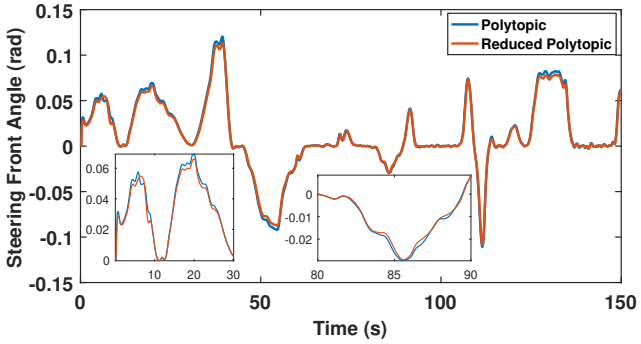

FIGURE 4.12: Steering front angle δ using the polytopic approaches (rad)

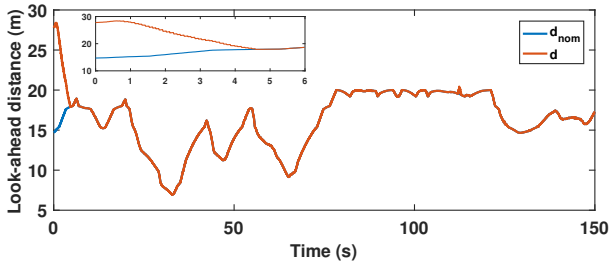

FIGURE 4.13: Look-ahead distance d (m)

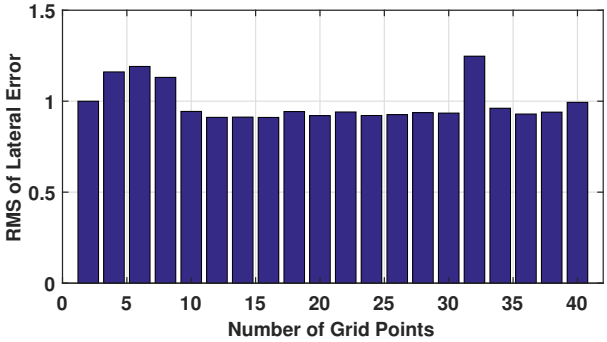

FIGURE 4.14: Normalized RMS of the lateral error with respect to different number of gridding points n_g

considered in the control design (i.e. $v_x < 3\ m/s$), the controller still can be interpolated with negative coefficients. Designing a gridded-based LPV controller, the gridded axis of the varying parameter should be drawn. This axis can be gridded starting from two grid-points until infinity. Thus, it is worthy to study the effect of increasing the number of gridding points on the performance of the system.

A set of tests is done at each chosen number of gridding points and the RMSs of the lateral errors are computed. The chosen number of gridding points are the even numbers from 2 to 40 grid-points (2,4,...,38,40). Fig. 4.14 shows the normalised RMS of the lateral errors from each test. Notice that all of them are normalized with respect to the test of $n_g = 2$ to make it easier for comparison, being the first test RMS equals to 0.263. It is clearly shown that increasing the number of gridding points may not always improve the performance.

Thus, it can be concluded that, in the used model, the performance of the gridded controller is not significantly affected by the number of gridding points.

LFT Approach

The implementation of the LFT controller (4.28) is simpler where it consists of a state-space control system which varies with an input parameter Δ_θ, unlike the previous approaches that have a set of controllers to be interpolated between each other. However, an online inverse must be done at each sample time. This may lead to a limitation during simulation or specifically in real implementations. Thus, a method has been used in [374] to avoid online calculations. A look-up table of the inverted matrix is computed at each chosen grid-point along the parameter range, and then, an interpolation is done during simulation.

The controller with online inverse, the one with interpolation and the nominal controller (at $v_x = 17.5m/s$) are tested (see Fig. 4.15 and 4.16 for details). Table 4.2 presents the RMS lateral error, where there is no significant difference between the tracking performances of the tested controllers. Fig. 4.15 shows that the performance of the interpolated controller (yellow line) differs a bit from the one with online inverse (red line) when the parameter variation rate increases (i.e. $t \in [40, 60]s$). On the other hand, it can be clearly observed that when the speed approaches the nominal speed ($v_x = 17.5m/s$), the nominal LFT controller (blue line) acts more closely to the one with online inverse (red line) ($t \in [135, 140]s$). Notice that at high speeds ($t \in [90, 100]$), the nominal LFT controller is showing a small difference in the lateral error, whereas the other two controllers are having exactly the same performance regarding also the steering action (see Fig. 4.16). As a result, the interpolated LFT controller showed a similar performance as the actual one which may help in reducing the computational cost in real implementations.

TABLE 4.2: RMS of the lateral error using the LFT approaches

	Nominal LFT	LFT with online inverse	Interpolated LFT
RMS	0.1849	0.1683	0.17

4.4.2 LPV Approaches Robustness Test

The most promising result of each LPV approach is retained and tested again with the LTI one (at $v_x = 17.5m/s$) by modifying some vehicle parameters (vehicle mass and tire stiffness). The mass of the vehicle changes by the number of passengers. Moreover, the tire stiffness is hard to be estimated (see [375] for instance), and it

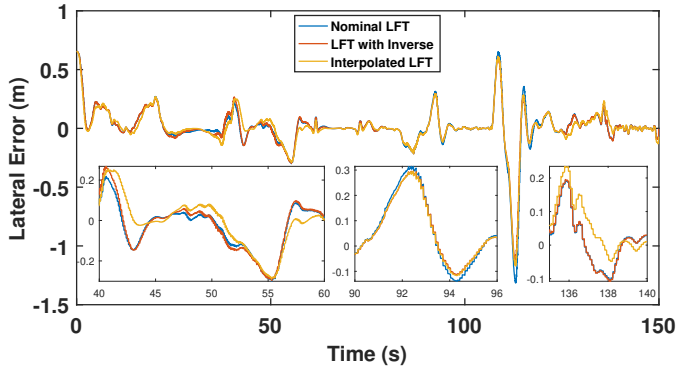

FIGURE 4.15: Lateral error using the LFT approaches (m)

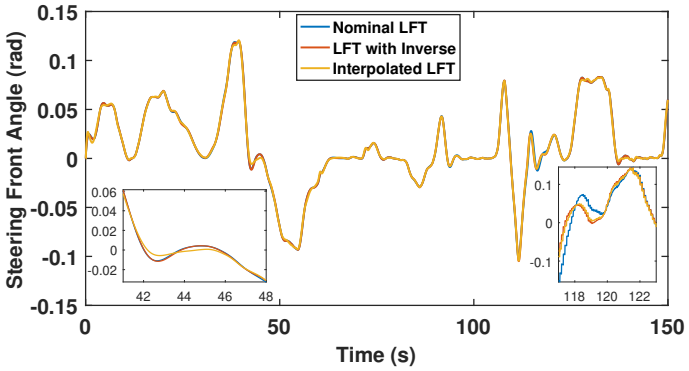

FIGURE 4.16: Steering front angle δ using the LFT approaches (rad)

varies by time when the tire loses its quality. Then, the following test is important to study the robustness of the designed controllers in terms of such uncertainties. In this test, the mass of the vehicle is chosen arbitrarily to be increased by $400Kg$ and each front and rear tire stiffness is adjusted by 30%.

The obtained results are shown in Fig. 4.17 and 4.18. Again, one can appreciate the success of the look-ahead system which helps in minimizing the initial lateral error smoothly, i.e. low steering actuation (see Fig. 4.18). Fig. 4.17 and Table 4.3 show that the tested controllers achieve comparable minimization of the lateral error, with the best tracking performance achieved by the gridded controller. The interpolated LFT seems to have the lowest robustness where it maintains the highest RMS lateral error with more steering overshoots as observed in Fig. 4.18. The steering rate RMS of the reduced polytopic controller shows the highest value in Table 4.3, and it has the highest overshoot when performing the initial lateral error (Fig. 4.18). Finally, all the compared controllers are considered to be robust to the injected uncertainties thanks to the used $\mathcal{H}_\infty$ concept.

TABLE 4.3: RMS of the lateral error for robustness comparison

	LTI	Reduced Polytopic	*Gridding* $(n_g = 16)$	Interpolated LFT
RMS	0.257	0.266	0.251	0.33

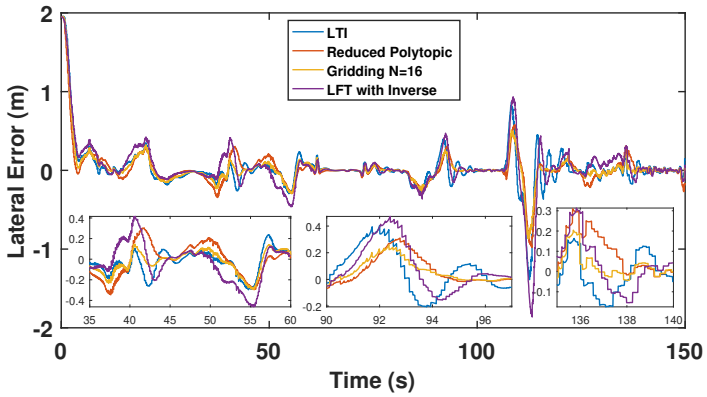

FIGURE 4.17: Lateral error for robustness comparison (m)

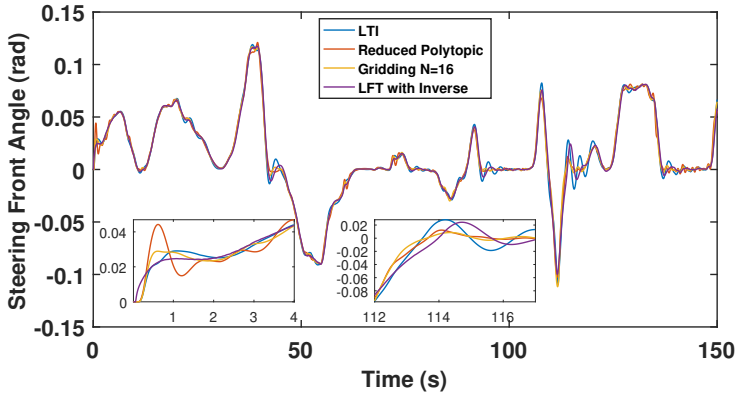

FIGURE 4.18: Steering front angle for robustness comparison (m)

4.5 Real Implementation

The last four controllers, compared in simulation, are then tested on a robotized electric Renault ZOE shown in Fig. 4.19. This automated vehicle is adapted for lateral and longitudinal controls by computer-controlled steering and pedal actuators. Vehicle speed and the global coordinates are measurable using GPS and IMU, see more details in Chapter 3. The vehicle is employed using a dSPACE MicroAutoBox in discrete time sampled by $T_s = 10ms$. As previously stated, actuator dynamics are modelled using an LTI model which influence uncertain dynamics between the real plant and the designed model. The test results of the designed controllers are discussed concerning their implementation, the acceptability of the resulted performance and the actuator limitations.

The tests are done in the closed track *Satory* shown in Fig. 4.20. This track contains bad road conditions and road-inclinations which allows to evaluate the controller robustness. The first part of the test describes the response of the controllers at high speeds. The second part concerns the precision of lateral control at optimal speeds chosen coherently depending on the road curvature. Fig. 4.21 shows the longitudinal speed evolution over time which is considered as an external parameter of the LPV mode. For the coming analysis, the limitations of the used steering actuator are as follows:

$$|\dot{\delta}|_{max} = 0.2, |\delta|_{max} = 0.4, \tag{4.30}$$

Fig. 4.22 and Table 4.5 show that all the controllers succeed to minimize the

FIGURE 4.19: Renault ZOE automated vehicle

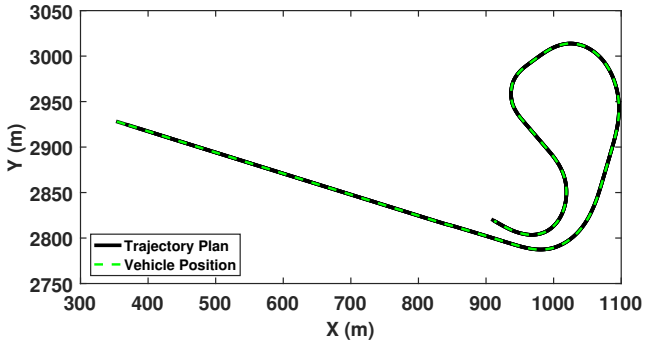

FIGURE 4.20: Satory trajectory plan and vehicle position

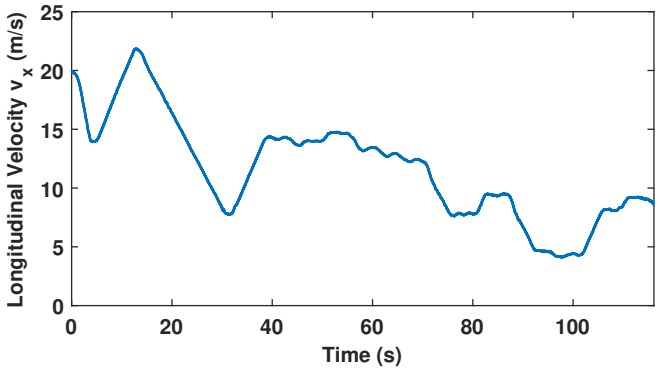

FIGURE 4.21: Experimental longitudinal speed (m/s)

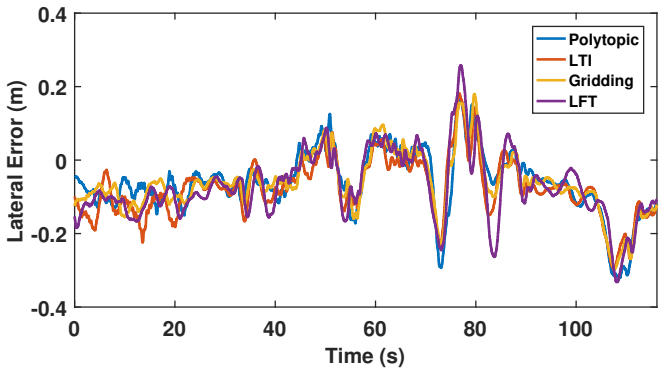

FIGURE 4.22: Experimental lateral error of the LTI and LPV controllers (m)

TABLE 4.4: RMS of the steering front rate for robustness comparison

	LTI	Reduced Polytopic	*Gridding* ($n_g = 16$)	Interpolated LFT
RMS	0.017	0.018	0.017	0.017

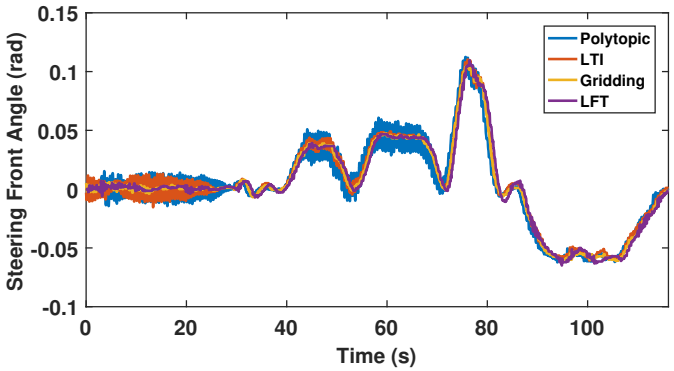

FIGURE 4.23: Experimental steering front angle of the LTI and LPV controllers (rad)

lateral error, however Fig. 4.23 and 4.24 show that the control input effort is quiet different. One can observe that both the polytopic and the LTI controllers are sensitive to noises, especially at high speeds (when $t \leq 60\ s$). This can be justified by the conservatism problem of the polytopic approach, and the highly uncertain dynamics reached at high speeds worsen the LTI performance. In fact, this uncertainty is not caused only by the bicycle model, but by the actuator model. Since G_{act} is used as an LTI system where actually it varies with speed and quiet changes at high speeds. Then, reaching speeds around 13 m/s and below, both controllers perform better with lower sensitivity to noises. On the other hand, the LFT and the gridding controllers show better performance in all situations with a little difference in the minimization of the lateral error. Regarding the steering front angle in Fig. 4.23, these two controllers have the same evolution with less noises even at high speeds.

Fig. 4.24 shows the steering rate input for the tested controllers. Again the LFT and the gridding controllers are less noisy than the one obtained by the LTI and the polytopic controllers. Table 4.6 presents that the gridding approach shows the less control effort. Notice that these results support the frequency domain analysis in paragraph 4.3.5, especially the analysis of noise sensitivity at high frequencies.

4.6 Summary of Comparison

This section presents a general review on the comparison done between the three approaches under the main proposed criteria. It is divided into two main parts, each one discusses the main collected comparisons introduced above:

TABLE 4.5: RMS of the lateral error for experimental comparison

	Polytopic	LTI	Gridding	LFT
RMS	0.1473	0.1105	0.1025	0.1096

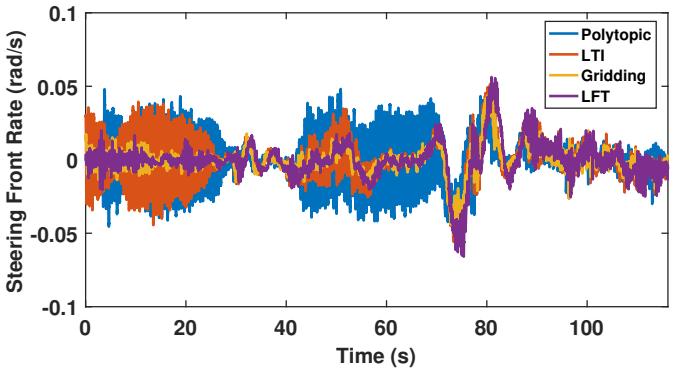

FIGURE 4.24: Experimental steering front rate of the LTI and LPV controllers (rad/s)

TABLE 4.6: RMS of the steering front rate for experimental comparison

	Polytopic	LTI	Gridding	LFT
RMS	0.0263	0.0149	0.0107	0.0129

4.6.1 About The Three LPV Approaches

LPV Formulations

In section 4.2, the nonlinear model was reformulated using the LPV approaches. It has shown that the type of parameter-dependency of the model affects the shape and the complexity of the LPV state-space representation.

For the polytopic approach, the system should be written in a way to be affine with respect to the varying parameters, and the input and output matrices should be constant. This may increase the number of parameters which increases the conservatism of the optimisation problem. Regarding the LFT model in (4.13), a varying parameter leaded a 4-dimensional parameter block Θ by the cause of its number of occurrences. This explains a real problem facing the applications of LFT approach. Some research studies are done on how to reduce the LFT state-space model [376], especially by the researchers working on aircraft control. Finally, the gridding approach showed a simplicity in model formulation where a set of state-space matrices are obtained at a chosen number of operating points, regardless of the parameter-dependency and its occurrences.

LPV/$\mathcal{H}_\infty$ Control Design

Section 4.3 introduced the $\mathcal{H}_\infty$ control design applied to the studied LPV approaches. It has stated the complexity of the existence conditions of each approach in terms of its LMI size and the number of decision variables. Regarding those LMIs, the polytopic approach has the simplest optimisation problem where the known concept of LTI/$\mathcal{H}_\infty$ is applied at the vertices of the polytope with a constant Lyapunov function. However, its LMI size grows exponentially when n_p increases, $\mathcal{O}(2^{n_p})$. This leads to conservatism which is decreased by reducing some vertices [372], but still can not be totally erased. The LFT approach comes to decrease the size of LMIs in polytopic approach, but it requires bigger number of decision variables [14]. The problem of conservatism can be solved using a parameter-dependent Lyapunov function which exists in the grid-based approach. The LMI size in this approach grows by $\mathcal{O}_g^{n_\rho}$, so it

TABLE 4.7: Overview of discussed approaches

Controller	Parameter dependency	Conservatism with large n_p	LMI size/ memory growth	Number of decision variables	Simulation results	Experimental results
Polytopic	Affine	High	$\mathcal{O}(2^2)$	6	Polytopic reduction leads better performance	High sensitivity to noises
LFT	Rational	Medium	$\mathcal{O}(2)$	78	Matrix inverse can be replaced by interpolation using a look-up table	Low sensitivity to noises
Grid-based	General	Low	$\mathcal{O}(n_g)$	9	Performance and n_g are not proportional	Low sensitivity to noises

is much bigger than that in the polytopic and LFT approaches when having $n_g > 2$. Also, the complexity of the grid-based approach appears significantly when increasing the order of the parameter-dependent Lyapunov function (n_ρ^X).

4.6.2 Implementation Part

This part plays a vital role in choosing the suitable controller of real applications, where there are many limitations in terms of computer power and costs.

Simulation Results

Section 4.4 has presented the performance of each control approach with its implementation limitation. The main concluding remarks obtained are:

- The reduction of the polytope decreases the conservatism of the optimisation problem, and thus obtaining better performance.
- Using the gridding approach, the system performance is independent from the number of chosen grid-points.
- The interpolated LFT controller could be used instead of its gain-scheduling (with inverse (4.28)) without losing its performance.

Real Implementation Procedure

Starting with the way of implementation of each approach, the polytopic controller is known to be interpolated as a convex combination of the designed LTI controllers at the polytopic vertices. Thus, those LTI controllers must be saved in a look-up table and then interpolated at each sampling time. It is similar with the gridding approach, but the set of gridded controllers will be linearly interpolated. However, the scheduling of the LFT approach is different, where the matrix Δ_θ contains a matrix which must be inverted online at each sample time, and this increases the computational time. Since the interpolated LFT shows a performance close to the gain-scheduling, it can be implemented using linear interpolation as the gridding approach.

Experimental Results

The figures of the experimental results show how the studied controllers deal with different situations. For example, the LTI and the polytopic controllers are more sensitive to noises at high speeds, i.e. when the system dynamics change significantly. However, the LFT and the gridding controllers are more robust to handle this kind of uncertainty when the approximated model used in the control design differs from the actual system.

As a result, although the grid-based approach needs to solve more LMIs for more decision variables compared to the polytopic one, it provides a general formulation for any parameter-dependency, and it is has the lowest conservatism among the three discussed approaches. On the other hand, the gain-scheduling structure of the LFT approach seems to be the most complex, and its LMIs contain huge number of decision variables compared to the other two. Thus, the grid-based approach could be proposed as a powerful and performant for LPV control applications. That is why it is widely used in aerospace applications [377], [378].

4.7 Conclusion

This chapter has proposed a theoretical and experimental comparison of the LPV approaches for the lateral control of autonomous vehicle. The gridded-based model has the simplest structure with less conservatism in optimisation among the others. The weighting parameters used in control design can physically translate the real actuator limitations to a filter added to the optimisation problem.

The practical limitations of each approach have been discussed by observing the simulation results that have been obtained from different chosen critical scenarios. Then the results obtained in real implementation have shown interesting results regarding the minimization of the lateral error, which encourages the application of LPV/robust approaches on autonomous vehicles. In fact, such approaches help to control parameter-variant systems and to handle with environmental disturbances (wind speed, bad road conditions/slopes, etc...).

As a consequence of the practical limitations, mainly at high speeds, the next chapters propose a switching scheme between multiple LPV controllers to improve the vehicle performance over the whole speed range. The switching strategy is based on Youla-Kucera (YK) Parameterization, where several LPV-YK control structures are designed and validated on the ZOE car.

Chapter 5

Advanced LPV-YK Control Structures: Theoretical Proofs

5.1 Introduction

Previous chapter compared the polytopic and the grid-based approach on the automated robotized platform. It has been concluded that a single Lyapunov function for models with large parameter variations (as ranging between low and fast vehicle speeds) leads to degraded performance at some parameter subsets. In addition, several kinds of lateral control performances may be needed such as lane-tracking, lane-changing, urgent maneuvers, parking, etc.

The current chapter proposes several switching/interpolating control architectures based on Youla-Kucera (YK) parameterization aiming to achieve robust and adaptive closed-loop specifications (rising time, steady-state error, ...). The LPV-YK control architecture incorporates multiple LPV or LTI controllers which can switch/interpolate between them with ensuring stability. It can be used to interpolate between different control performances aiming to achieve different closed-loop specifications, or to switch over partitioned parameter subsets when dealing with large parameter variations. Indeed, as introduced in Chapter 2, the interest behind YK concept is to parameterize a set of linear stabilizing controllers $K(Q)$ where each one is parameterized by its corresponding YK parameter Q [268]. This kind of configuration is structured by mapping a set of linear stabilizing controllers onto a Q-based controller.

The main contributions in this chapter lie in the LPV world and are:

1. Design an interpolating LPV-YK control scheme to achieve different closed-loop specifications.
2. Design a switching LPV-YK control scheme aiming to switch between partitioned parameter subsets.

The theoretical results in this chapter have been represented in:

- *Interpolation of Multi-LPV Control Systems Based on Youla–Kucera Parameterization, published in Automatica*, see [300].
- *Multi-Variable and Multi-Objective Gain Scheduled Control Based on Youla-Kucera Parameterization: Application to Autonomous Vehicles, under review in International Journal on Robust and Nonlinear Control*.
- *Advanced LPV-YK Control Design with Experimental Validation on Autonomous Vehicles, under review in Automatica*.

The following table summarizes briefly the LPV-YK structures presented in this chapter:

- The first two structures are proposed to achieve multiple closed-loop specifications, i.e. rising time, settling time, overshoot, etc. Both of them ensure closed-loop quadratic stability regardless the parameter variations and interpolating signals. The difference is just that the interpolated LPV controllers can be designed either using standard polytopic approach, or based on LTI-YK parameterization. Refer to Sections 5.5.1 and 5.5.2 for more illustration.
- The other structures are introduced aiming to provide robust performance over large parameter regions by designing a local LPV controller at each parameter subset. Quadratic or exponential closed-loop stability is possible depending on the parameter partitioning. Sections 5.6.3 and 5.6.4 illustrates the difference in more details.

TABLE 5.1: Overview of discussed approaches

Objective	Section	LPV-YK Structure	Closed-loop stability
Multiple closed-loop specifications	Section 5.5.1	Interpolation of polytopic-based LPV controllers	Quadratic
	Section 5.5.2	Interpolation of polytopic-based LPV controllers	Quadratic
Maintain robust performance	Section 5.6.3	Switching of partitioned YK-based LPV controllers	Quadratic
	Section 5.6.4	Switching of grid-based LPV controllers	Exponential

The structure is as follows: Section 5.2 states the motivations behind designing LPV-YK control structures. In Section 5.3, some fundamental lemmas are introduced to be used later . Section 5.4 defines a general LPV model with its parameter-varying region. Two LPV-YK control approaches for multi-objective control are presented in Section 5.5. Section 5.6 introduces two switching LPV-YK control structures over partitioned parameter regions. Finally, a discussion and summary is given in Section 5.7.

5.2 Motivation

YK parameterization has been successfully used for steering control of autonomous vehicles considering two LTI controllers designed separately (one for lane-changing and one for lane-tracking) [293]. The YK control scheme of both controllers has shown interesting performance for small and large lateral errors. On the other hand, the YK controller is parameterized for a fixed-speed (LTI lateral dynamics). The objective in this chapter is to generalize the LPV-YK control structures that interpolates/switches between multiple LPV controllers obtaining a multi-variable and multi-objective switched/interpolated controller.

The LPV-YK control approaches are proposed in this thesis to improve the performance of the switched/interpolated LPV controllers, with lower conservatism and design complexities. Indeed, previous works which have shown successful and

smooth LPV switching controllers as in [142], [229], and [208], require the re-design of the local LPV controllers using proposed LMIs, depending on the switching signals (e.g. hysteresis switching, switching with average dwell-time, etc.). It is worth mentioning that the re-design of all local LPV controllers together may cause conservatism when increasing the number of controllers.

The theoretical developments presented here are of interest to:

1. Simplify the design of the LPV switching/interpolating control system by decreasing the complexity of the LMI conditions (no need to re-design the local LPV controllers), using parameterization instead.
2. Avoid any limitation on the switching signals without requiring the use of a constant Lyapunov function.
3. Smooth the control and state responses during the switching instants.
4. Ensure a Plug&Play structure, avoiding the re-design of the switching control scheme if one needs to add or remove any of the local LPV controllers.

5.3 Preliminaries

This section introduces some notations and assumptions regarding LPV systems and LTI-YK parameterization. In addition, useful concepts and several lemmas are reviewed.

5.3.1 State Transformation

The concept of state transformation is to transform the states of a system without affecting its input/output property. Consider a state transformation matrix T (of appropriate dimension) which transforms the state of system W (with state-space matrices A, B, C, D). Then, the transformed system $\bar{W}$ is computed as:

$$\bar{W} : \left[\begin{array}{c|c} TAT^{-1} & TB \\ \hline CT^{-1} & D \end{array}\right]. \tag{5.1}$$

Lemma 5. *Consider a set of matrices A_i corresponding to each vertex of a convex hull $\mathcal{J} = \mathcal{C}_{\mathcal{O}}\{\rho_1, ..., \rho_{n_p}\}$, The following statements are equivalent:*

(i) A_i is Hurwitz $\forall i \in \mathbb{I}[1, n_p]$

(ii) there exist n_p transformation matrices T_i such that the LPV matrix

$$\bar{A}(\rho) = \sum_{i=1}^{n_p} \alpha_i(\rho)\bar{A}_i = \sum_{i=1}^{n_p} \alpha_i(\rho) T_i A_i T_i^{-1} \tag{5.2}$$

is quadratically stable $\forall \rho \in \mathcal{J}$, where $\rho = \sum_{i=1}^{n_p} \alpha_i(\rho)\rho_i$ such that $\sum_{i=1}^{n_p} \alpha_i(\rho) = 1$.

The proof is introduced in [297] as follows:

$(i) \Rightarrow (ii)$. If A_i is Hurwitz, then $\exists X_i > 0$ such that $X_i A_i + A_i^T X_i < 0$, $i \in \mathbb{I}_{n_p}$. According to [274], it is always possible to find state transformations T_i (e.g. $T_i = X_i^{1/2}$) such that,

$$P\bar{A}_i + \bar{A}_i P < 0, \qquad \forall i \in \mathbb{I}_{n_p} \tag{5.3}$$

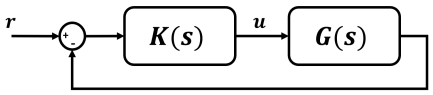

FIGURE 5.1: Negative feedback loop

for a common $P > 0$, with $\bar{A}_i = T_i A_i T_i^{-1}$. Finding the coordinates $\alpha_i(\rho)$, with ρ as a convex combination of the vertices of $\mathcal{J}$, the LPV matrix (5.2) can be constructed. Based on $\alpha_i \geq 0, \forall i \in \mathbb{I}_{n_p}$, inequalities (5.3) and linearity,

$$P\Big(\sum_{i=1}^{n_p} \alpha_i(\rho)\bar{A}_i\Big) + \Big(\sum_{i=1}^{n_p} \alpha_i(\rho)\bar{A}_i\Big)^T P < 0, \tag{5.4}$$

and thus the quadratic stability of $\bar{A}(\rho)$ is proved.

$(ii) \Rightarrow (i)$. Take $\rho = \rho_m$, with ρ_m one of the vertices of $\mathcal{J}$; then $\alpha_m = 1$, and $\alpha_i = 0, \forall i \neq m$. Therefore, $\bar{A}(\rho) = \bar{A}_m$, and from (5.4) it can be concluded that $\bar{A}_m$ is Hurwitz, and thus A_m.

5.3.2 YK Parameter Definition

Observing the control scheme in Fig. 5.1, assume a Single-Input-Single-Output (SISO) LTI plant $G(s)$ connected to a controller $K(s)$ in a stable feedback structure. Then, the closed-loop transfer function is obtained as:

$$CL(s) = \frac{G(s)K(s)}{1 + G(s)K(s)} \tag{5.5}$$

Moreover, let's define a transfer function $Q(s)$ from the reference r to the control input u, then:

$$Q(s) = \frac{K(s)}{1 + G(s)K(s)} \tag{5.6}$$

Thus, if $G(s)$ and $Q(s)$ are known, the controller $K(s)$ can be expressed as:

$$K(s) = \frac{Q(s)}{1 - G(s)Q(s)} \tag{5.7}$$

From (5.6), it is shown that if $K(s)$ stabilizes $G(s)$, then $Q(s)$ is stable and proper. Equivalently, if $Q(s)$ is stable and proper, then $K(s)$ given by (5.7) stabilizes $G(s)$.

In addition, reformulating the closed-loop expression to be written in terms of $Q(s)$, we obtain a transfer function affine with respect to $Q(s)$ expressed as:

$$CL(s) = Q(s)G(s) \tag{5.8}$$

From this point, the concept of a controller based on YK parameter $Q(s)$ which is parameterized by a transfer function is opened. Then a set of stabilizing controllers can be parameterized in terms of all stable and proper functions $Q(s)$ for any LTI plant $G(s)$.

5.3.3 Doubly Coprime Factorisation

YK parameterisation uses the doubly coprime factorisation concepts to reduce the algebraic complexity of Q computation. Consider the LTI plant G stabilized by a set of LTI controllers K_i, then they can be factorized (from left and right) as a product of

a stable transfer function matrix and a transfer function matrix with a stable inverse as shown below:

$$\begin{aligned} G &= NM^{-1} = \tilde{M}^{-1}\tilde{N} \\ K_i &= U_i V_i^{-1} = \tilde{V}_i^{-1}\tilde{U}_i, \quad \forall i \end{aligned} \tag{5.9}$$

Lemma 6. *If the coprime factors M, N, $\tilde{M}$, $\tilde{N}$, U_i, V_i, $\tilde{U}_i$, $\tilde{V}_i \in \mathcal{RH}_\infty \forall i$, and if they satisfy the following Bezout Identity:*

$$\begin{bmatrix} \tilde{V}_i & -\tilde{U}_i \\ -\tilde{N} & \tilde{M} \end{bmatrix} \begin{bmatrix} M & U_i \\ N & V_i \end{bmatrix} = \begin{bmatrix} M & U_i \\ N & V_i \end{bmatrix} \begin{bmatrix} \tilde{V}_i & -\tilde{U}_i \\ -\tilde{N} & \tilde{M} \end{bmatrix} = \begin{bmatrix} I & 0 \\ 0 & I \end{bmatrix} \tag{5.10}$$

then, all the factorized controllers K_i stabilize G (proof in [269]).

5.3.4 Q Parameterisation

Consider the YK parameter Q_i as a transfer function which characterizes the dynamic switching between a base controller K_0 and K_i $\forall i$.

Lemma 7. *Assume an LTI plant $G = NM^{-1}$ stabilized by the LTI controllers $K_i = U_i V_i^{-1}, \forall i$, which have been already designed separately, with M and N are coprime, U_i and V_i are coprime, and M, N, U_i and $V_i \in \mathcal{RH}_\infty \forall i$. Let us choose K_0 as a nominal controller factorised as $K_0 = U_0 V_0^{-1}$, then the set of parameterized LTI controllers $\tilde{K}_i$ ($\forall i \neq 0$) is defined as:*

$$\begin{aligned} \tilde{K}_i = \tilde{K}(Q_i) &= (U_0 + MQ_i)(V_0 + NQ_i)^{-1} \\ &= (\tilde{V}_0 + Q_i\tilde{N})^{-1}(\tilde{U}_0 + Q_i\tilde{M}) \end{aligned}$$

where $Q_i \in \mathcal{RH}_\infty$ by construction [269].

5.3.5 Exponential Stability of A Triangular Matrix

The following Lemma shows that a triangular matrix is exponentially stable if its diagonal elements are exponentially stable with bounded off-diagonal elements.

Notice that a matrix $A(\rho)$ is said to be exponentially stable if there exists a positive definite matrix function $X(\rho)$ such that

$$\pi = \dot{X}(\rho) + X(\rho)A(\rho) + A^T(\rho)X(\rho) < 0 \tag{5.11}$$

Lemma 8. *Assume that the matrices $A_{11}(\rho)$ and $A_{22}(\rho)$ are exponentially stable, every continuous and bounded block triangular matrix whose diagonal matrices consist of $A_{11}(\rho)$ and $A_{22}(\rho)$ is also exponentially stable.*

To prove the following Lemma, consider an upper triangular matrix:

$$A(\rho) = \begin{bmatrix} A_{11}(\rho) & A_{12}(\rho) \\ 0 & A_{22}(\rho) \end{bmatrix} \tag{5.12}$$

According to the assumption, there exists bounded positive definite matrix functions $X_1(\rho)$ and $X_2(\rho)$, positive real numbers α_1 and α_2, satisfying the following inequalities [379]:

$$\begin{aligned} \dot{X}_1(\rho) + X_1(\rho)A_{11}(\rho) + A_{11}^T(\rho)X_1(\rho) &\leq -\alpha_1 I \\ -\alpha_2 I \leq \dot{X}_2(\rho) + X_2(\rho)A_{22}(\rho) + A_{22}^T(\rho)X_2(\rho) &< 0 \end{aligned} \tag{5.13}$$

Since the off-diagonal matrix $A_{12}(\rho)$ is assumed to be bounded, there exists a positive real number α_3 satisfying

$$X_1(\rho)A_{12}(\rho) \leq \alpha_3 I \tag{5.14}$$

Choose

$$X(\rho) = \begin{bmatrix} X_1(\rho) & 0 \\ 0 & \lambda X_2(\rho) \end{bmatrix}$$

Then,

$$\pi = \begin{bmatrix} \dot{X}_1(\rho) + X_1(\rho)A_{11}(\rho) + A_{11}^T(\rho)X_1(\rho) & X_1(\rho)A_{12}(\rho) \\ A_{12}^T(\rho)X_1(\rho) & \lambda\left(\dot{X}_2(\rho) + X_2(\rho)A_{22}(\rho) + A_{22}^T(\rho)X_2(\rho)\right) \end{bmatrix}$$

Now, let us find a positive real number $\lambda > 0$ which satisfies (5.11) such that π is negative definite. Using Schur complement, inequality (5.11) is equivalent to the following two inequalities:

$$\begin{gathered} \pi(2,2) < 0 \\ \pi = \pi(1,1) - \pi(1,2)\pi(2,2)^{-1}\pi(2,1) < 0 \end{gathered} \tag{5.15}$$

The first inequality holds for any $\lambda > 0$ (from (5.13)). Considering (5.13) and (5.14) in (5.15), then

$$\pi \leq -\alpha_1 I + \lambda^{-1}\alpha_2\pi(1,2)\pi(2,1) \leq -\alpha_1 I + \lambda^{-1}\alpha_2\alpha_3^2 I \tag{5.16}$$

Therefore, $\pi < 0$ for any $\lambda > 0$ satisfying $\alpha_2\alpha_3^2/\lambda < \alpha_1$. A similar proof could be deduced for the lower triangular matrices.

Notations. *For the rest of the thesis, general notations are considered as follows.* $\mathbb{I}[a,b]$ *denotes the integer set from a to b.* $\mathbb{R}$ *stands for the set of real numbers.* $\mathbb{R}^{m\times n}$ *is the set of real* $m \times n$ *matrices. The transpose of a real matrix* M *is denoted by* M^T*.* I *and* 0 *denote an identity matrix and a zero matrix, respectively, of appropriate dimensions.* $diag(X_1, X_2, ..., X_N)$ *denotes a matrix with matrices* X_1*,* X_2*, ..., and* X_N *as diagonal blocks. It is worth noting that* γ_∞ *corresponds to the known* γ*-performance design, whereas* γ *is a switching/interpolating signal.*

5.4 LPV Model Definition

In this section, a general LPV model is defined to be used in the following sections. Consider a Multi-Input-Multi-Output (MIMO) LPV system $G(\rho)$ with m inputs and p outputs:

$$G(\rho)\begin{cases} \dot{x}(t) = A(\rho(t))x(t) + B_1(\rho(t))w(t) + B_2(\rho(t))u(t) \\ z(t) = C_1(\rho(t))x(t) + D_{11}(\rho(t))w(t) + D_{12}(\rho(t))u(t) \\ y(t) = C_2(\rho(t))x(t) + D_{21}(\rho(t))w(t) + D_{22}(\rho(t))u(t) \end{cases} \tag{5.17}$$

where $x(t) \in \mathbb{R}^{n_x}$, $y(t) \in \mathbb{R}^p$, $u(t) \in \mathbb{R}^m$, $z(t) \in \mathbb{R}^{n_z}$ are the state, output, input, controlled output vectors respectively. $w(t) = \begin{bmatrix} r & n & d \end{bmatrix}^T \in \mathbb{R}^{n_w}$ contains the exogenous inputs of the tracking reference r, measurable noise n and input disturbance d. $\rho(t) := \rho \in \mathbb{R}^{n_p}$ is a vector of n_p measurable time-varying parameters.

5.4.1 Polytopic-based LPV Model

To design quadratically stabilizing LPV controllers, the LPV model should be defined based on the polytopic approach, i.e. assuming affine parameter-dependency. Define a convex polytopic region $\mathcal{P}$ by the parameters extremums $[\underline{\rho}, \overline{\rho}]$ as:

$$\mathcal{P} := \mathcal{C}_{\mathcal{O}}\{w_1, ..., w_{2^{n_p}}\} \tag{5.18}$$

where w_i represent the vertices of $\mathcal{P}$ $\forall i \in \mathbb{I}[1, 2^{n_p}]$.

The polytopic approach for LPV control design requires two assumptions: 1) the system must be strictly proper ($D_{22}(\rho) = 0$); and 2) the input and output matrices B_2, C_2, D_{12} and D_{21} must be parameter-independent [15]. For what follows, we then assume that the LPV system is given as:

$$G(\rho) \begin{cases} \dot{x}(t) = A(\rho)x(t) + B_1(\rho)w(t) + B_2u(t) \\ z(t) = C_1(\rho)x(t) + D_{11}(\rho)w(t) + D_{12}u(t) \\ y(t) = C_2x(t) + D_{21}w(t) \end{cases} \tag{5.19}$$

Note that the second assumption doesn't impose any serious constraints where, if needed, it can be fulfilled by filtering the input u and output y [7]. Here, ρ belongs to $\mathcal{P}$ and is written as:

$$\rho = \sum_{i=1}^{2^{n_p}} \alpha_i w_i, \tag{5.20}$$

where $\sum_{i=1}^{2^{n_p}} \alpha_i = 1$, $\alpha_i \geq 0$ $\forall i$. Therefore, the system representation at any operating point $\rho \in \mathcal{P}$ is given as a convex combination of the state-space realizations of the LTI systems given at the vertices w_i:

$$\left[\begin{array}{c|cc} A(\rho) & B_1(\rho) & B_2 \\ \hline C_1(\rho) & D_{11}(\rho) & D_{12} \\ C_2 & D_{21} & 0 \end{array}\right] = \sum_{i=1}^{2^{n_p}} \alpha_i(\rho) \left[\begin{array}{c|cc} A_i & B_{1,i} & B_2 \\ \hline C_{1,i} & D_{11,i} & D_{12} \\ C_2 & D_{21} & 0 \end{array}\right] \tag{5.21}$$

5.5 Multi-Objective Control Interpolation

This section aims to design an interpolation scheme between different multi-objective controllers based on LPV-YK parameterization. Nowadays, systems are getting more and more complex leading to control algorithms able to consider online varying objectives for performance and safety. For instance, the field of autonomous systems, in particular autonomous vehicles, is indicative of such an evolution. However, it is difficult to design a single controller covering a large parameter range and achieving multiple objectives.

Fig. 5.2 shows an interpolation example between two control performances, where two controllers $K^{(1)}(\rho)$ and $K^{(2)}(\rho)$ are designed over the same convex parameter region $\mathcal{P}$, satisfying closed-loop quadratic stability. It is assumed that each controller has been designed separately achieving different closed-loop specification such as rising time, actuator bandwidth, steady-state error, etc.

The following two sections introduce two LPV-YK control structures aiming to interpolate between different control objectives satisfying the closed-loop quadratic stability for any interpolating signal. To do so, the polytopic LPV model $G(\rho)$ (5.19) is used for both control architectures.

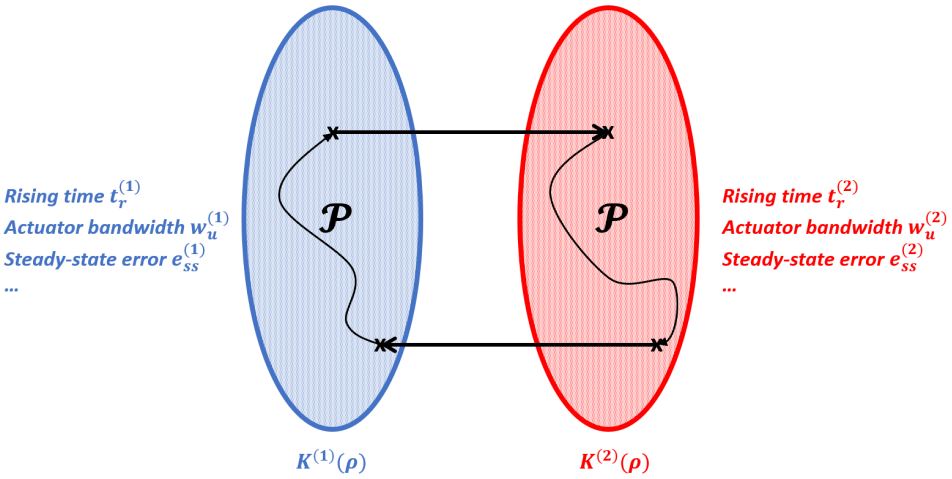

FIGURE 5.2: Interpolation of multiple control performances

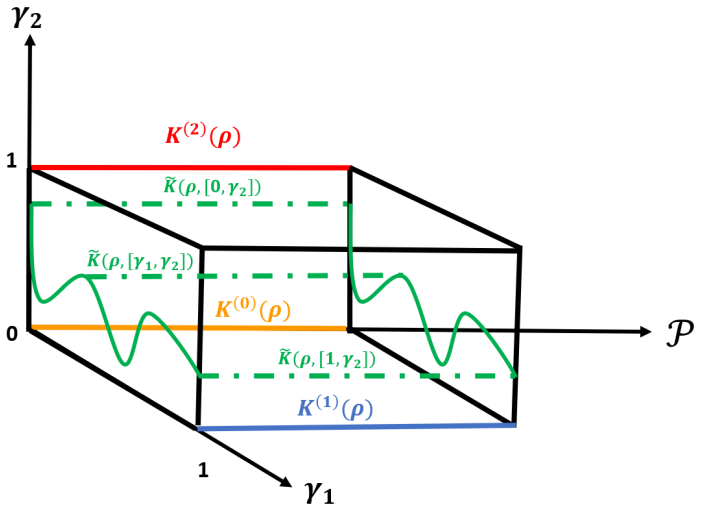

FIGURE 5.3: Interpolation between three polytopic-based LPV controllers along the convex parameter space $\mathcal{P}$. The LPV-YK controller $\tilde{K}(\rho,\gamma)$ interpolates, using $\gamma = [\gamma_1,\gamma_2]$, between $K^{(0)}(\rho)$ (for $\gamma = [0,0]$), $K^{(1)}(\rho)$ (for $\gamma = [1,0]$), and $K^{(2)}(\rho)$ (for $\gamma = [0,1]$)

Notations. *The following notations are used in the next two subsections 5.5.1 and 5.5.2. The subscript i of a system/matrix/variable of an LPV system (e.g. G_i, A_i, w_i) denotes the local LTI system/matrix/variable at the i^{th} vertex of a polytope $\mathcal{P}$. The superscript (j) denotes the j^{th} controller (e.g. $K^{(j)}$) in the set of the designed controllers. For example, $A_{k,i}^{(j)}$ represents the LTI state matrix of the j^{th} LPV controller at the i^{th} vertex of $\mathcal{P}$.*

5.5.1 Interpolation between polytopic-based LPV controllers

Let $\mathcal{K} = \{K^{(1)}(\rho), K^{(2)}(\rho), \ldots, K^{(j)}(\rho), \ldots, K^{(\zeta)}(\rho)\}$ be a finite set of quadratically stabilizing LPV controllers of $G(\rho)$ (5.19) that are designed achieving different objectives and closed-loop specifications. Thus, $\forall j \in \mathbb{I}[0,\zeta]$:

$$K^{(j)}(\rho) : \left[\begin{array}{c|c} A_k^{(j)}(\rho) & B_k^{(j)}(\rho) \\ \hline C_k^{(j)}(\rho) & D_k^{(j)}(\rho) \end{array}\right] \tag{5.22}$$

with the polytopic controllers:

$$\left[\begin{array}{c|c} A_k^{(j)}(\rho) & B_k^{(j)}(\rho) \\ \hline C_k^{(j)}(\rho) & D_k^{(j)}(\rho) \end{array}\right] = \sum_{i=1}^{2^{n_p}} \alpha_i(\rho) \left[\begin{array}{c|c} A_{k,i}^{(j)} & B_{k,i}^{(j)} \\ \hline C_{k,i}^{(j)} & D_{k,i}^{(j)} \end{array}\right] \tag{5.23}$$

where $A_k^{(j)}(\rho) \in \mathbb{R}^{n_k^{(j)} \times n_k^{(j)}}$, $B_k^{(j)}(\rho) \in \mathbb{R}^{n_k^{(j)} \times m_k}$, $C_k^{(j)}(\rho) \in \mathbb{R}^{p_k \times n_k^{(j)}}$ and $D_k^{(j)}(\rho) \in \mathbb{R}^{p_k \times m_k}$.

Based on the statements on LPV concepts and YK parameterization, a quadratically stable interpolation procedure between ζ LPV controllers is formulated (as mentioned by the next theorem). The interpolation is performed using an interpolating signal vector $\gamma = [\gamma_1, \ldots, \gamma_j, \ldots, \gamma_\zeta]$.

Let's assume that

(A.1.1). *There exists an LPV output-feedback controller $K^{(0)}(\rho)$ which quadratically stabilizes $G(\rho)$ over $\mathcal{P}$ (following the approach in [7]), defined as:*

$$K^{(0)}(\rho) : \left[\begin{array}{c|c} A_k^{(0)}(\rho) & B_k^{(0)}(\rho) \\ \hline C_k^{(0)}(\rho) & D_k^{(0)}(\rho) \end{array}\right] \tag{5.24}$$

being,

$$\left[\begin{array}{c|c} A_k^{(0)}(\rho) & B_k^{(0)}(\rho) \\ \hline C_k^{(0)}(\rho) & D_k^{(0)}(\rho) \end{array}\right] = \sum_{i=1}^{2^{n_p}} \alpha_i(\rho) \left[\begin{array}{c|c} A_{k,i}^{(0)} & B_{k,i}^{(0)} \\ \hline C_{k,i}^{(0)} & D_{k,i}^{(0)} \end{array}\right] \tag{5.25}$$

where $A_k^{(0)}(\rho) \in \mathbb{R}^{n_k^{(0)} \times n_k^{(0)}}$, $B_k^{(0)}(\rho) \in \mathbb{R}^{n_k^{(0)} \times m_k}$, $C_k^{(0)}(\rho) \in \mathbb{R}^{p_k \times n_k^{(0)}}$ and $D_k^{(0)}(\rho) \in \mathbb{R}^{p_k \times m_k}$.

(A.1.2). *A group of ζ LPV controllers $K^{(j)}(\rho)$ (5.22)-(5.23) ($j \in \mathbb{I}[1, \zeta]$) have been designed separately to quadratically stabilize $G(\rho)$ achieving different objectives and closed-loop specifications for all operating conditions.*

For illustration, Figure 5.3 represents an example of an interpolation between three polytopic-based LPV controllers $K^{(0)}(\rho)$, $K^{(1)}(\rho)$, and $K^{(2)}(\rho)$, along the convex parameter space $\mathcal{P}$. The orange solid line represents the chosen nominal LPV controller $K^{(0)}(\rho)$. The blue/red solid lines are two LPV controllers $K^{(1)}(\rho)$/$K^{(2)}(\rho)$ that are designed using the standard polytopic approach, achieving different required objectives. The overall interpolation is performed using the interpolating signal $\gamma = [\gamma_1, \gamma_2]$, and is represented by the LPV-YK controller $\tilde{K}(\rho, \gamma)$.

Notice that for every $\rho \in \mathcal{P}$ and for every continuous/discontinuous interpolating signal γ, $\tilde{K}(\rho, \gamma)$ quadratically stabilizes $G(\rho)$. Some interpolation cases can be mentioned to show how $\tilde{K}(\rho, \gamma)$ recovers a single gain-scheduled controller $K^{(j)}(\rho)$ by varying γ_j:

- if $\gamma_j = 0 \; \forall j$, $\tilde{K}(\rho, \gamma) \equiv K^{(0)}(\rho)$
- if $\gamma_j = 1$ for $j = c \in [1, \zeta]$ and $\gamma_j = 0 \; \forall j \neq c$, $\tilde{K}(\rho, \gamma) \equiv K^{(c)}(\rho)$
- else, the performance of $\tilde{K}(\rho, \gamma)$ is interpolated among $K^{(j)}(\rho)$ according to the chosen γ_j.

The following theorem proves that $\tilde{K}(\rho, \gamma)$ quadratically stabilizes $G(\rho)$ for every ρ and for any continuous/discontinuous interpolating vector signal γ.

Theorem 5. *Consider an LPV plant $G(\rho)$ (5.19), and given a set of LPV controllers $\mathcal{K}$ (5.22) that quadratically stabilizes $G(\rho)$. Let us choose $K^{(0)}(\rho)$ as the nominal (central) controller for YK parameterization. Then, the parameterized LPV-YK controller $\tilde{K}(\rho,\gamma)$ (5.28), represented in Fig. 5.4, stabilizes $G(\rho)$ for any continuous/discontinuous interpolating signal $\gamma = [\gamma_1, \gamma_2, \ldots, \gamma_\zeta]$, if there exist symmetric, positive definite matrices $X_g \in \mathbb{R}^{n_x \times n_x}$, $X_k \in \mathbb{R}^{n_k^{(0)} \times n_k^{(0)}}$ such that:*

$$A(\rho)X_g + X_g A^T(\rho) + B_2 W(\rho) + W^T(\rho)B_2^T < 0 \tag{5.26}$$

$$A_k^{(0)}(\rho)X_k + X_k A_k^{(0)T}(\rho) + B_k^{(0)}(\rho)V(\rho) + V(\rho)^T(\rho)B_k^{(0)T}(\rho) < 0 \tag{5.27}$$

The state space matrices of the parameterized LPV-YK controller $\tilde{K}(Q(\rho)) = \tilde{K}(\rho,\gamma)$ are written as:

$$\tilde{A}_k(\rho,\gamma) = \begin{bmatrix} A(\rho) + B_2F_g(\rho) - B_2D_q(\rho,\gamma)C_2 & -B_2D_q(\rho,\gamma)F_k^{(0)}(\rho) & B_2C_q(\rho,\gamma) \\ -B_k^{(0)}(\rho)C_2 & A_k^{(0)}(\rho) & 0 \\ -B_q(\rho)C_2 & -B_q(\rho)F_k^{(0)}(\rho) & A_q(\rho) \end{bmatrix}$$

$$\tilde{B}_k(\rho,\gamma) = \begin{bmatrix} B_2D_q(\rho,\gamma) \\ B_k^{(0)}(\rho) \\ B_q(\rho) \end{bmatrix}$$

$$\tilde{C}_k(\rho,\gamma) = \begin{bmatrix} F_g(\rho) - (D_k^{(0)}(\rho) + D_q(\rho,\gamma))C_2 & \\ & C_k^{(0)}(\rho) - D_q(\rho,\gamma)F_k^{(0)}(\rho) \quad C_q(\rho,\gamma) \end{bmatrix}$$

$$\tilde{D}_k(\rho,\gamma) = D_k^{(0)}(\rho) + D_q(\rho,\gamma) \tag{5.28}$$

where

$$\begin{aligned} A_q(\rho) &= diag(A_q^{(1)}, \ldots, A_q^{(j)}, \ldots, A_q^{(\zeta)}), \\ B_q(\rho) &= \begin{bmatrix} B_q^{(1)} & \ldots & B_q^{(j)} & \ldots & B_q^{(\zeta)} \end{bmatrix}^T, \\ C_q(\rho,\gamma) &= \begin{bmatrix} \gamma_1 C_q^{(1)} & \ldots & \gamma_j C_q^{(j)} & \ldots & \gamma_\zeta C_q^{(\zeta)} \end{bmatrix}, \\ D_q(\rho,\gamma) &= \sum_{j=1}^{\zeta} \gamma_j D_q^{(j)}, \end{aligned} \tag{5.29}$$

being $F_g(\rho) = W(\rho)X_g^{-1}$, $F_k^{(0)}(\rho) = V(\rho)X_k^{-1}$, and $A_q^{(j)}$, $B_q^{(j)}$, $C_q^{(j)}$, and $D_q^{(j)}$ the state-space matrices of $Q^{(j)}(\rho,\gamma)$ $\forall j \in \mathbb{I}[1,\zeta]$ represented in (5.31). Notice that γ_j is multiplied by the output of $Q^{(j)}(\rho)$, i.e. $Q^{(j)}(\rho,\gamma) = \gamma_j \times Q^{(j)}(\rho)$.

Proof 1. *According to YK parameterisation concept, the parameterized controller can be formulated as a Linear Fractional Transformation (LFT) system [269], i.e. $\tilde{K}^{(j)}(\rho,\gamma) = \mathcal{F}_l(J(\rho), Q^{(j)}(\rho,\gamma))$ $\forall j$ (see Fig. 5.4), where $J(\rho)$ and $Q^{(j)}(\rho,\gamma))$ derived as shown in (5.30)-(5.31).*

$$J(\rho) = \sum_{i=1}^{2^{n_p}} \alpha_i(\rho) \left[\begin{array}{cc|cc} A_i + B_2F_{g,i} & 0 & 0 & B_2 \\ -B_{k,i}^{(0)}C_2 & A_{k,i}^{(0)} & B_{k,i}^{(0)} & 0 \\ \hline F_{g,i} - D_{k,i}^{(0)}C_2 & C_{k,i}^{(0)} & D_{k,i}^{(0)} & I \\ -C_2 & -F_{k,i}^{(0)} & I & 0 \end{array}\right] \tag{5.30}$$

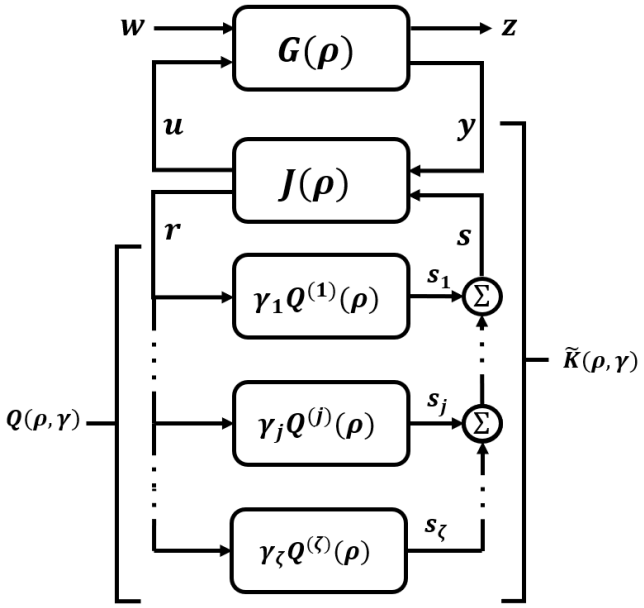

FIGURE 5.4: Polytopic-based LPV-YK general configuration

At each vertex w_i, the closed-loop system $CL_i(\gamma)$ (5.33) is derived from the LFT interconnection between G_i and $\tilde{K}_i(\gamma)$ (see Fig. 5.5).

$$Q^{(j)}(\rho,\gamma)=\sum_{i=1}^{2^{n_p}}\alpha_i(\rho)\left[\begin{array}{cc:c|c} A_i+B_2D_{k,i}^{(j)}C_2 & B_2C_{k,i}^{(j)} & B_2[D_{k,i}^{(j)}-D_{k,i}^{(0)}]F_{k,i}^{(0)}-B_2C_{k,i}^{(0)} & B_2[D_{k,i}^{(j)}-D_{k,i}^{(0)}] \\ B_{k,i}^{(j)}C_2 & A_{k,i}^{(j)} & B_{k,i}^{(j)}F_{k,i}^{(0)} & B_{k,i}^{(j)} \\ \hdashline 0 & 0 & A_{k,i}^{(0)}+B_{k,i}^{(0)}F_{k,i}^{(0)} & B_{k,i}^{(0)} \\ \hline \gamma[D_{k,i}^{(j)}C_2-F_{g,i}] & \gamma C_{k,i}^{(j)} & \gamma[(D_{k,i}^{(j)}-D_{k,i}^{(0)})F_{k,i}^{(0)}-C_{k,i}^{(0)}] & \gamma[D_{k,i}^{(j)}-D_{k,i}^{(0)}] \end{array}\right] \tag{5.31}$$

$$\begin{aligned}\bar{A}_{cl,i}(\gamma) &= TA_{cl,i}(\gamma)T^{-1} \\ &= \left[\begin{array}{cc:cc} A_i+B_2F_{g,i} & B_2C_{q,i} & -B_2(F_{g,i}-(D_{k,i}^{(0)}+D_{q,i}(\gamma))C_2) & B_2(C_{k,i}^{(0)}-D_{q,i}F_{k,i}^{(0)}) \\ 0 & A_{q,i} & B_{q,i}C_2 & -B_{q,i}F_{k,i}^{(0)} \\ \hdashline 0 & 0 & A_i+B_2D_{k,i}^{(0)}C_2 & B_2C_{k,i}^{(0)} \\ 0 & 0 & B_{k,i}^{(0)}C_2 & A_{k,i}^{(0)} \end{array}\right]\end{aligned} \tag{5.32}$$

$$CL_i(\gamma) = \left[\begin{array}{ccc|c} A_i + B_2(D_{k,i}^{(0)} + D_{q,i}(\gamma))C_2 & B_2(F_{g,i} - (D_{k,i}^{(0)} + D_{q,i}(\gamma))C_2) & B_2(C_{k,i}^{(0)} - D_{q,i}(\gamma)F_{k,i}^{(0)}) & B_2C_{q,i}(\gamma) & B_{1,i} + B_2(D_{k,i}^{(0)} + D_{q,i}(\gamma))D_{21} \\ B_2D_{q,i}(\gamma)C_2 & A_i + B_2(F_{g,i} - D_{q,i}(\gamma)C_2) & -B_2D_{q,i}(\gamma)F_{k,i}^{(0)} & B_2C_{q,i}(\gamma) & B_2D_{q,i}(\gamma)D_{21} \\ B_{k,i}^{(0)}C_2 & -B_{k,i}^{(0)}C_2 & A_{k,i}^{(0)} & 0 & B_{k,i}^{(0)}D_{21} \\ B_{q,i}C_2 & -B_{q,i}C_2 & -B_{q,i}F_{k,i}^{(0)} & A_{q,i} & B_{q,i}D_{21} \\ \hline C_{1,i} + D_{12}(D_{k,i}^{(0)} + D_{q,i}(\gamma))C_2 & D_{12}(F_{g,i} - (D_{k,i}^{(0)} + D_{q,i}(\gamma))C_2) & D_{12}(C_{k,i}^{(0)} - D_{q,i}(\gamma)F_{k,i}^{(0)}) & D_{12}C_{q,i}(\gamma) & D_{11,i} + D_{12}(D_{k,i}^{(0)} + D_{q,i}(\gamma))D_{21} \end{array}\right] \tag{5.33}$$

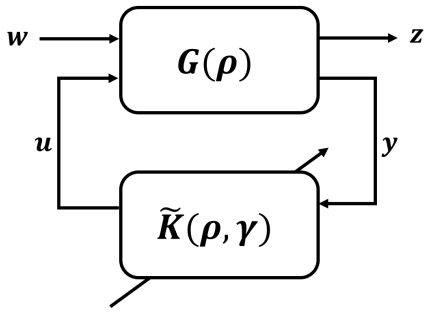

FIGURE 5.5: $G - \tilde{K}$ LFT interconnection

Now, the closed-loop state matrix $A_{cl}(\rho,\gamma) = \sum_{i=1}^{2^{n_p}} \alpha_i(\rho) A_{cl,i}(\gamma)$ *is quadratically stable if there exist a symmetric, positive definite, parameter-invariant matrix* X_{cl} *such that:*

$$X_{cl} A_{cl}(\rho,\gamma) + A_{cl}^T(\rho,\gamma) X_{cl} < 0 \;\; \forall\gamma \tag{5.34}$$

To prove this, let $T = \begin{bmatrix} I & 0 & 0 & 0 \\ 0 & 0 & 0 & I \\ I & -I & 0 & 0 \\ 0 & 0 & I & 0 \end{bmatrix}$ *be a state transformation matrix which is applied to* $CL(\rho,\gamma)$*, without changing its input-output nature, so* $T^{-1} = \begin{bmatrix} I & 0 & 0 & 0 \\ I & 0 & -I & 0 \\ 0 & 0 & 0 & I \\ 0 & I & 0 & 0 \end{bmatrix}$.

Due to the block-triangular form of $\bar{A}_{cl,i}(\gamma)$ *(5.32) , (5.34) is satisfied if the following equations hold (check Lemma 2 in [296]):*

$$\sum_{i=1}^{2^{n_p}} \alpha_i(\rho)(Y_g(A_i + B_2 F_{g,i}) + (A_i + B_2 F_{g,i})^T Y_g) < 0 \tag{5.35}$$

$$\sum_{i=1}^{2^{n_p}} \alpha_i(\rho)(Y_q A_{q,i} + A_{q,i}^T Y_q) < 0 \tag{5.36}$$

$$\sum_{i=1}^{2^{n_p}} \alpha_i(\rho)(Y_0 \mathcal{A}_i^{(0)} + \mathcal{A}_i^{(0)T} Y_0) < 0 \tag{5.37}$$

where $Y_g \in \mathbb{R}^{n_x \times n_x}$, $Y_q \in \mathbb{R}^{n_q \times n_q}$ *and* $Y_0 \in \mathbb{R}^{(n_x+n_k^{(0)})\times(n_x+n_k^{(0)})}$ *are symmetric, positive definite, parameter-invariant matrices, and choosing* $X_{cl} = T^T \, diag(Y_g, Y_q, Y_0) \, T$*, and*

$$\mathcal{A}_i^{(0)} = \begin{bmatrix} A_i + B_2 D_{k,i}^{(0)} C_2 & B_2 C_{k,i}^{(0)} \\ B_{k,i}^{(0)} C_2 & A_{k,i}^{(0)} \end{bmatrix} \tag{5.38}$$

Inequality (5.35) can be linearized by $Y_g = X_g^{-1}$ *which leads to (5.26) when choosing* $W(\rho) = \sum_{i=1}^{2^{n_p}} \alpha_i(\rho) F_{g,i} X_g$*. Due to the diagonal shape of* $A_q(\rho)$*, it is quadratically stable if each diagonal term* $A_q^{(j)}(\rho)$ *is quadratically stable. Regarding (5.31), the state matrix of each LPV-YK parameter* $A_q^{(j)}(\rho)$ *is quadratically stable if there exist symmetric, positive definite,*

constant matrices $P_1 \in \mathbb{R}^{(n_x+n_k^{(1)})\times(n_x+n_k^{(1)})}$ *and* $P_2 \in \mathbb{R}^{n_k^{(0)}\times n_k^{(0)}}$ *such that:*

$$\sum_{i=1}^{2^{np}} \alpha_i(\rho)(P_1\mathcal{A}_i^{(j)} + \mathcal{A}_i^{(j)T}P_1) < 0 \tag{5.39}$$

$$\sum_{i=1}^{2^{np}} \alpha_i(\rho)(P_2(A_{k,i}^{(0)} + B_{k,i}^{(0)}F_{k,i}^{(0)}) + (A_{k,i}^{(0)} + B_{k,i}^{(0)}F_{k,i}^{(0)})^T P_2) < 0 \tag{5.40}$$

being,

$$\mathcal{A}_i^{(j)} = \begin{bmatrix} A_i + B_2 D_{k,i}^{(j)} C_2 & B_2 C_{k,i}^{(j)} \\ B_{k,i}^{(j)} C_2 & A_{k,i}^{(j)} \end{bmatrix} \tag{5.41}$$

The condition in (5.39) is verified given that $K^{(j)}(\rho) \in \mathcal{K}$ *quadratically stabilizes* $G(\rho)$. *Moreover, the inequality (5.40) satisfies (5.27) by choosing* $P_2 = X_k^{-1}$ *and* $V(\rho) = \sum_{i=1}^{2^{np}} \alpha_i(\rho)F_{k,i}^{(0)}X_k$. *Thus,* $\forall j \in \mathbb{I}[1,j]$ $A_q^{(j)}(\rho)$, *is quadratically stable, consequently* $A_q(\rho)$, *and (5.36) is verified. Finally, (5.37) is fulfilled given that* $K^{(0)}(\rho)$ *quadratically stabilizes* $G(\rho)$.

Notice that the closed-loop state matrix $A_{cl}(\rho,\gamma)$ is proved to be quadratically stable regardless the switching signal γ. It is worth mentioning that this is achieved without requiring an instantaneous design of all the local LPV controllers including the interpolating signals.

5.5.2 Interpolation between YK-based LPV controllers

Unlike the previous polytopic-based LPV-YK control, the current section proposes a more advanced one aiming to reduce the problem conservatism caused by the condition of requiring polytopic-based LPV controllers, i.e. relaxing assumption (A.1.2) and the LMI condition (5.27). Generally speaking, it has been found that it is not necessary to have $Q^{(j)}(\rho,\gamma)$ quadratically stable by design. It is only necessary to have each $Q_i^{(j)}(\gamma)$ stable $\forall w_i$. Then, a state transformation (as in Lemma 5) can be used to obtain a quadratically stabilizing LPV-YK parameter $\bar{Q}(\rho,\gamma)$. To do so, and to improve the closed-loop performance, the local LPV controllers are supposed now to be designed using YK-based gain-scheduling, i.e. the local interpolated LPV controllers are designed based on YK parameterization of their corresponding LTI controllers.

As a result, the current section expresses deeply the necessary LMI conditions to design a quadratically stabilizing LPV-YK interpolation scheme, whereas the LMIs in Theorem 5 are considered to be sufficient conditions.

Considering the polytopic-based LPV model $G(\rho)$ (5.19), assume that

(A.2.1). *There exists an LPV output-feedback controller* $K^{(0)}(\rho)$ *which quadratically stabilizes* $G(\rho)$ *over* $\mathcal{P}$ *(following the approach in [7]), defined as:*

$$K^{(0)}(\rho) : \left[\begin{array}{c|c} A_k^{(0)}(\rho) & B_k^{(0)}(\rho) \\ \hline C_k^{(0)}(\rho) & D_k^{(0)}(\rho) \end{array}\right] \tag{5.42}$$

being,

$$\left[\begin{array}{c|c} A_k^{(0)}(\rho) & B_k^{(0)}(\rho) \\ \hline C_k^{(0)}(\rho) & D_k^{(0)}(\rho) \end{array}\right] = \sum_{i=1}^{2^{np}} \alpha_i(\rho) \left[\begin{array}{c|c} A_{k,i}^{(0)} & B_{k,i}^{(0)} \\ \hline C_{k,i}^{(0)} & D_{k,i}^{(0)} \end{array}\right] \tag{5.43}$$

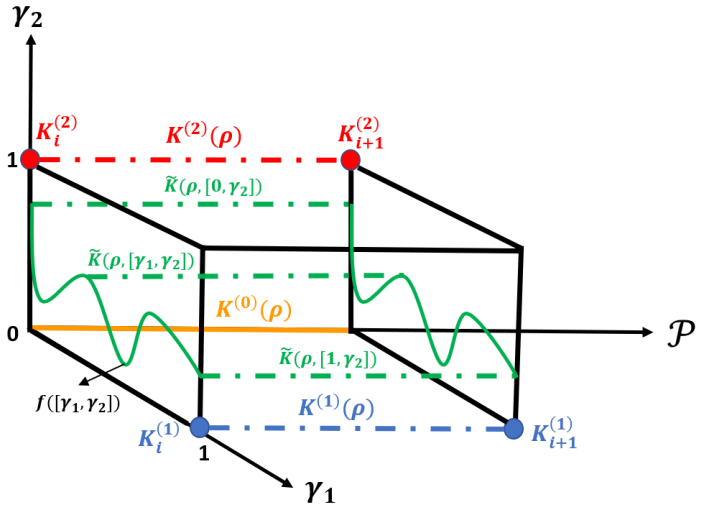

FIGURE 5.6: Interpolation between three LPV controllers; two YK-based gain-scheduled controllers $K^{(1)}(\rho)$ and $K^{(2)}(\rho)$, and a polytopic-based LPV controller $K^{(0)}(\rho)$ along the convex parameter space $\mathcal{P}$. The LPV-YK controller $\tilde{K}(\rho,\gamma)$ interpolates, using $\gamma = [\gamma_1,\gamma_2]$, between $K^{(0)}(\rho)$ (for $\gamma = [0,0]$), $K^{(1)}(\rho)$ (for $\gamma = [1,0]$), and $K^{(2)}(\rho)$ (for $\gamma = [0,1]$)

where $A_k^{(0)}(\rho) \in \mathbb{R}^{n_k^{(0)} \times n_k^{(0)}}$, $B_k^{(0)}(\rho) \in \mathbb{R}^{n_k^{(0)} \times m_k}$, $C_k^{(0)}(\rho) \in \mathbb{R}^{p_k \times n_k^{(0)}}$ *and* $D_k^{(0)}(\rho) \in \mathbb{R}^{p_k \times m_k}$.

(A.2.2). *At each vertex* w_i ($i \in \mathbb{I}[1, 2^{n_p}]$) *of the polytope* $\mathcal{P}$, *a group of* ζ *local LTI controllers* $K_i^{(j)}$ ($j \in \mathbb{I}[1,\zeta]$) *have been designed separately to stabilize* G_i *achieving different objectives and performances for all operating conditions.*

The objective of the proposed strategy is to:

1. Design a set of gain-scheduled controllers $K^{(j)}(\rho)$, $j \in \mathbb{I}[1,\zeta]$. Each one is designed by interpolating its corresponding LTI controllers $K_i^{(j)}$ ($i \in \mathbb{I}[1, 2^{n_p}]$) based on YK parameterization.

2. Create an overall interpolation scheme between the gain-scheduled controllers $K^{(j)}(\rho)$ ($j \in \mathbb{I}[0,\zeta]$), by an interpolating signal vector γ, which is referred to as $\tilde{K}(\rho,\gamma)$, such that the resultant LPV-YK controller $\tilde{K}(\rho,\gamma)$ quadratically stabilizes $G(\rho)$ $\forall \rho \in \mathcal{P}$ and for every $\gamma = [\gamma_1, ..., \gamma_j, ..., \gamma_\zeta]$.

Figure 5.6 represents an example of an LPV-YK based interpolation between three gain scheduled-scheduled controllers $K^{(0)}(\rho)$, $K^{(1)}(\rho)$, and $K^{(2)}(\rho)$, along the convex parameter space $\mathcal{P}$. The orange solid line represents the chosen nominal LPV controller $K^{(0)}(\rho)$, as defined by (A.2.1). The blue/red points represent the local LTI controllers $K_i^{(1)}/K_i^{(2)}$ ($i \in \mathbb{I}[1, 2^{n_p}]$) as defined in (A.2.2). The blue/red dashed line is the gain-scheduled controller $K^{(1)}(\rho)/K^{(2)}(\rho)$ that is designed by the YK-based interpolation of the LTI controllers $K_i^{(1)}/K_i^{(2)}$. The overall interpolation is performed using the interpolating signal $\gamma = [\gamma_1,\gamma_2]$, and is represented by the LPV-YK controller $\tilde{K}(\rho,\gamma)$. It is worth mentioning that the difference between this figure and Fig. 5.3 is that the interpolated LPV controllers $K^{(1)}(\rho)$ and $K^{(2)}(\rho)$ are designed using the standard polytopic approach in Fig. 5.3, whereas here they are designed using YK-based gain-scheduling as proposed by [300].

The LPV-YK controller $\tilde{K}(\rho,\gamma)$ is designed based on a Linear Matrix Inequality (LMI) optimization problem, where it is defined as

$$\tilde{K}(\rho,\gamma) : \left[\begin{array}{c|c} \tilde{A}_k(\rho,\gamma) & \tilde{B}_k(\rho,\gamma) \\ \hline \tilde{C}_k(\rho,\gamma) & \tilde{D}_k(\rho,\gamma) \end{array}\right] \tag{5.44}$$

It is worth mentioning that for every $\rho \in \mathcal{P}$ and for every continuous/discontinuous interpolating signal γ, $\tilde{K}(\rho,\gamma)$ quadratically stabilizes $G(\rho)$.

The interpolation cases can be mentioned to show how $\tilde{K}(\rho,\gamma)$ recovers a single gain-scheduled controller $K^{(j)}(\rho)$ by varying γ_j:

- if $\gamma_j = 0\ \forall j$, $\tilde{K}(\rho,\gamma) \equiv K^{(0)}(\rho) = \sum_{i=1}^{2^{n_p}} \alpha_i(\rho) K_i^{(0)}$
- if $\gamma_j = 1$ for $j = c \in [1,\zeta]$ and $\gamma_j = 0\ \forall j \neq c$, $\tilde{K}(\rho,\gamma) \equiv K^{(c)}(\rho) = \sum_{i=1}^{2^{n_p}} \alpha_i(\rho) K_i^{(c)}$
- else, the performance of $\tilde{K}(\rho,\gamma)$ is interpolated among $K^{(j)}(\rho)$ according to the chosen γ_j.

The next theorem proves that the LPV-YK controller $\tilde{K}(\rho,\gamma)$ (5.47) quadratically stabilizes $G(\rho)\ \forall\rho$, and for every continuous/discontinuous interpolating vector signal γ.

Theorem 6. *Consider an LPV plant $G(\rho)$ (5.19), satisfying assumptions (A.2.1) and (A.2.2). Then, the following generalized LPV-YK controller $\tilde{K}(\rho,\gamma)$ (5.47), as represented in Fig. 5.7, quadratically stabilizes $G(\rho)$ for any $\rho \in \mathcal{P}$ and for any continuous/discontinuous interpolating signals $\gamma_j \in [0,1]$ $(j \geq 1)$, if there exist symmetric, positive definite, constant matrices $X_g \in \mathbb{R}^{n_x \times n_x}$, $X_{k,i} \in \mathbb{R}^{n_k^{(0)} \times n_k^{(0)}}$, and matrices $W_i \in \mathbb{R}^{m \times n_x}$ and $V_i \in \mathbb{R}^{m \times n_k^{(0)}}$ such that $\forall i$:*

$$A_i X_g + X_g A_i^T + B_2 W_i + W_i^T B_2^T < 0 \quad \forall w_i \tag{5.45}$$

$$A_{k,i}^{(0)} X_{k,i} + X_{k,i} A_{k,i}^{(0)T} + B_{k,i}^{(0)} V_i + V_i^T B_{k,i}^{(0)T} < 0 \quad \forall w_i \tag{5.46}$$

The state-space matrices of $\tilde{K}(\rho,\gamma)$ are

$$\begin{aligned}
\tilde{A}_k(\rho,\gamma) &= \sum_{i=1}^{2^{n_p}} \alpha_i(\rho) \begin{bmatrix} A_i + B_2 F_{g,i} - B_2 \tilde{D}_{q,i}(\gamma) C_2 & -B_2 \tilde{D}_{q,i}(\gamma) F_{k,i}^{(0)} & B_2 \tilde{C}_{q,i}(\gamma) \\ -B_{k,i}^{(0)} C_2 & A_{k,i}^{(0)} & 0 \\ -\tilde{B}_{q,i} C_2 & -\tilde{B}_{q,i} F_{k,i}^{(0)} & \tilde{A}_{q,i} \end{bmatrix} \\
\tilde{B}_k(\rho,\gamma) &= \sum_{i=1}^{2^{n_p}} \alpha_i(\rho) \begin{bmatrix} B_2 \tilde{D}_{q,i}(\gamma) \\ B_{k,i}^{(0)} \\ \tilde{B}_{q,i} \end{bmatrix} \\
\tilde{C}_k(\rho,\gamma) &= \sum_{i=1}^{2^{n_p}} \alpha_i(\rho) \begin{bmatrix} F_{g,i} - (D_{k,i}^{(0)} + \tilde{D}_{q,i}(\gamma)) C_2 & C_{k,i}^{(0)} - \tilde{D}_{q,i}(\gamma) F_{k,i}^{(0)} & \tilde{C}_{q,i}(\gamma) \end{bmatrix} \\
\tilde{D}_k(\rho,\gamma) &= \sum_{i=1}^{2^{n_p}} \alpha_i(\rho) [D_{k,i}^{(0)} + \tilde{D}_{q,i}(\gamma)]
\end{aligned} \tag{5.47}$$

where $\forall i \in \mathbb{I}[1, 2^{n_p}]$,

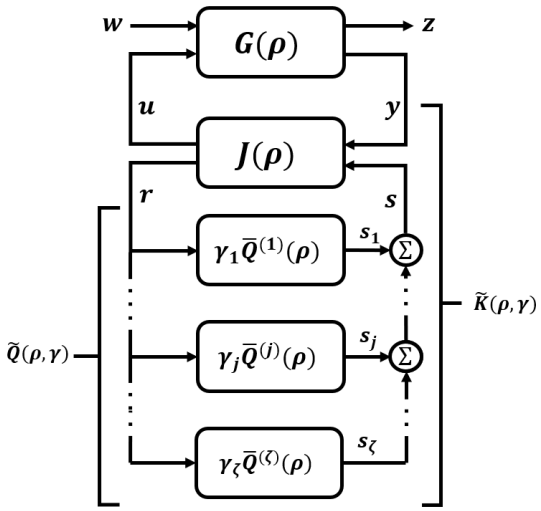

FIGURE 5.7: LPV-YK general configuration

$$
\begin{aligned}
\tilde{A}_{q,i} &= diag(Z_i^{(1)} A_{q,i}^{(1)} (Z_i^{(1)})^{-1}, \ldots, Z_i^{(j)} A_{q,i}^{(j)} (Z_i^{(j)})^{-1}, \ldots, Z_i^{(\zeta)} A_{q,i}^{(\zeta)} (Z_i^{(\zeta)})^{-1}), \\
\tilde{B}_{q,i} &= \begin{bmatrix} Z_i^{(1)} B_{q,i}^{(1)} & \ldots & Z_i^{(j)} B_{q,i}^{(j)} & \ldots & Z_i^{(\zeta)} B_{q,i}^{(\zeta)} \end{bmatrix}^T, \\
\tilde{C}_{q,i}(\gamma) &= \begin{bmatrix} \gamma_1 C_{q,i}^{(1)} (Z_i^{(1)})^{-1} & \ldots & \gamma_j C_{q,i}^{(j)} (Z_i^{(j)})^{-1} & \ldots & \gamma_\zeta C_{q,i}^{(\zeta)} (Z_i^{(\zeta)})^{-1} \end{bmatrix}, \\
\tilde{D}_{q,i}(\gamma) &= \sum_{j=1}^{\zeta} \gamma_j D_{q,i}^{(j)},
\end{aligned}
\tag{5.48}
$$

*$A_{q,i}^{(j)}$, $B_{q,i}^{(j)}$, $C_{q,i}^{(j)}$ and $D_{q,i}^{(j)}$ are the state-space matrices of $Q^{(j)}(\rho)$ given in (5.54) at the polytopic vertices w_i, $F_{g,i} = W_i X_g^{-1}$, $F_{k,i}^{(0)} = V_i X_{k,i}^{-1}$, and $Z_i^{(j)}$ are state transformation matrices chosen to satisfy **Lemma 5** such that $\bar{A}_q^{(j)}(\rho) = \sum_{i=1}^{2^{np}} \alpha_i(\rho) Z_i^{(j)} A_{q,i}^{(j)} (Z_i^{(j)})^{-1}$ is quadratically stable $\forall j \geq 1$.*

Proof 2. *According to YK parameterization concept, each parameterized controller can be formulated as a Linear Fractional Transformation (LFT) system [269]. Then, the LPV-YK controller can be written as $\tilde{K}(\rho,\gamma) = \mathcal{F}_l(J(\rho), \tilde{Q}(\rho,\gamma))$ (see Fig. 5.7), where $J(\rho)$ is represented in (5.49), and $\tilde{Q}(\rho,\gamma) = \sum_{i=1}^{\zeta} \gamma_j(t) \bar{Q}^{(j)}(\rho)$ being $\bar{Q}^{(j)}(\rho)$ a transformed system of $Q^{(j)}(\rho)$ (5.54) satisfying **Lemma 5**, to be shown later in the proof.*

$$
J(\rho) = \sum_{i=1}^{2^{np}} \alpha_i(\rho) \left[\begin{array}{cc|cc} A_i + B_2 F_{g,i} & 0 & 0 & B_2 \\ -B_{k,i}^{(0)} C_2 & A_{k,i}^{(0)} & B_{k,i}^{(0)} & 0 \\ \hline F_{g,i} - D_{k,i}^{(0)} C_2 & C_{k,i}^{(0)} & D_{k,i}^{(0)} & I \\ -C_2 & -F_{k,i}^{(0)} & I & 0 \end{array}\right]
\tag{5.49}
$$

The following proof is achieved by two steps:

1. *Prove that the LPV-YK parameter $\tilde{Q}(\rho,\gamma)$ is quadratically stable $\forall \rho \in \mathcal{P}$, $\forall \gamma$.*
2. *Prove the closed-loop quadratic stability $\forall \rho \in \mathcal{P}$, $\forall \gamma$.*

Step 1: *$\tilde{Q}(\rho,\gamma)$ can be proved to be quadratically stable $\forall\rho\in\mathcal{P}$ and $\forall\gamma$ as follows: Assuming (A.2.2), and since inequality (5.46) is satisfied, there exist symmetric, positive definite matrices $S_i^{(j)}\in\mathbb{R}^{(n_x+n_k^{(j)})\times(n_x+n_k^{(j)})}$ and $R_i\in\mathbb{R}^{n_k^{(0)}\times n_k^{(0)}}$ such that $\forall i,\forall j\geq 1$:*

$$S_i^{(j)}\mathcal{A}_i^{(j)}+\mathcal{A}_i^{(j)T}S_i^{(j)}<0 \tag{5.50}$$

$$(A_{k,i}^{(0)}+B_{k,i}^{(0)}F_{k,i}^{(0)})R_i+R_i(A_{k,i}^{(0)}+B_{k,i}^{(0)}F_{k,i}^{(0)})^T<0 \tag{5.51}$$

being,

$$\mathcal{A}_i^{(j)}=\begin{bmatrix}A_i+B_2D_{k,i}^{(j)}C_2 & B_2C_{k,i}^{(j)}\\ B_{k,i}^{(j)}C_2 & A_{k,i}^{(j)}\end{bmatrix} \tag{5.52}$$

with $R_i=X_{k,i}$ and $F_{k,i}^{(0)}=V_iX_{k,i}^{-1}$. Thus, $A_{q,i}^{(j)}$ is Hurwitz $\forall i,j$ and there exist symmetric, positive definite matrices $X_{q,i}^{(j)}=diag(S_i^{(j)},R_i)\in\mathbb{R}^{n_{q,i}^{(j)}\times n_{q,i}^{(j)}}$ such that:

$$X_{q,i}^{(j)}A_{q,i}^{(j)}+(A_{q,i}^{(j)})^TX_{q,i}^{(j)}<0\quad\forall i,\forall j \tag{5.53}$$

*Following **Lemma 5**, for any $j\geq 1$, there exist transformation matrices $Z_i^{(j)}$ such that the transformed system $\bar{Q}^{(j)}(\rho)$ is quadratically stable $\forall\rho\in\mathcal{P}^{(j)}$, choose $Z_i^{(j)}=(X_{q,i}^{(j)})^{1/2}$. As a result, $\tilde{Q}(\rho,\gamma)=\sum_{j=1}^{\zeta}\gamma_j\bar{Q}^{(j)}(\rho)$ is quadratically stable $\forall\rho\in\mathcal{P}$ and $\forall\gamma\in[0,1]$.*

$$
\begin{aligned}
Q^{(j)}(\rho) &= \sum_{i=1}^{2^{n_p}} \alpha_i(\rho) \left[\begin{array}{c|c} A_{q,i}^{(j)} & B_{q,i}^{(j)} \\ \hline C_{q,i}^{(j)} & D_{q,i}^{(j)} \end{array}\right] \\
&= \sum_{i=1}^{2^{n_p}} \alpha_i(\rho) \left[\begin{array}{cc:c|c} A_i + B_2 D_{k,i}^{(j)} C_2 & B_2 C_{k,i}^{(j)} & B_2[D_{k,i}^{(j)} - D_{k,i}^{(0)}]F_{k,i}^{(0)} - B_2 C_{k,i}^{(0)} & B_2[D_{k,i}^{(j)} - D_{k,i}^{(0)}] \\ B_{k,i}^{(j)} C_2 & A_{k,i}^{(j)} & B_{k,i}^{(j)} F_{k,i}^{(0)} & B_{k,i}^{(j)} \\ \hdashline 0 & 0 & A_{k,i}^{(0)} + B_{k,i}^{(0)} F_{k,i}^{(0)} & B_{k,i}^{(0)} \\ \hline [D_{k,i}^{(j)} C_2 - F_{g,i}] & C_{k,i}^{(j)} & [(D_{k,i}^{(j)} - D_{k,i}^{(0)})F_{k,i}^{(0)} - C_{k,i}^{(0)}] & [D_{k,i}^{(j)} - D_{k,i}^{(0)}] \end{array}\right]
\end{aligned} \tag{5.54}
$$

$$
\begin{aligned}
\bar{A}_{cl}(\rho,\gamma) &= \sum_{i=1}^{2^{n_p}} \alpha_i(\rho) T A_{cl,i}(\gamma) T^{-1} \\
&= \sum_{i=1}^{2^{n_p}} \alpha_i(\rho) \left[\begin{array}{cc:cc} A_i + B_2 F_{g,i} & B_2 \tilde{C}_{q,i}(\gamma) & -B_2(F_{g,i} - (D_{k,i}^{(0)} + \tilde{D}_{q,i}(\gamma))C_2) & B_2(C_{k,i}^{(0)} - \tilde{D}_{q,i}(\gamma)F_{k,i}^{(0)}) \\ 0 & \tilde{A}_{q,i} & \tilde{B}_{q,i} C_2 & -\tilde{B}_{q,i} F_{k,i}^{(0)} \\ \hdashline 0 & 0 & A_i + B_2 D_{k,i}^{(0)} C_2 & B_2 C_{k,i}^{(0)} \\ 0 & 0 & B_{k,i}^{(0)} C_2 & A_{k,i}^{(0)} \end{array}\right]
\end{aligned} \tag{5.55}
$$

$$CL(\rho,\gamma)=\sum_{i=1}^{2^{n_p}}\alpha_i(\rho)\left[\begin{array}{ccc|c} A_i+B_2(D_{k,i}^{(0)}+\tilde{D}_{q,i}(\gamma))C_2 & B_2(F_{g,i}-(D_{k,i}^{(0)}+\tilde{D}_{q,i}(\gamma))C_2) & B_2(C_{k,i}^{(0)}-\tilde{D}_{q,i}(\gamma)F_{k,i}^{(0)}) & B_2\tilde{C}_{q,i}(\gamma) & B_{1,i}+B_2(D_{k,i}^{(0)}+\tilde{D}_{q,i}(\gamma))D_{21} \\ B_2\tilde{D}_{q,i}(\gamma)C_2 & A_i+B_2(F_{g,i}-\tilde{D}_{q,i}(\gamma)C_2) & -B_2\tilde{D}_{q,i}(\gamma)F_{k,i}^{(0)} & B_2\tilde{C}_{q,i}(\gamma) & B_2\tilde{D}_{q,i}(\gamma)D_{21} \\ B_{k,i}^{(0)}C_2 & -B_{k,i}^{(0)}C_2 & A_{k,i}^{(0)} & 0 & B_{k,i}^{(0)}D_{21} \\ \tilde{B}_{q,i}C_2 & -\tilde{B}_{q,i}C_2 & -\tilde{B}_{q,i}F_{k,i}^{(0)} & \tilde{A}_{q,i} & \tilde{B}_{q,i}D_{21} \\ \hline C_{1,i}+D_{12}(D_{k,i}^{(0)}+\tilde{D}_{q,i}(\gamma))C_2 & D_{12}(F_{g,i}-(D_{k,i}^{(0)}+\tilde{D}_{q,i}(\gamma))C_2) & D_{12}(C_{k,i}^{(0)}-\tilde{D}_{q,i}(\gamma)F_{k,i}^{(0)}) & D_{12}\tilde{C}_{q,i}(\gamma) & D_{11,i}+D_{12}(D_{k,i}^{(0)}+\tilde{D}_{q,i}(\gamma))D_{21} \end{array}\right] \tag{5.56}$$

Step 2: *The closed-loop system $CL(\rho,\gamma)$ (5.56) is derived from the LFT interconnection between $G(\rho)$ and $\tilde{K}(\rho,\gamma)$ (see Fig. 5.5). Its state matrix $A_{cl}(\rho,\gamma) = \sum_{i=1}^{2^{n_p}} \alpha_i(\rho) A_{cl,i}(\gamma)$ is quadratically stable if there exist a symmetric, positive definite, constant matrix X_{cl} such that:*

$$X_{cl} A_{cl}(\rho,\gamma) + A_{cl}^T(\rho,\gamma) X_{cl} < 0 \quad \forall\gamma \tag{5.57}$$

Now , let $T = \begin{bmatrix} I & 0 & 0 & 0 \\ 0 & 0 & 0 & I \\ I & -I & 0 & 0 \\ 0 & 0 & I & 0 \end{bmatrix}$ *be a state transformation matrix which is applied to $CL(\rho,\gamma)$ without changing its input-output nature, with* $T^{-1} = \begin{bmatrix} I & 0 & 0 & 0 \\ I & 0 & -I & 0 \\ 0 & 0 & 0 & I \\ 0 & I & 0 & 0 \end{bmatrix}$.

Due to the block-triangular form of $\bar{A}_{cl}(\rho,\gamma)$ (5.55) , (5.57) is satisfied if the following equations hold (check Lemma 2 in [296]):

$$\sum_{i=1}^{2^{n_p}} \alpha_i(\rho)(Y_g(A_i + B_2 F_{g,i}) + (A_i + B_2 F_{g,i})^T Y_g) < 0 \tag{5.58}$$

$$\sum_{i=1}^{2^{n_p}} \alpha_i(\rho)(Y_q \tilde{A}_{q,i} + \tilde{A}_{q,i}^T Y_q) < 0 \tag{5.59}$$

$$\sum_{i=1}^{2^{n_p}} \alpha_i(\rho)(Y_0 \mathcal{A}_i^{(0)} + \mathcal{A}_i^{(0)T} Y_0) < 0 \tag{5.60}$$

where $Y_g \in \mathbb{R}^{n_x \times n_x}$, $Y_q \in \mathbb{R}^{n_q^{(1)} \times n_q^{(1)}}$ and $Y_0 \in \mathbb{R}^{(n_x+n_k^{(0)})\times(n_x+n_k^{(0)})}$ are symmetric, positive definite, parameter-invariant matrices, choosing $X_{cl} = T^T\, diag(Y_g, Y_q, Y_0)\, T$, with

$$\mathcal{A}_i^{(0)} = \begin{bmatrix} A_i + B_2 D_{k,i}^{(0)} C_2 & B_2 C_{k,i}^{(0)} \\ B_{k,i}^{(0)} C_2 & A_{k,i}^{(0)} \end{bmatrix} \tag{5.61}$$

Therefore,

- *Inequality (5.58) is equivalent to (5.45) by choosing $Y_g = X_g^{-1}$ and $W_i = F_{g,i} X_g$.*
- *Since $\tilde{Q}(\rho,\gamma)$ is proved to be quadratically stable, inequality (5.36) is satisfied.*
- *(5.60) is fulfilled given that $K^{(0)}(\rho)$ quadratically stabilizes $G(\rho)$.*

It is worth mentioning that the problem complexity refers mainly to find a nominal LPV controller $K^{(0)}(\rho)$ which must quadratically stabilize $G(\rho)$, i.e. assumption (A.2.1). The rest is carried out using classical LTI control approaches. This shows an interest since a quadratically stabilizing gain-scheduled controller $K^{(j)}(\rho)$ can be designed based on an interpolation of LTI controllers, with lower conservatism compared to the standard polytopic design. In addition, the interpolation of several gain-scheduled controllers, with any finite continuous/discontinuous interpolating signals γ_j, provides a general multi-variable and multi-objective controller $\tilde{K}(\rho,\gamma)$ based on LPV-YK concept.

The next sections introduce LPV-YK control structures aiming to achieve stable smooth switching between parameter partitions.

5.6 Switching between Parameter Subsets

This section proposes two different LPV-YK structures aiming to switch between different parameter subsets. This is usually needed when dealing with large number of varying parameters or large variations. Thus, the aim is not to change the closed-loop performance, but to maintain a closed-loop robust performance over the wide parameter variations. The following two subsections discuss the limitations of both polytopic and grid-based approaches, and some solutions that have been proposed in the literature.

5.6.1 Polytopic Approach

As discussed in Chapter 2, the polytopic approach is known to be the most conservative one [14]. One of the main causes is that the polytopic LPV synthesis requires a constant Lyapunov function to ensure quadratic stability, which increases the problem conservatism.

Moreover, the overbounding of the parameter set is considered as a main cause of conservatism. The operating region of the underlying LPV model is defined by a convex polytope containing the parameter trajectories. This convex parameter region may include vertices that are not attained by the real plant, resulting in conservatism. The reason is that the construction of the polytope is based on the assumption that all parameters vary independently (in the affine parameter dependency formulation), whereas they could be related to each other by inherent couplings. For example, the known bicycle model describing the lateral dynamics of an autonomous vehicle is parameterized by the scheduling parameters "v_x" and "$1/v_x$" [23] (being v_x the longitudinal speed). Such a situation might cause unstable models at the polytopic vertices. In addition, the parameters could be physically correlated with each other, such that some combinations of extreme values of the parameters do not occur in real operation. For example, an LPV model describing the vertical flight dynamics of an aeroplane might be parameterized by the external scheduling signals (i.e., parameters) “speed” and “altitude.” But usually, the maximum speed is not reached for minimum altitude and vice versa [24].

Several solutions have been investigated in the literature to find a reduced convex parameter region, as presented in the recent survey [25]. [380] has recently proposed a methodology for polytopic vertices reduction. [26] suggests to construct convex polyhedrons along given parameter trajectories, and solve the control design problem using affine parameter-dependent LMIs. Unfortunately, these methods often result in a huge number of vertices or nonconvex parameter sets and thus in increased computational burden. Scheduling Dimension Reduction (SDR) approach is proposed in [24] which reduces the parameter set based on experimental data, and yields the benefit of tailoring a control design to specific trajectories. In [31], a Deep Neural Network (DNN) approach is used to develop the SDR methods and achieve higher model accuracy under scheduling dimension reduction. In [32] and [33], authors develop an LPV switching controller and prove its stability when switching among the overlapped subsets of a polytopic parameter region.

Concerning YK methods, in [298], a YK configuration is proposed to improve the performance of a polytopic LPV control. On the other hand, [297] proposes a YK-based gain-scheduled controller by interpolating LTI controllers designed separately at the different vertices of a polytopic parameter region. The interpolation is performed as a function of the varying parameters of the LPV model. Closed-loop quadratic stability and performance are guaranteed at intermediate interpolation

points of the convex domain. In [299], a fixed pole-assignment application is introduced using an LPV YK-based method to preserve the closed-loop poles at the same location by interpolating between different controllers.

In addition, in our previous work [300], an LPV-YK control scheme has been proposed to interpolate between two LPV controllers, each one designed over a full polytopic region, to achieve multiple control performances. On the other hand, all the previous YK-based solutions are still conservative for systems having overbounding polytopic parameter region.

5.6.2 Grid-based Approach

The grid-based approach uses a parameter-dependent Lyapunov function to solve a set of parameter-dependent LMIs (pLMIs). Since a single parameter-dependent Lyapunov function could not be efficient for complex designs and large parameter regions, a first solution has been proposed in [142]. The objective is to design multiple LPV controllers based on multiple parameter-varying Lyapunov functions, each suitable for a specific parameter subregion, and switch between them to achieve better performance. The switching stability has been studied for hysteresis switching and switching with average dwell-time strategies. This methodology enhances the use of the switched LPV techniques in several applications, see for instance [173], [199], [184] ,[206].

On the other hand, it has been stated in [142] that the switched LPV controllers may not provide a smooth transient response during switching, where aggressive performance is obtained at switching instants. Such a case may lead to mechanical damage, decrease material lifetime, or signal saturation which is out of real application objectives. Following this work, several research studies have been involved in solving the switching smoothness. For instance, a bumpless transfer of switching controllers is proposed in [238] followed by some developments in [239], [229], and [240].

Finally, a smooth switching LPV controller has been proposed in [208]. It is designed in considering adjustable interpolation functions and a higher order differential control signal. An iterative descent algorithm is applied to optimize three decision variables (the parameter-dependent Lyapunov functions, the local controllers, and the interpolation functions). It also augments the problem to two dimensional parameter regions. This concept is developed in the recent works [210] and [214], however, it increases the complexity and the design constraints of the local LPV controllers to achieve their objectives.

Notations. *The following notations are used in the next two subsections 5.6.3 and 5.6.4. The subscript i of a system/matrix/variable of an LPV plant (e.g. $G(\rho)$) denotes the LPV system/matrix/variable of the plant when the varying-parameter $\rho \in \mathcal{P}_i$, where $\mathcal{P}_i$ is a subset of the full parameter region $\mathcal{P}$. In addition, the second subscript j, when used, corresponds to the j^{th} vertex of a polytope. For example, $A_{k,ij}$ represents the state matrix of the i^{th} LPV local controller in the polytope $\mathcal{P}_i$ at the j^{th} vertex of $\mathcal{P}_i$.*

5.6.3 Partitioned Gain-scheduled Control

This section proposes a partitioned gain-scheduled controller which solves the overbounding and conservatism problems of the standard polytopic controller. It presents an LPV-YK control scheme which:

1. Formulates a YK-based gain-scheduling between LTI controllers that have been already designed separately at the polytopic vertices of each parameter subset.

2. Switches between the formulated gain-scheduling controllers over the partitioned polytopic subregions.

The closed-loop system is proved to guarantee the quadratic stability for any continuous/discontinuous switching signals in terms of a set of Linear Matrix Inequalities (LMIs).

Define $\mathcal{P}_0$ as a convex polytope that contains all the parameter trajectories $\rho \in \mathbb{R}^{n_p}$. Let $\mathcal{P}_i$, $i \in Z_N = \{1, \ldots, N\}$, be the convex polytopic subsets, that could intersect by a boundary or surface, defined in $\mathcal{P}_0$ along the parameter trajectories, i.e. $\rho \in \mathcal{P} = \bigcup_{i \geq 1} \mathcal{P}_i \subset \mathcal{P}_0$. Each $\mathcal{P}_i$ ($i \geq 0$) is defined as:

$$\mathcal{P}_i := \mathcal{C}_{\mathcal{O}}\{w_{i1}, ..., w_{i2^{n_p}}\} \tag{5.62}$$

where w_{ij} represent the polytopic vertices of $\mathcal{P}_i$ $\forall j \in \mathbb{I}[1, 2^{n_p}]$. ρ is then scheduled as:

$$\forall \rho \in \mathcal{P}_i, \quad \rho = \sum_{j=1}^{2^{n_p}} \alpha_{ij}(\rho) w_{ij}, \qquad i \in \{1, \ldots, N\} \tag{5.63}$$

and $\forall i \sum_{j=1}^{2^{n_p}} \alpha_{ij}(\rho) = 1$, $\alpha_{ij}(\rho) \geq 0$ $\forall i, j$, being $\alpha_{ij}(\rho)$ the scheduling coefficients in the convex region $\mathcal{P}_i$.

Fig. 5.8 shows an example of a convex parameter region defined by two varying parameters $\rho_1 \in [\underline{\rho}_1, \bar{\rho}_1]$, and $\rho_2 \in [\underline{\rho}_2, \bar{\rho}_2]$, with $\rho_2 = 1/\rho_1$. The convex region $\mathcal{P}_0$ is represented in solid orange, and the convex subregions $\mathcal{P}_i$ ($i \geq 1$) are bounded within dashed green polygons.

The LPV representation of $G(\rho)$ is defined over $\mathcal{P}_0$ as a convex combination of the state-space realizations of the local LTI systems G_{0j} at the vertices w_{0j}:

$$\left[\begin{array}{c|cc} A(\rho) & B_1(\rho) & B_2 \\ \hline C_1(\rho) & D_{11}(\rho) & D_{12} \\ C_2 & D_{21} & 0 \end{array}\right] = \sum_{j=1}^{2^{n_p}} \alpha_{0}j(\rho) \left[\begin{array}{c|cc} A_{0j} & B_{1,0j} & B_2 \\ \hline C_{1,0j} & D_{11,0j} & D_{12} \\ C_2 & D_{21} & 0 \end{array}\right] \tag{5.64}$$

Notice that $G(\rho)$ could be defined equivalently in terms of the LTI plants G_{ij} (at w_{ij}) as, for $\rho \in \mathcal{P}_i$:

$$\left[\begin{array}{c|cc} A(\rho) & B_1(\rho) & B_2 \\ \hline C_1(\rho) & D_{11}(\rho) & D_{12} \\ C_2 & D_{21} & 0 \end{array}\right] = \sum_{j=1}^{2^{n_p}} \alpha_{ij}(\rho) \left[\begin{array}{c|cc} A_{ij} & B_{1,ij} & B_2 \\ \hline C_{1,ij} & D_{11,ij} & D_{12} \\ C_2 & D_{21} & 0 \end{array}\right] \tag{5.65}$$

Now, assume that

(A.3.1). *There exists an LPV output-feedback controller $K_0(\rho)$ which quadratically stabilizes $G(\rho)$ (using the standard polytopic approach in [7]) over the full parameter region $\mathcal{P}_0$, defined as:*

$$K_0(\rho) : \left[\begin{array}{c|c} A_{k,0}(\rho) & B_{k,0}(\rho) \\ \hline C_{k,0}(\rho) & D_{k,0}(\rho) \end{array}\right] \tag{5.66}$$

being,

$$\left[\begin{array}{c|c} A_{k,0}(\rho) & B_{k,0}(\rho) \\ \hline C_{k,0}(\rho) & D_{k,0}(\rho) \end{array}\right] = \sum_{j=1}^{2^{n_p}} \alpha_{0j}(\rho) \left[\begin{array}{c|c} A_{k,0j} & B_{k,0j} \\ \hline C_{k,0j} & D_{k,0j} \end{array}\right] \tag{5.67}$$

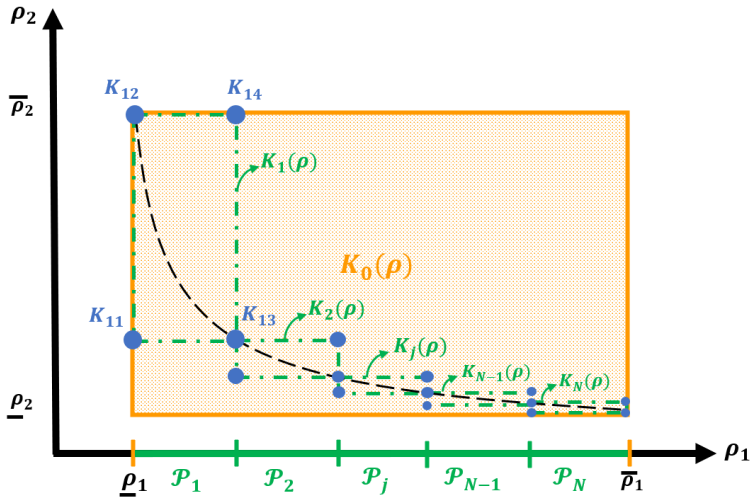

FIGURE 5.8: Partitioned polytopic regions

where $A_{k,0}(\rho) \in \mathbb{R}^{n_{k,0} \times n_{k,0}}$, $B_{k,0}(\rho) \in \mathbb{R}^{n_{k,0} \times m_k}$, $C_{k,0}(\rho) \in \mathbb{R}^{p_k \times n_{k,0}}$ *and* $D_{k,0}(\rho) \in \mathbb{R}^{p_k \times m_k}$.

(A.3.2). *At each vertex* w_{ij} ($j \in \mathbb{I}[1, 2^{n_p}]$, $i \geq 1$), *a local LTI controller* K_{ij} *is designed separately to stabilize the local plant* G_{ij}. *It is worth mentioning that, at each intersecting boundary, a unique LTI controller should be designed at the intersecting extremums of the adjacent subsets respectively.*

Regarding the example in Fig. 5.8, the local LTI controllers at the intersecting boundaries w_{i3} (at K_{i3}) and $w_{(i+1)2}$ (at $K_{(i+1)2}$), $\forall i \in \mathbb{I}[1, N-1]$, are designed similarly. Consequently, the switching between two successive subsets ($\mathcal{P}_i$ and $\mathcal{P}_{i+1}$) undergoes using the same LTI controller ($K_{i3} \equiv K_{(i+1)2}$). In such a case, the state and control input energies, just before and just after switching, are not affected.

The objective of the work in this section is to:

1. Design multiple YK-based gain-scheduled controllers $\tilde{K}_i(\rho)$, $i \in \mathbb{I}[1, N]$. Each one is designed by interpolating its corresponding LTI controllers K_{ij} ($j \in \mathbb{I}[1, 2^{n_p}]$) based on YK concept (refer to Fig. 5.8).

2. Create an overall switched LPV-YK controller $\tilde{K}_\sigma(\rho)$ to switch between $\tilde{K}_i(\rho)$, such that $\tilde{K}_\sigma(\rho)$ quadratically stabilizes $G(\rho)$ $\forall \rho \in \mathcal{P}$ and for every continuous/discontinuous switching signal $\sigma(t)$. The switched closed-loop system is represented as

$$\tilde{CL}_\sigma(\rho) : \left[\begin{array}{c|c} \tilde{A}_{cl,\sigma}(\rho) & \tilde{B}_{cl,\sigma}(\rho) \\ \hline \tilde{C}_{cl,\sigma}(\rho) & \tilde{D}_{cl,\sigma}(\rho) \end{array}\right] \tag{5.68}$$

To illustrate the proposed approach, Fig. 5.8 represents an example of a convex parameter set partitioning. The dashed black curve represents the actual operating conditions of the parameters ($\rho_2 = 1/\rho_1$). The orange solid polygon represents the nominal LPV controller $K_0(\rho)$ designed using standard polytopic approach over the convex region $\mathcal{P}_0$. The blue points represent the local LTI controllers K_{ij} ($j \in \mathbb{I}[1, 4]$, $i \in \mathbb{I}[1, N]$) designed separately to stabilize G_{ij} at w_{ij} using any LTI control approaches. The green dashed polygons are the subsets chosen along the parameter trajectory. Over each subset $\mathcal{P}_i$, a gain-scheduled controller $\tilde{K}_i(\rho)$ is designed based

on the YK interpolation of the local LTI controllers K_{ij}. The overall switching scheme between the $\tilde{K}_i(\rho)$ is represented by the LPV-YK controller $\tilde{K}_\sigma(\rho)$.

The LPV-YK controllers $\tilde{K}_i(\rho)$ are designed based on a Linear Matrix Inequality (LMI) optimization problem, where they are defined as

$$\tilde{K}_i(\rho) : \left[\begin{array}{c|c} \tilde{A}_{k,i}(\rho) & \tilde{B}_{k,i}(\rho) \\ \hline \tilde{C}_{k,i}(\rho) & \tilde{D}_{k,i}(\rho) \end{array}\right] \tag{5.69}$$

The next theorem proves the quadratic stability of the closed-loop system $\tilde{CL}_\sigma(\rho)$ (5.68) for every $\rho \in \mathcal{P}$.

Theorem 7. *Consider an LPV plant $G(\rho)$ (5.19), satisfying assumptions (A.3.1) and (A.3.2). Then, the switched LPV-YK controller $\tilde{K}_\sigma(\rho)$ (5.69)-(5.72), represented in Fig. 5.9, quadratically stabilizes $G(\rho)$ for any $\rho \in \mathcal{P}$ and for any continuous/discontinuous switching signals $\gamma_i \in [0,1]$ ($\forall i \geq 1$), if there exist symmetric, positive definite, constant matrices $X_g \in \mathbb{R}^{n_x \times n_x}$, $X_{k,ij} \in \mathbb{R}^{n_{k,ij} \times n_{k,ij}}$, and matrices $W_j \in \mathbb{R}^{m \times n_x}$ and $V_{ij} \in \mathbb{R}^{m_k \times n_{k,ij}}$ such that:*

$$A_{0j}X_g + X_g A_{0j}^T + B_2 W_j + W_j^T B_2^T < 0 \quad \forall w_{0j} \tag{5.70}$$

$$A_{k,0}(w_{ij})X_{k,ij} + X_{k,ij}A_{k,0}^T(w_{ij}) + B_{k,0}(w_{ij})V_{ij} + V_{ij}^T B_{k,0}^T(w_{ij}) < 0 \quad \forall w_{ij} \tag{5.71}$$

with the state-space matrices of $\tilde{K}_i(\rho)$ are

$$\begin{aligned}
\tilde{A}_{k,i}(\rho) &= \sum_{j=1}^{2^{n_p}} \alpha_{ij}(\rho) \begin{bmatrix} A_{ij} + B_2 F_{g,ij} - B_2 \bar{D}_{q,ij} C_2 & -B_2 \bar{D}_{q,ij} F_{k,ij} & B_2 \bar{C}_{q,ij} \\ -B_{k,0}(w_{i,j}) C_2 & A_{k,0}(w_{i,j}) & 0 \\ -\bar{B}_{q,ij} C_2 & -\bar{B}_{q,ij} F_{k,ij} & \bar{A}_{q,ij} \end{bmatrix} \\
\tilde{B}_{k,i}(\rho) &= \sum_{j=1}^{2^{n_p}} \alpha_{ij}(\rho) \begin{bmatrix} B_2 \bar{D}_{q,ij} & B_{k,0}(w_{i,j}) & \bar{B}_{q,ij} \end{bmatrix} \\
\tilde{C}_{k,i}(\rho) &= \sum_{j=1}^{2^{n_p}} \alpha_{ij}(\rho) \begin{bmatrix} F_{g,ij} - (D_{k,ij} + D_{q,ij}) C_2 & \\ & C_{k,0}(w_{i,j}) - D_{q,ij} F_{k,ij} \quad \bar{C}_{q,ij} \end{bmatrix} \\
\tilde{D}_{k,i}(\rho) &= \sum_{j=1}^{2^{n_p}} \alpha_{ij}(\rho) [D_{k,0}(w_{i,j}) + \bar{D}_{q,ij}]
\end{aligned} \tag{5.72}$$

$\forall i \in \mathbb{I}[1, N]$,

*where $\bar{A}_{q,ij} = Z_{ij} A_{q,ij} (Z_{ij})^{-1}$, $\bar{B}_{q,ij} = Z_{ij} B_{q,ij}$, and $\bar{C}_{q,ij} = C_{q,ij}(Z_{ij})^{-1}$ $\forall i, j$, and Z_{ij} are state transformation matrices chosen, to satisfy **Lemma 5**, such that $\bar{A}_{q,i}(\rho) = \sum_{j=1}^{2^{n_p}} \alpha_j(\rho) Z_{ij} A_{q,ij} (Z_{ij})^{-1}$ is quadratically stable $\forall i \geq 1$. $A_{q,ij}$, $B_{q,ij}$, $C_{q,ij}$ and $D_{q,ij}$ are the state-space matrices of $Q_i(\rho)$ (5.74) at the polytopic vertices w_{ij}. In addition, $F_{g,j} = W_j X_g^{-1}$, $F_{k,ij} = V_{ij}(X_{k,ij})^{-1}$, and $F_{g,ij} = F_g(w_{ij})$.*

Proof 3. *As mentioned in the previous proofs, each parameterized controller can be formulated as a Linear Fractional Transformation (LFT) system [269]. Each LPV-YK controller can be written as $\tilde{K}_i(\rho) = \mathcal{F}_l(J(\rho), \bar{Q}_i(\rho))$ $\forall \rho \in \mathcal{P}_i$ (see Fig. 5.9), where $J(\rho)$ is represented in (5.73), and $\bar{Q}_i(\rho)$ is the transformed system of $Q_i(\rho)$ (5.74).*

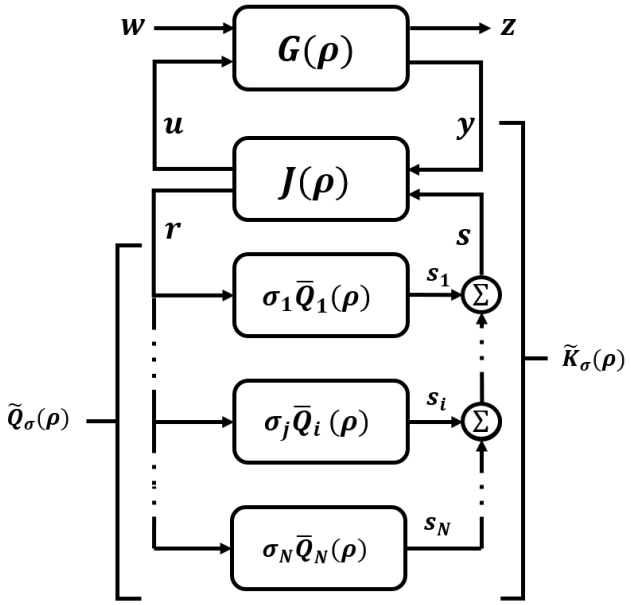

FIGURE 5.9: Partitioned polytopic-based generalized LPV-YK configuration

$$J(\rho) = \sum_{j=1}^{2^{n_p}} \alpha_i j(\rho) \left[\begin{array}{cc|cc} A_{ij} + B_2 F_{g,ij} & 0 & 0 & B_2 \\ -B_{k,0}(w_{ij})C_2 & A_{k,0}(w_{ij}) & B_{k,0}(w_{ij}) & 0 \\ \hline F_{g,ij} - D_{k,0}(w_{ij})C_2 & C_{k,0}(w_{ij}) & D_{k,0}(w_{ij}) & I \\ -C_2 & -F_{k,ij} & I & 0 \end{array}\right] \tag{5.73}$$

$$Q_i(\rho) = \sum_{j=1}^{2^{n_p}} \alpha_{ij}(\rho) \left[\begin{array}{cc:c|c} A_{ij} + B_2 D_{k,ij} C_2 & B_2 C_{k,ij} & B_2[D_{k,ij} - D_{k,0}(w_{ij})]F_{k,ij} - B_2 C_{k,0}(w_{ij}) & B_2[D_{k,ij} - D_{k,0}(w_{ij})] \\ B_{k,ij} C_2 & A_{k,ij} & B_{k,ij} F_{k,ij} & B_{k,ij} \\ \hdashline 0 & 0 & A_{k,0}(w_i ij) + B_{k,0}(w_{ij}) F_{k,ij} & B_{k,0}(w_{ij}) \\ \hline D_{k,ij} C_2 - F_{g,ij} & C_{k,ij} & (D_{k,ij} - D_{k,0}(w_{ij}))F_{k,ij} - C_{k,0}(w_{ij}) & D_{k,ij} - D_{k,0}(w_{ij}) \end{array}\right] \tag{5.74}$$

$$\begin{aligned} \bar{A}_{cl,i}(\rho) &= \sum_{j=1}^{2^{n_p}} \alpha_{ij}(\rho) T A_{cl,ij}(\gamma) T^{-1} \\ &= \sum_{j=1}^{2^{n_p}} \alpha_{ij}(\rho) \left[\begin{array}{cc:c:c} A_{ij} + B_2 F_{g,ij} & B_2 \bar{C}_{q,ij} & -B_2(F_{g,ij} - (D_{k,0}(w_{ij}) + \bar{D}_{q,ij})C_2) & B_2(C_{k,0j}(w_{ij}) - \tilde{D}_{q,ij} F_{k,ij}) \\ 0 & \bar{A}_{q,ij} & \bar{B}_{g,ij} C_2 & -\bar{B}_{q,ij} F_{k,ij} \\ \hdashline 0 & 0 & A_{ij} + B_2 D_{k,0}(w_{ij}) C_2 & B_2 C_{k,0}(w_{ij}) \\ 0 & 0 & B_{k,0}(w_{ij}) C_2 & A_{k,0}(w_{ij}) \end{array}\right] \end{aligned} \tag{5.75}$$

The following proof is achieved by two steps: 1) Prove that the LPV-YK parameter $\bar{Q}_i(\rho)$ is quadratically stable $\forall \rho \in \{\mathcal{P}_i\}_{i\in Z_N}$; and 2) Prove the closed-loop quadratic stability $\forall \rho \in \{\mathcal{P}_i\}_{i\in Z_N}$, $\forall \sigma$.

Step 1:

*Knowing that: 1) K_{ij} stabilizes G_{ij} $\forall i \geq 1, \forall j \in [1, 2^{n_p}]$; and 2) (5.71) is satisfied, it can be shown that the triangular elements of $A_{q,ij}$ $\forall i, j$ are Hurwitz, and consequently, $A_{q,ij}$ is Hurwitz $\forall i, j$. According to **Lemma 5**, for any $i \geq 1$, there exist transformation matrices Z_{ij} such that the transformed system $\bar{Q}_i(\rho)$ is quadratically stable $\forall \rho \in \mathcal{P}_i$, choose $Z_{ij} = (X_{q,ij})^{1/2}$. As a result, $\bar{Q}_i(\rho)$ is quadratically stable $\forall \rho \in \mathcal{P}_i$.*

Step 2:

The switched closed-loop system $CL_\sigma(\rho)$ is derived from the LFT interconnection between $G(\rho)$ and $\tilde{K}_\sigma(\rho)$ (see Fig. 5.9).

The switched closed-loop state matrix $A_{cl,\sigma}(\rho) = \sum_{j=1}^{2^{n_p}} \alpha_{\sigma j}(\rho) A_{cl,\sigma j}$ is quadratically stable if:

1. *There exist symmetric, positive definite, constant matrices $X_{cl,i}$ such that $\forall i \geq 1$*

$$X_{cl,i}\tilde{A}_{cl,i}(\rho) + \tilde{A}_{cl,i}^T(\rho)X_{cl,i} < 0 \quad \forall \rho \in \mathcal{P}_i \tag{5.76}$$

2. *$\forall t_k \in [0, T]$, $V(x_{cl}(t_k)) \leq V(x_{cl}(t_k^-))$*

Taking the same state transformation matrix $T = \begin{bmatrix} I & 0 & 0 & 0 \\ 0 & 0 & 0 & I \\ I & -I & 0 & 0 \\ 0 & 0 & I & 0 \end{bmatrix}$, the transformed closed-loop state matrix $\bar{A}_{cl,i}(\rho)$ is represented in (5.75).

Due to its block-triangular form, (5.76) is then satisfied if the following equations hold (check Lemma 2 in [296]):

$$\sum_{j=1}^{2^{n_p}} \alpha_{ij}(\rho)(Y_{g,i}(A_{ij} + B_2F_{g,ij}) + (A_{ij} + B_2F_{g,ij})^T Y_{g,i}) < 0 \tag{5.77}$$

$$\sum_{j=1}^{2^{n_p}} \alpha_{ij}(\rho)(Y_{q,i}\bar{A}_{q,ij} + \bar{A}_{q,ij}^T Y_{q,i}) < 0 \tag{5.78}$$

$$\sum_{j=1}^{2^{n_p}} \alpha_{ij}(\rho)(Y_i\mathcal{A}_{ij} + \mathcal{A}_{ij}^T Y_i) < 0 \tag{5.79}$$

where $Y_{g,i} \in \mathbb{R}^{n_x \times n_x}$, $Y_{q,i} \in \mathbb{R}^{n_q \times n_q}$ and $Y_i \in \mathbb{R}^{(n_x+n_{k,0})\times(n_x+n_{k,0})}$ are symmetric, positive definite, constant matrices, choosing $X_{cl,i} = T^T\, diag(Y_{g,i}, Y_{q,i}, Y_i)\, T$, with

$$\mathcal{A}_{ij} = \begin{bmatrix} A_{ij} + B_2D_{k,0}(w_{ij})C_2 & B_2C_{k,0}(w_{ij}) \\ B_{k,0}(w_{ij})C_2 & A_{k,0}(w_{ij}) \end{bmatrix} \tag{5.80}$$

- *Inequality (5.77) is equivalent to (5.70) by choosing $Y_{g,i} = X_g^{-1}$ and $W_j = F_{g,ij}X_g$ for every $\rho \in \mathcal{P}_i$.*

- *Since $\bar{Q}_i(\rho)$) is proved to be quadratically stable $\forall i$, inequality (5.78) is satisfied.*
- *(5.79) is fulfilled given that $K_0(\rho)$ quadratically stabilizes $G(\rho)$ over $\mathcal{P}_0$, and consequently over any $\mathcal{P}_i \subset \mathcal{P}_0$.*

Therefore condition (5.76) is satisfied.

Assume a sequence of finite switching time over the interval $[0, T]$ is $t_0, t_1, \ldots, t_n$ with $t_0 = 0$, knowing that the closed-loop Lyapunov function is defined as $V(x_{cl}) = x_{cl}^T X_{cl,\sigma} x_{cl}$. From the YK basic concept, the closed-loop is written as $\mathcal{F}_l(G, J, Q)$. Consider a switching between any two adjacent subsets $\mathcal{P}_i$ and $\mathcal{P}_{i+1}$ $\forall i \geq 1$ at time t_k, then, the closed-loop dynamics switches from $\mathcal{F}_l(G, J, Q_{i,3})$ to $\mathcal{F}_l(G, J, Q_{i+1,2})$, or vise-versa. According to (A.3.2), $K_{i,3} \equiv K_{i+1,2}$ $\forall i \geq 1$, consequently $Q_{i,3} \equiv Q_{i+1,2}$. Then, for any switching time t_k, $\mathcal{F}_l(G, J, Q_{i,3}) = \mathcal{F}_l(G, J, Q_{i+1,2})$, and thus $V(x_{cl}(t_k)) = V(x_{cl}(t_k^-))$.

As a result, the switched closed-loop system $CL_\sigma(\rho)$ is quadratically stable $\forall \rho \in \mathcal{P}$, and for any switching signal σ.

5.6.4 Grid-based LPV-YK Control

In this section, a switching between consecutive parameter partitions is attained with a closed-loop exponential stability. Recall that the grid-based LPV approach has shown interesting results for our experimental results shown in Chapter 5. However, to achieve robust closed-loop performance with large parameter variations, multiple grid-based LPV controllers can be designed each suitable for its corresponding parameter subset. Specifically, the nominal LPV controller $K_0(\rho)$ and the others $K_i(\rho)$ ($i \in \{1, \ldots, N\}$) exponentially stabilize the LPV plant. This is performed without asking an affine parameter dependency assumption of the LPV model. Consider the general LPV system $G(\rho)$ (5.17) with m inputs and p outputs. All the state-space data are continuous functions of the parameter vector ρ. Assume that ρ is in a compact set $\mathcal{P} \subset \mathbb{R}^s$ with its parameter variation rate bounded by $\underline{\nu_k} \leq \dot{\rho}_k \leq \overline{\nu}_k$ for $k = 1, 2, ..., s$. Moreover, let us assume the following:

- $(A(\rho), B_2(\rho), C_2(\rho))$ triple is parameter-dependent stabilizable and detectable $\forall \rho \in \mathcal{P}$.
- $\begin{bmatrix} B_2^T(\rho) & D_{12}^T(\rho) \end{bmatrix}$ and $\begin{bmatrix} C_2(\rho) & D_{21}(\rho) \end{bmatrix}$ have full row ranks $\forall \rho \in \mathcal{P}$.
- $D_{22}(\rho) = 0$.

Suppose that the parameter set $\mathcal{P}$ is covered by a finite number of closed subsets $\{\mathcal{P}_i\}_{i \in Z_N}$, where the index set $Z_N = \{1, 2, \ldots, N\}$, and $\mathcal{P} = \bigcup \mathcal{P}_i$. At the boundaries between each adjacent subsets, there exist at least a single intersecting boundary or an intersecting surface.

Now, assume that

(A.4.1). *There exists an LPV output-feedback controller $K_0(\rho)$ which exponentially stabilizes $G(\rho)$ at the full parameter region $\mathcal{P}_0 := \mathcal{P}$. (following the grid-based approach in [18]),*

(A.4.2). *Over each parameter subset $\{\mathcal{P}_i\}_{i \in Z_N}$, there exists an LPV controller $K_i(\rho)$ predesigned separately and exponentially stabilize $G(\rho)$ over $\{\mathcal{P}_i\}_{i \in Z_N}$. Each $K_i(\rho)$ is designed, based on grid-based approach, to achieve a suitable performance in its corresponding parameter region $\{\mathcal{P}_i\}_{i \in Z_N}$*

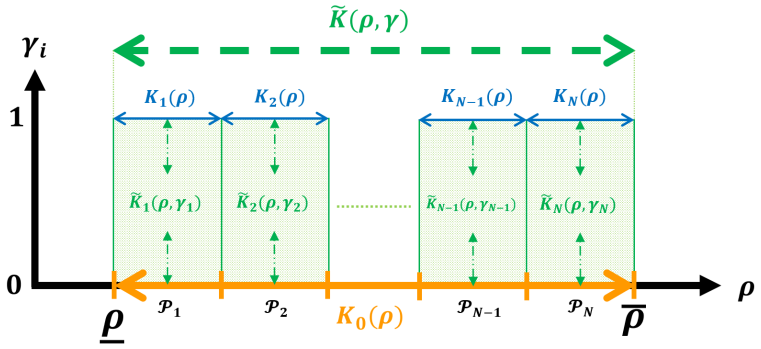

FIGURE 5.10: LPV-YK gridded controller

The defined LPV controllers $K_i(\rho)$ $(i \geq 0)$ are described over $\mathcal{P}_i$ as

$$K_i(\rho) : \left[\begin{array}{c|c} A_{k,i}(\rho,\dot{\rho}) & B_{k,i}(\rho) \\ \hline C_{k,i}(\rho) & D_{k,i}(\rho) \end{array}\right] \quad , i \in \{0, Z_N\} \tag{5.81}$$

where $A_{k,i}(\rho,\dot{\rho}) \in \mathbb{R}^{n_{k,i}\times n_{k,i}}$, $B_{k,i}(\rho) \in \mathbb{R}^{n_{k,i}\times m_k}$, $C_{k,i}(\rho) \in \mathbb{R}^{p_k\times n_{k,i}}$ and $D_{k,i}(\rho) \in \mathbb{R}^{p_k\times m_k}$.

The closed-loop system performance is achieved in each parameter subregion and under given switching/interpolating logics via YK parameterization concept. The switching occurs when the parameter trajectory hits one of the subsets boundaries. A switching signal could be any continuous/discontinuous switching signal γ. The LPV closed-loop system of each pre-defined controller $K_i(\rho)$ over $\mathcal{P}_i$ can be described by

$$CL_i(\rho) : \left[\begin{array}{c|c} A_{cl,i}(\rho,\dot{\rho}) & B_{cl,i}(\rho) \\ \hline C_{cl,i}(\rho) & D_{cl,i}(\rho) \end{array}\right] \quad , i \in \{0, Z_N\} \tag{5.82}$$

where $x_{cl,i}^T = \begin{bmatrix} x^T & x_{k,i}^T \end{bmatrix} \in \mathbb{R}^{n_x+n_{k,i}}$ $(i \geq 0)$. For any $i \in \{0, Z_N\}$, the closed-loop LPV system (5.82) is required to satisfy the bounded real lemma over $\mathcal{P}_i$ with a performance level $\gamma_{\infty,i}$, i.e. $\|z\|_2 < \gamma_{\infty,i} \|w\|_2$ and there exists a symmetric, positive definite matrix functions $X_{cl,i}(\rho)$, each of them is smooth over the corresponding parameter subset $\mathcal{P}$, such that

$$\begin{bmatrix} \left\{\begin{array}{c} A_{cl,i}^T(\rho)X_{cl,i}(\rho) + X_{cl,i}(\rho)A_{cl,i}(\rho) \\ + \sum_{k=1}^{s} \pm\{\underline{\nu}_k, \overline{\nu}_k\}\frac{\partial X_{cl,i}}{\partial \rho_k} \end{array}\right\} & X_{cl,i}(\rho)B_{cl,i}(\rho) & C_{cl,i}^T(\rho) \\ B_{cl,i}^T(\rho)X_{cl,i}(\rho) & -\gamma_{\infty,i}I_{n_w} & D_{cl,i}^T(\rho) \\ C_{cl,i}(\rho) & D_{cl,i}(\rho) & -\gamma_{\infty,i}I_{n_z} \end{bmatrix} < 0 \tag{5.83}$$

The objective of grid-based LPV-YK control structure is to obtain exponential stability of the closed-loop system based on YK parameterisation. Moreover, a smooth interpolation scheme $\tilde{K}(\rho,\gamma)$ is formulated between multiple pre-designed LPV controllers $K_i(\rho)$ $(i \in Z_N)$, using the switching signal $\gamma = [\gamma_1, ..., \gamma_i, ..., \gamma_N]$, where each $K_i(\rho)$ is designed to be suitably used for a certain parameter subregion $\mathcal{P}_i$. This could be achieved by two steps:

1. Parameterize each LPV controller $K_i(\rho)$ with respect to the nominal LPV controller $K_0(\rho)$, by an LPV-YK parameter $Q_i(\rho)$.

2. At each boundary of two adjacent subsets $\mathcal{P}_i$ and $\mathcal{P}_{i+1}$, the interpolating signals γ_i and γ_{i+1} are adjusted in a way to switch smoothly from $K_i(\rho)$ to $K_{i+1}(\rho)$

or vise-versa. As a result, the overall parameterized LPV-YK controller $\tilde{K}(\rho,\gamma)$ stabilizes $G(\rho)$ $\forall\rho\in\mathcal{P}$ and for every continuous/discontinuous interpolating signals γ_i, $i\in Z_N$.

In order to illustrate the approach, Figure 5.10 shows the partitioned parameter region $\mathcal{P}$ with intersecting boundaries. The orange solid line represents the chosen nominal LPV controller $K_0(\rho)$, as defined by (A.4.1). The blue solid lines represent the local LPV controllers $K_i(\rho)$ ($i\in Z_N$) as defined in (A.4.2). The overall switching controller is performed using the interpolating signal $\gamma=[\gamma_1,...,\gamma_N]$ ($\gamma_i\in[0,1]$ $\forall i$), and is represented by the LPV-YK controller $\tilde{K}(\rho,\gamma)$. These LPV and LPV-YK controllers are designed in the next section.

The overall interpolation scheme which is referred to $\tilde{K}(\rho,\gamma)$ (see Fig. 5.11) is designed based on a Parametric Linear Matrix Inequality (PLMI) optimization problem, where its state-space matrices are represented as

$$\tilde{K}(\rho,\gamma):\left[\begin{array}{c|c}\tilde{A}_k(\rho,\gamma) & \tilde{B}_k(\rho,\gamma)\\ \hline \tilde{C}_k(\rho,\gamma) & \tilde{D}_k(\rho,\gamma)\end{array}\right] \tag{5.84}$$

being $\gamma(\rho)$ the vector of the parameter-dependent switching signals $\gamma_i(\rho)$ $(i\in Z_N)$ that are chosen here as follows:

- if $\gamma_i(\rho)=0\ \forall i$, $\tilde{K}(\rho,\gamma)\equiv K_0(\rho)$.
- For any $\rho\in\mathcal{P}_m$, $\gamma_m(\rho)=1$ and $\gamma_i(\rho)=0\ \forall i\neq m$, which implies that $\tilde{K}(\rho,\gamma)$ is equivalent to $\mathcal{F}_l(J(\rho),Q_m(\rho))$ that recovers $K_m(\rho)$ (refer to Fig. 5.11).

The following theorem aims to prove that $\tilde{K}(\rho,\gamma)$ exponentially stabilizes $G(\rho)$ for every $\rho\in\mathcal{P}$ and for every continuous/discontinuous interpolating signals γ_i.

Theorem 8. *Consider an LPV plant $G(\rho)$ (5.17), and that the assumptions (A.4.1) and (A.4.2) are satisfied. Let $K_0(\rho)$ be the nominal LPV controller designed over the full parameter region $\mathcal{P}_0$. Then, the parameterized LPV-YK controller $\tilde{K}(\rho,\gamma)$ (5.84)-(5.87), as represented in Fig. 5.11, exponentially stabilizes $G(\rho)$, with an achieved performance $\|z\|_2<\gamma_\infty\|w\|_2$, where $\gamma_\infty=\max\{\gamma_{\infty,i}\}_{i\in Z_N}$, for any continuous/discontinuous bounded switching signal $\gamma_i\in[0,1]$, if there exist symmetric positive definite matrix functions $X_g(\rho)\in\mathbb{R}^{n_x\times n_x}$, $X_{k,0}(\rho)\in\mathbb{R}^{n_{k,0}\times n_{k,0}}$, and matrices $V(\rho)$ and $W(\rho)$ such that for any $\rho\in\mathcal{P}$:*

$$A(\rho)X_g(\rho)+X_g(\rho)A^T(\rho)+\sum_{j=1}^{s}\pm\{\underline{\nu}_j,\overline{\nu}_j\}\frac{\partial X_g}{\partial\rho_j}+B_2(\rho)V(\rho)+V^T(\rho)B_2^T(\rho)<0 \tag{5.85}$$

$$A_{k,0}(\rho)X_{k,0}(\rho)+X_{k,0}(\rho)A_{k,0}^T(\rho)+\sum_{j=1}^{s}\pm\{\underline{\nu}_j,\overline{\nu}_j\}\frac{\partial X_{k,0}}{\partial\rho_j}+B_{k,0}(\rho)W(\rho)+W^T(\rho)B_{k,0}^T(\rho)<0 \tag{5.86}$$

And $\forall\rho\in\mathcal{P}$, the state-space matrices of $\tilde{K}(\rho,\gamma)$ in (5.84) are

$$\tilde{A}_k(\rho,\gamma)=\left[\begin{array}{cc}A(\rho)+B_2(\rho)F_g(\rho)-B_2(\rho)D_q(\rho,\gamma)C_2(\rho) & -B_2(\rho)D_q(\rho,\gamma)F_{k,0}(\rho)\\ -B_{k,0}(\rho)C_2(\rho) & A_{k,0}(\rho)\\ -B_q(\rho)C_2(\rho) & -B_q(\rho)F_{k,0}(\rho)\end{array}\right.$$
$$\left.\begin{array}{c}B_2(\rho)C_q(\rho,\gamma)\\ 0\\ A_q(\rho)\end{array}\right],$$

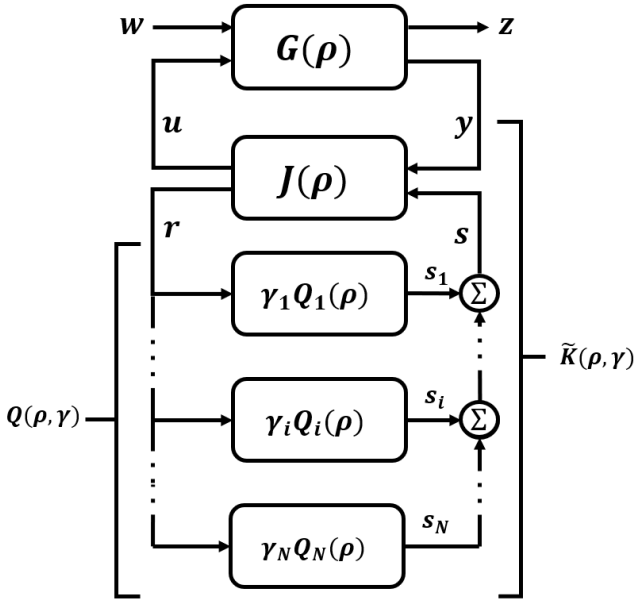

FIGURE 5.11: Generalized YK configuration

$$\begin{aligned}
\tilde{B}_k(\rho,\gamma) &= \begin{bmatrix} B_2(\rho)D_q(\rho,\gamma) & B_{k,0}(\rho) & B_q(\rho) \end{bmatrix}^T, \\
\tilde{C}_k(\rho,\gamma) &= \begin{bmatrix} F_g(\rho) - (D_{k,0}(\rho) + D_q(\rho,\gamma))C_2(\rho) & C_{k,0}(\rho) - D_q(\rho,\gamma)F_{k,0}(\rho) & C_q(\rho,\gamma) \end{bmatrix}, \\
\tilde{D}_k(\rho,\gamma) &= D_{k,0}(\rho) + D_q(\rho,\gamma).
\end{aligned} \tag{5.87}$$

where

$$\begin{aligned}
A_q(\rho) &= diag(A_{q,1}, \ldots, A_{q,i}, \ldots, A_{q,N}), \\
B_q(\rho) &= \begin{bmatrix} B_{q,1} & \ldots & B_{q,i} & \ldots & B_{q,N} \end{bmatrix}^T, \\
C_q(\rho,\gamma) &= \begin{bmatrix} \gamma_1 C_{q,1} & \ldots & \gamma_i C_{q,i} & \ldots & \gamma_N C_{q,N} \end{bmatrix}, \\
D_q(\rho,\gamma) &= \sum_{i=1}^{N} \gamma_i D_{q,i},
\end{aligned} \tag{5.88}$$

being $A_{q,i}$, $B_{q,i}$, $C_{q,i}$, and $D_{q,i}$ the state-space matrices of $Q_i(\rho)$ represented in (5.91), $F_g(\rho) = V(\rho)X_g^{-1}(\rho)$, and $F_{k,0}(\rho) = W_{k,0}(\rho)X_{k,0}^{-1}(\rho)$.

Proof 4. *According to YK concept, the parameterized controller can be formulated as a Linear Fractional Transformation (LFT) system [269], i.e. $\tilde{K}(\rho,\gamma) = \mathcal{F}_l(J(\rho), Q(\rho,\gamma))$ (see Fig. 5.11), where $J(\rho)$ is defined as:*

$$J(\rho) = \left[\begin{array}{cc|cc} A(\rho) + B_2(\rho)F_g(\rho) & 0 & 0 & B_2(\rho) \\ -B_{k,0}(\rho)C_2(\rho) & A_{k,0}(\rho,\dot{\rho}) & B_{k,0}(\rho) & 0 \\ \hline F_g(\rho) - D_{k,0}(\rho)C_2(\rho) & C_{k,0}(\rho) & D_{k,0}(\rho) & I \\ -C_2(\rho) & -F_{k,0}(\rho) & I & 0 \end{array}\right] \tag{5.89}$$

and $Q(\rho,\gamma) = \sum_{i=1}^{N} \gamma_i(\rho)Q_i(\rho)$ (see $Q_i(\rho)$ in (5.91)). Specifically, a defined LPV controller $K_m(\rho)$ ($m \in [1, N]$) can be formulated as $\mathcal{F}_l(J(\rho), Q_m(\rho)))$, i.e. $K_m(\rho) \equiv \mathcal{F}_l(J(\rho), Q(\rho,\gamma))$ for $\gamma_m = 1$ and $\gamma_i = 0\ \forall i \neq m$.

The following proof is achieved by two steps: 1) Prove that the LPV-YK parameter

$Q(\rho,\gamma)$ is exponentially stable $\forall\rho \in \mathcal{P}$ and $\forall\gamma$; and 2) Prove the closed-loop exponential stability $\forall\rho \in \mathcal{P}, \forall\gamma$.

Step 1:

$Q_i(\rho)$ can be proved to be exponentially stable $\forall\rho \in \{\mathcal{P}_i\}_{i\geq 1}$ as follows:

Following (A.4.2) and (5.86), there exist symmetric positive definite matrix functions $P_{cl,i}$, and $P_{k,0}$ such that $\forall\rho \in \{\mathcal{P}_i\}_{i\geq 1}$

$$A_{cl,i}^T(\rho)P_{cl,i}(\rho) + P_{cl,i}(\rho)A_{cl,i}(\rho) + \sum_{k=1}^{s}\dot{\rho}_k\frac{\partial P_{cl,i}(\rho)}{\partial\rho_k} < 0 \tag{5.90a}$$

$$A_{F_k}(\rho)P_{k,0}(\rho) + P_{k,0}(\rho)A_{F_k}^T(\rho) + \sum_{k=1}^{s}\dot{\rho}_k\frac{\partial P_{k,0}(\rho)}{\partial\rho_k} < 0 \tag{5.90b}$$

where $A_{F_k}(\rho) = A_{k,0}(\rho) + B_{k,0}(\rho)F_{k,0}(\rho)$.

*(5.90a) can be deduced from (5.83) by choosing $P_{cl,i}(\rho) = X_{cl,i}(\rho)$, and (5.90b) can be satisfied from (5.86) by choosing $P_{k,0}(\rho) = X_{k,0}(\rho)$ and $W_{k,0}(\rho) = F_{k,0}(\rho)X_{k,0}(\rho)$. Following **Lemma 8**, $A_{q,i}(\rho)$, consequently $Q_i(\rho)$, is exponentially stable over $\mathcal{P}_i$ $\forall i \geq 1$. As a result, $Q(\rho,\gamma) = \sum_{i=1}^{N}\gamma_i Q_i(\rho)$ is exponentially stable over $\bigcup\mathcal{P}_i = \mathcal{P}$ for every bounded signals $\gamma \in [0,1]$.*

Step 2:

The closed-loop system $CL(\rho,\gamma)$ (5.92) is derived from the LFT interconnection between $G(\rho)$ (5.17) and $\tilde{K}(\rho,\gamma)$ (5.87) (see Fig. 5.11).

$$Q_i(\rho) = \left[\begin{array}{cc:c|c} A(\rho)+B_2(\rho)D_{k,i}(\rho)C_2(\rho) & B_2(\rho)C_{k,i}(\rho) & B_2(\rho)[D_{k,i}(\rho)-D_{k,0}(\rho)]F_k - B_2(\rho)C_{k,0}(\rho) & B_2(\rho)[D_{k,i}(\rho)-D_{k,0}(\rho)] \\ B_{k,i}(\rho)C_2(\rho) & A_{k,i}(\rho,\dot\rho) & B_{k,i}(\rho)F_{k,0} & B_{k,i}(\rho) \\ \hdashline 0 & 0 & A_{k,0}(\rho)+B_{k,0}(\rho)F_{k,0}(\rho) & B_{k,0}(\rho) \\ \hline D_{k,i}^{(1)}C_2 - F_{g,i} & C_{k,i}(\rho) & [D_{k,i}(\rho)-D_{k,0}(\rho)]F_{k,0}(\rho) - C_{k,0}(\rho) & D_{k,i}(\rho)-D_{k,0}(\rho) \end{array}\right] \tag{5.91}$$

$$CL(\rho,\gamma) = \left[\begin{array}{ccc} A(\rho)+B_2(\rho)(D_{k,0}(\rho)+D_q(\rho,\gamma))C_2(\rho) & B_2(\rho)(F_g(\rho)-(D_{k,0}(\rho)+D_q(\rho,\gamma))C_2(\rho)) & B_2(\rho)(C_{k,0}(\rho)-D_q(\rho,\gamma)F_k(\rho)) \\ B_2(\rho)D_q(\rho,\gamma)C_2(\rho) & A(\rho)+B_2(\rho)(F_g(\rho)-D_q(\rho,\gamma)C_2(\rho)) & -B_2(\rho)D_q(\rho,\gamma)F_k(\rho) \\ B_{k,0}(\rho)C_2(\rho) & -B_{k,0}(\rho)C_2(\rho) & A_{k,0}(\rho,\dot\rho) \\ B_q(\rho)C_2(\rho) & -B_q(\rho)C_2(\rho) & -B_q(\rho)F_k(\rho) \\ \hline C_1(\rho)+D_{12}(\rho)(D_{k,0}(\rho)+D_q(\rho,\gamma))C_2(\rho) & D_{12}(\rho)(F_g(\rho)-(D_{k,0}(\rho)+D_q(\rho,\gamma))C_2(\rho)) & D_{12}(\rho)(C_{k,0}(\rho)-D_q(\rho,\gamma)F_k(\rho)) \end{array}\right.$$

$$\left.\begin{array}{c|c} B_2(\rho)C_q(\rho,\gamma) & B_1(\rho)+B_2(\rho)(D_{k,0}(\rho)+D_q(\rho,\gamma))D_{21}(\rho) \\ B_2(\rho)C_q(\rho,\gamma) & B_2(\rho)D_q(\rho,\gamma)D_{21}(\rho) \\ 0 & B_{k,0}(\rho)D_{21}(\rho) \\ A_q(\rho,\dot\rho) & B_q(\rho)D_{21}(\rho) \\ \hline D_{12}(\rho)C_q(\rho,\gamma) & D_{11}(\rho)+D_{12}(\rho)(D_{k,0}(\rho)+D_q(\rho,\gamma))D_{21}(\rho) \end{array}\right] \tag{5.92}$$

$$\begin{aligned} \bar A_{cl}(\rho,\gamma) &= TA_{cl}(\rho,\gamma)T^{-1} \\ &= \left[\begin{array}{cc:c|c} A(\rho)+B_2(\rho)F_g(\rho) & B_2(\rho)C_q(\rho,\gamma) & -B_2(\rho)(F_g(\rho)-(D_{k,0}(\rho)+D_q(\rho,\gamma))C_2(\rho)) & B_2(\rho)(C_{k,0}(\rho)-D_q(\rho,\gamma)F_k(\rho)) \\ 0 & A_q(\rho,\dot\rho) & B_q(\rho)C_2(\rho) & -B_q(\rho)F_k(\rho) \\ \hdashline 0 & 0 & A(\rho)+B_2(\rho)D_{k,0}(\rho)C_2(\rho) & B_2(\rho)C_{k,0}(\rho) \\ 0 & 0 & B_{k,0}(\rho)C_2(\rho) & A_{k,0}(\rho,\dot\rho) \end{array}\right] \end{aligned} \tag{5.93}$$

The closed-loop state matrix $A_{cl}(\rho,\gamma)$ is exponentially stable if $\forall\rho\in\mathcal{P}$, $\dot{\rho}\in[\underline{\nu},\overline{\nu}]$, there exists a symmetric, positive definite matrix function $X_{cl}(\rho)$ such that $\forall\gamma$:

$$A_{cl}^T(\rho,\gamma)X_{cl}(\rho)+X_{cl}(\rho)A_{cl}(\rho,\gamma)+\sum_{k=1}^{s}\dot{\rho}_k\frac{\partial X_{cl}}{\partial\rho_k}<0 \tag{5.94}$$

Let $T=\begin{bmatrix}I&0&0&0\\0&0&0&I\\I&-I&0&0\\0&0&I&0\end{bmatrix}$ *be a state transformation matrix which is applied to* $CL(\rho,\gamma)$ *without changing its input-output nature, with* $T^{-1}=\begin{bmatrix}I&0&0&0\\I&0&-I&0\\0&0&0&I\\0&I&0&0\end{bmatrix}$.

*Due to the block-triangular form of $\bar{A}_{cl}(\rho,\gamma)$ (5.93), (5.94) is satisfied if the following equations hold $\forall\rho\in\mathcal{P}$ (check **Lemma 8**):*

$$Y_g(\rho)(A(\rho)+B_2(\rho)F_g(\rho))^T+(A(\rho)+B_2(\rho)F_g(\rho))Y_g(\rho)+\sum_{k=1}^{s}\dot{\rho}_k\frac{\partial Y_g}{\partial\rho_k}<0 \tag{5.95a}$$

$$Y_q(\rho)A_q^T(\rho)+A_q(\rho)Y_q(\rho)+\sum_{k=1}^{s}\dot{\rho}_k\frac{\partial Y_q}{\partial\rho_k}<0 \tag{5.95b}$$

$$A_{cl,0}^T(\rho)Y_{cl,0}(\rho)+Y_{cl,0}(\rho)A_{cl,0}(\rho)+\sum_{k=1}^{s}\dot{\rho}_k\frac{\partial Y_{cl,0}}{\partial\rho_k}<0 \tag{5.95c}$$

where $Y_g(\rho)\in\mathbb{R}^{n_x\times n_x}$, $Y_q(\rho)\in\mathbb{R}^{n_q\times n_q}$ and $Y_{cl,0}(\rho)\in\mathbb{R}^{(n_x+n_{k,0})\times(n_x+n_{k,0})}$ are symmetric, positive definite matrix functions, choosing $X_{cl}(\rho)=T^T\,diag(Y_g,Y_q,Y_{cl,0})\,T$.

Therefore,

- *Inequality (5.95a) can be deduced from (5.85) by choosing $Y_g(\rho)=X_g(\rho)$ and considering that $F_g(\rho)=V(\rho)X_g^{-1}(\rho)$ in (5.85).*
- *(5.95b) is satisfied since $Q(\rho,\gamma)$ has been proved in Step 1 to be exponentially stable over $\mathcal{P}$.*
- *(5.95c) is fulfilled given that $K^{(0)}(\rho)$ exponentially stabilizes $G(\rho)$ according to (A.4.1).*

Now, assume a sequence of finite switching time over the interval $[0,T]$ is $t_0,t_1,\ldots,t_N$ with $t_0=0$, knowing that the closed-loop Lyapunov function is $V(x_{cl})=x_{cl}^TX_{cl}(\rho)x_{cl}$. From the YK basic concept [269], a parameterized controller $\tilde{K}=\mathcal{F}_l(J,Q)$ recovers the performance of its actual controller K. Thus, the closed-loop performance of $\mathcal{F}_l(G,\tilde{K})$ is equivalent to the performance of $\mathcal{F}_l(G,K)$. In the current work, it can be deduced that the closed-loop performance of $CL(\rho,\gamma)$ (5.92) is equivalent to that of $CL_i(\rho)$ (5.82) within each parameter subset $\mathcal{P}_i$. Notice that according to (5.83), the following inequality describes the performance of $CL_i(\rho)$ $\forall\rho\in\{\mathcal{P}_i\}_{i\in Z_N}$

$$\frac{d}{dt}(x_{cl,i}^TX_{cl,i}(\rho)x_{cl,i})+\frac{1}{\gamma_{\infty,i}}z^Tz-\gamma_{\infty,i}w^Tw<0 \tag{5.96}$$

On the other hand, it is worth mentioning that $X_{cl}(\rho)$ is independent of the switching signal γ, so, for any switching time t_k, $V(x_{cl}(t_k))=V(x_{cl}(t_k^-))$, and thus

$$V(x_{cl}(t_k))\leq V(x_{cl}(t_k^-)) \tag{5.97}$$

Given the initial condition $x_{cl}(0) = 0$, *from (5.96)-(5.97), it can be shown that the inequality*

$$\dot{V}(x_{cl}) + \frac{1}{\gamma_\infty} z^T z - \gamma_\infty w^T w < 0, \quad \gamma_\infty = \max\{\gamma_{\infty,i}\}_{i \in Z_N} \tag{5.98}$$

holds within each parameter subset. Integrate on both sides, we get

$$V(x_{cl}(T)) - V(x_{cl}(0)) + \frac{1}{\gamma_\infty} \|z\|_2^2 - \gamma_\infty \|w\|_2^2 < 0$$

Since $V(x_{cl}(T)) \geq 0$ *and* $V(x_{cl}(0)) = 0$, $\|z\|_2 < \gamma_\infty \|w\|_2$ *is achieved. Therefore, the closed-loop is exponentially stable with an achieved performance* $\|z\|_2 < \gamma_\infty \|w\|_2$, *where* $\gamma_\infty = \max\{\gamma_{\infty,i}\}_{i \in Z_N}$.

5.7 Discussion

This chapter has presented four LPV-YK control structures:

1. **Interpolation of polytopic-based LPV controllers:** It is used to interpolate between already designed LPV controllers, knowing that all the interpolated LPV controllers should quadratically stabilize the LPV model for any parameter variations.

2. **Interpolation of YK-based LPV controllers:** This structure uses the LTI-YK parameterization to first design multiple quadratically stabilizing LPV controllers. Then interpolates between these YK-based LPV controllers providing a whole closed-loop quadratic stability.

3. **Switching of partitioned YK-based LPV controllers:** It is designed aiming to solve the conservatism of the quadratic stability problem due to overbounding (in convex regions), large number of varying parameters, and their large range of variations. A YK-based LPV controller is designed in each parameter subset, and the switching appears at the intersection boundary between each two consecutive subsets.

4. **Switching of grid-based LPV controllers:** This structure is formulated to switch between multiple grid-based LPV controllers, each is designed to be useful over its subset. Each parameter subset is gridded and the local LPV controllers are required to be exponentially stabilizing.

Notice that one can combine multiple parameter subsets with multiple closed-loop specifications in one structure. Such a structure can be the most generalized control scheme including parameter-variations, robustness, and different control objectives. For instance, one can partition $\mathcal{P}$ into N parameter subsets, and design ζ YK-based LPV controllers in each subset $\mathcal{P}_i$. As a result, the LPV-YK controller $\tilde{K}(\rho, \gamma)$ switches and interpolates between $(N \times \zeta)$ LPV controllers $\tilde{K}_i^{(j)}(\rho)$, $i \in \mathbb{I}[1, N]$, $j \in \mathbb{I}[1, \zeta]$.

Chapter 6

Application of the LPV-YK Structures on Vehicle Lateral Control

6.1 Introduction

The main thesis motivation behind considering an interpolation scheme between multiple LPV controllers is the application to autonomous vehicles. Indeed, several studies have involved the LPV control approaches to solve the lateral tracking problem over the full speed-range (speed as the varying parameter) [23]. However, it is not sufficient to achieve different tracking performances (e.g. smooth and aggressive). On the other hand, [293] has proposed an LTI-YK control structure for both lane-tracking and lane-changing control performances, but works only for a constant speed.

Indeed, the driving capabilities have been recently improved for highly, and even fully, autonomous driving thanks to advanced control theory. A fully autonomous car needs to perform several tasks including longitudinal control, lateral control, chassis control, etc. Moreover, the lateral dynamics of an autonomous vehicle varies significantly with respect to its longitudinal speed [138], [139]. Specifically, at low speeds, the lateral dynamics becomes harder to be controlled (due to approaching system singularity), whereas at high speeds, robustness and system stability decrease [140]. Even at nominal speeds, the lateral control aims to achieve various objectives such as lane tracking, lane changing, obstacle avoidance, etc. Consequently, various performances are required accordingly for different driving situations that are facing the vehicle.

The following chapter uses the LPV-YK control structures, presented in the previous chapter, to improve the vehicle tracking performance over a large speed range. First, the implementation architecture with its designing steps are shown, then, simulation and experimental results are presented to validate the efficiency of the proposed LPV-YK control structures.

The simulation and experimental results shown in this chapter have been presented in:

- *Multi-Variable and Multi-Objective Gain Scheduled Control Based on Youla-Kucera Parameterization: Application to Autonomous Vehicles, under review in International Journal on Robust and Nonlinear Control.*
- *Advanced LPV-YK Control Design with Experimental Validation on Autonomous Vehicles, under review in Automatica.*

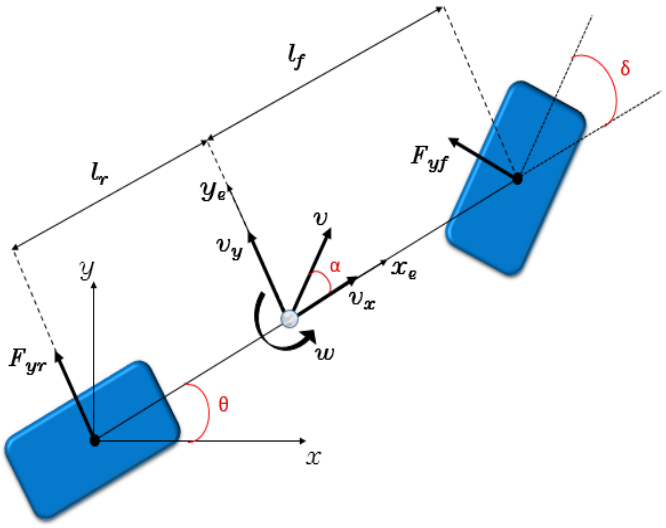

FIGURE 6.1: Vehicle Bicycle Model

This chapter is organized as follows: Section 6.2 states the formulated LPV models for the lateral bicycle model. In Section 6.3, the generalized LPV model including the weighting functions is introduced. Section 6.4 defines LPV/$\mathcal{H}_\infty$ control design problem to be used later. The general LPV-YK control scheme is defined in Section 6.5. Section 6.6 presents the implementation of the Interpolation of polytopic-based LPV controllers. The interpolation of YK-based LPV controllers is depicted in Section 6.7. The partitioned LPV-YK controller is presented in Section 6.8. Section 6.9 shows the implementation of the grid-based LPV-YK controller. Finally, a summary and conclusion is given in Section 6.10.

6.2 LPV Model Formulation

The following section describes the LPV model that is used for each of the LPV-YK control structures, considering both the general and affine parameter-dependency.

6.2.1 Lateral Bicycle Model

Recall that the lateral bicycle model has been used to control the lateral motion of our automated car. Notice that the chosen bicycle model is one type of Pacejkas' models only [138]. As previously mentioned in Chapter 3, the bicycle model is represented as shown in Fig. 6.1, with

$$\begin{cases} \dot{v}_y = \frac{F_{yf}\cos\delta + F_{yr}}{m} - wv_x \\ \dot{w} = \frac{F_{yf} l_f \cos\delta - F_{yr} l_r}{I} \end{cases} \tag{6.1}$$

F_{yf} and F_{yr} can be modelled using Pacejka's tire model [138] as follows:

$$\begin{array}{ll} F_{yf} = c_3 \sin(c_2 \tan^{-1}(c_1 \alpha_f)) & \alpha_f = \delta - \tan^{-1}(\frac{v_y}{v_x} - \frac{l_f w}{v_x}) \\ F_{yr} = c_3 \sin(c_2 \tan^{-1}(c_1 \alpha_r)) & \alpha_r = -\tan^{-1}(\frac{v_y}{v_x} - \frac{l_r w}{v_x}) \end{array} \tag{6.2}$$

where c_1, c_2 and c_3 are constants.

Assuming small α (refer to Section 3.2.8), the tire forces are linearized resulting the following:

$$\begin{aligned} F_{yf} &= C_f(\delta - \tfrac{v_y}{v_x} - \tfrac{l_f w}{v_x}) \\ F_{yr} &= C_r(-\tfrac{v_y}{v_x} + \tfrac{l_r w}{v_x}) \end{aligned} \tag{6.3}$$

where C_f and C_r represent the tires' stiffness of the front and rear wheels.

6.2.2 LPV Bicycle Model Structures

Referring to Chapter 4, taking $\rho(t) = v_x \in \mathbb{R}^{n_\rho}$ as a varying parameter, and assuming small steering front angles ($\sin(\delta) \approx \delta$), and small slip angles, the LPV state-space representation can be written as:

$$\Sigma(\rho) \begin{cases} \dot{x}(t) = A_\Sigma(\rho)x(t) + B_\Sigma u(t) \\ y(t) = C_\Sigma x(t) + D_\Sigma u(t) \end{cases} \tag{6.4}$$

where:

$$\begin{aligned} x(t) = \begin{bmatrix} v_y \\ w \end{bmatrix} \in \mathbb{R}^{n_x},\ u(t) = \delta, ,y(t) = w,\ B_\Sigma = \begin{bmatrix} \frac{1}{m}C_f \\ \frac{1}{I}C_f l_f \end{bmatrix}, \\ A_\Sigma(\rho) = \begin{bmatrix} -\frac{C_r+C_f}{m\rho} & -\frac{l_f C_f - l_r C_r}{m\rho} - \rho \\ -\frac{l_f C_f - l_r C_r}{I\rho} & -\frac{l_f^2 C_f + l_r^2 C_r}{I\rho} \end{bmatrix}. \end{aligned} \tag{6.5}$$

Grid-based Model

The grid-based LPV model is a model interpolated over a set of LTI models that are linearized at different operating points. This approach considers the general parameter dependency of the model (without model reformulation). Thus, the model in (6.4)-(6.5) can be used for the grid-based LPV-YK control structure. Refer to Section 4.2.2 for more details.

Polytopic Model

Since the polytopic model must be affine with respect to the varying parameters. So, the state matrix in (6.5) is reformulated as:

$$A_\Sigma(\rho) = \begin{bmatrix} -\frac{C_r+C_f}{m}\rho_2 & -\frac{C_f l_f - C_r l_r}{m}\rho_2 - \rho_1 \\ -\frac{C_f l_f - l_r C_r}{I}\rho_2 & -\frac{C_f l_f^2 + l_r^2 C_r}{I}\rho_2 \end{bmatrix}, \tag{6.6}$$

where $\rho = [\rho_1, \rho_2] = [v_x, \frac{1}{v_x}]$. Refer to Section 4.2.2 for more details.

6.3 Generalized LPV Model

This section shows the components of the generalized LPV model $G(\rho)$, that is used later for control design.

6.3.1 Actuator model

The actuator model is included to achieve a more realistic model. Thus, the bicycle model is extended by considering an identified steering actuator dynamics Σ_{act}.

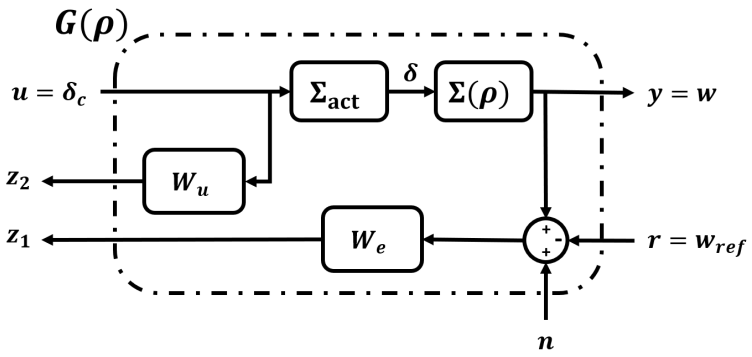

FIGURE 6.2: Generalized Plant $G(\rho)$

Recall from Chapter 3 that the steering actuator model is identified at the nominal longitudinal speed $v_x = 12\ m/s$ as an LTI model. A second order transfer function has been obtained in the following form:

$$\Sigma_{act} = \frac{k}{s^2 + 2\zeta w_n s + w_n^2} e^{-T_d s} \tag{6.7}$$

where k, ζ, w_n, and T_d are the static gain, the damping, the natural frequency and the time delay, respectively. The time delay term- $e^{-T_d s}$ is represented as:

$$e^{-T_d s} = \frac{1 - \frac{T_d s}{2} + \frac{(T_d s)^2}{12}}{1 + \frac{T_d s}{2} + \frac{(T_d s)^2}{12}} \tag{6.8}$$

6.3.2 Weighting functions

In this thesis, the LPV and LTI controllers are designed using the robust $\mathcal{H}_\infty$ concept. For control design purpose, two weighting transfer functions $W_e(s)$ and $W_u(s)$ are designed to present the closed-loop tracking performance and the actuator limitations respectively. Then, the state-space representation of $G(\rho)$ is obtained from the generalized plant shown in Fig. 6.2. Having a second order $\Sigma(\rho)$, Σ_{act} of order 4, $W_e(s)$ and $W_u(s)$ of first order each, then, the obtained generalized LPV model $G(\rho)$ is of order 8.

6.4 LPV/$\mathcal{H}_\infty$ Control Design

In this chapter, all the LPV lateral controllers $K(\rho)$ are designed using the LPV/$\mathcal{H}_\infty$ control design approaches, either polytopic or grid-based. The objective of the lateral control is to track a given yaw-rate reference $r = w_{ref}$ with rejecting the measurement noises n. Fig 6.3 presents the control design scheme where $w_r = [w_{ref} \quad n]^T$ is a vector of the yaw-rate reference w_{ref} and measurement noises n, δ_c is the steering control input, and w is the measured yaw-rate of the vehicle. $z = [z_1 \quad z_2]^T$ is the controlled output vector containing the required yaw-rate tracking performance $z_1 = W_e \times (w_{ref} - w)$ and steering actuator limitations $z_2 = W_u \times \delta_c$.

The objective is to minimize the $\mathcal{L}_2$ induced gain from the external input w_r to the controlled output $z = \begin{bmatrix} z_1 & z_2 \end{bmatrix}^T$. This is achieved by solving the following $\mathcal{L}_2$ induced minimization problem:

$$\|z\|_2 \leq \gamma_\infty \|w_r\|_2$$

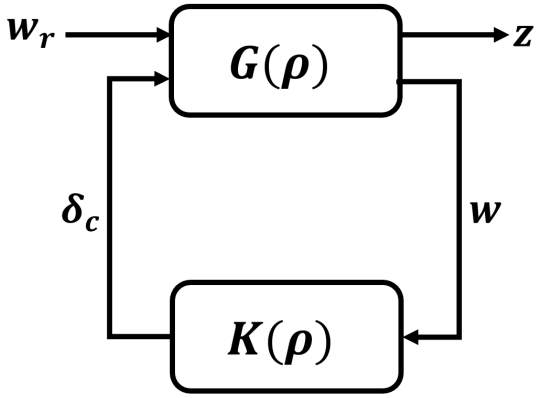

FIGURE 6.3: LPV/$\mathcal{H}_\infty$ Control Design Scheme

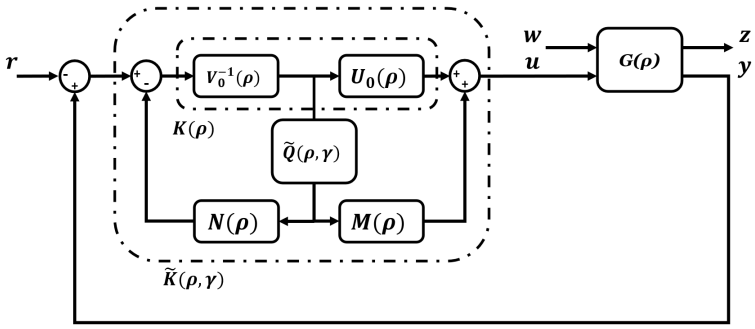

FIGURE 6.4: LPV-YK control structure

and $\gamma_\infty > 0$, to be minimized. Note that the obtained controller $K(\rho)$ is an *LPV Dynamic Output Feedback Controller*.

6.5 General LPV-YK Control Scheme

In this section, a general implementation scheme of an LPV-YK controller $\tilde{K}(\rho,\gamma)$ is defined as shown in Fig. 6.4. Note that the LFT representation of the generalized LPV-YK controller in Fig. 5.11 can be equivalently reformulated as in Fig. 6.4. This scheme is considered to be general among all the LPV-YK control structures that are discussed in the previous chapter. Among these structures, the definitions of $M(\rho)$, $N(\rho)$, $U_0(\rho)$, and $V_0^{-1}(\rho)$ are similar. The only difference between a structure and another is the LPV-YK parameter $\tilde{Q}(\rho,\gamma)$. The implementation scheme of the LPV-YK control is formulated using the doubly coprime factorization [272].

6.5.1 LPV Coprime Factorization

LPV-YK parameterisation uses the LPV coprime factorisation concept to reduce the algebraic complexity of Q computation. Consider the LPV plant $G(\rho)$ stabilized by a set of LPV controllers $K_i(\rho)$, then they can be factorized (from left and right) as a product of a stable transfer function matrix and a transfer function matrix with a stable inverse as shown below:

$$\begin{aligned} G(\rho) &= N(\rho)M^{-1}(\rho) = \tilde{M}^{-1}(\rho)\tilde{N}(\rho) \\ K_i(\rho) &= U_i(\rho)V_i^{-1}(\rho) = \tilde{V}_i^{-1}(\rho)\tilde{U}_i(\rho), \quad \forall i \end{aligned} \tag{6.9}$$

where the LPV coprime factors are computed such that $M(\rho)$, $N(\rho)$, $\tilde{M}(\rho)$, $\tilde{N}(\rho)$, $U_i(\rho)$, $V_i(\rho)$, $\tilde{U}_i(\rho)$, $\tilde{V}_i(\rho)$ are stable and proper, and satisfying the following *Bezout Identity*:

$$\begin{bmatrix} \tilde{V}_i(\rho) & -\tilde{U}_i(\rho) \\ -\tilde{N}(\rho) & \tilde{M}(\rho) \end{bmatrix} \begin{bmatrix} M(\rho) & U_i(\rho) \\ N(\rho) & V_i(\rho) \end{bmatrix} = \begin{bmatrix} M(\rho) & U_i(\rho) \\ N(\rho) & V_i(\rho) \end{bmatrix} \begin{bmatrix} \tilde{V}_i(\rho) & -\tilde{U}_i(\rho) \\ -\tilde{N}(\rho) & \tilde{M}(\rho) \end{bmatrix} = \begin{bmatrix} I & 0 \\ 0 & I \end{bmatrix} \tag{6.10}$$

The LPV coprime factors are computed at each vertex using the state-space representations written in (6.11)-(6.12).

$$\begin{bmatrix} M(\rho) & U_i(\rho) \\ N(\rho) & V_i(\rho) \end{bmatrix} : \left[\begin{array}{cc|cc} A(\rho)+B_2(\rho)F_g(\rho) & 0 & B_2(\rho) & 0 \\ 0 & A_{k,i}(\rho)+B_{k,i}(\rho)F_{k,i}(\rho) & 0 & B_{k,i}(\rho) \\ \hline F_g(\rho) & C_{k,i}(\rho)+D_{k,i}(\rho)F_{k,i}(\rho) & I & D_{k,i}(\rho) \\ C_2(\rho) & F_{k,i}(\rho) & 0 & I \end{array}\right] \tag{6.11}$$

$$\begin{bmatrix} \tilde{V}_i(\rho) & -\tilde{U}_i(\rho) \\ -\tilde{N}(\rho) & \tilde{M}(\rho) \end{bmatrix} : \left[\begin{array}{cc|cc} A(\rho)+B_2(\rho)D_{k,i}(\rho)C_2(\rho) & B_2(\rho)C_{k,i}(\rho) & -B_2(\rho) & B_2(\rho)D_{k,i}(\rho) \\ B_{k,i}(\rho)C_2(\rho) & A_{k,i}(\rho) & 0 & B_{k,i}(\rho) \\ \hline F_{g,i}(\rho)-D_{k,i}(\rho)C_2(\rho) & -C_{k,i}(\rho) & I & -D_{k,i}(\rho) \\ C_2(\rho) & -F_{k,i}(\rho) & 0 & I \end{array}\right] \tag{6.12}$$

6.5.2 LPV-YK Control Structure

Choosing $K_0(\rho) = U_0(\rho)V_0^{-1}(\rho) = \tilde{V}_0^{-1}(\rho)\tilde{U}_0(\rho)$ (or $K^{(0)}(\rho)$ as notated in some structures) as the nominal LPV controller, the LPV-YK controller $\tilde{K}(\rho,\gamma)$ in Fig. 6.4 is then expressed as:

$$\begin{aligned} \tilde{K}(\rho,\gamma) &= \Big(U_0(\rho)+M(\rho)\tilde{Q}(\rho,\gamma)\Big)\Big(V_0(\rho)+N(\rho)\tilde{Q}(\rho,\gamma)\Big)^{-1} \\ &= \Big(\tilde{V}_0(\rho)+\tilde{Q}(\rho,\gamma)\tilde{N}(\rho)\Big)^{-1}\Big(\tilde{U}_0(\rho)+\tilde{Q}(\rho,\gamma)\tilde{M}(\rho)\Big) \end{aligned} \tag{6.13}$$

The next sections define the LPV coprime factors $M(\rho)$, $N(\rho)$, $U_0(\rho)$, $V_0(\rho)$, and the LPV-YK parameter $\tilde{Q}(\rho,\gamma)$, for each of the discussed LPV-YK control structures.

6.6 Interpolation of polytopic-based LPV controllers

This section presents the steps done to design an LPV-YK controller aiming to interpolate between polytopic-based LPV controllers, as has been shown in Fig. 5.3. Simulation results are also presented after the design steps. The objective of this method is to:

1. Design three LPV controllers $K^{(j)}(\rho)$, $j \in \mathbb{I}[0,2]$. Each one is designed based on the standard polytopic approach.

2. Create an overall interpolation scheme between the gain-scheduled controllers $K^{(j)}(\rho)$ ($j \in \mathbb{I}[0,2]$), by an interpolating signal vector γ, which is referred to as $\tilde{K}(\rho,\gamma)$, such that the resultant LPV-YK controller $\tilde{K}(\rho,\gamma)$ quadratically stabilizes $G(\rho)$ $\forall\rho \in \mathcal{P}$ and for every $\gamma = [\gamma_1, \gamma_2]$.

6.6.1 Lateral Control Design

Here, the longitudinal speed is bounded in $[3, 30] m/s$. Indeed it has been observed that considering speeds lower than $3m/s$, the performance of lateral controllers deteriorates significantly (due to the conservatism of the polytopic approach). $G(\rho)$ is written as a convex combination of the vertices of the triangular polytope

$$\mathcal{P} = \mathcal{CO}\{(\underline{\rho_1}, \underline{\rho_2}), (\underline{\rho_1}, \overline{\rho_2}), (\overline{\rho_1}, \underline{\rho_2})\} = \mathcal{CO}\{(3, \frac{1}{30}), (3, \frac{1}{3}), (30, \frac{1}{30})\} \tag{6.14}$$

with the state-space representation as described in (6.4)-(6.6). Notice that the fourth vertex has been removed to decrease the problem conservatism.

Referring to Fig. 5.3, assumptions (A.1.1)-(A.1.2), and **Theorem** 5 in Section 5.5.1, a highly robust LPV controller $K^{(0)}(\rho)$, and two gain-scheduled controllers $K^{(1)}(\rho)$ and $K^{(2)}(\rho)$ are designed to perform different required performances. The three controllers are designed using the standard polytopic-based LPV/$\mathcal{H}_\infty$ concept following a method similar to [7], having the weighting functions as follows:

- $K^{(0)}(\rho)$: A slow transient response and noise rejection performances are required using the weighting functions $W_e^{(0)}$ and $W_u^{(0)}$:

$$W_e^{(0)}(s) = \frac{s+2}{2s+0.002}, \quad W_u^{(0)}(s) = \frac{s+5}{0.01s+5} \tag{6.15}$$

  The following closed-loop step responses are obtained:

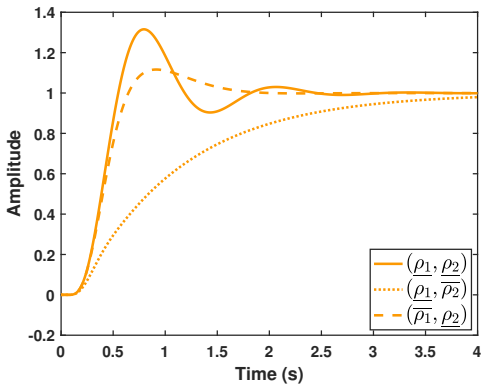

FIGURE 6.5: Closed-loop step response with $K^{(0)}(\rho)$

- $K^{(1)}(\rho)$: needs to perform smooth lateral transitions which is important to provide comfort riding. This is achieved using the following weighting functions $W_e^{(1)}$ and $W_u^{(1)}$:

$$W_e^{(1)}(s) = \frac{s+2}{2s+0.002}, \quad W_u^{(1)}(s) = \frac{s+10}{0.01s+10} \tag{6.16}$$

  The following closed-loop step responses are obtained:

- $K^{(2)}(\rho)$: to perform fast lateral transitions to handle the vehicle when facing aggressive maneuvers and lateral oscillations. The chosen weighting functions $W_e^{(2)}$ and $W_u^{(2)}$ are:

$$W_e^{(2)}(s) = \frac{s+20}{2s+0.02}, \quad W_u^{(2)}(s) = \frac{10s+25}{0.1s+500} \tag{6.17}$$

  The following closed-loop step responses are obtained:

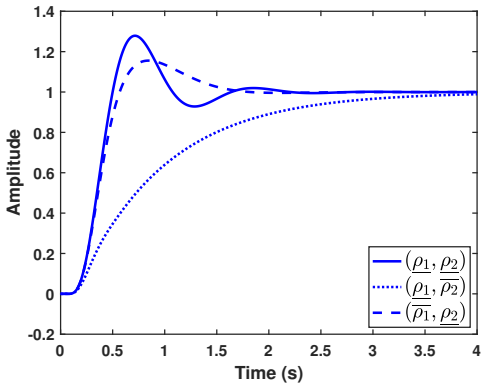

FIGURE 6.6: Closed-loop step response with $K^{(1)}(\rho)$

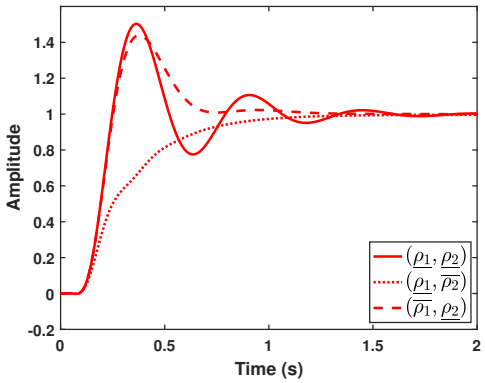

FIGURE 6.7: Closed-loop step response with $K^{(2)}(\rho)$

6.6.2 Design the LPV-YK Control Structure

The following steps are done to design the LPV-YK control:

1. According to the method explained in Section 5.5.1 and **Theorem 5**, the LPV polytopic-based state-feedback controllers $F_g(\rho)$ and $F_k^{(0)}(\rho)$ are designed using the LMIs (5.26)-(5.27). After finding the decision variables $W(\rho)$ and X_g from (5.26), and $V(\rho)$ and X_k from (5.27), $F_g(\rho)$ and $F_k^{(0)}(\rho)$ are computed as

$$\begin{aligned} F_g(\rho) &= W(\rho)X_g^{-1}, \\ F_k^{(0)}(\rho) &= V(\rho)X_k^{-1} \end{aligned} \tag{6.18}$$

2. The state-space representations of $M(\rho)$, $N(\rho)$, $U^{(0)}(\rho)$ and $V^{(0)}(\rho)$ are computed as illustrated in Section 6.5.1. $\tilde{Q}(\rho,\gamma)$ is formulated as:

$$\tilde{Q}(\rho,\gamma) = \sum_{j=1}^{2} \gamma_j Q^{(j)}(\rho) \tag{6.19}$$

where $Q^{(j)}(\rho)$ are obtained from (5.31), $\forall j \in \{1,2\}$.

3. Here, the interpolating signal $\gamma(t)$ is a vector of dimension two $[\gamma_1(t), \gamma_2(t)]$, where each γ_j multiplies its corresponding $Q^{(j)}(\rho)$. In this example, and based

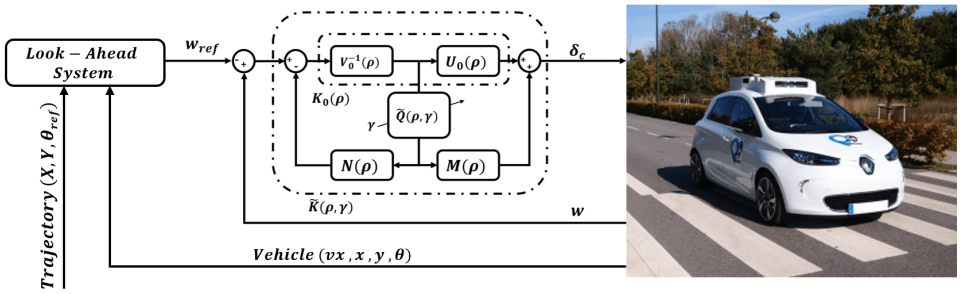

FIGURE 6.8: Simulation scheme

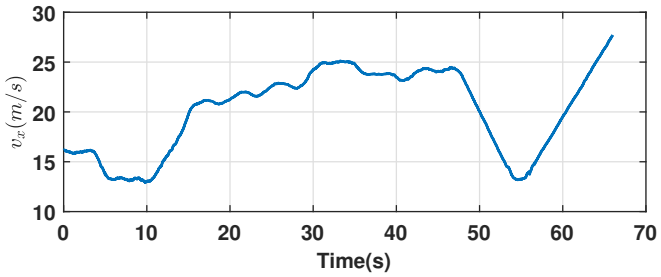

FIGURE 6.9: Simulation: Parameter-varying longitudinal speed v_x (m/s)

on an experimental experience, $\gamma_2(t)$ is chosen to vary according to the demanded control tasks. Linear relations are proposed between different variables as follows:

- if $\theta_e \leq 0.1$, $\gamma_2(t) = sat(-y_L + 1.4 + 0.1\dot{\delta}, [0, 1])$
- if $\theta_e > 0.1$, $\gamma_2(t) = sat(-0.7y_e + 1.4, [0, 1])$
- $\gamma_1(t) = 1 - \gamma_2(t)$

where θ_e and y_e represent the heading and lateral errors between the vehicle and the current point on the reference path, respectively. $\dot{\delta}$ is the steering speed, and y_L is the lateral error at a look-ahead distance L [353].

More illustration about the choice of the interpolating signals γ_j is shown in the next chapter.

6.6.3 Simulation Results

The parameterized LPV-YK controller $\tilde{K}(\rho, \gamma)$ is simulated on a nonlinear full car model designed for the Renault ZOE vehicle. The simulation is done using a part of a real trajectory map (*Satory*) (see Fig. 3.6) where its coordinates are obtained from a pre-recorded map using the positioning system mounted on the robotized ZOE car. The simulation in performed with MATLAB/Simulink with fixed sampling-time$= 0.01s$ using the scheme shown in Fig. 6.8. The real vehicle speed from this recording is multiplied by 1.7 gain and used as a speed profile reference, to test the controllers within critical high speeds.

A scenario is chosen to cover several lateral tasks and critical situations as follows:

1. The vehicle is required to start its Autonomous Driving (AD) with a large lateral error ($y_e > 2\ m$).

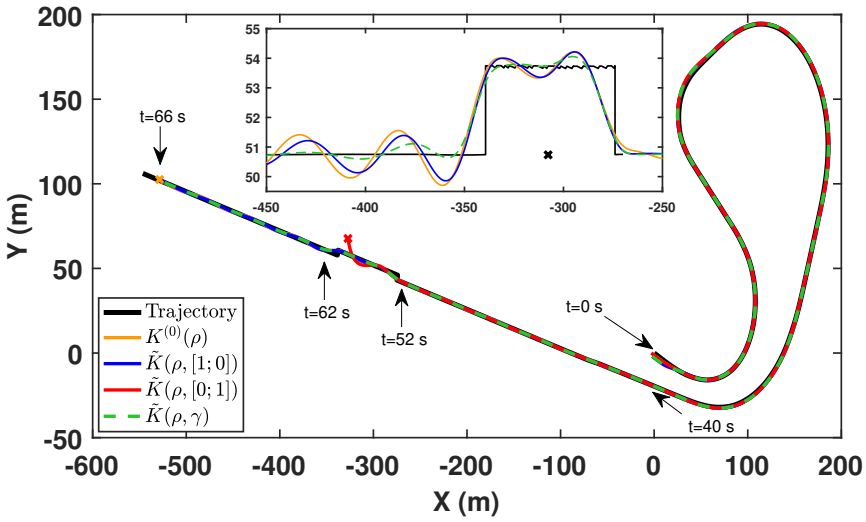

FIGURE 6.10: Simulation: Planned and controlled trajectories

2. When $t \in [10, 40]s$, the vehicle performs four successive turns at a high speed ($v_x > 20m/s$).

3. When $t \in [40, 50]s$, the vehicle is subjected to some sensor noises (due to real measurements) on a straight stretch.

4. An obstacle is detected when $t \in [50, 60]s$, the navigation modifies the trajectory suddenly as two successive lateral steps (each one of 3 m), aiming to avoid a collision.

The scenario is tested with different controllers:

- The nominal highly robust controller: $\tilde{K}(\rho,[0,0]) \equiv K^{(0)}(\rho)$,
- The smooth tracker: $\tilde{K}(\rho,[1,0]) \equiv K^{(1)}(\rho)$,
- The aggressive tracker: $\tilde{K}(\rho,[0,1]) \equiv K^{(2)}(\rho)$,
- The proposed LPV-YK controller: $\tilde{K}(\rho,\gamma)$ with $\gamma = [\gamma_1, \gamma_2]$ varies in real-time

Fig. 6.9 shows the speed profile for all the tests. Fig. 6.10 shows the (X-Y) coordinates of the reference trajectory and the vehicle positioning response of the different tested controllers. Fig. 6.11a depicts the lateral error from the reference trajectory to the vehicle Center of Gravity (CoG), and the steering control input is shown in Fig. 6.11b. Fig. 6.11c represents the steering speed which reflects the driving comfort. Fig. 6.12 shows the evolution of the interpolating signal γ for $\tilde{K}(\rho,\gamma)$.

The results are studied along time evolution as follows:

- At $t = 0s$, it is shown in Fig. 6.11a that only some of the tested controllers are activated to start with high lateral error ($y_e > 2.5m$), since both controllers $K^{(0)}(\rho)$ and $\tilde{K}(\rho,[0,1])$ can't deal with large lateral errors (observed from pre-testing). On the other hand, $\tilde{K}(\rho,[1,0])$ and $\tilde{K}(\rho,\gamma)$ perform better with the initial high lateral error, where $\tilde{K}(\rho,\gamma)$ shows a lower overshoot (see Fig. 6.11a when $t \in [2, 5]s$) with a smoother steering action (see Fig. 6.11b when $t \in [2, 4]s$).

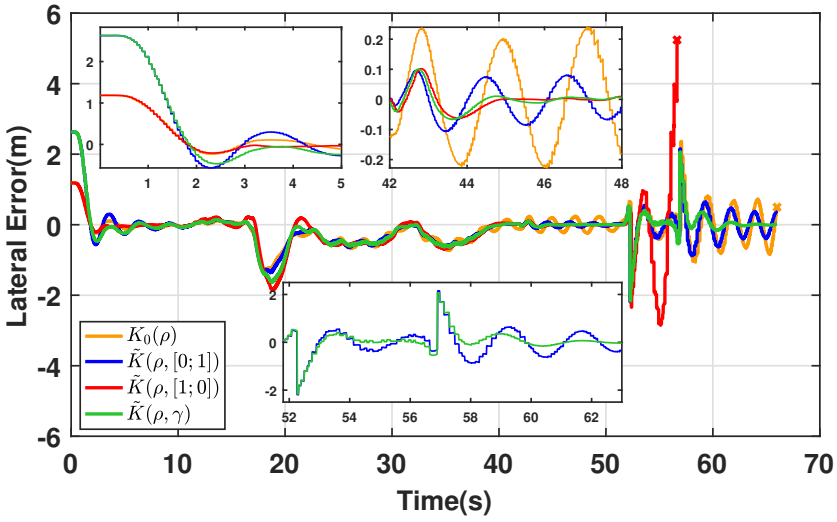

(A) Lateral error y_e (m)

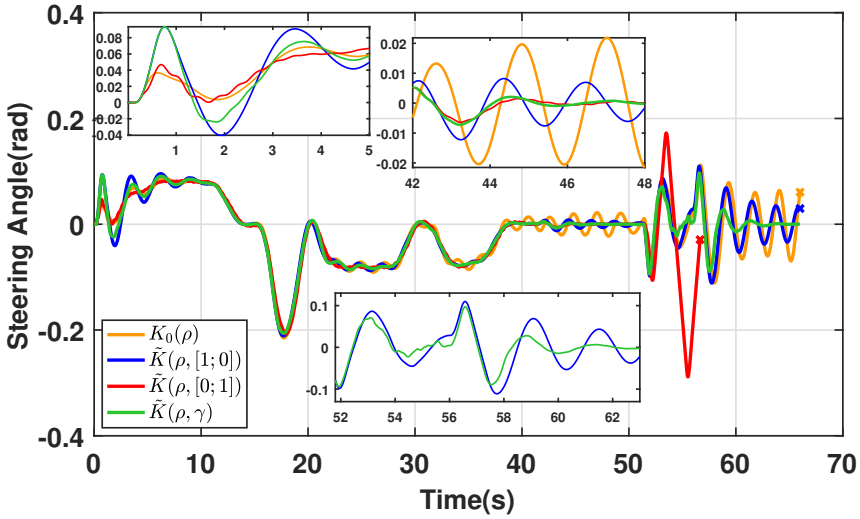

(B) Control input steering wheel angle (rad)

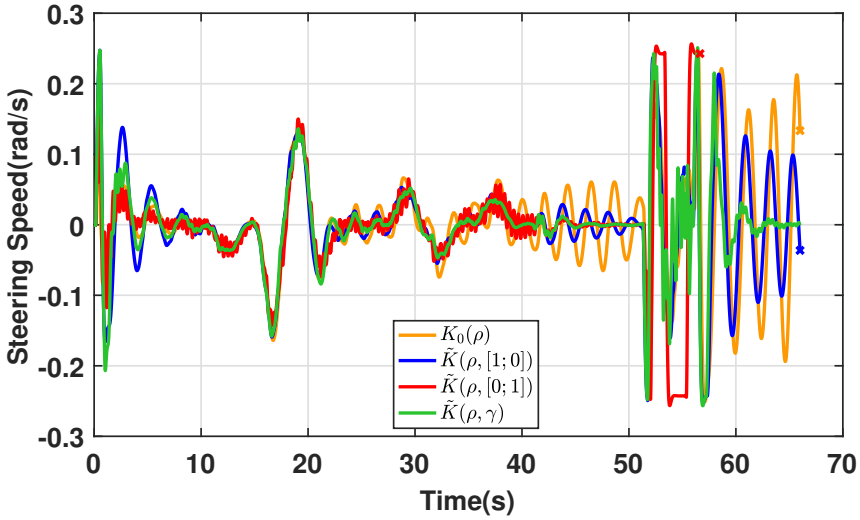

(C) Steering speed $\dot{\delta}$ (rad/s)

FIGURE 6.11: Simulation results

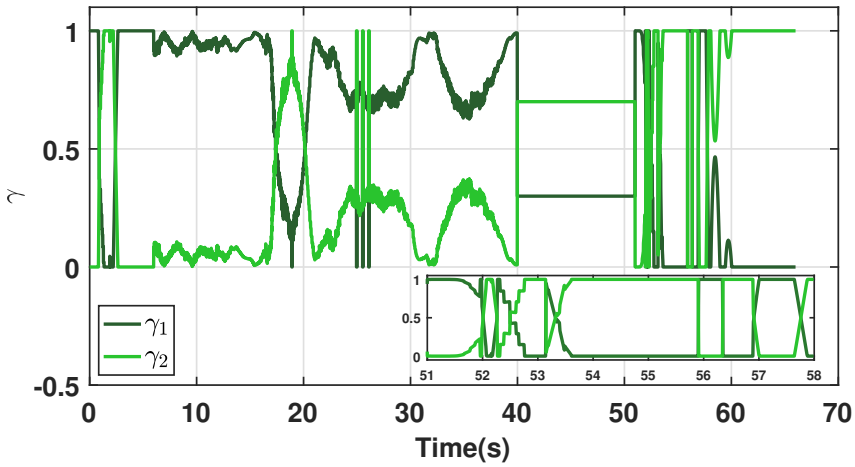

FIGURE 6.12: Interpolating signal γ

- When $t \in [5, 40]s$, during the four successive turns, the four tested controllers have almost similar tracking performance (check Fig. 6.11a), where there exists low steering noises using the fast controller $\tilde{K}(\rho, [0, 1])$ as shown in Fig. 6.11c.
- When $t \in [42, 48]s$, on the straight highway, Fig. 6.11a shows that the slow controllers ($K^{(0)}(\rho)$, $\tilde{K}(\rho, [1, 0])$) have lateral oscillations due to actuator limitations (for smoothness). On the other hand, the fast controller $\tilde{K}(\rho, [0, 1])$ and $\tilde{K}(\rho, \gamma)$ could handle the vehicle. This is achieved due to the use of the steering speed in the proposed equations of γ_2, γ changes to $[0.3, 0.7]$.
- Finally, when $t \in [52, 62]s$, Fig. 6.10 shows that only $\tilde{K}(\rho, [0, 1])$ could not perform a fast double lane-change to overcome an obstacle (represented as "x"). Although the nominal and the smooth controllers $K^{(0)}(\rho)$ and $\tilde{K}(\rho, [1, 0])$ could succeed in performing it, however, the vehicle performs high lateral oscillations. On the other hand, $\tilde{K}(\rho, \gamma)$ shows better performance without any lateral overshoots (see Fig. 6.11a) and with a very smooth and optimized steering action (see Fig. 6.11b and 6.11c when $t \in [52, 62]s$).

Thanks to the variations of γ which reflects the needed lateral task to the proposed parameterized controller $\tilde{K}(\rho, \gamma)$, obtaining a combination between the designed performances.

The next section introduces the improvement obtained by interpolating between YK-based LPV controllers instead of polytopic-based.

6.7 Interpolation of YK-based LPV controllers

In this section, a more advanced interpolation scheme is introduced, where the interpolation LPV controllers are designed based on YK parameterization as has been discussed in Section 5.5.2. The objective of this method is to:

1. Design two of gain-scheduled controllers $K^{(j)}(\rho)$, $j \in \mathbb{I}[1, 2]$. Each one is designed by interpolating its corresponding LTI controllers $K_i^{(j)}$ ($i \in \mathbb{I}[1, 2^{n_p}]$) based on YK parameterization. The nominal controller $K^{(0)}(\rho)$ is design based on the standard polytopic LPV approach.

2. Create an overall interpolation scheme between the gain-scheduled controllers $K^{(j)}(\rho)$ ($j \in \mathbb{I}[0,2]$), by an interpolating signal vector γ, which is referred to as $\tilde{K}(\rho,\gamma)$, such that the resultant LPV-YK controller $\tilde{K}(\rho,\gamma)$ quadratically stabilizes $G(\rho)$ $\forall \rho \in \mathcal{P}$ and for every $\gamma = [\gamma_1, \gamma_2]$.

6.7.1 Lateral Control Design

The first improvement that can be mentioned about using YK-based LPV controllers instead of polytopic-based, is that the control design conservatism can be decreased. Consequently, in this section, the longitudinal speed can be considered in $[1,30]m/s$ (while it has been in $[3,30]m/s$ in Section 6.7). $G(\rho)$ is written as a convex combination of the vertices of the polytope

$$\mathcal{P} = \mathcal{C}_{\mathcal{O}}\{(\underline{\rho_1},\underline{\rho_2}),(\underline{\rho_1},\overline{\rho_2}),(\overline{\rho_1},\underline{\rho_2})\} = \mathcal{C}_{\mathcal{O}}\{(1,\frac{1}{30}),(1,\frac{1}{1}),(30,\frac{1}{30})\} \tag{6.20}$$

with the state-space representation as is described in (6.4)-(6.6).

Referring to Fig. 5.6, assumptions (A.2.1)-(A.2.2) and **Theorem** 6 in Section 5.5.2, a highly robust LPV controller $K^{(0)}(\rho)$, and two gain-scheduled controllers $K^{(1)}(\rho)$ and $K^{(2)}(\rho)$ are designed to perform different required performances as follows:

- The polytopic-based LPV controller $K^{(0)}(\rho)$ is designed using the standard polytopic approach. A slow transient response and noise rejection performances are required for the nominal controller $K^{(0)}(\rho)$ using weighting functions $W_e^{(0)}$ and $W_u^{(0)}$ as follows:

$$W_e^{(0)}(s) = \frac{s+2}{2s+0.002}, \quad W_u^{(0)}(s) = \frac{s+5}{0.01s+5} \tag{6.21}$$

The closed-loop step responses are obtained as shown in Fig. 6.13.

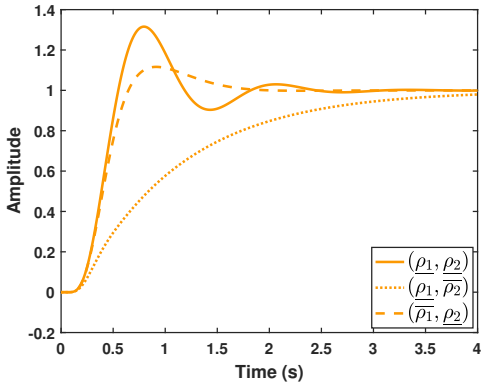

FIGURE 6.13: Closed-loop step response with $K^{(0)}(\rho)$

- LTI controllers $K_i^{(1)}$ are designed separately using LTI/$\mathcal{H}_\infty$ concept at each vertex w_i to perform smooth lateral transitions which is important to provide comfort riding. This is achieved using the following weighting functions $W_e^{(1)}$ and $W_u^{(1)}$ $\forall i$:

$$W_e^{(1)}(s) = \frac{s+2}{2s+0.002}, \quad W_u^{(1)}(s) = \frac{s+10}{0.01s+10} \tag{6.22}$$

The closed-loop step responses are obtained as shown in Fig. 6.14.

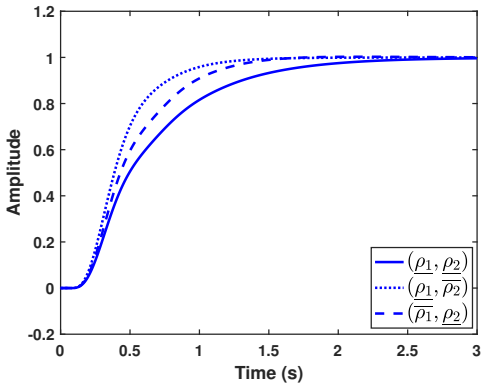

FIGURE 6.14: Closed-loop step response with $K_1^{(1)}$, $K_2^{(1)}$, and $K_3^{(1)}$ at the polytopic vertices

- LTI controllers $K_i^{(2)}$ are designed separately using LTI/$\mathcal{H}_\infty$ concept at each vertex w_i to perform fast lateral transitions to handle the vehicle when facing aggressive maneuvers and lateral oscillations. The chosen weighting functions are $W_e^{(2)}$ and $W_u^{(2)}$ $\forall i$ as:

$$W_e^{(2)}(s) = \frac{s+20}{2s+0.02}, \quad W_u^{(2)}(s) = \frac{10s+25}{0.1s+500} \tag{6.23}$$

The closed-loop step responses are obtained as shown in Fig. 6.15.

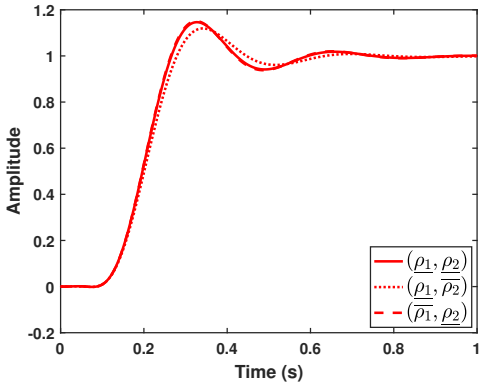

FIGURE 6.15: Closed-loop step response with $K_1^{(2)}$, $K_2^{(2)}$, and $K_3^{(2)}$ at the polytopic vertices

It is worth noting the difference in closed-loop step responses between the ones in Fig. 6.6 and Fig. 6.14, and Fig. 6.7 and Fig. 6.15. The difference of using polytopic-based control design and LTI control design is clearly observed at each polytopic vertex.

6.7.2 Design the LPV-YK Control Structure

The following steps are done to design the LPV-YK control shown in Fig. 6.4:

1. According to the LMIs explained in Section **Theorem** 6, the LPV polytopic-based state-feedback controller $F_g(\rho)$, and the LTI state-feedback controllers $F_{k,i}^{(0)}$, $\forall i \in \mathbb{I}[1,4]$, are designed. After finding the decision variables W_i ($i \in$

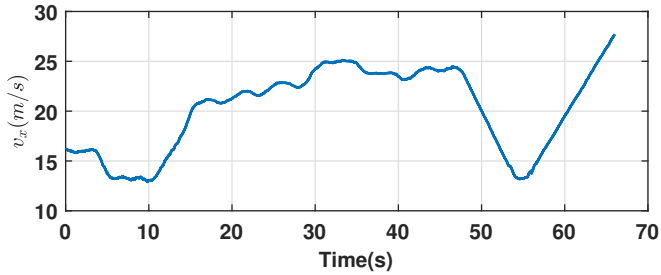

FIGURE 6.16: Simulation: Parameter-varying longitudinal speed v_x (m/s)

$\{1,2,3\}$) and X_g from (5.45), and V_i and $X_{k,i}$ ($i \in \{1,2,3\}$) from (5.46). Then , $F_g(\rho)$ and $F_k^{(0)}(\rho)$ are computed as

$$\begin{aligned} F_g(\rho) &= \sum_{i=1}^{3} W_i X_g^{-1}, \\ F_k^{(0)}(\rho) &= \sum_{i=1}^{3} V_i X_{k,i}^{-1} \end{aligned} \tag{6.24}$$

2. The state-space representations of $M(\rho)$, $N(\rho)$, $U^{(0)}(\rho)$ and $V^{(0)}(\rho)$ are computed as illustrated in Section 6.5.1. $\tilde{Q}(\rho,\gamma)$ is formulated as:

$$\tilde{Q}(\rho,\gamma) = \sum_{j=1}^{2} \gamma_j Q^{(j)}(\rho) \tag{6.25}$$

where $Q^{(j)}(\rho)$ are obtained from (5.54), $\forall j \in \{1,2\}$.

3. Here, the interpolating signal $\gamma(t) = [\gamma_1(t), \gamma_2(t)]$ is chosen as in the previous section as follows:

   - if $\theta_e \leq 0.1$, $\gamma_2(t) = sat(-y_L + 1.4 + 0.1\dot{\delta}, [0,1])$
   - if $\theta_e > 0.1$, $\gamma_2(t) = sat(-0.7y_e + 1.4, [0,1])$
   - $\gamma_1(t) = 1 - \gamma_2(t)$

The following two sub-sections introduce simulation and experimental results of the designed LPV-YK control structure.

6.7.3 Simulation Results

The parameterized LPV-YK controller $\tilde{K}(\rho,\gamma)$ is simulated on a nonlinear full car model designed for a Renault ZOE vehicle. The performed simulation is similar to the one in the previous section, using the scheme shown in Fig. 6.8. The scenario, the test track, the longitudinal speed profile are exactly the same used in the previous section.

The scenario is tested with different controllers:

- The nominal highly robust controller: $\tilde{K}(\rho,[0,0]) \equiv K^{(0)}(\rho)$,
- The smooth tracker: $\tilde{K}(\rho,[1,0]) \equiv K^{(1)}(\rho)$,
- The aggressive tracker: $\tilde{K}(\rho,[0,1]) \equiv K^{(2)}(\rho)$,

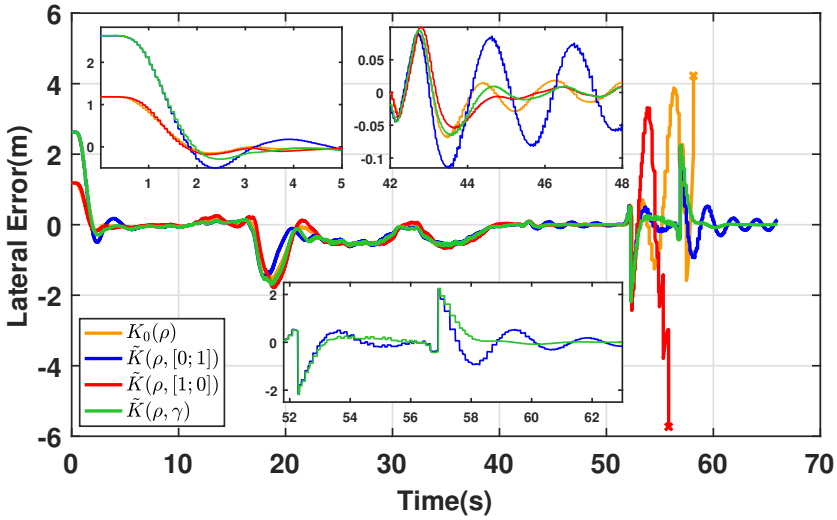

(A) Lateral error y_e (m)

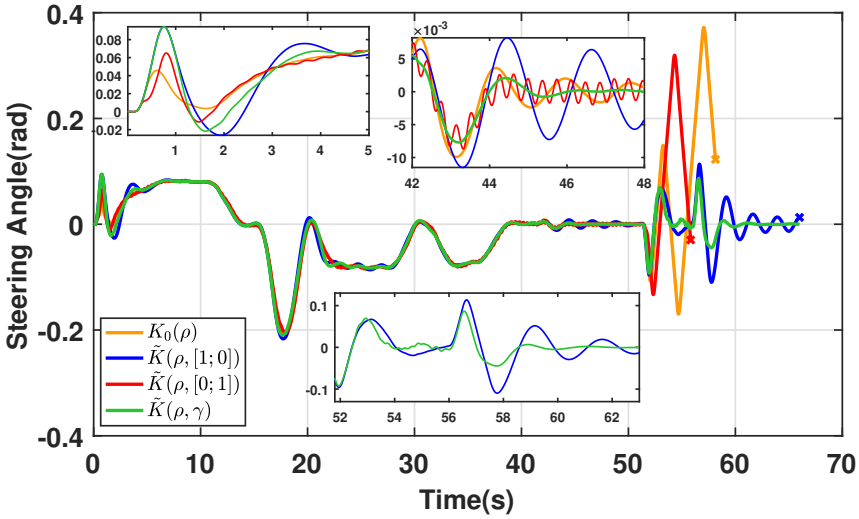

(B) Control input steering wheel angle (rad)

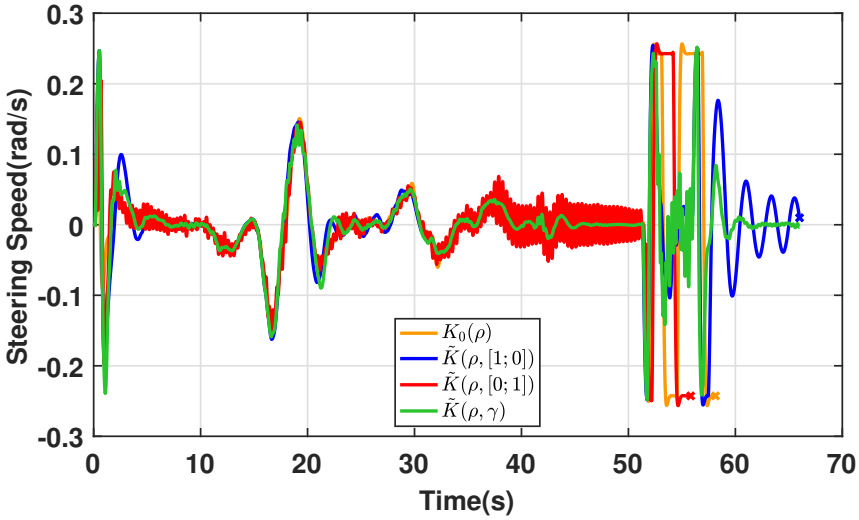

(C) Steering speed $\dot{\delta}$ (rad/s)

FIGURE 6.17: Simulation results

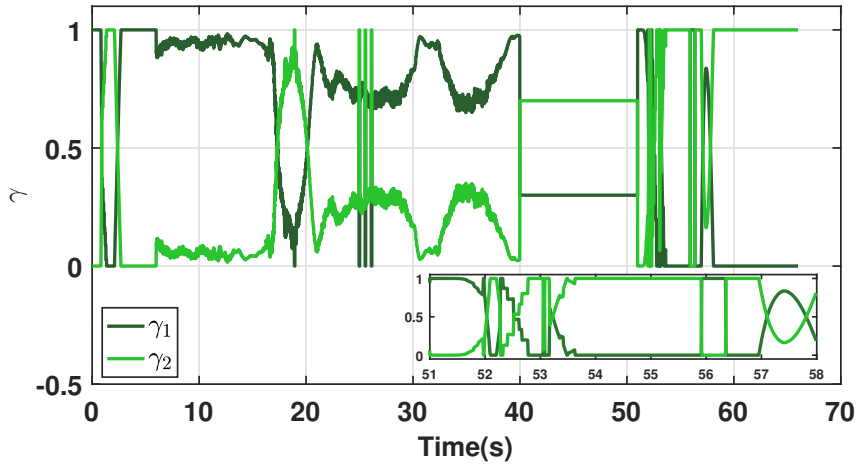

FIGURE 6.18: Interpolating signal γ

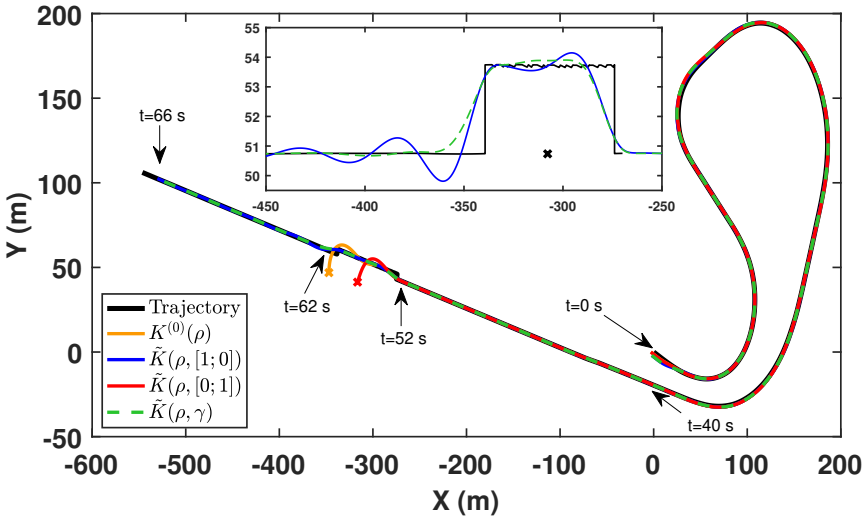

FIGURE 6.19: Simulation: Planned and controlled trajectories

- The proposed LPV-YK controller: $\tilde{K}(\rho,\gamma)$ with $\gamma = [\gamma_1, \gamma_2]$ varies in real-time

Fig. 6.16 shows the speed profile for all the tests. Fig. 6.17a depicts the lateral error from the reference trajectory to the vehicle Center of Gravity (CoG), and the steering control input is shown in Fig. 6.17b. Fig. 6.17c represents the steering speed which reflects the driving comfort. Fig. 6.18 shows the evolution of the interpolating signal γ for $\tilde{K}(\rho,\gamma)$, and Fig. 6.19 shows the (X-Y) coordinates of the reference trajectory and the vehicle positioning response of the different tested controllers.

- At $t = 0s$, it is shown in Fig. 6.17a that only some of the tested controllers are activated to start at high lateral error ($y_e > 2.5m$), since both controllers $K^{(0)}(\rho)$ and $\tilde{K}(\rho,[0,1])$ can't deal with large lateral errors (observed from pre-testing). On the other hand, $\tilde{K}(\rho,[1,0])$ and $\tilde{K}(\rho,\gamma)$ perform better with the initial high lateral error, where $\tilde{K}(\rho,\gamma)$ shows a lower overshoot (see Fig. 6.17a when $t \in [2,5]s$) with a smoother steering action (see Fig. 6.17b when $t \in [2,4]s$).

- When $t \in [5,40]s$, during the four successive turns, the four tested controllers have almost similar tracking performance (check Fig. 6.17a), where there exists low steering noises using the fast controller $\tilde{K}(\rho,[0,1])$ as shown in Fig. 6.17c.

- When $t \in [42,48]s$, on the straight highway, Fig. 6.17a shows that the slow controllers ($K^{(0)}(\rho)$, $\tilde{K}(\rho,[1,0])$) have lateral oscillations due to actuator limitations (for smoothness). On the other hand, the fast controller $\tilde{K}(\rho,[0,1])$ could handle the situation, but demanding more steering effort with noises (see Fig. 6.17c when $t \in [42,48]s$). However, due to the use of the steering speed in the proposed equations of γ_2, γ changes to $[0.3, 0.7]$, and $\tilde{K}(\rho,\gamma)$ achieves a perfect trade-off between decreasing the lateral oscillations (in Fig. 6.17a) and relaxing the steering action (in Fig. 6.17b and 6.17c).

- Finally, when $t \in [52,62]s$, it is clear in Fig. 6.19 that both $K^{(0)}(\rho)$ and $\tilde{K}(\rho,[0,1])$ could not perform a fast double lane-change to overcome an obstacle (represented as "**x**"). Although the smooth controller $\tilde{K}(\rho,[1,0])$ could succeed in performing it, however, the vehicle performs high lateral oscillations. On the other hand, $\tilde{K}(\rho,\gamma)$ shows better performance without any lateral overshoots (see Fig. 6.17a) and with a very smooth and optimized steering action (see Fig. 6.17b and 6.17c when $t \in [52,62]s$).

Thanks to the variations of γ which reflects the needed lateral task to the proposed parameterized controller $\tilde{K}(\rho,\gamma)$, obtaining a combination between the designed performances.

Table 6.1 summarizes the conclusions behind the simulation results that are considered similar between the YK-based and polytopic-based interpolation, with much performance improvement using the YK-based interpolation.

6.7.4 Experimental Results

The LPV-YK controller $\tilde{K}(\rho,\gamma)$ is tested on the robotized electric Renault ZOE vehicle. Previously in Chapter 4, we have tested a polytopic-based LPV controller $K_1(\rho)$ (see Section 4.5) which has been designed with the weights $W_e^{(1)}$ and $W_u^{(1)}$ (i.e. the same weights used to design $\tilde{K}(\rho,[1,0])$), and using the standard polytopic optimisation problem [12]. Notice that the interpolating signal vector γ is switched manually during the test. This experimental test mainly aims to:

TABLE 6.1: Overview of the tested controllers in simulation

Controller	Value of interpolating vector γ	Control objective	Advantages	Disadvantages
$\tilde{K}(\rho,[0,0])$ $\equiv K^{(0)}(\rho)$	[0,0]	Highly robust	High noise rejection due to bad environment conditions, sensor faults, etc.	Inaccurate tracking performance and conservative
$\tilde{K}(\rho,[1,0])$ $\equiv K^{(1)}(\rho)$	[1,0]	Smooth tracker	Good tracking performance with smooth steering	Oscillatory and cannot perform well at high lateral accelerations
$\tilde{K}(\rho,[0,1])$ $\equiv K^{(2)}(\rho)$	[0,1]	Aggressive tracker	Fast tracking performance and could achieve high lateral accelerations	Too sensitive to noises
$\tilde{K}(\rho,\gamma)$	variant as in Fig. 6.18	Multiple objectives by varying the interpolating vector γ.	All the mentioned advantages and even more by choosing the optimal combination of controllers by γ	No bad performance is observed

1. Compare both controllers $K_1(\rho)$ and $\tilde{K}(\rho,[1,0])$.
2. Observe the controller response when γ switches aggressively as a step function.

The test is done in a part of *Satory* test-track shown in Fig. 6.20. Fig. 6.21 shows the variation of the measured longitudinal speed in *Kph* which is considered to be coherent with respect to the road curvature. The vehicle starts on a straight highway using the smooth controller $\tilde{K}(\rho,[1,0])$. Then, it switches to the faster controller $\tilde{K}(\rho,[0,1])$ when approaching two successive maneuvers (at $t = 20s$) aiming to achieve the lowest lateral error. After exiting the successive maneuvers, it switches again to the smooth controller $\tilde{K}(\rho,[1,0])$ (at $t = 50s$) and enters a second maneuver to compare its performance to the previously tested polytopic LPV controller $K_1(\rho)$.

Regarding Figs. 6.22a and 6.22b, it is clearly shown that the vehicle performance is not affected during the switching times (at $t = 20s$ and $t = 50s$) with negligible transient response.

- When $t \in [20,50]s$, $\tilde{K}(\rho,[0,1])$ achieves smaller lateral error compared to $K_1(\rho)$ (see Fig. 6.22a), but with low steering noises as shown in Fig. 6.22b. Notice that these steering noises has been observed also in simulation section for $\tilde{K}(\rho,[0,1])$.
- When $t \in [65,85]s$, $\tilde{K}(\rho,[1,0])$ shows lower lateral error during maneuvering compared to $K_1(\rho)$. This appears since the LPV-YK controller $\tilde{K}(\rho,[1,0])$ is less conservative than the polytopic LPV controller $K_1(\rho)$.

The next two sections implements the LPV-YK control structure to switch between multiple parameter subsets aiming to maintain a unique closed-loop performance over the whole parameter region.

6.8 Partitioned LPV-YK controller

This section implements the partitioned LPV-YK controller, proposed in Section 5.6.3, to the lateral dynamics of an autonomous vehicle, since it contains a non-affine scheduling parameter which causes an overbounding convex parameter region when implementing the polytopic approach. Designing steps and experimental results are depicted in the following subsections.

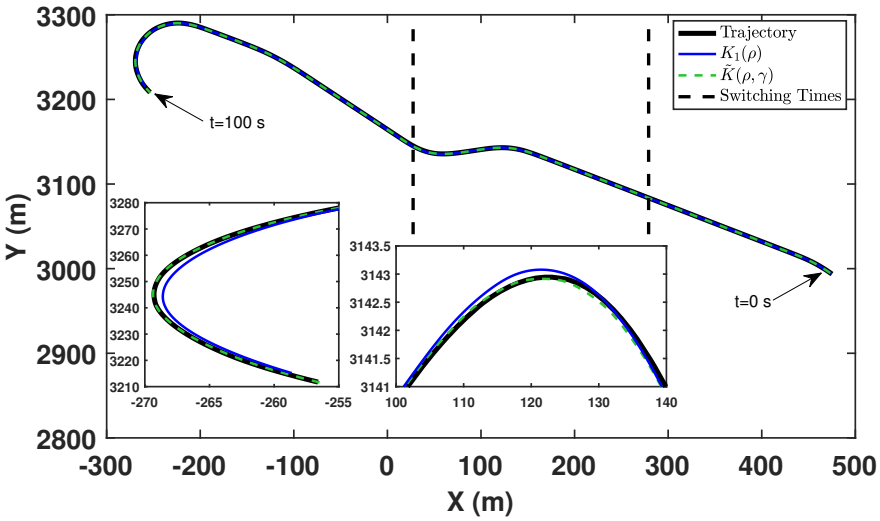

FIGURE 6.20: Experimental planned and controlled trajectories

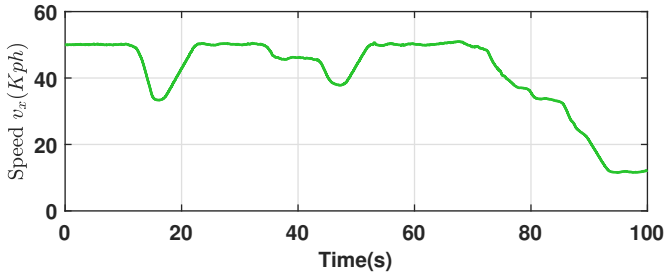

FIGURE 6.21: Experimental longitudinal speed v_x (Kph)

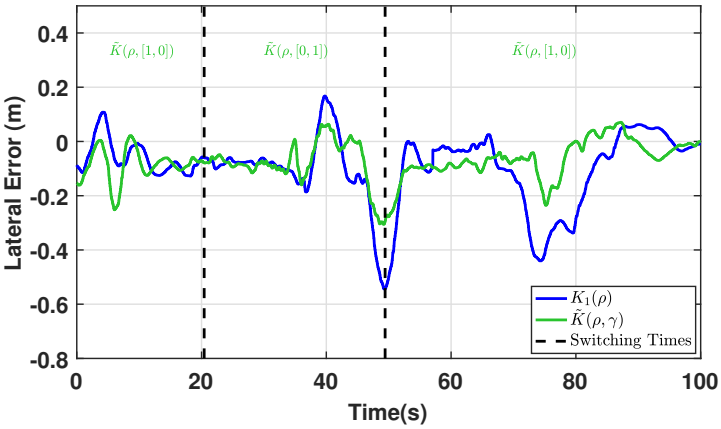

(A) Lateral error y_e (m)

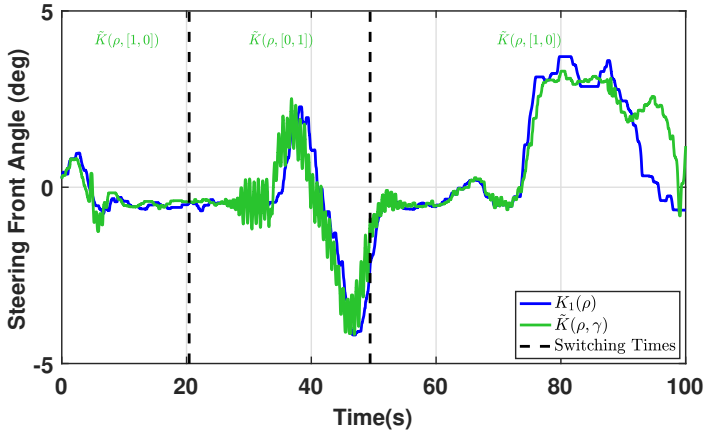

(B) Steering front angle δ (deg)

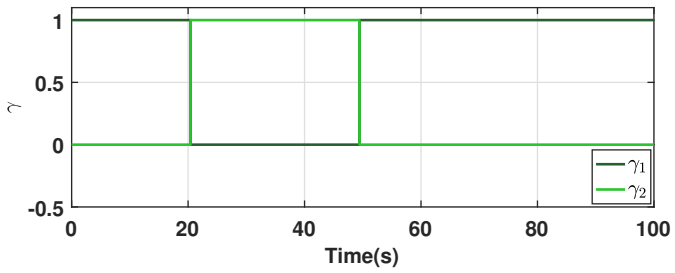

(C) Interpolating signal γ

FIGURE 6.22: Experimental results

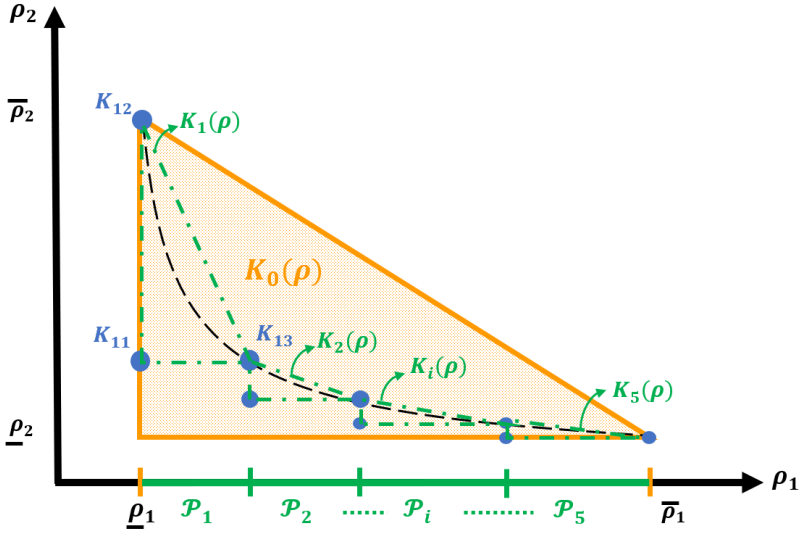

FIGURE 6.23: Partitioned parameter region

The longitudinal speed is assumed to vary within the range $v_x[5, 30]\ m/s$. Since the system dynamics changes significantly in this speed range, it could be conservative to design a single LPV controller over the full parameter region. Thus, the parameter region is divided into 5 subsets as:

$$v_x \in [5, 10] \cup [10, 15] \cup [15, 20] \cup [20, 25] \cup [25, 30] \tag{6.26}$$

The objective of this method is to:

1. Design multiple YK-based gain-scheduled controllers $\tilde{K}_i(\rho)$, $i \in \mathbb{I}[1, 5]$. Each one is designed by interpolating its corresponding LTI controllers K_{ij} ($j \in \mathbb{I}[1, 2^{n_p}]$) based on YK concept (refer to Fig. 6.23).

2. Create an overall switched LPV-YK controller $\tilde{K}_\sigma(\rho)$ to switch between $\tilde{K}_i(\rho)$, such that $\tilde{K}_\sigma(\rho)$ quadratically stabilizes $G(\rho)$ $\forall \rho \in \mathcal{P}$ and for every continuous/discontinuous switching signal $\sigma(t)$.

6.8.1 Lateral Control Design

$G(\rho)$ is written here as a convex combination of the vertices of a triangular polytope $\mathcal{P}_0 = \mathcal{CO}\{(\underline{\rho_1}, \underline{\rho_2}), (\underline{\rho_1}, \overline{\rho_2}), (\overline{\rho_1}, \underline{\rho_2})\}$ as shown in Fig. 6.23 with the state-space representation as is described in (6.4)-(6.6). This section aims to design the partitioned polytopic-based LPV-YK control. Five triangular convex subsets ($\mathcal{P}_1 \dots \mathcal{P}_5$) are chosen along the parameter trajectory as shown in Fig. 6.23.

The nominal LPV controller $K_0(\rho)$ is designed, based on (A.3.1), using the weighting functions $W_{e,0}$ and $W_{u,0}$ defined as:

$$W_{e,0}(s) = \frac{s+2}{2s+0.002}, \quad W_{u,0}(s) = \frac{s+5}{0.01s+5} \tag{6.27}$$

The following closed-loop step responses are obtained as shown in Fig. 6.24.

In addition, at the polytopic vertices w_{ij} $\forall i \in \mathbb{I}[1, 5], \forall j \in \mathbb{I}[1, 3]$, LTI controllers K_{ij} are designed, based on (A.3.2), separately using the same weighting functions W_e and W_u chosen to present the tracking performance and the actuator limitations respectively. as:

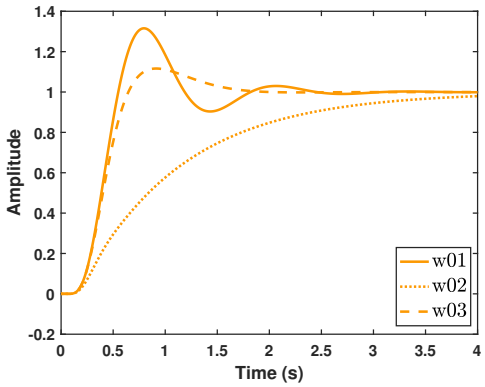

FIGURE 6.24: $K_0(\rho) \in \mathcal{P}_0$

$$W_e(s) = \frac{s+2}{2s+0.002}, \quad W_u(s) = \frac{s+10}{0.01s+10} \tag{6.28}$$

The closed-loop step responses are shown in Fig. 6.25.

6.8.2 Design the LPV-YK Control Structure

Referring to Fig. 6.23, assumptions (A.3.1)-(A.3.2) and **Theorem** 7 in Section 5.6.3, the design of the partitioned polytopic-based LPV-YK (shown in Fig. 6.4) is done according to the following steps:

1. According to the LMIs in Theorem 7, the LPV polytopic-based state-feedback controller $F_g(\rho)$, and the LTI state-feedback controllers $F_{k,i}(\rho)$, $\forall i \in \mathbb{I}[1,5]$, are designed. After finding the decision variables W_{0j} ($j \in \{1,2,3\}$) and X_g from (5.70), and V_{ij} and $X_{k,ij}$ ($i \in \mathbb{I}[1,5]$,$j \in \{1,2,3\}$) from (5.71). Then, $F_g(\rho)$ and $F_k^{(0)}(\rho)$ are computed as

$$\begin{aligned} F_g(\rho) &= \sum_{j=1}^{3} W_{0j} X_g^{-1}, \\ F_{k,i}^{(0)}(\rho) &= \sum_{j=1}^{3} V_{ij} (X_{k,ij})^{-1}, \quad \forall i \in \mathbb{I}[1,5] \end{aligned} \tag{6.29}$$

2. The state-space representations of $M(\rho)$, $N(\rho)$, $U_0(\rho)$ and $V_0(\rho)$ are computed as illustrated in Section 6.5.1. $\tilde{Q}(\rho,\gamma)$ is defined here as $Q_\sigma(\rho)$, recall that σ represents the switching signals which changes at the intersecting boundaries of the parameter subsets. $Q_i(\rho)$ are obtained from (5.74), $\forall j \in \{1,5\}$. It is worth mentioning that the switching signal is called σ instead of γ, since the signal does not appear in the closed-loop state matrix, whereas the closed-loop state matrix switches from one to another.

3. Here, the switching signal σ depends only on the varying parameter ρ, where switching occurs at the intersecting boundaries of the parameter subsets.

The current structure has been directly experimentally validated on the ZOE vehicle as shown in the next shown.

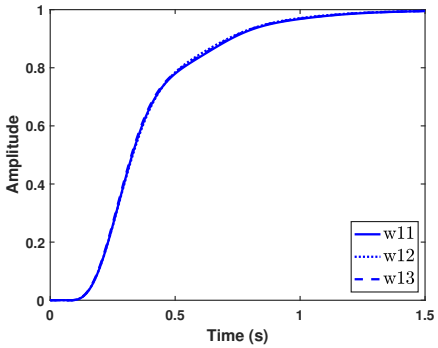

(A) K_{11}, K_{12}, and $K_{13} \in \mathcal{P}_1$

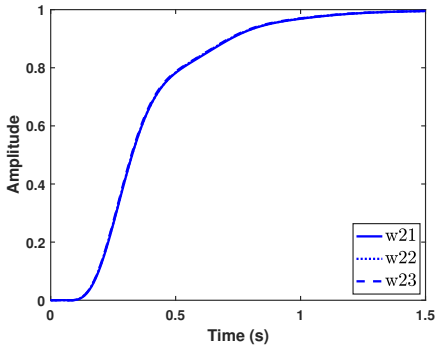

(B) K_{21}, K_{22}, and $K_{23} \in \mathcal{P}_2$

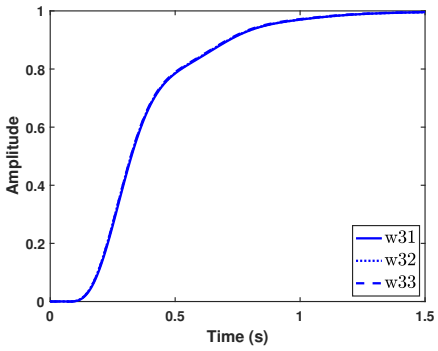

(C) K_{31}, K_{32}, and $K_{33} \in \mathcal{P}_3$

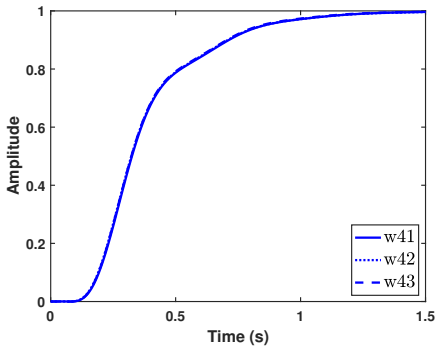

(D) K_{41}, K_{42}, and $K_{43} \in \mathcal{P}_4$

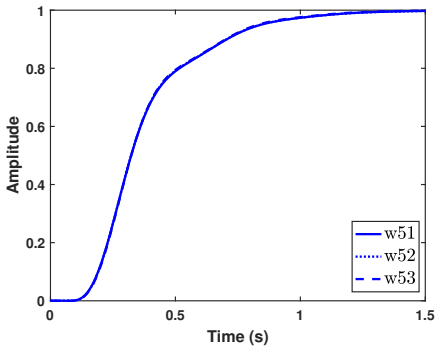

(E) K_{51}, K_{52}, and $K_{53} \in \mathcal{P}_5$

FIGURE 6.25: Closed-loop step response with K_{ij} $\forall i \in \mathbb{I}[1,5]$ and $\forall j \in \mathbb{I}[1,3]$

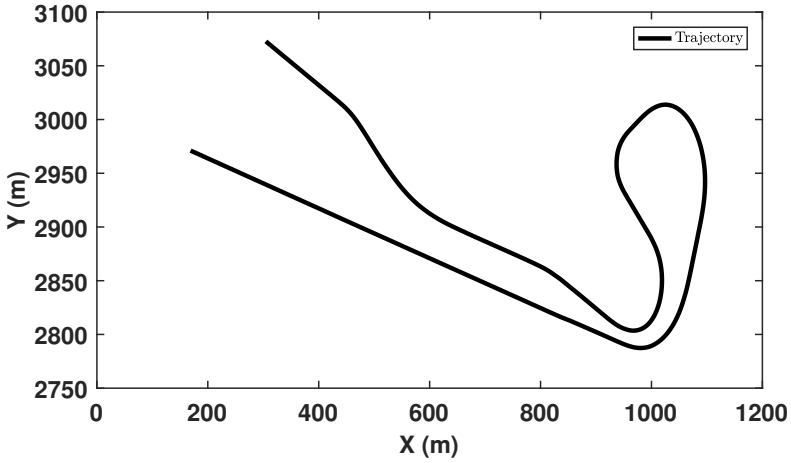

FIGURE 6.26: Experimental planned and controlled trajectories

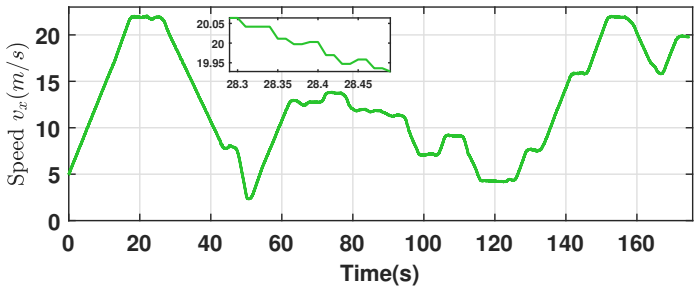

FIGURE 6.27: Experimental longitudinal speed v_x (Kph)

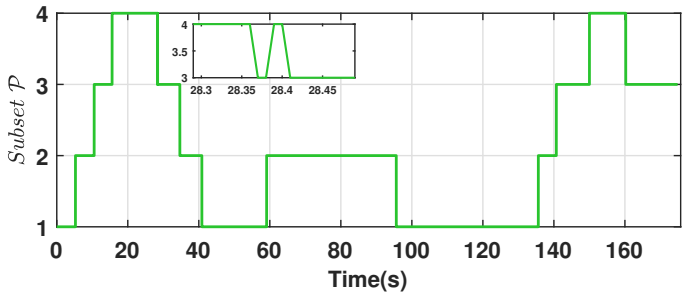

FIGURE 6.28: Parameter subsets

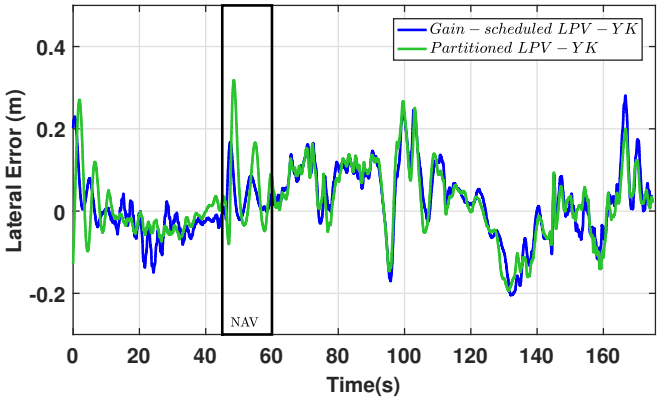

(A) Lateral error y_e (m)

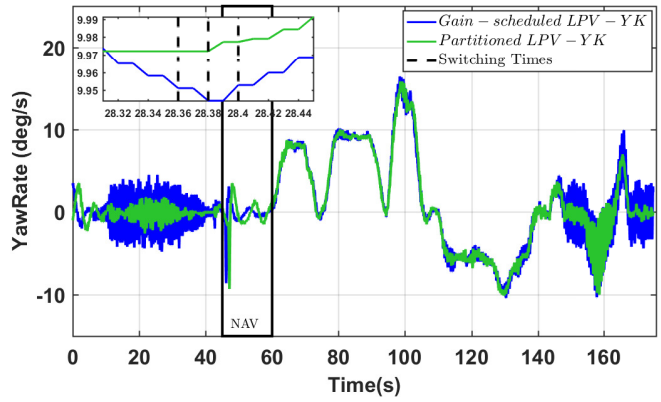

(B) Yaw rate w (deg/s)

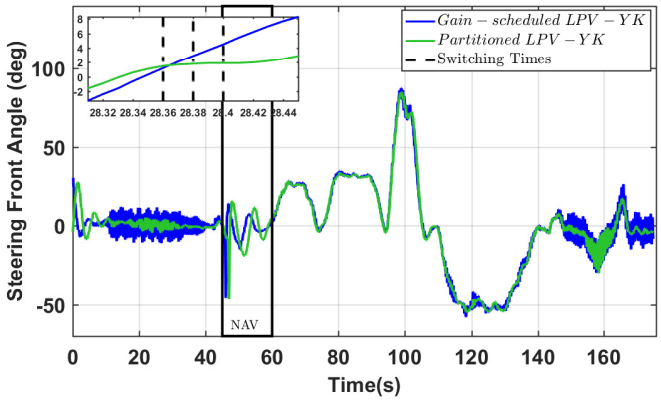

(C) Steering front angle δ (deg)

FIGURE 6.29: Partitioned polytopic-based LPV-YK control

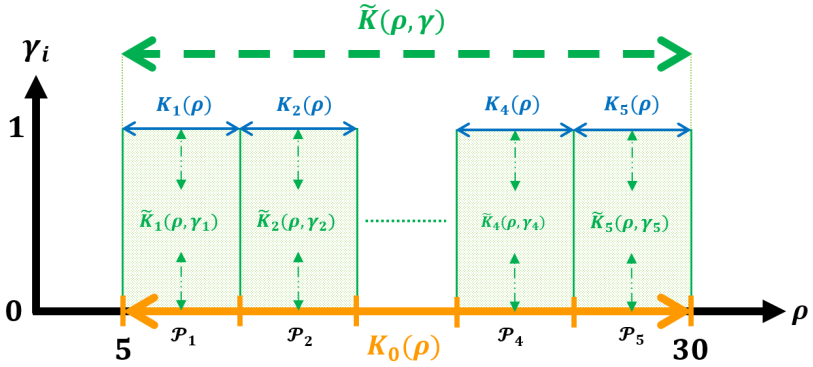

FIGURE 6.30: Multiple Parameter Subregions

6.8.3 Experimental Results

To validate the improvement caused by the proposed partitioned polytopic-based LPV-YK control, the vehicle performance is analyzed and compared to a gain-scheduled LPV-YK controller. The gain-scheduled LPV-YK controller is referred to a YK-based polytopic LPV controller that is designed over the whole parameter region $\mathcal{P}_0$ (for instance, as the design on $K^{(1)}(\rho)$ in the previous section). Notice that, in all the tests, a restarting mode of the navigation systems appears at the end of the highway. Consequently, the results analysis doesn't concern the boarded part marked "NAV".

The experiments shown here have been carried out on the Renault ZOE vehicle. The test results of the designed controllers are discussed concerning their implementation and the analysis of the obtained performance. The tests are done in a private test track in *Satory* as shown in Fig. 6.26. The first part of the test describes the response of the controllers at a straight highway with high speeds. The second part concerns the precision of lateral control at optimal speeds chosen coherently depending on the road curvature.

The longitudinal speed is considered as an external parameter of the LPV mode that is shown in Fig. 6.27. Fig. 6.28 presents the operating parameter subset that switches according to the speed evolution. Fig. 6.29a depicts the lateral error from the reference trajectory to the vehicle Center of Gravity (CoG). Fig. 6.29b represents the yaw rate of the vehicle, and the steering control input is shown in Fig. 6.29c.

It is shown in Fig. 6.29a that both controllers, the proposed partitioned and gain-scheduled LPV-YK, could successfully achieve lateral error minimization. On the other hand, the gain-scheduled LPV-YK controller leads to higher steering oscillations, compared to the partitioned LPV-YK controller, as shown in Figs. 6.29b and 6.29c.

When $t \in [28.3, 28.5]s$, it is observed in Fig. 6.28 switches hysterically back and forth between the subsets $\mathcal{P}_3$ and $\mathcal{P}_4$. However, the hysterical switching of the partitioned LPV-YK controller between both subsets didn't affect the performance of the steering input and consequently the yaw rate (see the zoomed part in Figs. 6.29c and 6.29b). This is expected since, at that instants, the operating controllers at that intersecting boundary are dynamically equivalent, i.e. $\mathcal{F}_l(G, J_{33}, Q_{33}) \equiv \mathcal{F}_l(G, J_{42}, Q_{42})$.

6.9 Grid-based LPV-YK controller

This section implements the grid-based LPV-YK controller, proposed in Section 5.6.4, to the lateral dynamics of an autonomous vehicle, aiming to achieve robust performance. Designing steps and experimental results are depicted in the following subsections.

As in the previous section, the parameter region is divided into 5 subsets as:

$$\rho \in [5, 10] \cup [10, 15] \cup [15, 20] \cup [20, 25] \cup [25, 30] \tag{6.30}$$

Each parameter subset is gridded with six grid points spaced equally.

The objective of grid-based LPV-YK control structure is to obtain exponential stability of the closed-loop system based on YK parameterisation. Moreover, a smooth interpolation scheme $\tilde{K}(\rho, \gamma)$ is formulated between multiple pre-designed LPV controllers $K_i(\rho)$ ($i \in \mathbb{I}[1, 5]$), using the switching signal $\gamma = [\gamma_1, , ..., \gamma_5]$, where each $K_i(\rho)$ is designed to be suitably used for a certain parameter subregion $\mathcal{P}_i$. This could be achieved by two steps:

1. Parameterize each LPV controller $K_i(\rho)$ ($i \in \mathbb{I}[1, 5]$) with respect to the nominal LPV controller $K_0(\rho)$, by an LPV-YK parameter $Q_i(\rho)$.

2. At each boundary of two adjacent subsets $\mathcal{P}_i$ and $\mathcal{P}_{i+1}$, the interpolating signals γ_i and γ_{i+1} are adjusted in a way to switch from $K_i(\rho)$ to $K_{i+1}(\rho)$ or vise-versa. As a result, the overall parameterized LPV-YK controller $\tilde{K}(\rho, \gamma)$ stabilizes $G(\rho)$ $\forall \rho \in \mathcal{P}$ and for every continuous/discontinuous interpolating signals γ_i, $i \in \mathbb{I}[1, 5]$.

6.9.1 Lateral Control Design

In this section, $G(\rho)$ is not required to have affine parameter-dependency, so it is written as shown in (6.4)-(6.5), over the parameter region presented in Fig. 6.30.

- The nominal LPV controller $K_0(\rho)$ is designed using $W_{e,0}$ and $W_{u,0}$ in (6.27) over the full parameter region $\mathcal{P}$ satisfying (A.4.1).

  The following closed-loop step responses are obtained:

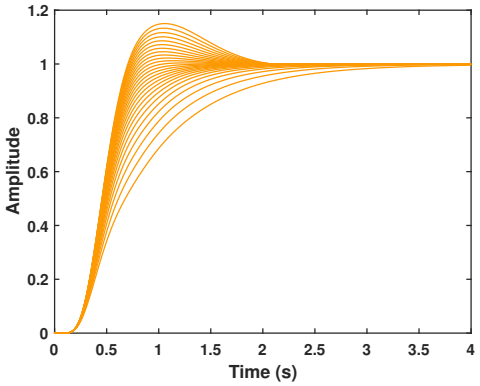

FIGURE 6.31: $K_0(\rho) \in \mathcal{P}_0$

- Following (A.4.2), the controllers $K_i(\rho)$ are designed separately over $\mathcal{P}_i$ ($i \in [1, 5]$), with the same weighting functions W_e and W_u in (6.28).

  The closed-loop step responses are shown in Fig. 6.32

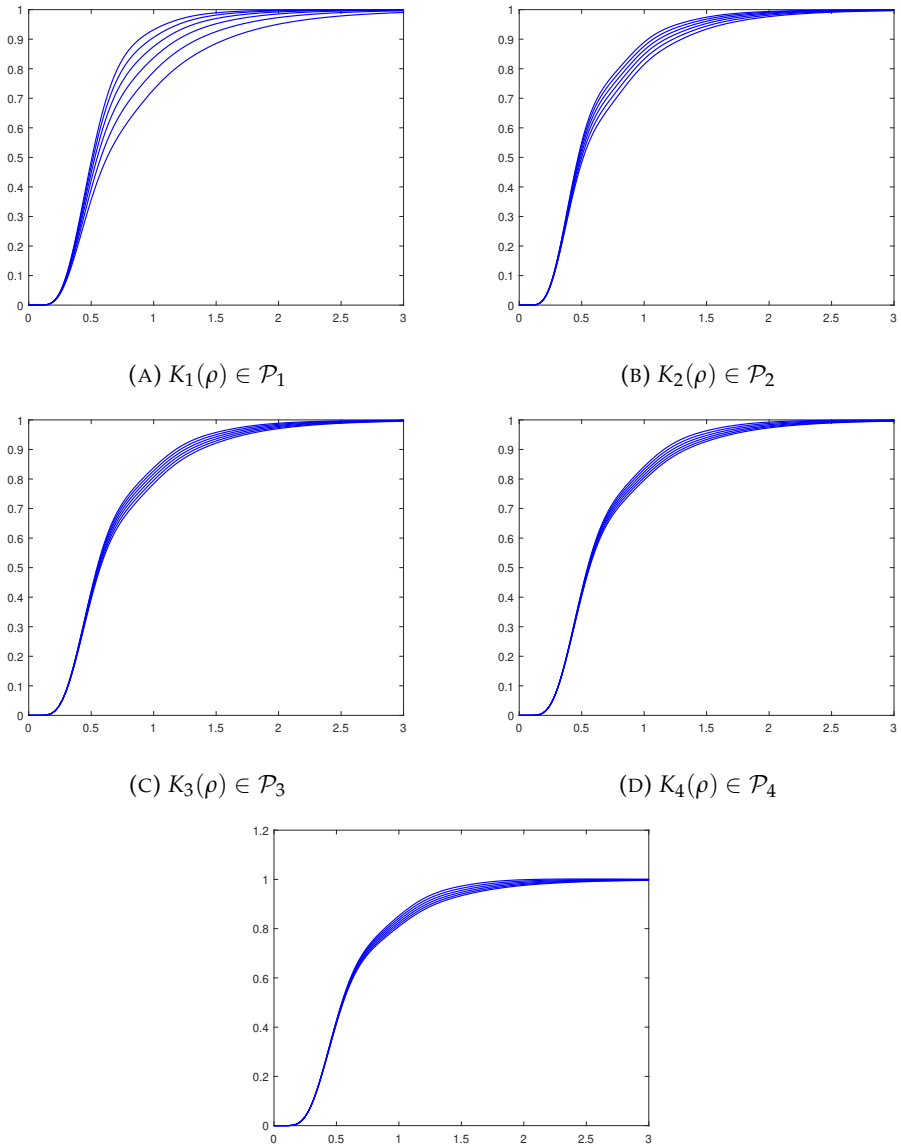

(A) $K_1(\rho) \in \mathcal{P}_1$

(B) $K_2(\rho) \in \mathcal{P}_2$

(C) $K_3(\rho) \in \mathcal{P}_3$

(D) $K_4(\rho) \in \mathcal{P}_4$

(E) $K_5(\rho) \in \mathcal{P}_5$

FIGURE 6.32: Closed-loop step response with K_{ij} $\forall i \in \mathbb{I}[1,5]$ and $\forall j \in \mathbb{I}[1,3]$

6.9.2 Design the LPV-YK Control Structure

Referring to Fig. 5.10, assumptions (A.4.1)-(A.4.2) and **Theorem** 8 in Section 5.6.4, the design of the grid-based LPV-YK (shown in Fig. 6.4) is achieved accordingly to the next steps:

1. Following the conditions of **Theorem 8**, the LPV state-feedback gains $F_g(\rho)$ and $F_{k,0}(\rho)$ are designed using the LMIs (5.85)-(5.86), where the multiple parameter-dependent Lyapunov functions at each subset are specified as affine and smooth functions of scheduling parameters. That is,

$$X_g(\rho) = X_g^0 + X_g^1\,\rho, \quad X_{k,0}(\rho) = X_{k,0}^0 + X_{k,0}^1\,\rho,$$

   where matrices X_g^j and $X_{k,0}^j$, $j = 0, 1$ are the optimization variables to be determined.

2. The state-space representations of $M(\rho)$, $N(\rho)$, $U_0(\rho)$ and $V_0(\rho)$ are computed as illustrated in Section 6.5.1. $\tilde{Q}(\rho,\gamma)$ is formulated as:

$$\tilde{Q}(\rho,\gamma) = \sum_{i=1}^{5} \gamma_i Q_i(\rho) \tag{6.31}$$

   where $Q_i(\rho)$ are obtained from (5.91), $\forall i \in \mathbb{I}[1,5]$.

3. $\gamma_i(\rho)$ is switched between {0,1} when $\rho(t)$ touches the switching boundaries. $Q_i(\rho)$ are obtained from (5.74), $\forall j \in \{1,5\}$. Then, the LPV-YK controller $\tilde{K}(\rho,\gamma)$ is ready to be implemented.

The current structure has been directly experimentally validated on the ZOE vehicle as shown in the next shown.

6.9.3 Experimental Results

To validate the proposed grid-based LPV-YK control, the vehicle performance is analyzed and compared to an LPV-switched controller designed using the Theorem presented in [142]. Similarly to the previous section, a restarting mode of the navigation systems appears at the end of the highway, and the results analysis doesn't concern the boarded part marked "NAV". The scenario in this experiment is exactly the same to the previous experiment with the reference trajectory and the longitudinal speed are as shown in Fig. 6.26 and 6.27 respectively.

Fig. 6.33a depicts the lateral error from the reference trajectory to the vehicle Center of Gravity (CoG). Fig. 6.33b represents the yaw rate of the vehicle, and the steering control input is shown in Fig. 6.33c.

Both controllers achieve minimized lateral error as show in Fig. 6.33a. However, Fig. 6.33b and 6.33c emphasize a clear difference in performances during switching from one subset to another. The zoomed parts in Fig. 6.33c show that the switching effect is negligible using the proposed grid-based LPV-YK controller, which is not the case for the switched LPV controller.

Moreover, it is worth mentioning that the control input response at high speeds is not noisy. However, it has been shown previously in Section 4.5 that designing a single LPV grid-based controller over the whole parameter region may cause noisy performance at high speed.

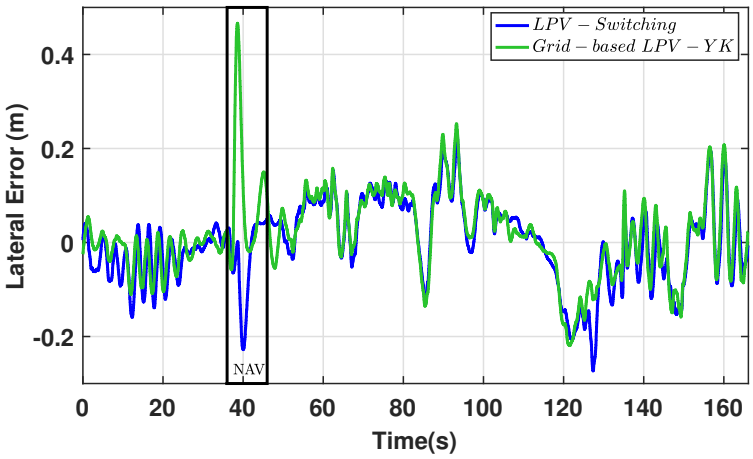

(A) Lateral error y_e (m)

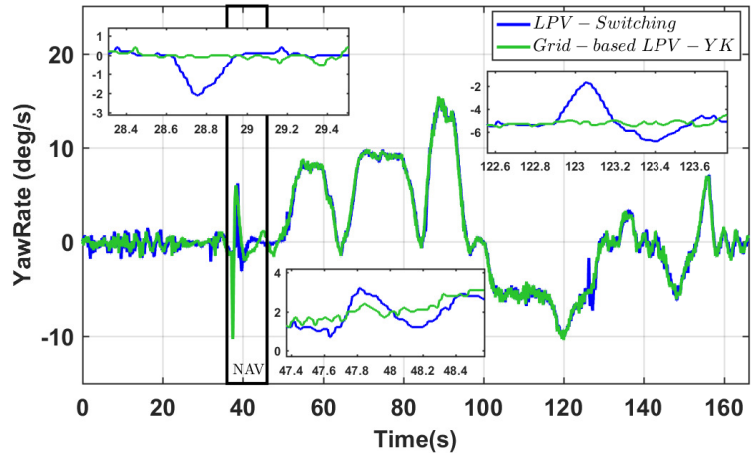

(B) Yaw rate w (deg/s)

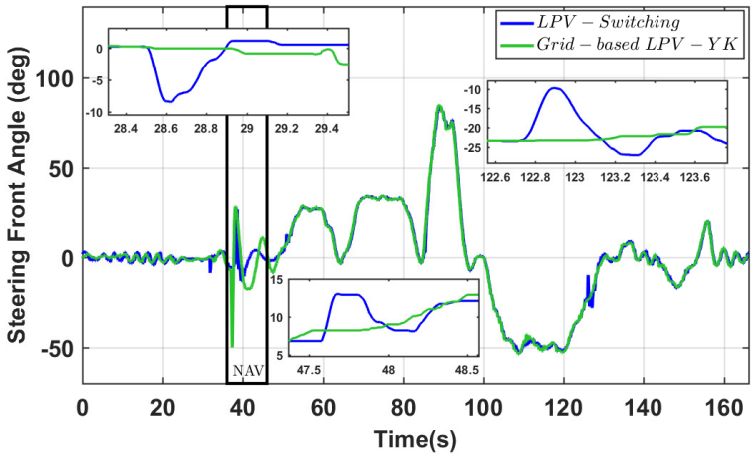

(C) Steering front angle δ (deg)

FIGURE 6.33: Grid-based LPV-YK control

6.10 Conclusion

This chapter has implemented the LPV-YK control structures proposed in the previous chapter. First, it has been used to improve the system performance, while dealing with various objectives and situations. The application to the autonomous vehicle lateral control is carried out. The simulation shows interesting results regarding the efficiency of the proposed method of providing high performance and ensuring safety at critical situations. In addition, experimental results are shown to validate its real performance by testing the approach on a real Renault ZOE vehicle.

Then, the partitioned and grid-based LPV-YK control structures have been implemented to maintain unique closed-loop specifications over the whole parameter region. Both structures have shown remarkable experimental results when compared to the standard LPV control appraoches.

Finally, it is worth mentioning that that the LPV-YK control structure facilitates adding any new controller, by introducing its corresponding LPV-YK parameter to the YK configuration (as shown in Fig. 5.9), without recalling all the control design procedure. This enhances real applications, such as in industries, where the systems are subjected to frequent instrumentation changes such as autonomous vehicles.

An interest appears to study the optimal choice of γ, and how to find always the best combination of a larger set of controllers, which will improve more the presented work. This study will be investigated in the next chapter.

Chapter 7

About The Interpolation Logic of LPV-YK Control: An Example Using Reinforcement Learning

7.1 Introduction

In this chapter, the structure of interpolation between YK-based LPV controllers is concerned aiming to find an optimal interpolation according to the required objectives. In Section 6.7, the interpolating signal γ has been chosen according to our previous experience in autonomous vehicle lane-tracking and lane-changing. The interpolation has shown good results, however, it could not be optimal. Since the whole closed-loop system can be complex including the LPV-YK control and the nonlinear vehicle model, Artificial Intelligence (AI) tools are proposed to learn how to find the optimal solution of γ.

Reinforcement Learning (RL) algorithms are highly recommended to find optimal actions according to a certain reward function. The reward function can be designed according to engineering experience, and the optimization objective is to maximize the reward function regarding the current vehicle and surrounding environment situations. Thanks to the stability conditions of the LPV-YK control, the interpolating signal γ can be any ad-hoc physically based, continuous/discontinuous, external or internal signal. Consequently, using the RL method does not affect the stability of the closed-loop system.

The current chapter proposes an RL-based LPV-YK interpolation scheme aiming to achieve an optimal performance with guaranteeing closed-loop quadratic stability. First, it is shown how the interpolating signals affect the closed-loop specifications using time-domain analysis. Then, the RL model is trained and simulated using the same simulation environment as in Section 6.7.

The results in this chapter has been represented in:

- *Intelligent Control Switching for Autonomous Vehicles based on Reinforcement Learning, published in 2022 33rd IEEE Intelligent Vehicles (IV) Symposium Conference*, refer to [381].

The chapter is organized as follows: Section 2 discusses the related works to our contribution. Section 3 defines some preliminaries on the fundamentals of Reinforcement Learning. A proof on control performance recovery of the LPV-YK control structure is shown in Section 4. A time-domain analysis on the affect of the interpolating signal on the closed-loop performance is depicted in Section 5. Section 6 represents the RL-based LPV-YK interpolation architecture. The training and testing

results of the RL model are shown in Section 7. Finally, some concluding remarks are given in Section 8.

7.2 Related Works

In the last decades, autonomous driving has involved different main domains such as automatic control theory and Artificial Intelligence (AI). For instance, [23] has presented the design and experimental validation of three Linear Parameter-Varying (LPV) control approaches for autonomous vehicles. On the other hand, a review has investigated Deep Reinforcement Learning (DRL) algorithms and provides automated driving tasks where DRL methods have been employed [382]. Each of these domains has proposed different kinds of approaches to solve the longitudinal and lateral control problems of autonomous driving.

On the other hand, recent studies have proposed AI learning tools due to its powerful performance, such as Reinforcement Learning (RL) [382],[383]. [384] presents a deep RL based approach for lateral motion control. Deep RL has proved to be able to solve many control tasks in different fields, however there is no stability guarantees for its behavior in real-world scenarios. Several studies have been investigated to provide stability guarantees either by adding dynamic constraints [385] or by combining deep RL with a theoretical optimization control [386],[387]. Moreover, recent works have proposed RL algorithms for decision-making and performance optimization for vehicles lane change [388],[389],[390].

As mentioned before, automated steering control should be able to address any circumstances such as activating the vehicle away from its reference trajectory with a significant error, or performing step lane changes. For ensuring stability and performance in such situations, a single controller could not be able to satisfy all critical situations. This chapter aims to propose an LPV-YK control interpolation based on RL to handle situations as large lateral deviations. Such deviations can be caused either by a first system activation, avoidance maneuver or even a localization discontinuity.

7.3 Preliminaries

This section presents some fundamentals of Reinforcement Learning to be used later in the chapter, readers can refer to [391] for more details.

7.3.1 Reinforcement Learning Elements

In order to explain the elements of the RL algorithms some definitions for the interaction to achieve a goal will be explained. The learner and decision-maker is called the *agent*, for e.g. the ego vehicle. The agent interacts with what is called the *environment* which includes everything outside the agent, in this case is the racetrack, the obstacles and the surrounding vehicles. The agent selects actions and the environment changes accordingly, which make them interact continually. This interaction is received by the agent with some representation of the environment described as *State* which includes information about its situation, it could be information about coordinates or speed of other vehicles, features of the road, among others. Refer to Fig. 7.1 to visualize the connection between these components.

The main sub-elements of RL algorithms are:

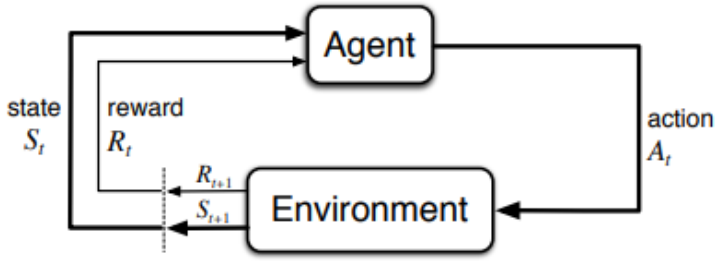

FIGURE 7.1: The agent–environment interaction in RL

- Policy: Is a mapping from perceived states of the environment to actions to be taken in those actions. It is sufficient to determine the behavior, policies may be stochastic.
- Reward: Defines the goal that is send as a number by the environment. The objective of the agent is to maximize the cumulative reward received over the long run. This value depends on the agents current action and the current state of the agent's environment at any time. The only way the agent can influence the reward signal is through its actions, which can have a direct effect on the total reward, or an indirect effect through changing the environment's state. The policy may be changed to select the action that will be followed by a higher reward on that situation in the future. Generally, reward signals may be stochastic functions of the state of the environment and the actions taken.
- Value function: Specifies what is good in the long run defined as episode. The value of a state can be described as the total amount of reward an agent can expect to accumulate over the future, starting from that state. Whereas rewards determine the immediate, intrinsic desirability of environmental states, values indicate the long-term desirability of states after taking into account the states that are likely to follow, and the rewards available in those states.
- Model: Is a representation of the behavior of the environment. When an action is made given a state the model might predict the resultant next state and reward due to this action. The model is used for planning and to consider possible future situations before they actually happen. There are two types of methods, model-free that are trial-and-error learners and model-based that integrate model and planning.

7.3.2 Reinforcement Learning Theory

The interaction between the agent and the environment occur at a sequence of discrete time steps t in which it receives some representation of the environment's state $S_t \in \mathcal{S}$ in the $\mathcal{S}$ set of possible states, and it selects an action $A_t \in \mathcal{A}(S_t)$ where $\mathcal{A}(S_t)$ is the set of actions available in state S_t. One time step later, in part as consequence of its action, the agent receives a numerical reward $R_{t+1} \in \mathcal{R} \subset \mathbb{R}$ and finds itself in a new state S_{t+1}. The Fig. 7.1 represents the agent-environment interaction.

At each time step, the agent implements a mapping from states to probabilities of selecting each possible action. This mapping is called the agent's policy and is denoted π_t, where $\pi_t(a \mid s)$ is the probability that $A_t = a$ if $S_t = s$. Reinforcement learning methods specify how the agent changes its policy as a result of its experience. The agent's goal, roughly speaking, is to maximize the total amount of reward it receives over the long run.

An agent can increase the long-term reward by exploiting knowledge learned about the discounted sum of expected future rewards of different state-action pairs. The learning agent has to exploit what it already knows in order to obtain rewards, but it also has to explore the unknown in order to make better action selections in the future. One of the main challenges in reinforcement learning is managing the trade-off between exploration and exploitation [382].

For some stochastic control problems when the models for sequential decision making outcomes are uncertain, Markov Decision Processes (MDP) are used. The MDP model consists of decision epochs, states $\boldsymbol{S}$, actions $\boldsymbol{A}$, rewards $\boldsymbol{R}$, and transition probabilities $\boldsymbol{T}$; a tuple $< S, A, T, R >$. Choosing an action a in a state s generates a reward *R(s,a)* and determines the state at the next decision epoch s' through a transition probability function *T(s,a,s')*. Policies are instructions of which action to choose under any occurrence at every future decision. The agent look for policies which are optimal. The mathematical representation of the policy which is a mapping from the state space to a probability over the set of actions, and $\pi_t(a \mid s)$ represents the probability of choosing action a at state s. The goal is to find the optimal policy π^* at time k, defined as:

$$\pi^* = \arg\max_{\pi} \mathbb{E}_{\pi}\{\sum_{k=0}^{H-1} \gamma^k R(s_k, a_k) \mid s_0 = s\} := \arg\max_{\pi} V_{\pi}(s) \tag{7.1}$$

Where γ is the discount factor that controls how an agent consider future rewards. When γ is low the agent will maximize short term rewards, on the contrary with high values of γ the agent will try to maximize rewards over a longer time frame. Eq. (7.1) represents the highest expected sum of discounted rewards in a time horizon H in the MDP. From the models directly, RL agents may learn value function estimates, policies and/or environment. Finding a policy π that maximizes the expected discounted sum of rewards over trajectories in the state space is what solving a RL task means.

7.3.3 Actor Critic Approach

Actor-critic methods are hybrid methods that combine value-based and policy-based algorithms. One actor is the one that selects the actions and this is the policy-structure. After an action is made by the 'actor', the estimated value function evaluates the action and this is known as the 'critic'. The value-based methods are model-free Temporal Difference (TD), are methods that can learn directly from raw experience without a model of the environment's dynamics and learn estimates of the utility of individual state-action pairs represented in Eq. (7.2). This scalar signal is the sole output of the critic and drives all learning in both actor and critic, as shown in Fig. 7.2

$$Q_{\pi}(s, a) = \mathbb{E}_{\pi}\{\sum_{k=0}^{H-1} \gamma^k R(s_k, a_k) \mid s_0 = s, a_0 = a\} \tag{7.2}$$

Q-learning will learn (near) optimal state-action values provided a big number of samples are obtained for each pair. Agents implementing Q-learning update their Q values according to the update rule of Eq. (7.3):

$$Q(s, a) \leftarrow Q(s, a) + \alpha \left[r + \gamma \max_{a' \in A} Q(s', a') - Q(s, a) \right] \tag{7.3}$$

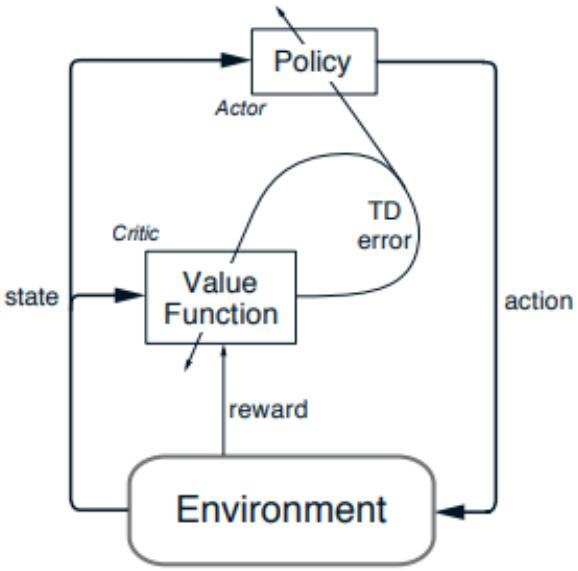

FIGURE 7.2: The actor–critic architecture

Where $Q(s,a)$ is an estimate of the utility of selecting action a in state s; α is the learning rate which controls the degree to which Q values are updated at each time step.

The policy-based methods aim to estimate the optimal policy directly, and the value is a secondary. Typically, a policy π_θ is parameterized as a neural network. Policy gradient methods use gradient descent to estimate the parameters of the policy that maximize the expected reward. The result can be a stochastic policy where actions are selected by sampling, or a deterministic policy. When selecting actions, exploration is performed by adding noise to the actor policy. To stabilize learning a replay buffer is used to minimize data correlation. A separate actor-critic specific target network is also used. Normal Q-learning is adapted with a restricted number of discrete actions the optimal Q-value and optimal action as Q^* and a^*.

$$Q^*(s,a) = \max_\pi Q_\pi(s,a)\ ,\ a^* = \arg\max a Q^*(s,a) \tag{7.4}$$

By correcting the Q-values towards the optimal values using the chosen action, the policy is updated towards the optimal action proposition. Thus two separate networks work at estimating Q^* and π^*.

7.3.4 Soft-Max Policy Approximation

In policy gradient methods, the policy $\pi(a|s,\theta)$ can be formulated in any way, as long as it is differentiable with respect to its parameters θ; i.e. as long as $\nabla\pi(a|s,\theta)$ (the column vector of partial derivatives of $\pi(a|s,\theta)$ with respect to the components of θ) exists and is finite for all $s \in \mathcal{S}$, $a \in \mathcal{A}(s)$, and $\theta \in \mathbb{R}^{d'}$.

In practice, parameterized numerical preferences $h(s,a,\theta) \in \mathbb{R}$, for each state–action pair, is chosen if the action space is discrete and not too large. Usually, an exponential soft-max distribution is used so that the actions having the highest preferences, in each state, are given the highest probabilities to be selected, the policy is then formulated as follows:

$$\pi(a|s,\theta) = \frac{e^{h(s,a,\theta)}}{\sum_b e^{h(s,b,\theta)}}, \tag{7.5}$$

where $e = 2.71828$ is the base of the natural logarithm. This policy parameterization is known as sof-max in action preferences. Notice that the action preferences $h(s,a,\theta)$ can be parameterized by a DNN or can be any linear function in features. An example which is usually used:

$$h(s,a,\theta) = \theta^T x(s,a), \tag{7.6}$$

where $x(s,a)$ is a state-action pair feature.

An advantage of the soft-max policy approximation is that the approximate policy can approach a deterministic policy.

7.4 Different Kinds of Interpolating Signals

In the autonomous vehicle field, an interpolation scheme with any ad-hoc interpolating signal can be beneficial to link between the decision-making and control systems, i.e. as a control supervisor. It can be expressed as a list of characters, floats or binaries which describes the decision taken. For example:

- As a character: it indicates the general task which should be taken by the vehicle, i.e. smooth/aggressive lane tracking, slow/fast lane change, far/ emergency collision avoidance, parking, autonomous-mode initialization, decrease lateral acceleration noises, sudden brake, etc.
- As a float: it represents all the ego vehicle information, i.e. position, lateral/longitudinal speed, lateral/longitudinal acceleration, vehicle parameters' change (mass, tire stiffness estimation, etc.), and others. Moreover, it gives the surrounding information such as: fixed/moving objects using cameras and LiDAR (vehicles, pedestrians, etc.), road conditions (holes, friction, slope, wet/ humid, traffic lights/ marks, lane lines, etc.), environment condition (weather, wind speed, etc.)
- As a binary: it displays driving conditions due to a certain situation, i.e. sport/ classic drive, emergency calls (heart attack), etc.

In this chapter, the interpolating signal is considered to be float ranging in $[0,1]$.

Considering the LPV-YK control structure in Section 6.7, the next section proves the control recovery of each already designed LTI controller.

7.4.1 Local LTI Control Performance Recovery

Regarding Fig. 5.7, the interpolation cases can be mentioned to show how $\tilde{K}(\rho,\gamma)$ recovers a single gain-scheduled controller $K^{(j)}(\rho)$ by varying γ_j:

- if $\gamma_j = 0\ \forall j$, $\tilde{K}(\rho,\gamma) \equiv K^{(0)}(\rho) = \sum_{i=1}^{2^{n_p}} \alpha_i(\rho) K_i^{(0)}$
- if $\gamma_j = 1$ for $j = c \in [1,\zeta]$ and $\gamma_j = 0\ \forall j \neq c$, $\tilde{K}(\rho,\gamma) \equiv K^{(c)}(\rho) = \sum_{i=1}^{2^{n_p}} \alpha_i(\rho) K_i^{(c)}$

- else, the performance of $\tilde{K}(\rho,\gamma)$ is interpolated among $K^{(j)}(\rho)$ according to the chosen γ_j.

In this section, the performance recovery of each pre-designed local LTI controller $K_i^{(j)}$ ($i \in [1, 2^{n_p}]$, $j \geq 1$), from the LPV-YK controller $\tilde{K}(\rho,\gamma)$, is verified. Let us choose an LTI controller $K_l^{(c)}$ (i.e. $\gamma_c = 1$ and $\gamma_j = 0\ \forall j \neq c$, and $\rho = w_l$). The following derivation shows the performance recovery of of $K_l^{(c)}$ from $\tilde{K}(\rho,\gamma)$:
Substitute the vertex $w_l^{(c)}$ and $\gamma = [0 \ldots 0\ \ \gamma_c = 1\ \ 0 \ldots 0]$ (denoted by $\gamma_c^* = 1$) in (6.13),

$$\tilde{K}(w_l, \gamma_c^* = 1) = \left(U_l^{(0)} + M_l \bar{Q}_l^{(c)}\right)\left(V_l^{(0)} + N_l \bar{Q}_l^{(c)}(\rho)\right)^{-1} \tag{7.7}$$

Since the input-output performance of Q and $\bar{Q}$ is similar (according to the state transformation concept), $\bar{Q}_l^{(0)} \equiv Q_l^{(0)}$. According to [269], (7.7) can be written as

$$\tilde{K}(w_l, \gamma_c^* = 1) = U_l^{(0)}(V_l^{(0)})^{-1} + (\tilde{V}_l^{(0)})^{-1} Q_l^{(c)} \left(I + (V_l^{(0)})^{-1} N_l^{(0)} Q_l^{(c)}\right)^{-1} (V_l^{(0)})^{-1} \tag{7.8}$$

Referring to YK concept, $Q_l^{(c)} = \tilde{U}_l^{(c)} V_l^{(0)} - \tilde{V}_l^{(c)} U_l^{(0)}$, after some derivations:

$$\begin{aligned} Q_l^{(c)} &= \tilde{V}_l^{(c)} (\tilde{V}_l^{(c)})^{-1} \tilde{U}_l^{(c)} V_l^{(0)} - \tilde{V}_l^{(c)} U_l^{(0)} (V_l^{(0)})^{-1} V_l^{(0)} \\ &= \tilde{V}_l^{(c)} K_l^{(c)} V_l^{(0)} - \tilde{V}_l^{(c)} K_l^{(0)} V_l^{(0)} \\ &= \tilde{V}_l^{(c)} (K_l^{(c)} - K_l^{(0)}) V_l^{(0)} \end{aligned} \tag{7.9}$$

Substitute and shape it, then

$$\tilde{K}(w_l, \gamma_c^* = 1) = K_l^{(0)} + [\tilde{V}_l^{(c)} V_l^{(0)} + (K_l^{(c)} - K_l^{(0)}) N_l \tilde{V}_l^{(0)}]^{-1} \times (K_l^{(c)} - K_l^{(0)}) \tag{7.10}$$

Knowing that $K_l^{(c)} = (\tilde{V}_l^{(c)})^{-1} \tilde{U}_l^{(c)}$, and applying the Bezout identities (1), we get:

$$\tilde{V}_l^{(c)} V_l^{(0)} + (K_l^{(c)} - K_l^{(0)}) N_l \tilde{V}_l^{(0)} = I. \tag{7.11}$$

Then,

$$\tilde{K}(w_l, \gamma_c^* = 1) = K_l^{(0)} + K_l^{(c)} - K_l^{(0)} = K_l^{(c)}. \tag{7.12}$$

Therefore, it is shown that the performance achieved by the LPV-YK controller $\tilde{K}(\rho,\gamma)$ at any vertex w_l is equivalent to the performance of its corresponding LTI controller $K_l^{(c)}$.

7.5 Variation of Closed-loop Performance With Respect to The Interpolating Signal

The objective of this section is to show how the closed-loop performance changes with respect to the interpolating signal γ. The analysis performed here can help later understand the change in the LPV-YK control performance while changing γ to certain values. The LPV-YK control structure designed in Section 6.7 is used here. Recall that the objective of this structure is to interpolate between three LPV controllers $K^{(j)}(\rho)$, $j \in \{0, 1, 2\}$, being:

- The highly robust polytopic-based LPV controller $K^{(0)}(\rho)$ is designed using the standard polytopic approach, achieving a slow transient response and noise rejection performances.
- The smooth YK-based LPV controller $K^{(1)}(\rho)$ designed to perform smooth lateral transitions to provide comfort riding.
- The fast YK-based LPV controller $K^{(2)}(\rho)$ achieving fast lateral transitions to handle the vehicle when facing aggressive maneuvers and lateral oscillations.

Figs. 7.3a, 7.3b, 7.3c show the closed-loop step responses of each LPV controller at the three polytopic vertices. In the following, the objective is to analyze the change of the closed-loop step response, at each vertex separately, when γ_1 changes from 0 to 1, while always ensuring $\gamma_2 = 1 - \gamma_1$. It is shown in these figures that the closed-loop specifications (i.e. rising time, overshoot, settling time, etc.) stay always between the two interpolated controllers $K_i^{(1)}$ and $K_i^{(2)}$ wherever γ_j's ($j = \{1,2\}$) vary between 0 and 1 with $\gamma_1 + \gamma_2 = 1$. To clarify this point, Figs. 7.4a and 7.4b show the monotonic decreasing of both rising and settling times when changing from the slow controller $K_i^{(1)}$ to the faster one $K_i^{(2)}$, with respect to $\gamma = [\gamma_1, 1 - \gamma_1]$. Notice that the colored points (from blue to red) in these figures correspond to the same legends in the Fig. 7.3a. Thus, multiple closed-loop specifications can be achieved from the interpolation of two LPV controllers, each corresponds to a certain value of γ, which can be used later to choose the required specifications during online implementation.

7.6 RL-based LPV-YK Interpolation Architecture

Reinforcement learning can teach how an agent act by interacting with its environment in order to maximize the expected cumulative rewards for a certain task. There are two general categories of RL algorithms, namely value-based method and policy-based method. While value-based methods can approximate the value function using neural networks in an off-policy way, the primary advantage of policy-based methods, such as the actor-critic [392], is that they can directly optimize the quantity of advantage, while remaining stable during function approximations. Our study thus focuses on policy-based RL methods. A detailed explanation of the actor-critic methods can be found in chapter 13 in [391].

7.6.1 Problem Description

In Section 6.7, it has been shown that using the LPV-YK interpolation is important to maintain an optimal performance for different lateral maneuvers, such as large lateral deviations. In our formulation, we focus on situations where explicit lane change intentions are already given by the trajectory planner as a 3 meters lateral step. Our task is to decide when and how to interpolate between the two designed controllers based on states of the ego vehicle with respect to the environment and the reference trajectory. Once a decision is made by the RL model, the LPV-YK control scheme achieves a new closed-loop performance and regulates the lateral movements. The applicable switching signal policy to be learned should incorporate the following three functionalities:

- Avoiding collisions with the lanes boundaries

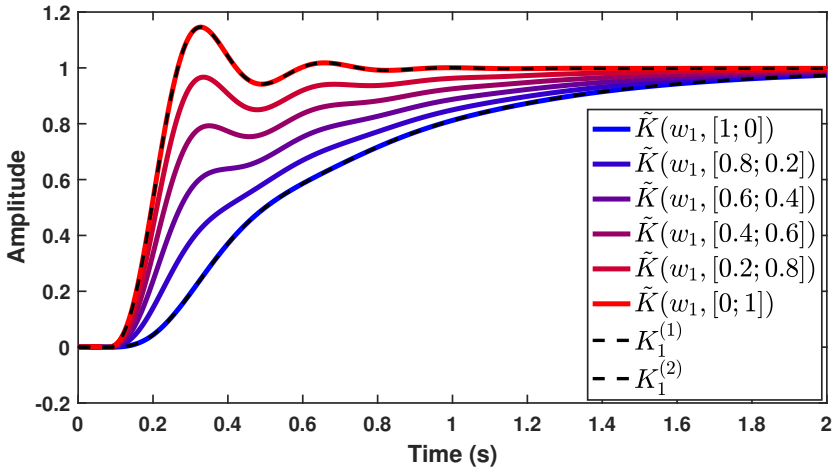

(A) At $\rho = w_1$

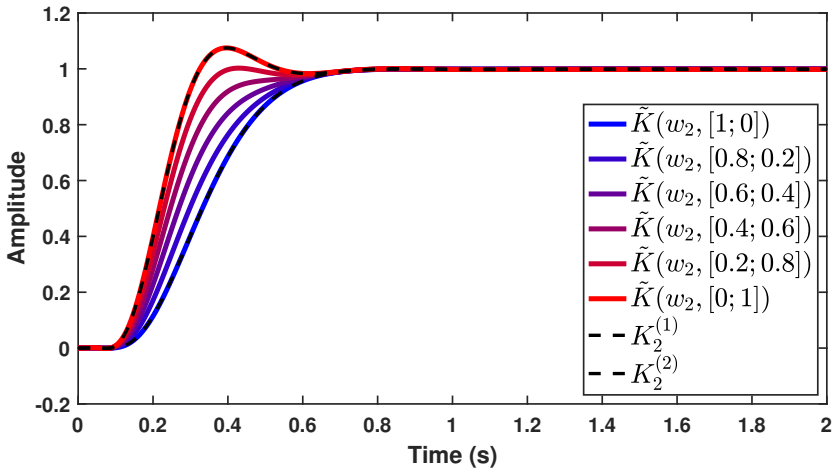

(B) At $\rho = w_2$

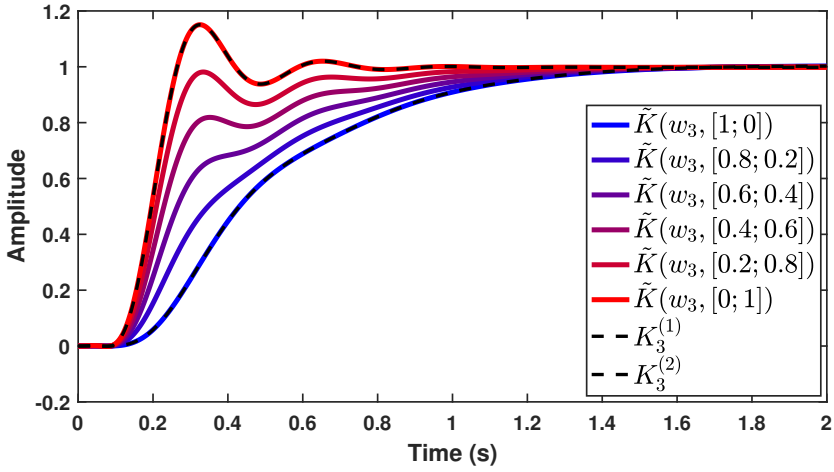

(C) At $\rho = w_3$

FIGURE 7.3: Closed-loop step responses at the three polytopic vertices with different γ values

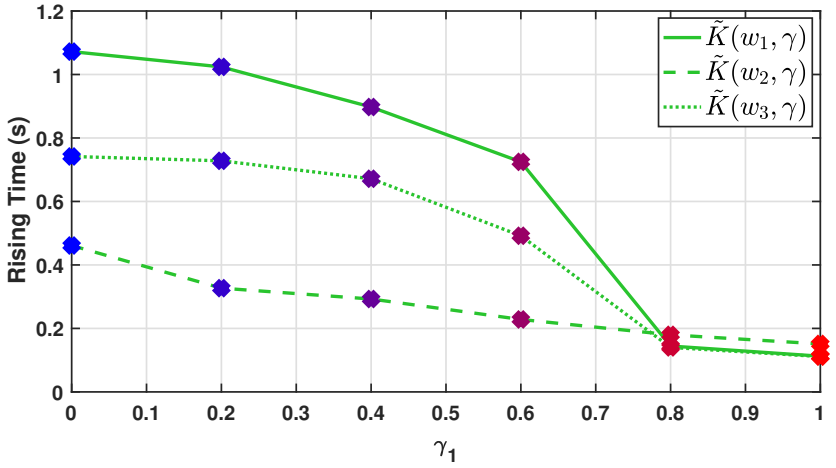

(A) Rising Time with respect to γ

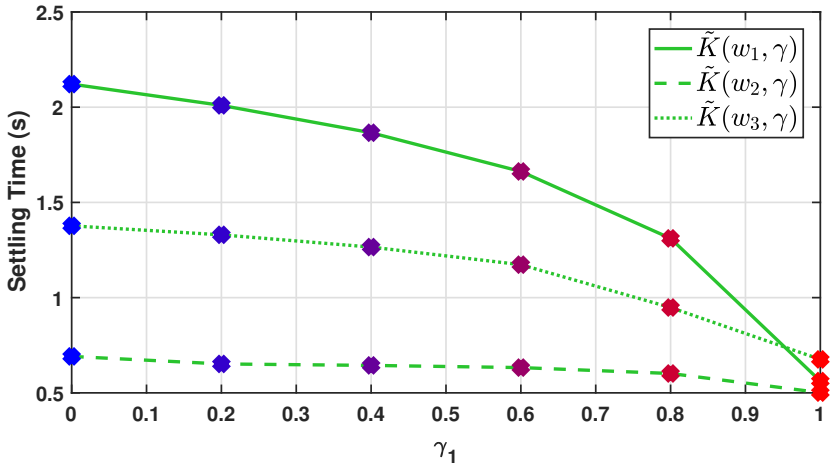

(B) Settling Time with respect to γ

FIGURE 7.4: Closed-loop specifications at the three polytopic vertices with different γ values

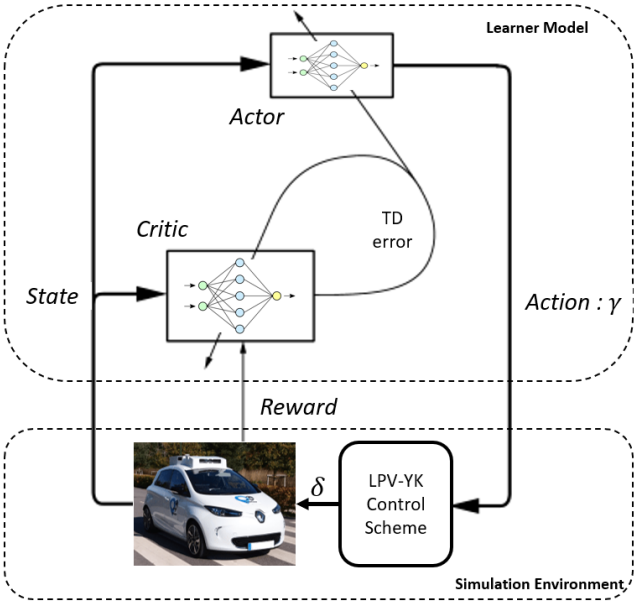

FIGURE 7.5: System architecture of RL-based switching

- Achieving high driving efficiency
- Executing smooth maneuvers

7.6.2 System Architecture

The overall system architecture for enabling automated switching is shown in Fig. 7.5. The system is composed of two main components:

1. Learner Model: uses the actor-critic algorithm to train the switching logic of the LPV-YK control scheme (agent), to learn a high-level policy while interacting with the environment.
2. Simulation Environment: includes the road network and different task scenarios, is generated using a RENAULT simulator on MATLAB, for a real automated ZOE car, that has been already used in the previous chapters, and it interacts with the training agent.

The vehicle and controllers information can be accessed, taking into account the vehicle and control dynamics generated in the simulation model. To enable safe, smooth, and efficient driving behaviors on highways, the learner model first receives the vehicle current state with respect to the reference trajectory from the simulator, which are passed through the policy network. Next, the learner model determines the high-level switching policy, which then sends the switching action back to the simulator to model the controllers' and vehicle's movement in the next time step, and compute the corresponding reward. Notice that the controller output is the steering angle δ.

7.6.3 Simulation Environment

The simulation environment in presented in Fig. 7.6. For a chosen value of the interpolating signal γ, the dynamics of the LPV-YK controller $\tilde{K}(\rho, \gamma)$ is adapted

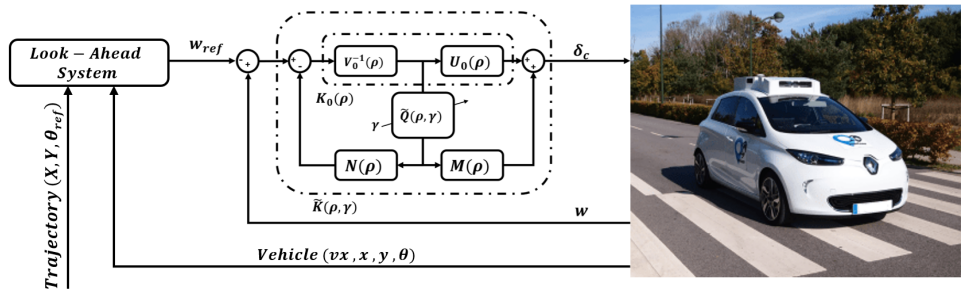

FIGURE 7.6: Simulation Environment

leading to an interpolated closed-loop performance from the yaw-rate reference w_{ref} to the measured vehicle yaw-rate w.

The vehicle model contains the nonlinear dynamics of the automated ZOE vehicle. This model provides all the needed observations and the state-space variables to be used in the learner model. The simulation environment is designed on MATLAB/Simulink with a fixed step-size $T_s = 0.01s$. The frequency of the interpolating signal γ is considered here to be similar to the closed-loop frequency. However, it can be taken slower for smoother interpolation.

7.6.4 Learner Model

The learner model is chosen here to be an RL model using the policy-based actor-critic method. The pseudo-code for the actor-critic algorithm can be expressed as follows [391]:

Algorithm 1 Actor-Critic method to estimate the policy $\pi_\theta \approx \pi_*$

Input: a differentiable policy parameterization $\pi(a|s,\theta)$
Input: a differentiable state-value function parameterization $\hat{v}(s,w)$
Algorithm parameters: $\lambda^w \in [0,1]$, $\lambda^\theta \in [0,1]$, $\alpha^w > 0$, $\alpha^\theta > 0$, $\alpha^{\bar{R}} > 0$
Initialize $\bar{R} \in \mathbb{R}$ (e.g., to 0)
Initialize state-value weights $w \in \mathbb{R}^d$ and policy parameters $\theta \in \mathbb{R}^{d'}$ (e.g., to **0**)
Initialize $S \in \mathcal{S}$ (e.g., to s_0)
$z^w \leftarrow 0$ (d-component eligibility trace vector)
$z^\theta \leftarrow 0$ (d'-component eligibility trace vector)
for Loop forever (for each time step) **do**
  $A \sim \pi(.|S,\theta)$
  Take action A, observe S' (next state), R (reward)
  $\Delta_{TD} \leftarrow R - \bar{R} + \hat{v}(S',w) - \hat{v}(S,w)$
  $\bar{R} \leftarrow \bar{R} + \alpha^{\bar{R}}\Delta_{TD}$
  $z^w \leftarrow \lambda^w z^w + \nabla\hat{v}(S,w)$
  $z^\theta \leftarrow \lambda^\theta z^\theta + \nabla \ln \pi(S,w)$
  $w \leftarrow w + \alpha^w \Delta_{TD} z^w$
  $\theta \leftarrow \theta + \alpha^\theta \Delta_{TD} z^\theta$
  $S \leftarrow S'$
end for

Two Deep Neural Network (DNN) models are to be trained expressing the policy π and the state-value function $\hat{v}$. Their weighting parameters θ and w, the average reward $\bar{R}$ are initialized by zeros. The initial state s_0 can be chosen depending on the initial state of the vehicle with respect to its surroundings. At each time-step:

1. The action is estimated from the trained policy (actor). This action is entered to the Simulation Environment resulting the reward R and the next state S'.
2. The Temporal-Difference error Δ_{TD} is then computed, and the average reward $\bar{R}$ is updated.
3. The weighting parameters of both actor and critic DNNs are updated using the gradient-descent method.
4. The current state is updated to the next state, and continue to the next time-step.

State Space

Before getting into the definition of the state space, we introduce an observation space to help modeling the surrounding environment. The observation of a vehicle consists of six variables $\{v_x, y_L, \theta_e, y_e, \dot{\delta}, y_L \times \theta_e\}$, where v_x, y_L , θ_e , y_e , $\dot{\delta}$ are the vehicle speed, lateral error at the look-ahead distance L, vehicle heading error, vehicle lateral error, and the steering speed, respectively. $y_L \times \theta_e$ is used to identify if the vehicle is going toward or away from the trajectory depending on its sign.

In real traffic flow, a driver can neither observe nor process all the above observations precisely and continuously. A human can possibly observe whether he is in close or far distance, approaching or moving away. Therefore, it is suggested here to discretize the observations into grids (4 grids for each). As a result, we end up with a state space S including $4^6 = 4096$ states.

Action Space

In this study, the action space A represents the switching signal γ which is discretized as $\{0, 0.2, 0.4, 0.6, 0.8, 1\}$. So, there are six actions achieving different closed-loop performances, and thus different vehicle behavior. Notice that we have already presented the possible closed-loop performances resulting from each γ action in the previous sections.

Reward Function

The reward function is designed to incorporate key objectives of this study, which is to develop an automated switching strategy to provide safety, efficiency, and comfort. Specifically,

1. Efficiency : evaluation of the relative distance toward the reference trajectory.
2. Comfort : evaluation of steering speed, which relates proportionally the yaw acceleration.
3. Safety : evaluations of collision risks and high lateral overshoots.

The sub-reward functions can be expressed as:

$$\begin{aligned} R_{eff} &= -v_x \times (a.|y_e| + b.|y_L| + c.|\theta_e|) \\ R_{comf} &= -v_x \times (d.|\dot{\delta}|) \\ R_{safe} &= -100 \end{aligned} \tag{7.13}$$

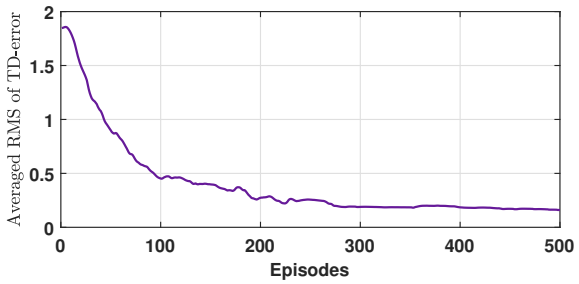

FIGURE 7.7: Averaged RMS of the TD-error

where a, b, c, and d are the weights chosen according to the required driving type, i.e. comfort or sportive driving. Then , the total reward function R is:

$$R = R_{eff} + R_{comf} + R_{safe} \tag{7.14}$$

Actor-Critic Model

A one-step softmax actor-critic episodic algorithm is used, see chapter 13 in [391] for more details. The state-action feature vector is formulated using a tile coding with 1 tilings and four tiles for each state. Having 4^6 states and 6 actions, results in $6 \times 1 \times 4^6 = 24576$ features. Notice that only one tiling has been chosen due to computation cost, and since it has achieved our requirements as presented in the next section. The actor and critic weights, Θ and W respectively, are initialized by zeros. The discount factor is 1. The actor and critic step-sizes are $\alpha^{\Theta} = 0.0625$ and $\alpha^{W} = 1$ respectively.

7.7 Simulation Experiment

The simulation is done using the nonlinear full car model designed for a Renault ZOE vehicle. The scenario is chosen as the one used in [369]. This scenario covers several lateral steps at different speeds. Fig. 7.8 depicts the planned and the controlled trajectories, and the longitudinal speed profile is shown in Fig. 7.9.

The first step is to train the actor-critic model. After training, tests are performed to compare the resultant performance using the RL-based switching with another switching logic. The averaged RMS of the TD-error is computed and represented in Fig. 7.7. It is shown how the TD-error is optimized and decreases along the number of episodes. In order to evaluate the trained policy of γ^{RL}, it is compared to the switching logic already used Section 6.7, which has been designed according to our experience.

7.7.1 Testing Results

The parameterized LPV-YK controller $\tilde{K}(\rho, \gamma)$ is structured as shown in Section 6.7 and simulated on the Renault simulator with the trained switching policy. The simulation is done on a designed trajectory containing consecutive lateral deviation steps over different longitudinal speeds.

The chosen scenario is tested with different controllers: $\tilde{K}(\rho, [1;0]) = K^{(1)}(\rho)$ (smooth tracker), $\tilde{K}(\rho, [0;1]) = K^{(2)}(\rho)$ (aggressive tracker), the LPV-YK controller with experienced switching logic $\tilde{K}(\rho, \gamma^{f})$, and the proposed RL-based LPV-YK switching control $\tilde{K}(\rho, \gamma^{RL})$. Fig. 7.9 shows the speed profile for all the tests. Fig. 7.10a

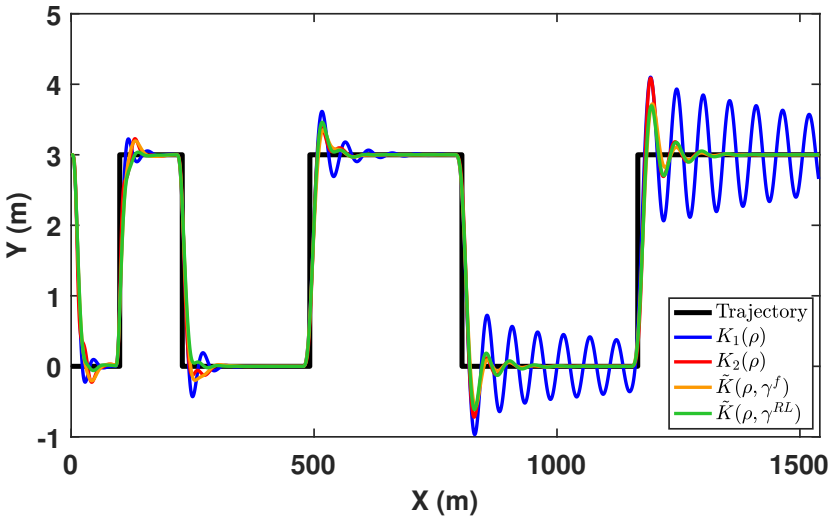

FIGURE 7.8: Planned and controlled trajectories

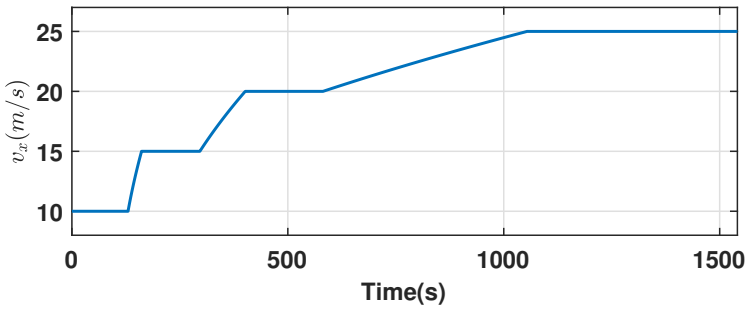

FIGURE 7.9: Longitudinal speed v_x (m/s)

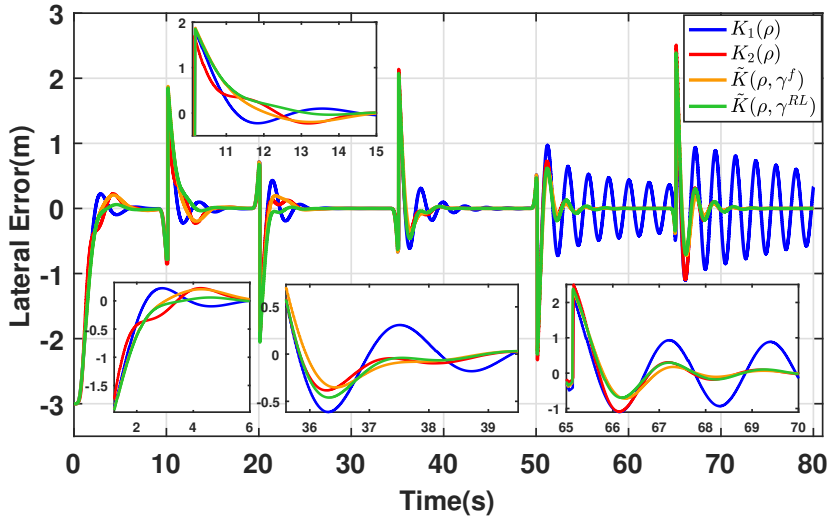

(A) Lateral error y_e (m)

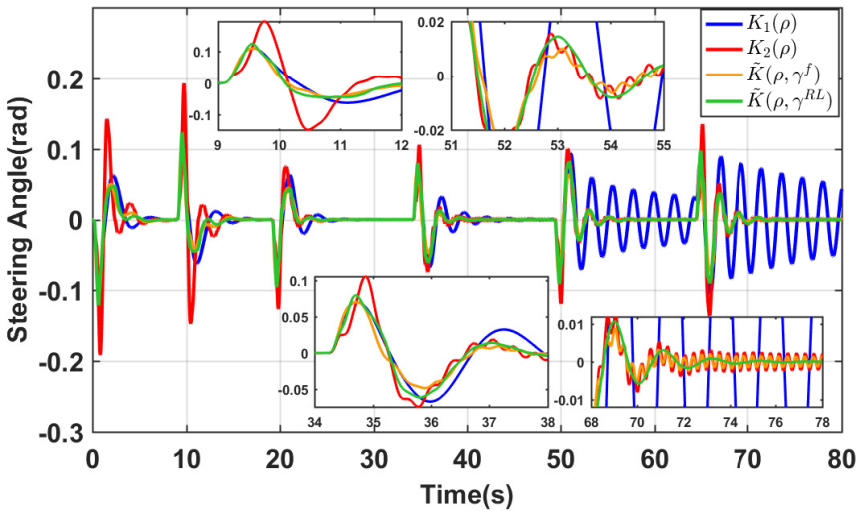

(B) Control input steering wheel angle (rad)

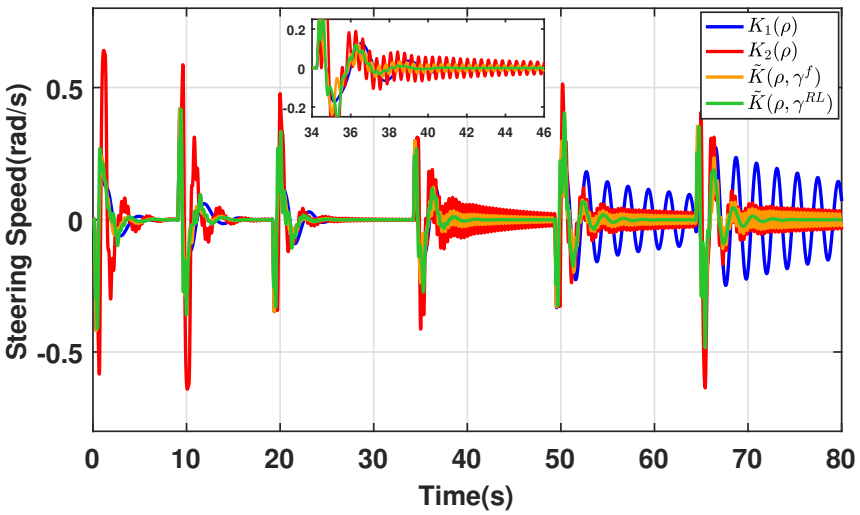

(C) Steering speed $\dot{\delta}$ (rad/s)

FIGURE 7.10: Simulation results

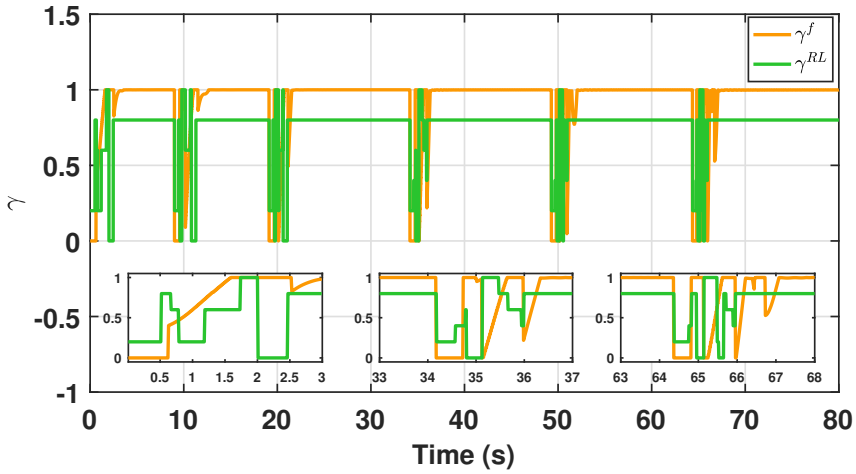

FIGURE 7.11: Interpolating signal γ

depicts the lateral error from the reference trajectory to the vehicle Center of Gravity (CoG), and the steering control input is shown in Fig. 7.10b. Fig. 7.10c represents the steering speed which reflects the driving comfort. Fig. 7.11 shows the evolution of the interpolating signals γ^f and γ^{RL}.

First, it is important noticing that neither $K^{(1)}(\rho)$ nor $K^{(2)}(\rho)$ could achieve an optimal performance regarding the lateral error optimization and steering comfort. Specifically, Fig. 7.10a shows the high lateral oscillations caused by $K^{(1)}(\rho)$, whereas $K^{(2)}(\rho)$ leads to steering speed noises, as shown in Figs. 7.10b and 7.10c, which affects the riding comfort.

On the other hand, the interpolation between both controllers using the LPV-YK control scheme achieves better performance on both tracking and steering speed noise attenuation, i.e. reaching more optimized performance. This is shown regarding the performance of $\tilde{K}(\rho, \gamma^f)$ and $\tilde{K}(\rho, \gamma^{RL})$ compared to $K^{(1)}(\rho)$ and $K^{(2)}(\rho)$. According to Fig. 7.11, it is presented how both switching logic γ^f and γ^{RL} have similar evolution with respect to time. This means that the trained RL-based switching model is close to what have been previously proposed based on our experience.

Regarding the zoomed parts in Figs. 7.10a, 7.10b, and 7.10c, it is shown that the overall vehicle performance is even better using the RL-based LPV-YK switching control. The steering angle and the steering speed are clearly shown to be smoother and optimized. Concerning the lateral error, Fig. 7.10a presents how $\tilde{K}(\rho, \gamma^{RL})$ performs the smoothest lateral deviations with lowest overshoot. The RMS are calculated for both $\tilde{K}(\rho, \gamma^f)$ and $\tilde{K}(\rho, \gamma^{RL})$ obtaining the following:

$$RMS_{y_e}^{f} = 0.47, \quad RMS_{y_e}^{RL} = 0.452 \tag{7.15}$$

7.8 Conclusion

This chapter has proposed an new combination between reinforcement learning and automatic control tools, to ensure both stability and high performance for autonomous vehicles. The LPV-YK switching control scheme is chosen since it ensures the closed-loop stability for any continuous/discontinuous interpolating signal. This signal can be used to incorporate any ad-hoc physically-based interpolation.

A rising topic, such as reinforcement learning, is used to supervise the switching logic to provide an optimized performance. Instead of estimating the switching logic depending on our experience and knowledge, a softmax actor-critic RL model has been used to observe the vehicle states with respect to the reference trajectory, and choose the best switching scenario.

The LPV-YK switching control with the highly performant RL model has provided interesting results in simulation. It has achieved safety, efficiency, and comfort compared to other simulated controllers. It is important mentioning that the LPV-YK control structure can be generalized to multiple controllers, and facilitates adding any new controller without recalling all the control design procedure. This can encourage to design a family of multiple controllers, and train an RL-based supervisor to interpolate between them depending on the vehicle-surrounding situation.

As future work, an interest appears to experimentally validate the proposed system architecture on the automated ZOE car. Moreover, the proposed architecture could aid also to strengthen the link between the decision-making and the control systems which leads to higher vehicle performance.

Chapter 8

Discussion

In this chapter, a summary and some concluding remarks are presented concerning the proposed LPV-YK controllers with their benefits on the lateral control of autonomous vehicles. In addition, several future perspectives are reported to aid the continuation of the thesis work.

8.1 Thesis Summary

The deployment of autonomous driving aims to avoid accidents, reduce fuel consumption, improve traffic flow. It also provides safety and passenger comfort in critical situations and make it possible to car travelling for everyone regardless of their abilities or conditions. However, control of autonomous vehicles is not trivial since it is required to handle various situations that may lead to use the maximum capabilities of the vehicle. This thesis have developed multi-variable and multi-objective control schemes aiming to achieve various control performances covering the whole vehicle speed range.

A general summary of each of the included chapters is shown below:

- Chapter 1 has introduced the main objectives and novelties of this thesis. In addition, the thesis organization is mentioned. Resulted publications such as journals, conferences, and patents are presented at the end of the chapter.
- Chapter 2 has reviewed the use of different switching and interpolating LPV control approaches in control fields. The most applied applications have been illustrated and classified over time evolution. The discussed approaches can be described as follows: 1) Standard LPV control: polytopic, grid-based, LFT: designed using one single (constant or parameter-dependent) Lyapunov function; 2) Switched-LPV control: designed using multiple parameter-dependent Lyapunov functions, and leads to aggressive controller states and output jumps at the switching instants; 3) Smooth LPV switching: designed sequentially or instantaneously, and uses iterative methods to smooth the switching transitions; 4) LPV interpolation based-on bumpless-transfer: tries to minimize the controller states or output differences at the switching transitions; and 5) LPV-YK control interpolation: designed by parameterizing the local controllers with respect to a single nominal controller. A timeline is provided at the end classifying their main applications.
- Chapter 3 has presented the autonomous vehicle architecture including the perception, motion planning, and control. A specific literature review is done on lateral control of autonomous vehicles based on the look-ahead approach. In addition, the simulation and experimental environments, that have been used in the work of this thesis, have been introduced.

- Chapter 4 has introduced a theoretical and experimental comparison of the LPV approaches for the lateral control of autonomous vehicles. It has been shown that the grid-based model has the simplest structure with less conservatism in optimization among the others. The weighting parameters used in the LPV/$\mathcal{H}_\infty$ control design can physically translate the real actuator limitations to a filter added to the optimization problem. The practical limitations of each approach have been discussed by observing the simulation results which were obtained from different chosen critical scenarios. Then, the real experiments showed interesting results regarding the minimization of the lateral error, which encourages the application of LPV/robust approaches on autonomous vehicles. A comparison table with pros and cons of each approach has been represented at the end. In fact, such approaches help to control parameter-variant systems and to handle with environmental disturbances (wind speed, bad road conditions/slopes, etc...).

- Chapter 5 has proposed four LPV-YK switching/interpolating methods to obtain smooth interpolation between different closed-loop specifications, and switching between consecutive parameter subregions. The switching signal can be parameter-dependent or any ad-hoc continuous/discontinuous signal. The main advantages behind these approaches, compared to the previous LPV-switched controllers in the literature are: 1) The pre-designed LPV controllers are parameterized with respect to a nominal LPV controller, instead of requiring the redesign in new constrained LMIs; 2) The design conditions proposed for LPV-YK switching control are more smooth and can be satisfied assuming just the LPV stabilizability of the system; 3) The interpolated/switched controllers can be designed using different control approaches, i.e. PID, $\mathcal{H}_\infty$, etc; and finally 4) The proposed LPV-YK control schemes don't pose any conditions or limitations on the switching signals.

- Chapter 6 has shown the implementation steps of the LPV-YK control schemes proposed in the previous chapter. These approaches improve the system performance, while dealing with various objectives and situations. An application to the autonomous vehicle lateral control has been carried out. The simulations have shown interesting results regarding the efficiency of the proposed methods of providing high performance and ensuring safety at critical situations. In addition, experimental results have been presented to validate their real performance by testing the approaches on a real Renault ZOE vehicle. Finally, notice that the LPV-YK control structures facilitate adding any new controller, by introducing its corresponding LPV-YK parameter to the YK configuration, without recalling all the control design procedure. This enhances real applications, such as in industries, where the systems are subjected to frequent instrumentation changes such as autonomous vehicles.

- Chapter 7 has proposed a new combination between Reinforcement Learning (RL) and automatic control tools, to ensure both stability and high performance for autonomous vehicles. The LPV-YK switching control scheme is chosen since it ensures the closed-loop stability for any continuous/discontinuous interpolating signal. This signal can be used to incorporate any ad-hoc physically-based interpolation. A rising topic, such as reinforcement learning, is used to supervise the switching logic to provide an optimized performance. Instead of estimating the switching logic depending on our experience and knowledge, a softmax actor-critic RL model has been used to observe the vehicle states with

respect to the reference trajectory, and choose the best switching scenario. The LPV-YK switching control with the highly performant RL model has provided interesting results in simulation. It has achieved safety, efficiency, and comfort compared to other simulated controllers. It is important mentioning that the LPV-YK control structure can be generalized to multiple controllers, and facilitates adding any new controller without recalling all the control design procedure. This encourages to design a family of multiple controllers, and train an RL-based supervisor to interpolate between them depending on the vehicle-surrounding situation.

8.2 Conclusions and Future Perspectives

To continue developing the work of this thesis, different future works are highly encouraged to be investigated regarding the obtained conclusions:

- The LPV-YK parameterization has shown significant improvement in the field of LPV switching control, where it simply ensures closed-loop stability without requiring an instantaneous design of the local LPV controllers. In addition, it achieves negligible switching effect, on the systems states and control inputs, at the switching instants. On the other hand, it is worth mentioning that it is important to analyze the output response of the LPV-YK parameter $\tilde{Q}(\rho, \gamma)$ which affects the performance of the LPV-YK controller $\tilde{K}(\rho, \gamma)$. A future work can be done to study the choice of the dynamics of $\tilde{Q}(\rho, \gamma)$, i.e. how to choose the best design of the LPV state-feedback gains $F_g(\rho)$ and $F_{k,0}(\rho)$, and how they affect the closed-loop performance.

- The LPV approaches, specifically the polytopic one, have achieved lower performance at high vehicle speeds which is resulted from dynamic model uncertainties. The actuator model has been identified as a speed-independent model, whereas in reality, it changes its dynamics with respect to the vehicle speed. Thus, it is suggested to identify the steering actuator model as an LPV model in the future works to obtain a more realistic LPV vehicle model. Then, implement again the LPV approaches and analyze the performance improvement at high vehicle speeds.

- The proposed LPV-YK control structures have shown interesting simulation and experimental results. In comparison with the LPV controllers, they have achieved better driving comfort at high vehicles speeds. Moreover, smoother switching transitions are resulted using the LPV-YK controllers. A next step can be done by testing them in more complex environments, i.e. friction drop, gust wind, higher lateral accelerations.

- Concerning the multi-objective LPV-YK control structures, their importance is shown by implementing them in different driving situations such as lane changing, lane tracking, collision avoidance. This has been achieved by regulating the interpolating signals accordingly with the vehicle-surrounding situations. For more development, an interest appears to study the optimal choice of the interpolating signals γ, and how to find always the best combination of a larger set of controllers, which will improve more the presented work.

- The LPV-YK switching control with the highly performant RL model has provided interesting results in simulation. It has achieved safety, efficiency, and

comfort compared to other simulated controllers. Such a combined architecture can be used in the future to strengthen the link between the decision-making and the control systems which leads to higher vehicle performance.

Appendix A

LMI-based LPV/$\mathcal{H}_\infty$ Solution

Theorem 9. ***LMI-based LPV/$\mathcal{H}_\infty$ Solution***

Assume that the dynamical output-feedback LPV/$\mathcal{H}_\infty$ controller has the form $K(\rho)=\left[\begin{array}{c|c} A_k(\rho) & B_k(\rho) \\ \hline C_k(\rho) & D_k(\rho) \end{array}\right]$.

This controller is obtained after solving the following LMIs in $(\boldsymbol{X}(\rho), \boldsymbol{Y}(\rho), \overline{\boldsymbol{A}}(\rho), \overline{\boldsymbol{B}}(\rho), \overline{\boldsymbol{C}}(\rho), \overline{\boldsymbol{D}}(\rho))$ *while minimizing* γ_∞,

$$\begin{bmatrix} M_{11} & (*)^T & (*)^T & (*)^T \\ M_{21} & M_{22} & (*)^T & (*)^T \\ M_{31} & M_{32} & M_{33} & (*)^T \\ M_{41} & M_{42} & M_{43} & M_{44} \end{bmatrix} < 0 \tag{A.1}$$

$$\begin{bmatrix} \boldsymbol{X}(\rho) & I_n \\ I_n & \boldsymbol{Y}(\rho) \end{bmatrix} > 0$$

Where:

$$\begin{aligned}
M_{11} &= A_p(\rho)\boldsymbol{X}(\rho) + \boldsymbol{X}(\rho)A_p^T(\rho) + \tfrac{\partial \boldsymbol{X}(\rho)}{\partial \rho}\dot{\rho} + B_2\overline{\boldsymbol{C}}(\rho) + \overline{\boldsymbol{C}}^T(\rho)B_2^T \\
M_{21} &= \overline{\boldsymbol{A}}(\rho) + A_p^T(\rho) + C_2^T\overline{\boldsymbol{D}}^T(\rho)B_2^T \\
M_{22} &= \boldsymbol{Y}(\rho)A_p(\rho) + A_p^T(\rho)\boldsymbol{Y}(\rho) + \tfrac{\partial \boldsymbol{Y}(\rho)}{\partial \rho}\dot{\rho} + \overline{\boldsymbol{B}}(\rho)C_2 + C_2^T\overline{\boldsymbol{B}}^T(\rho) \\
M_{31} &= B_1^T(\rho) + D_{21}^T(\rho)\overline{\boldsymbol{D}}^T(\rho)B_2^T \\
M_{32} &= B_1^T(\rho)\boldsymbol{Y}(\rho) + D_{21}^T(\rho)\overline{\boldsymbol{B}}^T(\rho) \\
M_{33} &= -\gamma_\infty I_{n_u} \\
M_{41} &= C_1(\rho)\boldsymbol{X}(\rho) + D_{12}(\rho)\overline{\boldsymbol{C}}(\rho) \\
M_{42} &= C_1(\rho) + D_{12}(\rho)\overline{\boldsymbol{D}}(\rho)C_2 \\
M_{43} &= D_{11}(\rho) + D_{12}\overline{\boldsymbol{D}}(\rho)D_{21}(\rho) \\
M_{44} &= -\gamma_\infty I_{n_y}
\end{aligned} \tag{A.2}$$

Then, we obtain the dynamical controller $K(\rho)$ *as follows (for* $\tfrac{\partial \boldsymbol{X}(\rho)}{\partial \rho}\dot{\rho} = 0$ *):*

$$\begin{cases}
D_k(\rho) = \overline{\boldsymbol{D}}(\rho) \\
C_k(\rho) = (\overline{\boldsymbol{C}}(\rho) - D_k(\rho)C_2(\rho)\boldsymbol{X}(\rho)M(\rho))^{-T} \\
B_k(\rho) = N^{-1}(\rho)(\overline{\boldsymbol{B}}(\rho) - \boldsymbol{Y}(\rho)B_2(\rho)D_k(\rho)) \\
A_k(\rho) = N^{-1}(\rho)(\overline{\boldsymbol{A}}(\rho) - \boldsymbol{Y}(\rho)A_p(\rho)\boldsymbol{X}(\rho) - \boldsymbol{Y}(\rho)B_2(\rho)D_k(\rho)C_2(\rho)\boldsymbol{X}(\rho) \\
\qquad -N(\rho)B_k(\rho)C_2(\rho)\boldsymbol{X}(\rho) - \boldsymbol{Y}(\rho)B_2(\rho)C_k(\rho)M^T(\rho))M^{-T}(\rho)
\end{cases} \tag{A.3}$$

where $M(\rho)$ *and* $N(\rho)$ *are defined such that* $M(\rho)N^T(\rho) = I_n - \boldsymbol{X}(\rho)\boldsymbol{Y}(\rho)$

Appendix B

$\mathcal{H}_\infty$ Control Theory

The $\mathcal{H}_\infty$ robust control is one of the most controllers used nowadays. The word robust means that, if a system is influenced by input external disturbances, model uncertainties, or sensors'/actuators' failure, the $\mathcal{H}_\infty$ controller will ensure the stability of the system to remain in the safe zone. The $\mathcal{H}_\infty$ control design is a mathematical optimization problem where it can be applied to multivariable systems. FIGURE B.1 represents how the $\mathcal{H}_\infty$ problem statement is expressed: Where:

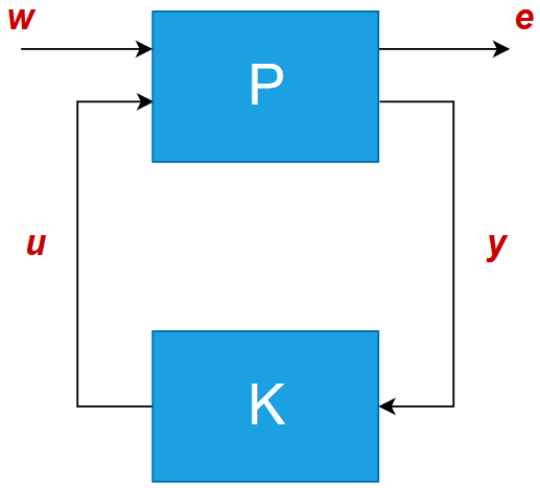

FIGURE B.1: $\mathcal{H}_\infty$ Control Design Configuration

- P is represented as a state space called the generalized plant which contains the LTI or LPV model system in addition to the weights that are added to the controlled outputs to achieve the required performances.
- K is the $\mathcal{H}_\infty$, static state-feedback or dynamic output-feedback, controller to be designed.
- w is the external input vector containing tracking references, input or output disturbances, or noises on the measured output.
- u is the controlled input to the LTI (LPV) model.
- y is the measured output from the LTI (LPV) model which will result an output-feedback dynamic controller K (a state-feedback controller is obtained if $y = x_p$ where x_p is the state vector of the generalized plant P).
- e is the controlled output which describes the objective of the controller.

The main objective of the mathematical optimization is to minimize the $\mathcal{H}_\infty$ norm of the energy-to-energy gain, which is the closed loop function $T_{ew}(s)$ in (B.1), from the external input $w(t)$ to the controlled output $e(t)$ ($\mathcal{L}_2$ to $\mathcal{L}_2$ norm). The $\mathcal{H}_\infty$ norm is defined as the maximum singular value of a function along the whole frequencies (In SISO systems, it is the highest magnitude reached by the transfer function). It is computed numerically using several algorithms where LMI method is the most popular one.

$$\|T_{ew}(s)\|_\infty = \sup_{w\in\mathbb{R}} \overline{\sigma}(T_{ew}(jw)) = \sup_{w(s)\in\mathcal{H}_2} \frac{\|e(s)\|_2}{\|w(s)\|_2} = \max_{w(t)\in\mathcal{L}_2} \frac{\|e(t)\|_2}{\|w(t)\|_2}$$
$$\|T_{ew}(s)\|_\infty \leq \gamma_\infty \tag{B.1}$$

Where γ_∞, to be minimized, represents how the demanded performance is achieved.

Bibliography

[1] Hussam Atoui et al. "Toward switching/interpolating LPV control: A review". In: *Annual Reviews in Control* (2022). ISSN: 1367-5788. DOI: https://doi.org/10.1016/j.arcontrol.2022.07.002. URL: https://www.sciencedirect.com/science/article/pii/S1367578822000888.

[2] Michael Safonov. "Origins of Robust Control: Early History and Future Speculations". In: *Annual Reviews in Control* 36 (Dec. 2012), 173–181. DOI: 10.1016/j.arcontrol.2012.09.001.

[3] DJ Leith and WE Leithead. "On formulating nonlinear dynamics in LPV form". In: *Proceedings of the 39th IEEE Conference on Decision and Control (Cat. No. 00CH37187)*. Vol. 4. IEEE. 2000, pp. 3526–3527.

[4] Jeff S Shamma. "Analysis and design of gain scheduled control systems". PhD thesis. Massachusetts Institute of Technology, 1988.

[5] P. Apkarian and R. J. Adams. "Advanced gain-scheduling techniques for uncertain systems". In: *IEEE Transactions on Control Systems Technology* 6.1 (1998), pp. 21–32. ISSN: 2374-0159. DOI: 10.1109/87.654874.

[6] P. Apkarian and P. Gahinet. "A convex characterization of gain-scheduled H_∞ controllers". In: *IEEE Transactions on Automatic Control* 40.5 (1995), pp. 853–864. ISSN: 2334-3303. DOI: 10.1109/9.384219.

[7] Pierre Apkarian, Pascal Gahinet, and Greg Becker. "Self-scheduled $\mathcal{H}_\infty$ control of linear parameter-varying systems: a design example". In: *Automatica* 31.9 (1995), pp. 1251–1261.

[8] Fen Wu et al. "Induced $\mathcal{L}_2$ norm control for LPV system with bounded parameter variation rates". In: *Proceedings of 1995 American Control Conference - ACC'95*. Vol. 3. 1995, 2379–2383 vol.3. DOI: 10.1109/ACC.1995.531398.

[9] Douglas J. Leith and William E. Leithead. "Survey of gain-scheduling analysis and design". In: *International Journal of Control* 73 (2000), pp. 1001 –1025.

[10] Javad Mohammadpour and Carsten W Scherer. *Control of linear parameter varying systems with applications*. Springer Science & Business Media, 2012.

[11] Olivier Sename, Peter Gaspar, and József Bokor (Eds). *Robust control and linear parameter varying approaches: application to vehicle dynamics*. Vol. 437. Springer, LNCIS, 2013.

[12] Andy Packard. "Gain scheduling via linear fractional transformations". In: *Systems & Control Letters* 22.2 (1994), pp. 79–92. ISSN: 0167-6911. DOI: https://doi.org/10.1016/0167-6911(94)90102-3. URL: https://www.sciencedirect.com/science/article/pii/0167691194901023.

[13] W. Rugh and J. Shamma. "Research on Gain Scheduling". In: *Automatica* 36 (Oct. 2000), pp. 1401–1425. DOI: 10.1016/S0005-1098(00)00058-3.

[14] C. Hoffmann and H. Werner. "A Survey of Linear Parameter-Varying Control Applications Validated by Experiments or High-Fidelity Simulations". In: *IEEE Transactions on Control Systems Technology* 23.2 (2015), pp. 416–433. ISSN: 2374-0159. DOI: 10.1109/TCST.2014.2327584.

[15] Georgo Z Angelis. "System analysis, modelling and control with polytopic linear models." In: (2003).

[16] Fen Wu. "Control of linear parameter varying systems". PhD thesis. University of California at Berkeley, 1995.

[17] Arnar Hjartarson, Peter J. Seiler, and Gary J. Balas. "LPV aeroservoelastic control using the LPVTools toolbox". In: 2013.

[18] Fen Wu et al. "Induced $\mathcal{L}_2$ Norm Control for LPV Systems with Bounded Parameter Variation Rates". In: *International Journal of Robust and Nonlinear Control* 6 (1996), pp. 983–998. DOI: 10.1002/(SICI)1099-1239(199611)6:9/10<983::AID-RNC263>3.0.CO;2-C.

[19] J.S. Shamma and M. Athans. "Gain scheduling: potential hazards and possible remedies". In: *IEEE Control Systems Magazine* 12.3 (1992), pp. 101–107. DOI: 10.1109/37.165527.

[20] Fen Wu. "A generalized LPV system analysis and control synthesis framework". In: *International Journal of Control* 74 (2001), pp. 745 –759.

[21] Fen Wu and Ke Dong. "Gain-scheduling control of LFT systems using parameter-dependent Lyapunov functions". In: *Proceedings of the 2005, American Control Conference, 2005.* 2005, 587–592 vol. 1. DOI: 10.1109/ACC.2005.1470020.

[22] Olivier Sename. "Review on LPV Approaches for Suspension Systems". In: *Electronics* 10.17 (2021). ISSN: 2079-9292. DOI: 10.3390/electronics10172120.

[23] Hussam Atoui et al. "LPV-Based Autonomous Vehicle Lateral Controllers: A Comparative Analysis". In: *IEEE Transactions on Intelligent Transportation Systems* 23.8 (2022), pp. 13570–13581. DOI: 10.1109/TITS.2021.3125771.

[24] A. Kwiatkowski and H. Werner. "PCA-Based Parameter Set Mappings for LPV Models With Fewer Parameters and Less Overbounding". In: *IEEE Transactions on Control Systems Technology* 16.4 (2008), pp. 781–788. DOI: 10.1109/TCST.2007.903094.

[25] Panshuo Li et al. "Polytopic LPV approaches for intelligent automotive systems: State of the art and future challenges". In: *Mechanical Systems and Signal Processing* 161 (2021), p. 107931. ISSN: 0888-3270. DOI: https://doi.org/10.1016/j.ymssp.2021.107931.

[26] T. Azuma et al. "A New LMI Approach to Analysis of Linear Systems Depending on Scheduling Parameter in Polynomial Forms". In: 48.4 (2000), pp. 199–199. DOI: doi:10.1524/auto.2000.48.4.199.

[27] Christian Hoffmann et al. "Synthesis of LPV Controllers With Low Implementation Complexity Based on a Reduced Parameter Set". In: *IEEE Transactions on Control Systems Technology* 22.6 (2014), pp. 2393–2398. DOI: 10.1109/TCST.2014.2303397.

[28] C. Hoffmann et al. "Synthesis of LPV controllers with reduced implementation complexity". In: *2014 American Control Conference*. 2014, pp. 3766–3771. DOI: 10.1109/ACC.2014.6858716.

[29] Pierre Apkarian and Hoang Duong Tuan. "Parameterized LMIs in Control Theory". In: *SIAM Journal on Control and Optimization* 38.4 (2000), pp. 1241–1264. DOI: 10.1137/S036301299732612X. eprint: https://doi.org/10.1137/S036301299732612X.

[30] H.D. Tuan and P. Apkarian. "Relaxations of parameterized LMIs with control applications". In: *Proceedings of the 37th IEEE Conference on Decision and Control (Cat. No.98CH36171)*. Vol. 2. 1998, 1747–1752 vol.2. DOI: 10.1109/CDC.1998.758548.

[31] P. J. W. Koelewijn and R. Tóth. "Scheduling Dimension Reduction of LPV Models - A Deep Neural Network Approach". In: *2020 American Control Conference (ACC)*. 2020, pp. 1111–1117. DOI: 10.23919/ACC45564.2020.9147310.

[32] Pan Zhao and R. Nagamune. "Optimal switching surface design for state-feedback switching LPV control". In: (2015), pp. 817–822. DOI: 10.1109/ACC.2015.7170835.

[33] P. Zhao and R. Nagamune. "Switching LPV controller design under uncertain scheduling parameters". In: *Automatica* 76 (2017), pp. 243–250.

[34] Florian Saupe and Harald Pfifer. "Applied LPV control exploiting the separation principle for the single axis positioning of an industrial manipulator". In: *2011 IEEE International Conference on Control Applications (CCA)*. 2011, pp. 1476–1481. DOI: 10.1109/CCA.2011.6044513.

[35] Florian Saupe and Harald Pfifer. "An Observer Based State Feedback LFT LPV Controller for an Industrial Manipulator". In: *IFAC Proceedings Volumes* 45.13 (2012). 7th IFAC Symposium on Robust Control Design, pp. 337–342. ISSN: 1474-6670. DOI: https://doi.org/10.3182/20120620-3-DK-2025.00017.

[36] Florian Saupe. "Linear Parameter Varying Control Design for Industrial Manipulators". In: 2013.

[37] Andy Packard. "Gain scheduling via linear fractional transformations". In: *Systems & control letters* 22.2 (1994), pp. 79–92.

[38] G. Scorletti and L. El Ghaoui. "Improved linear matrix inequality conditions for gain scheduling". In: *Proceedings of 1995 34th IEEE Conference on Decision and Control*. Vol. 4. 1995, 3626–3631 vol.4. DOI: 10.1109/CDC.1995.479152.

[39] Gérard Scorletti and Laurent El Ghaoui. "IMPROVED LMI CONDITIONS FOR GAIN SCHEDULING AND RELATED CONTROL PROBLEMS". In: *International Journal of Robust and Nonlinear Control* 8 (1998), pp. 845–877.

[40] Anders Helmersson. "Methods for robust gain scheduling". PhD thesis. Linköping University Electronic Press, 1995.

[41] Stephen Boyd et al. *Linear matrix inequalities in system and control theory*. Vol. 15. Siam, 1994, pp. 51–56.

[42] C.W. Scherer. "LPV control and full block multipliers". In: *Automatica* 37.3 (2001), pp. 361–375. ISSN: 0005-1098. DOI: https://doi.org/10.1016/S0005-1098(00)00176-X.

[43] C.W. Scherer. "A full block S-procedure with applications". In: *Proceedings of the 36th IEEE Conference on Decision and Control*. Vol. 3. 1997, 2602–2607 vol.3. DOI: 10.1109/CDC.1997.657769.

[44] Kursad Derinkuyu and Mustafa Ç. Pinar. "On the S-procedure and Some Variants". In: *Mathematical Methods of Operations Research* 64 (2006), pp. 55–77.

[45] Imre Pólik and Tamás Terlaky. "A Survey of the S-Lemma". In: *SIAM Rev.* 49 (2007), pp. 371–418.

[46] E. Feron, P. Apkarian, and P. Gahinet. "S-procedure for the analysis of control systems with parametric uncertainties via parameter-dependent Lyapunov functions". In: *Proceedings of 1995 American Control Conference - ACC'95*. Vol. 1. 1995, 968–972 vol.1. DOI: 10.1109/ACC.1995.529394.

[47] E. Feron, P. Apkarian, and P. Gahinet. "Analysis and synthesis of robust control systems via parameter-dependent Lyapunov functions". In: *IEEE Transactions on Automatic Control* 41.7 (1996), pp. 1041–1046. DOI: 10.1109/9.508913.

[48] M. Dettori and C.W. Scherer. "Robust stability analysis for parameter dependent systems using full block S-procedure". In: *Proceedings of the 37th IEEE Conference on Decision and Control (Cat. No.98CH36171)*. Vol. 3. 1998, 2798–2799 vol.3. DOI: 10.1109/CDC.1998.757879.

[49] Joost Veenman and Carsten W. Scherer. "A synthesis framework for robust gain-scheduling controllers". In: *Automatica* 50.11 (2014), pp. 2799–2812. ISSN: 0005-1098. DOI: https://doi.org/10.1016/j.automatica.2014.10.002. URL: https://www.sciencedirect.com/science/article/pii/S0005109814003835.

[50] Bei Lu, Heeju Choi, and G.D. Buckner. "LPV control design and experimental implementation for a magnetic bearing system". In: *2006 American Control Conference*. 2006, 6 pp.–. DOI: 10.1109/ACC.2006.1657440.

[51] Bei Lu et al. "Linear parameter-varying techniques for control of a magnetic bearing system". In: *Control Engineering Practice* 16.10 (2008), pp. 1161–1172. ISSN: 0967-0661. DOI: https://doi.org/10.1016/j.conengprac.2008.01.002.

[52] Alejandro Simon Ghersin, Roy S. Smith, and Ricardo S. Sánchez. "LPV CONTROL OF A MAGNETIC BEARING EXPERIMENT". In: *Latin American Applied Research* 40 (2010), pp. 303–310.

[53] Jasper Witte, H.M.N.K. Balini, and Carsten W. Scherer. "Robust and LPV control of an AMB system". In: *Proceedings of the 2010 American Control Conference*. 2010, pp. 2194–2199. DOI: 10.1109/ACC.2010.5531273.

[54] Alejandro Ghersin, Roy Smith, and Ricardo Sánchez-Peña. "Classical, Robust and LPV Control of a Magnetic-bearing Experiment". In: Jan. 2007, pp. 277–325. ISBN: 978-1-84628-898-2. DOI: 10.1007/978-1-84628-899-9_10.

[55] Masanori Narita, Gan Chen, and Isao Takami. "Gain scheduling controller synthesis for active magnetic bearing based on parameter dependent LMI with convexity condition". In: *2017 2nd International Conference on Control and Robotics Engineering (ICCRE)*. 2017, pp. 63–67. DOI: 10.1109/ICCRE.2017.7935043.

[56] I Kuseyri. "Adaptive vibration control of rotors with active magnetic bearings". In: *J Vib Eng Technol* 5.02 (2017), pp. 159–164.

[57] C. Hoffmann et al. "Benchmark problem — nonlinear control of a 3-DOF robotic manipulator". In: *52nd IEEE Conference on Decision and Control*. 2013, pp. 5534–5539. DOI: 10.1109/CDC.2013.6760761.

[58] Seyed Mahdi Hashemi and Herbert Werner. "Gain-scheduled H infinity control of a robotic manipulator with nonlinear joint friction". In: *Virtual Control Conference*. Jan. 2010.

[59] Ron J. Patton and S. Klinkhieo. "LPV fault estimation and FTC of a two-link manipulator". In: *Proceedings of the 2010 American Control Conference*. 2010, pp. 4647–4652. DOI: 10.1109/ACC.2010.5531057.

[60] Christian Paraiso Salah El-Dine, Seyed Mahdi Hashemi, and Herbert Werner. "Black-box versus grey-box LPV identification to control a mechanical system". In: *2012 IEEE 51st IEEE Conference on Decision and Control (CDC)*. 2012, pp. 5152–5157. DOI: 10.1109/CDC.2012.6426536.

[61] Seyed Mahdi Hashemi, Hossam Seddik Abbas, and Herbert Werner. "LPV modelling and control of a 2-DOF robotic manipulator using PCA-based parameter set mapping". In: *Proceedings of the 48h IEEE Conference on Decision and Control (CDC) held jointly with 2009 28th Chinese Control Conference*. 2009, pp. 7418–7423. DOI: 10.1109/CDC.2009.5400621.

[62] C. Hoffmann et al. "Closed-loop stability and performance optimization in LPV control based on a reduced parameter set". In: *2012 IEEE 51st IEEE Conference on Decision and Control (CDC)*. 2012, pp. 5146–5151. DOI: 10.1109/CDC.2012.6427053.

[63] Seyed Mahdi Hashemi, Hossam Seddik Abbas, and Herbert Werner. "Low-complexity linear parameter-varying modeling and control of a robotic manipulator". In: *Control Engineering Practice* 20.3 (2012), pp. 248–257. ISSN: 0967-0661. DOI: https://doi.org/10.1016/j.conengprac.2011.11.002.

[64] Mohammad Jabali and Mohammad Hosein Kazemi. "Uncertain polytopic LPV modelling of robot manipulators and trajectory tracking". In: *International Journal of Control, Automation and Systems* 15 (Mar. 2017). DOI: 10.1007/s12555-015-1432-1.

[65] Zhongwei Yu, Huitang Chen, and Peng-Yung Woo. "Polytopic gain scheduled $\mathcal{H}_\infty$ control for robotic manipulators". In: *Robotica* 21.5 (2003), 495–504. DOI: 10.1017/S0263574703005071.

[66] A Kwiatkowski et al. "Linear parameter varying PID controller design for charge control of a spark-ignited engine". In: *Control Engineering Practice* 17.11 (2009), pp. 1307–1317.

[67] Andrew P. White et al. "Mixed $\mathcal{H}_2/\mathcal{H}_\infty$ Observer-Based LPV Control of a Hydraulic Engine Cam Phasing Actuator". In: *IEEE Trans. Control. Syst. Technol.* 21 (2013), pp. 229–238.

[68] Felipe Castillo et al. "Fresh Air Fraction Control in Engines Using Dynamic Boundary Stabilization of LPV Hyperbolic Systems". In: *IEEE Transactions on Control Systems Technology* 23.3 (2015), pp. 963–974. DOI: 10.1109/TCST.2014.2356858.

[69] Cheng-Lun Chen and G.T.-C. Chiu. "Compensating for spatially repetitive disturbance with linear parameter varying repetitive control". In: *Proceedings of the 2004 IEEE International Conference on Control Applications, 2004.* Vol. 1. 2004, 736–741 Vol.1. DOI: 10.1109/CCA.2004.1387301.

[70] Lukas Bergmann et al. "Implementation of LPV $\mathcal{H}_\infty$ Loop-Shaping Control for a Variable Stiffness Actuator". In: *IFAC-PapersOnLine* 53.2 (2020). 21th IFAC World Congress, pp. 10129–10134. ISSN: 2405-8963. DOI: https://doi.org/10.1016/j.ifacol.2020.12.2738.

[71] Mokrane Boudaoud et al. "Gain scheduled control strategies for a nonlinear electrostatic microgripper: Design and real time implementation". In: *2012 IEEE 51st IEEE Conference on Decision and Control (CDC)*. 2012, pp. 3127–3132. DOI: 10.1109/CDC.2012.6426177.

[72] Christian Hoffmann, Christian Radisch, and Herbert Werner. "Active damping of container crane load swing by hoisting modulation — An LPV approach". In: *2012 IEEE 51st IEEE Conference on Decision and Control (CDC)*. 2012, pp. 5140–5145. DOI: 10.1109/CDC.2012.6426889.

[73] Vincent J. Ginter and Jeff K. Pieper. "Robust Gain Scheduled Control of a Hydrokinetic Turbine Part 2: Testing". In: *2009 IEEE Electrical Power Energy Conference (EPEC)*. 2009, pp. 1–5. DOI: 10.1109/EPEC.2009.5420971.

[74] Takahiro Sugiyama and Kenko Uchida. "SWITCHING FROM VELOCITY TO FORCE CONTROL FOR THE ELECTRO-HYDRAULIC SERVOSYSTEM BASED ON LPV SYSTEM MODELING". In: *IFAC Proceedings Volumes* 35 (2002), pp. 25–30.

[75] Yolanda Bolea et al. "LPV VS MULTI-MODEL PI(D) GAIN-SCHEDULING APPLIED TO CANAL CONTROL". In: *IFAC Proceedings Volumes* 38.1 (2005). 16th IFAC World Congress, pp. 13–18. ISSN: 1474-6670. DOI: https://doi.org/10.3182/20050703-6-CZ-1902.02173.

[76] Frans Wijnheijmer et al. "Modelling and LPV control of an electro-hydraulic servo system". In: *2006 IEEE Conference on Computer Aided Control System Design, 2006 IEEE International Conference on Control Applications, 2006 IEEE International Symposium on Intelligent Control*. 2006, pp. 3116–3121. DOI: 10.1109/CACSD-CCA-ISIC.2006.4777136.

[77] Alexandru Forrai, Takaharu Ueda, and Takashi Yumura. "Electromagnetic Actuator Control: A Linear Parameter-Varying (LPV) Approach". In: *IEEE Transactions on Industrial Electronics* 54.3 (2007), pp. 1430–1441. DOI: 10.1109/TIE.2007.893077.

[78] Samira Asadi et al. "Fault Reconstruction of Islanded Nonlinear DC Microgrids: An LPV-based Sliding Mode Observer Approach". In: *IEEE Journal of Emerging and Selected Topics in Power Electronics* (2020), pp. 1–1. DOI: 10.1109/JESTPE.2020.3043491.

[79] H. Hirano, Y. Kawai, and M. Fujita. "Automated driving for an experimental vehicle using visual feedback control". In: *SICE 2003 Annual Conference (IEEE Cat. No.03TH8734)*. Vol. 1. 2003, pp. 1016–1021.

[80] Roberto S. Inoue, Adriano A. G. Siqueira, and Marco H. Terra. "Experimental results on the nonlinear $\mathcal{H}_\infty$ control via quasi-LPV representation and game theory for wheeled mobile robots". In: *2007 IEEE International Conference on Control Applications*. 2007, pp. 1456–1461. DOI: 10.1109/CCA.2007.4389441.

[81] Jinghua Guo, Yugong Luo, and Keqiang Li. "Robust gain-scheduling automatic steering control of unmanned ground vehicles under velocity-varying motion". In: *Vehicle System Dynamics* (May 2018), pp. 1–22. DOI: 10.1080/00423114.2018.1475677.

[82] Eugenio Alcala et al. "Gain-scheduling LPV Control For Autonomous Vehicles Including Friction Force Estimation and Compensation Mechanism". In: *IET Control Theory & Applications* 12.12 (2018), pp. 1683–1693.

[83] Luiz Benicio Degli Esposte Rosa and Renan Pereira. "Discrete-time L2 loop-shaping control of a Maglev System using the LPV framework". In: *XXIII Brazilian Conference on Automation (CBA)*. Nov. 2020. DOI: 10.48011/asba.v2i1.1563.

[84] Damiano Rotondo, Fatiha Nejjari, and Vicenç Puig. "Quasi-LPV modeling, identification and control of a twin rotor MIMO system". In: *Control Engineering Practice* 21.6 (2013), pp. 829–846. ISSN: 0967-0661. DOI: https://doi.org/10.1016/j.conengprac.2013.02.004.

[85] H. Kajiwara, P. Apkarian, and P. Gahinet. "LPV techniques for control of an inverted pendulum". In: *IEEE Control Systems Magazine* 19.1 (1999), pp. 44–54. DOI: 10.1109/37.745767.

[86] Maifuz Ali and Herbert Werner. "Discrete-Time LPV Controller Synthesis Using Dilated LMIs with Application to an Arm-Driven Inverted Pendulum". In: vol. 18. Aug. 2011, pp. 7708–7712. DOI: 10.3182/20110828-6-IT-1002.03079.

[87] David Robert, Olivier Sename, and Daniel Simon. "An $\mathcal{H}_\infty$ LPV Design for Sampling Varying Controllers: Experimentation With a T-Inverted Pendulum". In: *IEEE Transactions on Control Systems Technology* 18.3 (2010), pp. 741–749. DOI: 10.1109/TCST.2009.2026179.

[88] X. Shu et al. "Design of structured discrete-time LPV gain-scheduling controllers through state augmentation and partial state feedback". In: *2013 American Control Conference*. 2013, pp. 6090–6095. DOI: 10.1109/ACC.2013.6580793.

[89] X. Shu et al. "Two-Parameter pLPV Modeling of Nonstationary Harmonically Related Multisine Disturbances for Reduced-Order Gain-Scheduling Control". In: Feb. 2013. DOI: 10.2316/P.2013.794-078.

[90] Pablo Ballesteros et al. "Reduced-order two-parameter pLPV controller for the rejection of nonstationary harmonically related multisine disturbances". In: *2013 European Control Conference (ECC)*. 2013, pp. 1835–1842. DOI: 10.23919/ECC.2013.6669358.

[91] Wiebke Heins, Pablo Ballesteros, and Christian Bohn. "GAIN-SCHEDULED STATE-FEEDBACK CONTROL FOR ACTIVE CANCELLATION OF MULTISINE DISTURBANCES WITH TIME-VARYING FREQUENCIES". In: *Mechanics and Control* 30 (2011), pp. 127–137.

[92] Masayuki Sato. "Robust Gain-Scheduled flight controller using inexact scheduling parameters". In: *2013 American Control Conference*. 2013, pp. 6829–6834. DOI: 10.1109/ACC.2013.6580911.

[93] Yuxiao Wang et al. "Gain scheduling controller of the aero-engine based on LPV model". In: *2016 IEEE Chinese Guidance, Navigation and Control Conference (CGNCC)*. 2016, pp. 2265–2270. DOI: 10.1109/CGNCC.2016.7829145.

[94] Hugo A. Pipino et al. "Nonlinear temperature regulation of solar collectors with a fast adaptive polytopic LPV MPC formulation". In: *Solar Energy* 209 (2020), pp. 214–225. ISSN: 0038-092X. DOI: https://doi.org/10.1016/j.solener.2020.09.005.

[95] Qilu Sun, Guanzhong Dai, and Wenping Pan. "LPV Model and Its Application in Web Server Performance Control". In: *2008 International Conference on Computer Science and Software Engineering*. Vol. 3. 2008, pp. 486–489. DOI: 10.1109/CSSE.2008.1219.

[96] G. Papageorgiou et al. "Taking robust LPV control into flight on the VAAC Harrier". In: *Proceedings of the 39th IEEE Conference on Decision and Control (Cat. No.00CH37187)*. Vol. 5. 2000, 4558–4564 vol.5. DOI: 10.1109/CDC.2001.914633.

[97] Masayuki Sato. "Robust Gain-Scheduled flight controller using inexact scheduling parameters". In: *2013 American Control Conference*. 2013, pp. 6829–6834. DOI: 10.1109/ACC.2013.6580911.

[98] M. Sato. "Robust H/sub 2/ problem for LPV systems and its application to model-following controller design for aircraft motions". In: *Proceedings of the 2004 IEEE International Conference on Control Applications, 2004.* Vol. 1. 2004, 442–449 Vol.1. DOI: 10.1109/CCA.2004.1387251.

[99] Pushkar Hingwe et al. "Linear parameter varying controller for automated lane guidance: experimental study on tractor-trailers". In: *IEEE Transactions on Control Systems Technology* 10.6 (2002), pp. 793–806. DOI: 10.1109/TCST.2002.804118.

[100] Hussam Atoui et al. "Parameter Varying Approach For A Combined (Kinematic + Dynamic) Model Of Autonomous Vehicles**Institute of Engineering Univ. Grenoble Alpes". In: *IFAC-PapersOnLine* 53.2 (2020). 21st IFAC World Congress, pp. 15071–15076. ISSN: 2405-8963. DOI: https://doi.org/10.1016/j.ifacol.2020.12.2028. URL: https://www.sciencedirect.com/science/article/pii/S2405896320326641.

[101] Van Tan Vu et al. "The design of an $\mathcal{H}_\infty$/LPV active braking control to improve vehicle roll stability". In: *7th IFAC Symposium on Systems Structure and Control (SSSC 2019)*. Sinaia, Romania, Sept. 2019.

[102] Kazusa Yamamoto et al. "Design and experimentation of an LPV extended state feedback control on Electric Power Steering systems". In: *Control Engineering Practice* 90 (2019), pp. 123–132.

[103] A. Kwiatkowski et al. "LPV controller synthesis for charge control of a car engine - A hybrid evolutionary algebraic approach". In: July 2007. DOI: 10.23919/ECC.2007.7068370.

[104] Abdelrahman Morsi et al. "Model Predictive Control Based on Linear Parameter-Varying Models of Active Magnetic Bearing Systems". In: *IEEE Access* 9 (2021), pp. 23633–23647. DOI: 10.1109/ACCESS.2021.3056323.

[105] Amirhossein Salimi et al. "Gain-scheduling control of a cable-driven MRI-compatible robotic platform for intracardiac interventions". In: *2013 American Control Conference*. 2013, pp. 746–751. DOI: 10.1109/ACC.2013.6579925.

[106] Zhongwei Yu, Huitang Chen, and Peng-Yung Woo. "Gain Scheduled LPV $\mathcal{H}_\infty$ Control Based on LMI Approach for a Robotic Manipulator". In: *J. Field Robotics* 19 (2002), pp. 585–593.

[107] Feng Zhang et al. "Transient lean burn air-fuel ratio control using input shaping method combined with linear parameter-varying control". In: *2006 American Control Conference*. 2006, 6 pp.–. DOI: 10.1109/ACC.2006.1657225.

[108] Feng Zhang et al. "Linear Parameter-Varying Lean Burn Air-Fuel Ratio Control". In: *Proceedings of the 44th IEEE Conference on Decision and Control*. 2005, pp. 2688–2693. DOI: 10.1109/CDC.2005.1582569.

[109] M. Jung and K. Glover. "Calibratable linear parameter-varying control of a turbocharged diesel engine". In: *IEEE Transactions on Control Systems Technology* 14.1 (2006), pp. 45–62. DOI: 10.1109/TCST.2005.860513.

[110] Farzad A Shirazi, Karolos M Grigoriadis, and Daniel Viassolo. "Wind turbine integrated structural and LPV control design for improved closed-loop performance". In: *International Journal of Control* 85.8 (2012), pp. 1178–1196.

[111] Hossam S. Abbas et al. "LPV gain-scheduled control of a control moment gyroscope". In: *2013 American Control Conference*. 2013, pp. 6841–6846. DOI: 10.1109/ACC.2013.6580913.

[112] Julian Theis, Christian Radisch, and Herbert Werner. "Self-Scheduled Control of a Gyroscope". In: *IFAC Proceedings Volumes* 47.3 (2014). 19th IFAC World Congress, pp. 6129–6134. ISSN: 1474-6670. DOI: https://doi.org/10.3182/20140824-6-ZA-1003.01058.

[113] Bei YANG, Xi WANG, and Penghui SUN. "Non-affine parameter dependent LPV model and LMI based adaptive control for turbofan engines". In: *Chinese Journal of Aeronautics* 32 (Mar. 2019). DOI: 10.1016/j.cja.2018.12.031.

[114] M. Dettori and C. W. Scherer. "Design and implementation of a gain scheduled controller for a compact disc player". In: *1999 European Control Conference (ECC)*. 1999, pp. 4508–4513. DOI: 10.23919/ECC.1999.7100045.

[115] M Dettori and CW Scherer. "Gain scheduling control for a CD player mechanism using LPV techniques". In: *Theory and Practice of Control and Systems*. World Scientific, 1998, pp. 385–390.

[116] M. Dettori and C.W. Scherer. "LPV design for a CD player: an experimental evaluation of performance". In: *Proceedings of the 40th IEEE Conference on Decision and Control (Cat. No.01CH37228)*. Vol. 5. 2001, 4711–4716 vol.5. DOI: 10.1109/CDC.2001.980950.

[117] Marco Dettori. "LMI techniques for control with application to a compact disc player mechanism". PhD thesis. Technische Universiteit Delft (The Netherlands), 2002.

[118] Klaus Trangbaek. "Linear Parameter Varying Control of Induction Motors". PhD thesis. Institut for Elektroniske Systemer, Aalborg Universitet, Jan. 2001.

[119] J.D. Bendtsen and K. Trangbaek. "Discrete-time LPV current control of an induction motor". In: *42nd IEEE International Conference on Decision and Control (IEEE Cat. No.03CH37475)*. Vol. 6. 2003, 5903–5908 Vol.6. DOI: 10.1109/CDC.2003.1271949.

[120] Ali Umut Gen. "Linear Parameter-Varying Modelling and Robust Control of Variable Cam Timing Engines". PhD thesis. Dept. Eng., Univ.Cambridge, Cambridge, U.K., 2002.

[121] Christophe Gauthier et al. "SOME EXPERIMENTAL RESULTS OF AN $\mathcal{H}_\infty$-LPV CONTROLLER APPLIED TO A DIESEL ENGINE COMMON RAIL INJECTION SYSTEM". In: *IFAC Proceedings Volumes* 40.10 (2007), pp. 417–424.

[122] Christophe Gauthier et al. "An LFT Approach to H Control Design for Diesel Engine Common Rail Injection System". In: *Oil & Gas Science and Technology-Revue de l'IFP* 62.4 (2007), pp. 513–522.

[123] M. B. Groot Wassink et al. "LPV control for a wafer stage: beyond the theoretical solution". In: *Control Engineering Practice* 13 (2005), pp. 231–245.

[124] H. Atoui et al. "Design And Experimental Validation Of A Lateral LPV Control Of Autonomous Vehicles". In: *2020 IEEE 23rd International Conference on Intelligent Transportation Systems (ITSC)*. 2020, pp. 1–6. DOI: 10.1109/ITSC45102.2020.9294459.

[125] Jonas S. Lauridsen and Ilmar Ferreira Santos. "Design of robust AMB controllers for rotors subjected to varying and uncertain seal forces". In: *European Journal of Emergency Medicine* 4 (2017), pp. 16–00618.

[126] Alican Sahinkaya and Jerzy T. Sawicki. "Cancelling Gyroscopic Effects in AMB Systems With Flexible Rotors via Modal Feedback". In: *Volume 4: Dynamics, Vibration, and Control* (2019).

[127] Charles Poussot-Vassal and Clement Roos. "Generation of a reduced-order LPV/LFT model from a set of large-scale MIMO LTI flexible aircraft models". In: *Control Engineering Practice* 20.9 (2012), pp. 919–930.

[128] Jean-Marc Biannic, Clement Roos, and Andreas Knauf. "Design and robustness analysis of fighter aircraft flight control laws". In: *European journal of control* 12.1 (2006), pp. 71–85.

[129] Rui Wang, Min Liu, and Yanhua Ma. "Fault estimation for aero-engine LPV systems based on LFT". In: *Asian Journal of Control* 23.1 (2021), pp. 351–361.

[130] Pablo Ballesteros et al. "LPV gain-scheduled output feedback for active control of harmonic disturbances with time-varying frequencies". In: *Advances on Analysis and Control of Vibrations-Theory and Applications* (2012).

[131] Pablo Ballesteros and Christian Bohn. "A frequency-tunable LPV controller for narrowband active noise and vibration control". In: *Proceedings of the 2011 American Control Conference*. 2011, pp. 1340–1345. DOI: 10.1109/ACC.2011.5990775.

[132] Pablo Ballesteros and Christian Bohn. "Disturbance Rejection through LPV Gain-Scheduling Control with Application to Active Noise Cancellation". In: *IFAC Proceedings Volumes* 44.1 (2011). 18th IFAC World Congress, pp. 7897–7902. ISSN: 1474-6670. DOI: https://doi.org/10.3182/20110828-6-IT-1002.00830.

[133] Xinyu Shu, Pablo Ballesteros, and Christian Bohn. "Active vibration control for harmonic disturbances with time-varying frequencies through LPV gain scheduling". In: *2011 Chinese Control and Decision Conference (CCDC)*. 2011, pp. 728–733. DOI: 10.1109/CCDC.2011.5968278.

[134] Franklyn Duarte et al. "An LPV discrete-time controller for the rejection of harmonic time-varying disturbances in a lightweight flexible structure". In: *2013 American Control Conference*. 2013, pp. 4092–4097. DOI: 10.1109/ACC.2013.6580467.

[135] Jihoon Lim, Patrick Kirchen, and Ryozo Nagamune. "LPV Controller Design for Diesel Engine SCR Aftertreatment Systems Based on Quasi-LPV Models". In: *IEEE Control Systems Letters* 5.5 (2021), pp. 1807–1812. DOI: 10.1109/LCSYS.2020.3046447.

[136] Christian Hoffmann and Herbert Werner. "Linear Parameter-Varying Control of Complex Mechanical Systems". In: *IFAC Proceedings Volumes* 47.3 (2014). 19th IFAC World Congress, pp. 6147–6152. ISSN: 1474-6670. DOI: https://doi.org/10.3182/20140824-6-ZA-1003.00118.

[137] C. Hoffmann et al. "Closed-loop stability and performance optimization in LPV control based on a reduced parameter set". In: *2012 IEEE 51st IEEE Conference on Decision and Control (CDC)*. 2012, pp. 5146–5151. DOI: 10.1109/CDC.2012.6427053.

[138] Hans Pacejka. *Tire and vehicle dynamics*. Elsevier, 2005.

[139] Rajesh Rajamani. *Vehicle dynamics and control*. New York, USA: Springer Science & Business Media, 2011.

[140] R Mariano, S Scalzi, and M Netto. "Nested PID steering control for lane keeping in autonomous vehicles". In: *Control Engineering Practice* 19.12 (Jan. 2011), pp 1459–1467. DOI: 10.1016/j.conengprac.2011.08.005.

[141] G.J. Balas and J.C. Doyle. "Robustness and performance trade-offs in control design for flexible structures". In: *IEEE Transactions on Control Systems Technology* 2.4 (1994), pp. 352–361. DOI: 10.1109/87.338656.

[142] B. Lu and F. Wu. "Switching LPV control designs using multiple parameter-dependent Lyapunov functions". In: *Automatica* 40 (Nov. 2004), pp. 1973–1980. DOI: 10.1016/j.automatica.2004.06.011.

[143] Grace S. Deaecto. "Dynamic output feedback $\mathcal{H}_\infty$ control of continuous-time switched affine systems". In: *Automatica* 71 (2016), pp. 44–49. ISSN: 0005-1098. DOI: https://doi.org/10.1016/j.automatica.2016.04.022.

[144] Xudong Zhao et al. "New Results on Stability of Slowly Switched Systems: A Multiple Discontinuous Lyapunov Function Approach". In: *IEEE Transactions on Automatic Control* 62.7 (2017), pp. 3502–3509. DOI: 10.1109/TAC.2016.2614911.

[145] Corentin Briat and Mustafa Khammash. "Stability analysis of LPV systems with piecewise differentiable parameters". In: *IFAC-PapersOnLine* 50.1 (2017). 20th IFAC World Congress, pp. 7554–7559. ISSN: 2405-8963. DOI: https://doi.org/10.1016/j.ifacol.2017.08.1191.

[146] Grace S. Deaecto and José C. Geromel. "Stability Analysis and Control Design of Discrete-Time Switched Affine Systems". In: *IEEE Transactions on Automatic Control* 62.8 (2017), pp. 4058–4065. DOI: 10.1109/TAC.2016.2616722.

[147] Franco Blanchini, Stefano Miani, and Carlo Savorgnan. "Stability results for linear parameter varying and switching systems". In: *Automatica* 43.10 (2007), pp. 1817–1823. ISSN: 0005-1098. DOI: https://doi.org/10.1016/j.automatica.2007.03.002.

[148] D. Liberzon. *Switching in systems and control*. Springer Science & Business Media, 2003.

[149] Shen Qu, Tianyi He, and Guoming G. Zhu. "LPV Modeling and Switched Control for EGR Valves with Dry Friction". In: *2019 IEEE Conference on Control Technology and Applications (CCTA)*. 2019, pp. 400–405. DOI: 10.1109/CCTA.2019.8920403.

[150] Tianyi He et al. "Switching State-Feedback LPV control with uncertain scheduling parameters". In: *2017 American Control Conference (ACC)*. 2017, pp. 2381–2386. DOI: 10.23919/ACC.2017.7963309.

[151] Chengzhi Yuan and Fen Wu. "Robust switching output-feedback control of time-varying polytopic uncertain systems". In: *International Journal of Control* 89 (2016), pp. 2262 –2276.

[152] J. P. Hespanha and A. S. Morse. "Stability of switched systems with average dwell-time". In: *Proceedings of the 38th IEEE Conference on Decision and Control (Cat. No.99CH36304)*. Vol. 3. 1999, 2655–2660 vol.3. DOI: 10.1109/CDC.1999.831330.

[153] D. Liberzon and A. S. Morse. "Basic problems in stability and design of switched systems". In: *IEEE Control Systems Magazine* 19.5 (1999), pp. 59–70. ISSN: 1941-000X. DOI: 10.1109/37.793443.

[154] Sungyung Lim and Kam Chan. "Analysis of hybrid linear parameter-varying systems". In: *Proceedings of the 2003 American Control Conference, 2003.* Vol. 6. 2003, 4822–4827 vol.6. DOI: 10.1109/ACC.2003.1242486.

[155] Hui Ye, A. N. Michel, and Ling Hou. "Stability theory for hybrid dynamical systems". In: *IEEE Transactions on Automatic Control* 43.4 (1998), pp. 461–474. ISSN: 2334-3303. DOI: 10.1109/9.664149.

[156] H. Lin and P. J. Antsaklis. "Stability and Stabilizability of Switched Linear Systems: A Survey of Recent Results". In: *IEEE Transactions on Automatic Control* 54.2 (2009), pp. 308–322.

[157] Sungyung Lim. *Analysis and control of linear-parameter-varying systems*. stanford university, 1999.

[158] Peng Yan, Hitay Özbay, and Murat Şansal. "Dwell time optimization in switching control of parameter varying time delay systems". In: *2011 50th IEEE Conference on Decision and Control and European Control Conference*. 2011, pp. 4909–4914. DOI: 10.1109/CDC.2011.6160365.

[159] Lixian Zhang and Peng Shi. "$\mathcal{L}_2 - \mathcal{L}_\infty$ Model Reduction for Switched LPV Systems With Average Dwell Time". In: *IEEE Transactions on Automatic Control* 53.10 (2008), pp. 2443–2448. DOI: 10.1109/TAC.2008.2007860.

[160] Peng Yan, Hitay Özbay, and Murat Şansal. "A switching control approach to stabilization of parameter varying time delay systems". In: *Proceedings of the 48h IEEE Conference on Decision and Control (CDC) held jointly with 2009 28th Chinese Control Conference*. 2009, pp. 7222–7226. DOI: 10.1109/CDC.2009.5400527.

[161] Bixuan Huang et al. "Average Dwell Time Based Smooth Switching Linear Parameter-Varying Proportional-Integral-Derivative Control for an F-16 Aircraft". In: *IEEE Access* 9 (2021), pp. 30979–30992. DOI: 10.1109/ACCESS.2021.3059900.

[162] Ligang GONG et al. "Switching control of morphing aircraft based on Q-learning". In: *Chinese Journal of Aeronautics* 33.2 (2020), pp. 672–687. ISSN: 1000-9361. DOI: https://doi.org/10.1016/j.cja.2019.10.005.

[163] Liqi Wang, Hui Ye, and Xiaofei Yang. "Development of a switched polytopic LPV model for the aircraft performing high angle of attack maneuver". In: *2017 4th International Conference on Information, Cybernetics and Computational Social Systems (ICCSS)*. 2017, pp. 566–571. DOI: 10.1109/ICCSS.2017.8091479.

[164] Dong Yang and Jun Zhao. "Observer-based $\mathcal{H}_\infty$ resilient control for a class of switched LPV systems and its application". In: *International Journal of Systems Science* 47 (Nov. 2015), pp. 1–12. DOI: 10.1080/00207721.2015.1110640.

[165] Yong He et al. "Robust control of morphing aircraft based on switched polytopic system". In: *2015 IEEE International Conference on Cyber Technology in Automation, Control, and Intelligent Systems (CYBER)*. 2015, pp. 1645–1649. DOI: 10.1109/CYBER.2015.7288192.

[166] Qiugang Lu et al. "Reference tracking control of hypersonic vehicles using switched linear parameter-varying approach". In: *2013 10th IEEE International Conference on Control and Automation (ICCA)*. 2013, pp. 670–675. DOI: 10.1109/ICCA.2013.6565016.

[167] Jian Li and Guang-Hong Yang. "Fault detection for switched linear parameter-varying systems: An average dwell-time approach". In: *Control Theory & Applications, IET* 7 (May 2013), pp. 1120–1130. DOI: 10.1049/iet-cta.2012.0832.

[168] Qiugang Lu et al. "Control design for a hypersonic aircraft using a switched linear parameter-varying system approach". In: *Proceedings of the Institution of Mechanical Engineers, Part I: Journal of Systems and Control Engineering* 227 (Feb. 2012), pp. 85–95. DOI: 10.1177/0959651812455897.

[169] Xu He, Georgi M. Dimirovski, and Jun Zhao. "Control of switched LPV systems using common Lyapunov function method and an F-16 aircraft application". In: *2010 IEEE International Conference on Systems, Man and Cybernetics*. 2010, pp. 386–392. DOI: 10.1109/ICSMC.2010.5641742.

[170] Xu He, Jun Zhao, and Georgi M. Dimirovski. "A blending method control of switched LPV systems with slow-varying parameters and its application to an F-16 aircraft model". In: *Proceedings of the 30th Chinese Control Conference*. 2011, pp. 1765–1770.

[171] Bei Lu and Fen Wu. "Switching-based fault-tolerant control for an F-16 aircraft with thrust vectoring". In: *Proceedings of the 48h IEEE Conference on Decision and Control (CDC) held jointly with 2009 28th Chinese Control Conference*. 2009, pp. 8494–8499. DOI: 10.1109/CDC.2009.5400385.

[172] Ke Dong and Fen Wu. "Online Switching Control of LFT Parameter-Dependent Systems". In: *Journal of Dynamic Systems Measurement and Control* 131 (Mar. 2009). DOI: 10.1115/1.3023140.

[173] Bei Lu, Fen Wu, and SungWan Kim. "Switching LPV control of an F-16 aircraft via controller state reset". In: *IEEE Transactions on Control Systems Technology* 14.2 (2006), pp. 267–277.

[174] Zong Guangdeng et al. "Fault-tolerant Control of Switched LPV Systems: A Bumpless Transfer Approach". In: *IEEE/ASME Transactions on Mechatronics* (2021), pp. 1–1. DOI: 10.1109/TMECH.2021.3096375.

[175] Dong Yang, Guangdeng Zong, and Hamid Reza Karimi. "Refined Anti-disturbance Control of Switched LPV Systems With Application to Aero-Engine". In: *IEEE Transactions on Industrial Electronics* 67.4 (2020), pp. 3180–3190. DOI: 10.1109/TIE.2019.2912780.

[176] Rui Wang, Cheng Liu, and Yan Shi. "Optimal control of aero-engine systems based on a switched LPV model". In: *Asian Journal of Control* 23 (Mar. 2021). DOI: 10.1002/asjc.2526.

[177] Peng Li et al. "Dynamic Event-Triggered Finite-Time $\mathcal{H}_\infty$ Tracking Control of Switched LPV Aero-Engine Models". In: *IEEE Transactions on Circuits and Systems II: Express Briefs* (2021), pp. 1–1. DOI: 10.1109/TCSII.2021.3114676.

[178] Dong Yang and Jun Zhao. "$\mathcal{H}_\infty$ output tracking control for a class of switched LPV systems and its application to an aero-engine model". In: *International Journal of Robust and Nonlinear Control* 27 (Sept. 2016). DOI: 10.1002/rnc.3673.

[179] Kongwei Zhu and Jun Zhao. "Event triggered control for a switched LPV system with applications to aircraft engines". In: *IET Control Theory & Applications* 12 (Mar. 2018). DOI: 10.1049/iet-cta.2017.0895.

[180] Kongwei Zhu, Jun Zhao, and Georgi M. Dimirovski. "$\mathcal{H}_\infty$ Tracking Control for Switched LPV Systems With an Application to Aero-Engines". In: *IEEE/CAA Journal of Automatica Sinica* 5.3 (2018), pp. 699–705. DOI: 10.1109/JAS.2016.7510025.

[181] Kongwei Zhu et al. "$\mathcal{H}_\infty$ filtering for switched linear parameter-varying systems and its application to aero-engines". In: *Iet Control Theory and Applications* 10 (2016), pp. 2552–2558.

[182] Kongwei Zhu, Chao Chen, and Jun Zhao. "$\mathcal{L}_2$ gain analysis of actuator saturation for switched LPV systems and applications to aero-engines". In: *2016 35th Chinese Control Conference (CCC)*. 2016, pp. 102–106. DOI: 10.1109/ChiCC.2016.7553068.

[183] Zhu Kongwei, Zhao Jun, and M. Dimirovski Georgi. "State feedback control for switched LPV systems with actuator saturation and its application to aero-engines". In: *2015 34th Chinese Control Conference (CCC)*. 2015, pp. 2224–2228. DOI: 10.1109/ChiCC.2015.7259979.

[184] M. Postma and R. Nagamune. "Air-Fuel Ratio Control of Spark Ignition Engines Using a Switching LPV Controller". In: *IEEE Transactions on Control Systems Technology* 20.5 (2012), pp. 1175–1187.

[185] Lili Tang, Jinquan Huang, and Muxuan Pan. "Switching LPV Control with Double-Layer LPV Model for Aero-Engines". In: *International Journal of Turbo & Jet-Engines* 34.4 (2017), pp. 313–320. DOI: doi:10.1515/tjj-2016-0014.

[186] Weilai Jiang et al. "Gain-scheduled control for morphing aircraft via switching polytopic linear parameter-varying systems". In: *Aerospace Science and Technology* 107 (2020), p. 106242. ISSN: 1270-9638. DOI: https://doi.org/10.1016/j.ast.2020.106242.

[187] Huan Li et al. "Linear Parameter-Varying Model of an Electro-Hydraulic Variable Valve Actuator for Internal Combustion Engines". In: *Journal of Dynamic Systems Measurement and Control-transactions of The Asme* 140 (2018), p. 011005.

[188] Shen Qu, Tianyi He, and Guoming G. Zhu. "Engine EGR Valve Modeling and Switched LPV Control Considering Nonlinear Dry Friction". In: *IEEE/ASME Transactions on Mechatronics* 25.3 (2020), pp. 1668–1678. DOI: 10.1109/TMECH.2020.2982315.

[189] Liang Nie et al. "Finite-time switched LPV control of quadrotors with guaranteed performance". In: *Journal of the Franklin Institute* 358.14 (2021), pp. 7032–7054. ISSN: 0016-0032. DOI: https://doi.org/10.1016/j.jfranklin.2021.07.018.

[190] Liang Nie et al. "Switched linear parameter-varying tracking control for quadrotors with large attitude angles and time-varying inertia". In: *Optimal Control Applications & Methods* (2021).

[191] G Gagliardi et al. "A Fault Detection Filter Design Method for Hybrid Switched Linear Parameter Varying Systems". In: *(ACD) 8th European Workshop on Advanced Control and Diagnosis* (2010), p. 247.

[192] Mohammad Bagher Abolhasani Jabali and Mohammad Hosein Kazemi. "Uncertain polytopic LPV modelling of robot manipulators and trajectory tracking". In: *International Journal of Control, Automation and Systems* 15 (2017), pp. 883–891.

[193] Xu Zhang et al. "Switched LPV Modeling and $\mathcal{H}_2$ Control for Hybrid Suspension with Mass Variation". In: *2020 Chinese Automation Congress (CAC)*. 2020, pp. 7644–7649. DOI: 10.1109/CAC51589.2020.9327563.

[194] M.Q. Nguyen, O. Sename, and L. Dugard. "A switched LPV observer for actuator fault estimation". In: *IFAC-PapersOnLine* 48.26 (2015). 1st IFAC Workshop on Linear Parameter Varying Systems LPVS 2015, pp. 194–199. ISSN: 2405-8963. DOI: https://doi.org/10.1016/j.ifacol.2015.11.136.

[195] He Xu et al. "Fault tolerant control with switched LPV method based on hysteresis strategy and an application to a microsatellite model". In: *2015 34th Chinese Control Conference (CCC)*. 2015, pp. 6153–6158. DOI: 10.1109/ChiCC.2015.7260604.

[196] Xu He et al. "Switching control for LPV polytopic systems using multiple Lyapunov functions". In: *Proceedings of the 30th Chinese Control Conference*. 2011, pp. 1771–1776.

[197] Bei Lu and Fen Wu. "Control design of switched LPV systems using multiple parameter-dependent Lyapunov functions". In: *Proceedings of the 2004 American Control Conference*. Vol. 4. 2004, 3875–3880 vol.4. DOI: 10.23919/ACC.2004.1384517.

[198] Xiangming Xue, Yiming Bu, and Bei Lu. "Hysteresis Switching LPV Control of a Wind Turbine System Covering Partial and Full Load Conditions". In: *ASME International Mechanical Engineering Congress and Exposition*. Vol. 57397. American Society of Mechanical Engineers. 2015, V04AT04A005.

[199] Fabien Lescher, Jing Yun Zhao, and Pierre Borne. "Switching LPV Controllers for a Variable Speed Pitch Regulated Wind Turbine". In: *The Proceedings of the Multiconference on "Computational Engineering in Systems Applications"*. Vol. 2. 2006, pp. 1334–1340. DOI: 10.1109/CESA.2006.4281844.

[200] Ehsan Azadi Yazdi et al. "Automated Multiple Robust Track-Following Control System Design in Hard Disk Drives". In: *IEEE Transactions on Control Systems Technology* 19.4 (2011), pp. 920–928. DOI: 10.1109/TCST.2010.2053541.

[201] Masih Hanifzadegan and Ryozo Nagamune. "Switching Gain-Scheduled Control Design for Flexible Ball-Screw Drives". In: *Journal of Dynamic Systems, Measurement, and Control* 136 (Jan. 2014), p. 014503. DOI: 10.1115/1.4025154.

[202] Lixian Zhang, Changhong Wang, and Lingjie Chen. "Stability and Stabilization of a Class of Multimode Linear Discrete-Time Systems With Polytopic Uncertainties". In: *IEEE Transactions on Industrial Electronics* 56.9 (2009), pp. 3684–3692. DOI: 10.1109/TIE.2009.2026375.

[203] Ehsan Azadi Yazdi and Ryozo Nagamune. "A parameter set division and switching gain-scheduling controllers design method for time-varying plants". In: *Systems & Control Letters* 60.12 (2011), pp. 1016–1023. ISSN: 0167-6911. DOI: https://doi.org/10.1016/j.sysconle.2011.09.004.

[204] P. H. Colmegna, F. D. Bianchi, and R. S. Sánchez-Peña. "Automatic Glucose Control During Meals and Exercise in Type 1 Diabetes: Proof-of-Concept in Silico Tests Using a Switched LPV Approach". In: *IEEE Control Systems Letters* 5.5 (2021), pp. 1489–1494. DOI: 10.1109/LCSYS.2020.3041211.

[205] Patricio H Colmegna et al. "Reducing glucose variability due to meals and postprandial exercise in T1DM using switched LPV control: In silico studies". In: *Journal of diabetes science and technology* 10.3 (2016), pp. 744–753.

[206] P. H. Colmegna et al. "Switched LPV Glucose Control in Type 1 Diabetes". In: *IEEE Transactions on Biomedical Engineering* 63.6 (2016), pp. 1192–1200.

[207] Grace Deaecto and José Geromel. "$\mathcal{H}_\infty$ state feedback switched control for discrete time-varying polytopic systems". In: *International Journal of Control* 86 (Apr. 2013). DOI: 10.1080/00207179.2012.750761.

[208] Masih Hanifzadegan and R. Nagamune. "Smooth switching LPV controller design for LPV systems". In: *Automatica* 50 (2014), pp. 1481–1488.

[209] Tianyi He. "Smooth Switching LPV Control and Its Applications". PhD thesis. Michigan State University, 2019.

[210] Tianyi He et al. "Simultaneous Design of Smooth Switching State-Feedback LPV Control". In: *Annual American Control Conference (ACC)*. 2018, pp. 3368–3373. DOI: 10.23919/ACC.2018.8431311.

[211] Tianyi He et al. "Smooth-switching LPV control for vibration suppression of a flexible airplane wing". In: *Aerospace Science and Technology* 84 (2019), pp. 895–903. ISSN: 1270-9638. DOI: https://doi.org/10.1016/j.ast.2018.11.029.

[212] Tianyi He, Guoming G. Zhu, and Sean Shan-Min Swei. "Sequential Design of Switching <tex>$\mathscr{H}_\infty$</tex> LPV State-Feedback Control". In: *2019 American Control Conference (ACC)*. 2019, pp. 4547–4552. DOI: 10.23919/ACC.2019.8815262.

[213] Tianyi He, Guoming Zhu, and Sean Swei. "A Sequential Design Approach for Switching $\mathcal{H}_\infty$ LPV Control". In: *International Journal of Control, Automation and Systems* 19 (Sept. 2021). DOI: 10.1007/s12555-020-0363-3.

[214] Tianyi He, Guoming Zhu, and Sean Swei. "Smooth Switching LPV Dynamic Output-feedback Control". In: *International Journal of Control, Automation and Systems* 18 (Dec. 2019), 1367–1377. DOI: 10.1007/s12555-019-0088-3.

[215] Tianyi He et al. "Active Vibration Suppression of BWB Airplane Using Smooth Switching LPV Control". In: *AIAA Scitech 2019 Forum* (2019).

[216] Weilai Jiang, Chaoyang Dong, and Qing Wang. "A systematic method of smooth switching LPV controllers design for a morphing aircraft". In: *Chinese Journal of Aeronautics* 28.6 (2015), pp. 1640–1649. ISSN: 1000-9361. DOI: https://doi.org/10.1016/j.cja.2015.10.005.

[217] Gaohua Cai et al. "Smooth control for a class of linear time-varying systems with input quantization and input saturation". In: *2016 35th Chinese Control Conference (CCC)*. 2016, pp. 10567–10572. DOI: 10.1109/ChiCC.2016.7555032.

[218] Haoyu Cheng et al. "Smooth switching linear parameter-varying fault detection filter design for morphing aircraft with asynchronous switching". In: *Transactions of the Institute of Measurement and Control* 40.8 (2018), pp. 2622–2638. DOI: 10.1177/0142331217708238. eprint: https://doi.org/10.1177/0142331217708238.

[219] Bixuan Huang et al. "Average Dwell Time Based Smooth Switching Linear Parameter-Varying Proportional-Integral-Derivative Control for an F-16 Aircraft". In: *IEEE Access* 9 (2021), pp. 30979–30992. DOI: 10.1109/ACCESS.2021.3059900.

[220] Zou Yiru, Liu Chunsheng, and Lu Ke. "Extended state observer based smooth switching control for tilt-rotor aircraft". In: *Journal of Systems Engineering and Electronics* 31.4 (2020), pp. 815–825. DOI: 10.23919/JSEE.2020.000025.

[221] Lei Song and Jianying Yang. "Smooth Switching Output Tracking Control for LPV Systems". In: *Asian Journal of Control* 14 (2012), pp. 1710–1716.

[222] Weilai Jiang, Chaoyang Dong, and Qing Wang. "Smooth switching linear parameter-varying control for hypersonic vehicles via a parameter set automatic partition method". In: *IET Control Theory & Applications* 9.16 (2015), pp. 2377–2386.

[223] Pan Zhao and Ryozo Nagamune. "Optimal switching surface design for switching LPV control and its application to air-fuel ratio control of an automotive engine". In: *2017 IEEE Conference on Control Technology and Applications (CCTA)*. 2017, pp. 898–903. DOI: 10.1109/CCTA.2017.8062573.

[224] Xiaofeng Liu and Siqi An. "Smooth Switching Controller Design for Multiobjective Control Systems and Applications". In: *Journal of Aerospace Engineering* 29 (Jan. 2016), p. 04016004. DOI: 10.1061/(ASCE)AS.1943-5525.0000596.

[225] Jingyi Zhao et al. "A Control Design of Rotor Speed Regulation for an Aeroengine based on Smooth Switching Strategy". In: *IFAC-PapersOnLine* 54.10 (2021). 6th IFAC Conference on Engine Powertrain Control, Simulation and Modeling E-COSM 2021, pp. 324–329. ISSN: 2405-8963. DOI: https://doi.org/10.1016/j.ifacol.2021.10.183.

[226] Pang-Chia Chen et al. "Smooth switching gain-scheduled control for large scale offshore wind turbine under full wind-speed conditions". In: *2016 International Conference on System Science and Engineering (ICSSE)*. 2016, pp. 1–4. DOI: 10.1109/ICSSE.2016.7551604.

[227] Lei Song and Jianying Yang. "Smooth switching output tracking control for a class of linear time-varying systems: An LMI approach". In: *Proceedings of the 29th Chinese Control Conference*. 2010, pp. 1977–1982.

[228] Masih Hanifzadegan and Ryozo Nagamune. "Smooth switching LPV controller design for LPV systems". In: *Autom.* 50 (2014), pp. 1481–1488.

[229] Pang-Chia Chen, Sun-Li Wu, and Hung-Shiang Chuang. "The smooth switching control for TORA system via LMIs". In: *IEEE ICCA 2010*. 2010, pp. 1338–1343. DOI: 10.1109/ICCA.2010.5524116.

[230] Pang-Chia Chen et al. "The smooth switching gain-scheduled control with $\mathcal{H}_\infty$ performance to the application of TORA systems". In: *International Journal of Modelling, Identification and Control* 22 (Oct. 2014), p. 261. DOI: 10.1504/IJMIC.2014.065344.

[231] Christopher Edwards and Ian Postlethwaite. "Anti-windup and bumpless-transfer schemes". In: *Automatica* 34.2 (1998), pp. 199–210.

[232] Mayuresh V. Kothare et al. "A unified framework for the study of anti-windup designs". In: *Automatica* 30.12 (1994), pp. 1869–1883. ISSN: 0005-1098. DOI: https://doi.org/10.1016/0005-1098(94)90048-5.

[233] William S Levine. *The Control Handbook (three volume set)*. CRC press, 2018.

[234] Christopher Edwards and Ian Postlethwaite. "Anti-windup and bumpless-transfer schemes". In: *Automatica* 34.2 (1998), pp. 199–210.

[235] R. Hanus, M. Kinnaert, and J.-L. Henrotte. "Conditioning technique, a general anti-windup and bumpless transfer method". In: *Automatica* 23.6 (1987), pp. 729–739. ISSN: 0005-1098. DOI: https://doi.org/10.1016/0005-1098(87)90029-X.

[236] M.C. Turner and D.J. Walker. "Modified linear quadratic bumpless transfer". In: *Proceedings of the 1999 American Control Conference (Cat. No. 99CH36251)*. Vol. 4. 1999, 2285–2289 vol.4. DOI: 10.1109/ACC.1999.786421.

[237] Matthew C Turner and Daniel J Walker. "Linear quadratic bumpless transfer". In: *Automatica* 36.8 (2000), pp. 1089–1101.

[238] Jan Dimon, Bendtsen Jakob, and Klaus Trangbaek. "Bumpless Transfer Between Observer-Based Gain Scheduled Controllers". In: *International Journal of Control* 78 (Jan. 2005). DOI: 10.1080/00207170500111028.

[239] Michel Kinnaert, Thomas Delwiche, and Joseph Yamé. "State resetting for bumpless switching in supervisory control". In: *2009 European Control Conference (ECC)*. 2009, pp. 2097–2102. DOI: 10.23919/ECC.2009.7074714.

[240] F. R. P. Safaei, J. Hespanha, and Gregory Stewart. "On controller initialization in multivariable switching systems". In: *Automatica* 48 (2012), pp. 3157–3165.

[241] Fatemeh Khani and Mohammad Haeri. "Smooth switching in a scheduled robust model predictive controller". In: *Journal of Process Control* 31 (2015), pp. 55–63. ISSN: 0959-1524. DOI: https://doi.org/10.1016/j.jprocont.2015.04.003.

[242] Ivan Malloci. "Sur les systèmes à commutation à deux échelles de temps: une application au contrôle de guidage de bande dans un laminoir à chaud". PhD thesis. Institut National Polytechnique de Lorraine, 2009.

[243] Kai Zheng et al. "Steady-state bumpless transfer under controller uncertainty using the state/output feedback topology". In: *IEEE Transactions on Control Systems Technology* 14.1 (2005), pp. 3–17.

[244] Kai Zheng and Joseph Bentsman. "Input/output structure of the infinite horizon LQ bumpless transfer and its implications for transfer operator synthesis". In: *International Journal of Robust and Nonlinear Control: IFAC-Affiliated Journal* 20.8 (2010), pp. 923–938.

[245] Guoxin Li et al. "Dynamic transfer of robust AMB controllers". In: *Proceedings of the Eighth International Symposium on Magnetic Bearings*. 2002, pp. 471–476.

[246] M Turner et al. "Switched control of a vehicle/short take-off land aircraft: An application of linear quadratic bumpless transfer". In: *Proceedings of The Institution of Mechanical Engineers Part I-journal of Systems and Control Engineering - PROC INST MECH ENG I-J SYST C* 220 (May 2006), pp. 157–170. DOI: 10.1243/09596518JSCE121.

[247] Ke Dong and Fen Wu. "Online Switching Control Designs of LFT Systems". In: *Proceedings of the 45th IEEE Conference on Decision and Control*. 2006, pp. 4075–4080. DOI: 10.1109/CDC.2006.376986.

[248] Ke Dong. *Advanced design techniques in linear parameter varying control*. North Carolina State University, 2006.

[249] Xiaofeng Liu et al. "Design for aircraft engine multi-objective controllers with switching characteristics". In: *Chinese Journal of Aeronautics* 27.5 (2014), pp. 1097–1110. ISSN: 1000-9361. DOI: https://doi.org/10.1016/j.cja.2014.08.002.

[250] Dong Yang and Jun Zhao. "$\mathcal{H}_\infty$ bumpless transfer for switched LPV systems and its application". In: *International Journal of Control* 92.8 (2019), pp. 1945–1958.

[251] Zong Guangdeng et al. "Fault-tolerant Control of Switched LPV Systems: A Bumpless Transfer Approach". In: *IEEE/ASME Transactions on Mechatronics* (2021), pp. 1–1. DOI: 10.1109/TMECH.2021.3096375.

[252] Dong Yang et al. "Bumpless Transfer $\mathcal{H}_\infty$ Anti-Disturbance Control of Switching Markovian LPV Systems Under the Hybrid Switching". In: *IEEE Transactions on Cybernetics* (2020), pp. 1–13. DOI: 10.1109/TCYB.2020.3024988.

[253] Ying Zhao et al. "Rate Bumpless Transfer Control for Switched Linear Systems With Stability and Its Application to Aero-Engine Control Design". In: *IEEE Transactions on Industrial Electronics* 67.6 (2020), pp. 4900–4910. DOI: 10.1109/TIE.2019.2931222.

[254] Yan Shi and Xi-Ming Sun. "Bumpless Transfer Control for Switched Linear Systems and its Application to Aero-Engines". In: *IEEE Transactions on Circuits and Systems I: Regular Papers* 68.5 (2021), pp. 2171–2182. DOI: 10.1109/TCSI.2021.3060745.

[255] Dong Yang, Guangdeng Zong, and Sing Nguang. "$\mathcal{H}_\infty$ bumpless transfer reliable control of Markovian switching LPV systems subject to actuator failures". In: *Information Sciences* 512 (July 2019). DOI: 10.1016/j.ins.2019.07.059.

[256] Penghui Sun et al. "Bumpless Transfer of Uncertain Switched System and Its Application to Turbofan Engines". In: *Energies* 14.16 (2021). ISSN: 1996-1073. DOI: 10.3390/en14165204.

[257] Raja M. Imran, D. M. Akbar Hussain, and Bhawani Shanker Chowdhry. "Parameterized Disturbance Observer Based Controller to Reduce Cyclic Loads of Wind Turbine". In: *Energies* 11.5 (2018). ISSN: 1996-1073. DOI: 10.3390/en11051296.

[258] Reza Yavari, Saeed Shamaghdari, and Arash Sadeghzadeh. "Robust H2 output-feedback bumpless transfer control of polytopic uncertain LPV systems". In: *European Journal of Control* 63 (2022), pp. 277–289. ISSN: 0947-3580. DOI: https://doi.org/10.1016/j.ejcon.2021.11.006.

[259] Guangdeng Zong, Chunxiao Huang, and Dong Yang. "Bumpless transfer fault detection for switched systems: a state-dependent switching approach". In: *Science China Information Sciences* 64.7 (2021), pp. 1–15.

[260] Xiaoqi Song and James Lam. "Bumpless $\mathcal{H}_\infty$ control for periodic piecewise linear systems". In: *Automatica* 135 (2022), p. 109941. ISSN: 0005-1098. DOI: https://doi.org/10.1016/j.automatica.2021.109941.

[261] Joseph Yame and Michel Kinnaert. "Parameterization of Linear Controllers for Bumpless Switching in Multi-Controller Schemes". In: 3 (Aug. 2004). DOI: 10.2514/6.2004-5108.

[262] Ying Zhao, Shuanghe Yu, and Jie Lian. "Anti-Disturbance Bumpless Transfer Control for Switched Systems With its Application to Switched Circuit Model". In: *IEEE Transactions on Circuits and Systems II: Express Briefs* 67.12 (2020), pp. 3177–3181. DOI: 10.1109/TCSII.2020.2970068.

[263] Joel Steenis, Kostas Tsakalis, and Raja Ayyanar. "An Approach to Bumpless Control for LPV Modeled Inverters in a Microgrid". In: *IEEE Transactions on Power Electronics* 29.11 (2014), pp. 6214–6223. DOI: 10.1109/TPEL.2014.2300820.

[264] Weilin Wu et al. "Design of Smooth Switching LPV Controller Based on Coprime Factorization and $\mathcal{H}_\infty$ Performance Realization". In: *IEEE Access* 9 (2021), pp. 117860–117867. DOI: 10.1109/ACCESS.2021.3102733.

[265] D. Youla, J. Bongiorno, and H. Jabr. "Modern Wiener–Hopf design of optimal controllers Part I: The single-input-output case". In: *IEEE Transactions on Automatic Control* 21.1 (1976), pp. 3–13. DOI: 10.1109/TAC.1976.1101139.

[266] D. Youla, H. Jabr, and J. Bongiorno. "Modern Wiener-Hopf design of optimal controllers–Part II: The multivariable case". In: *IEEE Transactions on Automatic Control* 21.3 (1976), pp. 319–338. DOI: 10.1109/TAC.1976.1101223.

[267] Vladimir Kucera. "Stability of Discrete Linear Feedback Systems". In: *IFAC Proceedings Volumes* 8 (1975), pp. 573–578.

[268] H. Niemann. "Dual Youla parameterisation". In: *IEE Proceedings - Control Theory and Applications* 150.5 (2003), pp. 493–. ISSN: 1350-2379. DOI: 10.1049/ip-cta:20030685.

[269] T. Tay, J. Moore, and I. Mareels. *High performance control*. Springer Science & Business Media, 1997.

[270] Jan Bendtsen and Klaus Trangbaek. "Multiple model adaptive control using dual youla-kucera factorisation". In: *IFAC Proceedings Volumes* 45.13 (2012), pp. 63–68.

[271] C. Desoer et al. "Feedback system design: The fractional representation approach to analysis and synthesis". In: *IEEE Transactions on Automatic Control* 25.3 (1980), pp. 399–412. ISSN: 2334-3303. DOI: 10.1109/TAC.1980.1102374.

[272] M. Vidyasagar. "Control system synthesis: a factorization approach, part II". In: *Synthesis lectures on control and mechatronics* 2.1 (2011), pp. 1–227.

[273] Luca Zaccarian and Andrew R. Teel. "The $\mathcal{L}_2$ bumpless transfer problem for linear plants: Its definition and solution". In: *Automatica* 41.7 (2005), pp. 1273–1280. ISSN: 0005-1098. DOI: https://doi.org/10.1016/j.automatica.2005.02.003.

[274] J. Hespanha and A. S. Morse. "Switching between stabilizing controllers". In: *Automatica* 38.11 (2002), pp. 1905–1917.

[275] J. Stoustrup and H. Niemann. "Starting up unstable multivariable controllers safely". In: *Proceedings of the 36th IEEE Conference on Decision and Control*. Vol. 2. 1997, 1437–1438 vol.2.

[276] J. Stoustrup. "Plug& play control: Control technology towards new challenges". In: *European Journal of Control* (2009), pp. 311–330.

[277] J.B. Moore, Lige Xia, and K. Glover. "On improving control-loop robustness of model-matching controllers". In: *Systems & Control Letters* 7.2 (1986), pp. 83–87. ISSN: 0167-6911. DOI: https://doi.org/10.1016/0167-6911(86)90012-5.

[278] I. Mahtout et al. "Advances in Youla-Kucera parametrization: A Review". In: *Annual Reviews in Control* (2020). DOI: 10.1016/j.arcontrol.2020.04.015.

[279] J. Hespanha and A. S. Morse. "Towards the High Performance Control of Uncertain Processes via Supervision". In: *In Proc. of the 30th Annual Conf. on Information Sciences and Syst*. 1996, pp. 405–410.

[280] O. Cifdaloz, A. A. Rodriguez, and J. M. Anderies. "Control of distributed parameter systems subject to convex constraints: Applications to irrigation systems and Hypersonic Vehicles". In: *2008 47th IEEE Conference on Decision and Control*. 2008, pp. 865–870.

[281] Klaus Trangbaek, Jakob Stoustrup, and Jan Dimon Bendtsen. "Stable controller reconfiguration through terminal connections". In: *IFAC Proceedings Volumes* 41 (2008), pp. 331–335.

[282] Klaus Trangbaek and Jan Bendtsen. "Stable controller reconfiguration through terminal connections — A practical example". In: *2009 IEEE International Conference on Control and Automation*. 2009, pp. 2037–2042. DOI: 10.1109/ICCA.2009.5410408.

[283] Simon Vestergaard Johansen et al. "Stepwise commissioning of a steam boiler with stability guarantees". In: *2016 European Control Conference (ECC)*. 2016, pp. 49–54. DOI: 10.1109/ECC.2016.7810262.

[284] I. Landau. "On the use of Youla-Kucera parametrization in adaptive active noise and vibration control-A review". In: *International Journal of Control* (Nov. 2018), pp. 1–25. DOI: 10.1080/00207179.2018.1548773.

[285] Xu Chen, Tianyu Jiang, and Masayoshi Tomizuka. "Pseudo Youla–Kucera parameterization with control of the waterbed effect for local loop shaping". In: *Automatica* 62 (2015), pp. 177–183. ISSN: 0005-1098. DOI: https://doi.org/10.1016/j.automatica.2015.09.029.

[286] John J. Martinez and Marouane Alma. "Improving playability of Blu-ray disc drives by using adaptive suppression of repetitive disturbances". In: *Automatica* 48.4 (2012), pp. 638–644. ISSN: 0005-1098. DOI: https://doi.org/10.1016/j.automatica.2012.01.016.

[287] Xu Chen and Masayoshi Tomizuka. "New Repetitive Control With Improved Steady-State Performance and Accelerated Transient". In: *IEEE Transactions on Control Systems Technology* 22.2 (2014), pp. 664–675. DOI: 10.1109/TCST.2013.2253102.

[288] Zhizheng Wu et al. "Youla parameterized adaptive vibration suppression with adaptive notch filter for unknown multiple narrow band disturbances". In: *Journal of Vibration and Control* 25.3 (2019), pp. 685–694. DOI: 10.1177/1077546318794539. eprint: https://doi.org/10.1177/1077546318794539.

[289] Masayoshi Tomizuka. "Dealing with periodic disturbances in controls of mechanical systems". In: *Annual Reviews in Control* 32.2 (2008), pp. 193–199. ISSN: 1367-5788. DOI: https://doi.org/10.1016/j.arcontrol.2008.07.002.

[290] M. Doumiati et al. "Road profile estimation using an adaptive Youla–Kučera parametric observer: Comparison to real profilers". In: *Control Engineering Practice* 61 (2017), pp. 270–278. ISSN: 0967-0661. DOI: https://doi.org/10.1016/j.conengprac.2015.12.020.

[291] Ioan Doré Landau, Aurelian Constantinescu, and Daniel Rey. "Adaptive narrow band disturbance rejection applied to an active suspension—an internal model principle approach". In: *Automatica* 41.4 (2005), pp. 563–574. ISSN: 0005-1098. DOI: https://doi.org/10.1016/j.automatica.2004.08.022.

[292] Sergio Valentinotti et al. "Optimal Operation of Fed-Batch Fermentations via Adaptive Control of Overflow Metabolite". In: *Control Engineering Practice* 11 (2003), pp. 665–674.

[293] I. Mahtout et al. "Youla-Kucera Based Lateral Controller for Autonomous Vehicle". In: *2018 21st International Conference on Intelligent Transportation Systems (ITSC)*. 2018, pp. 3281–3286. DOI: 10.1109/ITSC.2018.8569779.

[294] F. Navas, V. Milanés, and F. Nashashibi. "Using Plug & Play control for stable ACC-CACC system transitions". In: *2016 IEEE Intelligent Vehicles Symposium (IV)*. 2016, pp. 704–709. DOI: 10.1109/IVS.2016.7535464.

[295] Francisco Navas and Vicente Milanés. "Mixing V2V- and non-V2V-equipped vehicles in car following". In: *Transportation Research Part C: Emerging Technologies* (2019).

[296] W. Xie and T. Eisaka. "Design of LPV control systems based on Youla parameterisation". In: *IEE Proceedings - Control Theory and Applications* 151.4 (2004), pp. 465–472. ISSN: 1350-2379. DOI: 10.1049/ip-cta:20040513.

[297] F. Bianchi and R.S. Peña. "Interpolation for gain-scheduled control with guarantees". In: *Automatica* 47.1 (2011), pp. 239–243.

[298] B. Rasmussen and Y. Chang. "Stable Controller Interpolation and Controller Switching for LPV Systems". In: *Journal of Dynamic Systems Measurement and Control-transactions of The Asme - J DYN SYST MEAS CONTR* 132 (Jan. 2010). DOI: 10.1115/1.4000075.

[299] F. Blanchini et al. "Stable LPV Realization of Parametric Transfer Functions and Its Application to Gain-Scheduling Control Design". In: *IEEE Transactions on Automatic Control* 55.10 (2010), pp. 2271–2281. ISSN: 2334-3303. DOI: 10.1109/TAC.2010.2044259.

[300] Hussam Atoui et al. "Interpolation of multi-LPV control systems based on Youla–Kucera parameterization". In: *Automatica* 134 (2021), p. 109963. ISSN: 0005-1098. DOI: https://doi.org/10.1016/j.automatica.2021.109963.

[301] Anamaria Luca, Pedro Rodriguez-Ayerbe, and Didier Dumur. "Control of disturbed LPV systems in a LMI setting". In: *IFAC Proceedings Volumes* 44.1 (2011), pp. 4149–4154.

[302] Jasper Witte, H. M. N. K. Balini, and Carsten W. Scherer. "Experimental results with stable and unstable LPV controllers for active magnetic bearing systems". In: *2010 IEEE International Conference on Control Applications*. 2010, pp. 950–955. DOI: 10.1109/CCA.2010.5611087.

[303] H. M. N. K. Balini, Carsten W. Scherer, and Jasper Witte. "Performance Enhancement for AMB Systems Using Unstable $\mathcal{H}_\infty$ Controllers". In: *IEEE Transactions on Control Systems Technology* 19.6 (2011), pp. 1479–1492. DOI: 10.1109/TCST.2010.2097264.

[304] Fernando Daniel Bianchi and Ricardo Salvador Sánchez Peña. "A novel design approach for switched LPV controllers". In: *International Journal of Control* 83 (2010), pp. 1710 –1717.

[305] H.M.N.K. Balini, Jasper Witte, and Carsten W. Scherer. "Synthesis and implementation of gain-scheduling and LPV controllers for an AMB system". In: *Automatica* 48.3 (2012), pp. 521–527. ISSN: 0005-1098. DOI: https://doi.org/10.1016/j.automatica.2011.08.061.

[306] Weilin Wu et al. "Switching Controller Parameterization Realization for an LPV Plant with $\mathcal{H}_\infty$ Performance". In: *2018 37th Chinese Control Conference (CCC)*. 2018, pp. 2571–2576. DOI: 10.23919/ChiCC.2018.8483715.

[307] Weilin Wu, Wei Xie, and Liejun Li. "Switching Linear Parameter-Varying Controller Design With $\mathcal{H}_\infty$ Performance Based on Youla Parameterization". In: *IEEE Access* 8 (2020), pp. 184765–184773. DOI: 10.1109/ACCESS.2020.3029589.

[308] Fen Wu and Xuejing Cai. "Switching fault-tolerant control of a flexible air-breathing hypersonic vehicle". In: *Proceedings of the Institution of Mechanical Engineers, Part I: Journal of Systems and Control Engineering* 227 (Feb. 2012), pp. 24–38. DOI: 10.1177/0959651812453914.

[309] Alexander Schirrer, Martin Kozek, and Stefan Jakubek. "Convex Design for Lateral Control of a Blended Wing Body Aircraft". In: *Mechanics and Model-Based Control of Advanced Engineering Systems*. Springer, 2014, pp. 255–264.

[310] Tong Wang et al. "Adaptive Damping Control Scheme for Wind Grid-Connected Power Systems with Virtual Inertia Control". In: *IEEE Transactions on Power Systems* (2022), pp. 1–1. DOI: 10.1109/TPWRS.2021.3140086.

[311] Lukas R. S. Theisen, Juan F. Camino, and Hans H. Niemann. "An application of gain-scheduled control using state-space interpolation to hydroactive gas bearings". In: *2016 IEEE Conference on Control Applications (CCA)*. 2016, pp. 1117–1122. DOI: 10.1109/CCA.2016.7587956.

[312] Jing Ma et al. "Application of Dual Youla Parameterization Based Adaptive Wide-Area Damping Control for Power System Oscillations". In: *IEEE Transactions on Power Systems* 29.4 (2014), pp. 1602–1610. DOI: 10.1109/TPWRS.2013.2296940.

[313] Klaus Trangbaek. "Safe lpv controller switching". In: *2011 50th IEEE Conference on Decision and Control and European Control Conference*. IEEE. 2011, pp. 3428–3433.

[314] Xuejing Cai and Fen Wu. "Switching fault-tolerant control by Youla parametrization". In: *Proceedings of the 29th Chinese Control Conference*. 2010, pp. 4099–4104.

[315] Anamaria Luca. "Control of disturbed LPV systems in a LMI setting". In: vol. 44. Aug. 2011, pp. 4149–4154. ISBN: 9783902661937. DOI: 10.3182/20110828-6-IT-1002.02127.

[316] Franco Blanchini et al. "On the LPV control design and its applications to some classes of dynamical systems". In: *Lecture Notes in Control and Information Sciences* 464 (2015), pp. 319–338.

[317] Stefan R. Friedrich and Martin Buss. "A Simple Architecture for Arbitrary Interpolation of State Feedback". In: *IEEE Control Systems Letters* 3.2 (2019), pp. 469–474. DOI: 10.1109/LCSYS.2019.2899532.

[318] Vicente Milanés et al. "The Tornado Project: An Automated Driving Demonstration in Peri-Urban and Rural Areas". In: *IEEE Intelligent Transportation Systems Magazine* (2021).

[319] Jorge Beltrán et al. "Towards autonomous driving: a multi-modal 360° perception proposal". In: *2020 IEEE 23rd International Conference on Intelligent Transportation Systems (ITSC)*. IEEE. 2020, pp. 1–6.

[320] Charles R. Qi et al. "Frustum PointNets for 3D Object Detection from RGB-D Data". In: *2018 IEEE/CVF Conference on Computer Vision and Pattern Recognition*. 2018, pp. 918–927. DOI: 10.1109/CVPR.2018.00102.

[321] E.A. Wan and R. Van Der Merwe. "The unscented Kalman filter for nonlinear estimation". In: *Proceedings of the IEEE 2000 Adaptive Systems for Signal Processing, Communications, and Control Symposium (Cat. No.00EX373)*. 2000, pp. 153–158. DOI: 10.1109/ASSPCC.2000.882463.

[322] A. Piazzi et al. "Quintic G^2-splines for the iterative steering of vision-based autonomous vehicles". In: *IEEE Transactions on Intelligent Transportation Systems* 3.1 (2002), pp. 27–36. DOI: 10.1109/6979.994793.

[323] Brian Paden et al. "A survey of motion planning and control techniques for self-driving urban vehicles". In: *IEEE Transactions on intelligent vehicles* 1.1 (2016), pp. 33–55.

[324] Oscar Martí Rubio. "LPV Control of an Autonomous Vehicle". MA thesis. Barcelona School of Industrial Engineering, 2016.

[325] J Christian Gerdes and Eric J Rossetter. "A unified approach to driver assistance systems based on artificial potential fields". In: *Journal of Dynamic Systems, Measurement, and Control* 123.3 (2001), pp. 431–438.

[326] Mattias Brannstrom, Erik Coelingh, and Jonas Sjoberg. "Model-based threat assessment for avoiding arbitrary vehicle collisions". In: *IEEE Transactions on Intelligent Transportation Systems* 11.3 (2010), pp. 658–669.

[327] Ardalan Vahidi and Azim Eskandarian. "Research advances in intelligent collision avoidance and adaptive cruise control". In: *IEEE transactions on intelligent transportation systems* 4.3 (2003), pp. 143–153.

[328] Francisco Navas. "Stability analysis for controller switching in autonomous vehicles". PhD thesis. Sciences Des Metiers De L'Ingenieur (SMI), 2018.

[329] Eugenio Alcala et al. "Autonomous Racing using Linear Parameter Varying - Model Predictive Control (LPV-MPC)". In: *Control Engineering Practice (under review)* 14.8 (2019).

[330] Van-Tan Vu et al. "$\mathcal{H}_\infty$ active anti-roll bar control to prevent rollover of heavy vehicles: a robustness analysis". In: *IFAC-PapersOnLine* 49.9 (2016), pp. 99–104.

[331] Jeff Wit, Carl D Crane III, and David Armstrong. "Autonomous ground vehicle path tracking". In: *Journal of Robotic Systems* 21.8 (2004), pp. 439–449.

[332] Carsten Scherer. "Theory of robust control". In: *Delft University of Technology* (2001), pp. 1–160.

[333] Jeroen Ploeg et al. "Controller Synthesis for String Stability of Vehicle Platoons". In: *IEEE Transactions on Intelligent Transportation Systems* 15 (2014), pp. 854–865.

[334] Balázs Németh, Zsuzsanna Bede, and Péter Gáspár. "Control design of traffic flow using look-ahead vehicles to increase energy efficiency". In: *2017 American Control Conference (ACC)*. 2017, pp. 3530–3535. DOI: 10.23919/ACC.2017.7963493.

[335] András Mihály, Balázs Németh, and Péter Gáspár. "Look-ahead control of road vehicles for safety and economy purposes". In: *2014 European Control Conference (ECC)*. 2014, pp. 714–719. DOI: 10.1109/ECC.2014.6862209.

[336] Lingyun Xiao and Feng Gao. "A comprehensive review of the development of adaptive cruise control systems". In: *Vehicle System Dynamics* 48.10 (2010), pp. 1167–1192. DOI: 10.1080/00423110903365910. eprint: https://doi.org/10.1080/00423110903365910. URL: https://doi.org/10.1080/00423110903365910.

[337] Shengbo Li et al. "Model Predictive Multi-Objective Vehicular Adaptive Cruise Control". In: *IEEE Transactions on Control Systems Technology* 19.3 (2011), pp. 556–566. DOI: 10.1109/TCST.2010.2049203.

[338] Carlos Flores and Vicente Milanés. "Fractional-order-based ACC/CACC algorithm for improving string stability". In: *Transportation Research Part C: Emerging Technologies* 95 (2018), pp. 381–393. ISSN: 0968-090X. DOI: https://doi.org/10.1016/j.trc.2018.07.026. URL: https://www.sciencedirect.com/science/article/pii/S0968090X18307150.

[339] Ching-Chih Tsai, Shih-Min Hsieh, and Chien-Tzu Chen. "Fuzzy longitudinal controller design and experimentation for adaptive cruise control and stop&go". In: *Journal of Intelligent & Robotic Systems* 59.2 (2010), pp. 167–189.

[340] Khaled Laib, Olivier Sename, and Luc Dugard. "String Stable $\mathcal{H}_\infty$ LPV Cooperative Adaptive Cruise Control with a Variable Time Headway". In: *IFAC-PapersOnLine* 53.2 (2020), pp. 15140–15145.

[341] Jarrod Snider. "Automatic Steering Methods for Autonomous Automobile Path Tracking". In: (Apr. 2011).

[342] Vicente Milanés et al. "Intelligent automatic overtaking system using vision for vehicle detection". In: *Expert Systems with Applications* 39.3 (Feb. 2012), pp. 3362–3373.

[343] Ching-Fu Lin, Jyh-Ching Juang, and Kun-Rui Li. "Active collision avoidance system for steering control of autonomous vehicles". In: *IET Intelligent Transport Systems* 8.6 (2014), pp. 550–557.

[344] Chuanyang Yu et al. "MPC-based Path Following Design for Automated Vehicles with Rear Wheel Steering". In: *2021 IEEE International Conference on Mechatronics (ICM)*. IEEE. 2021, pp. 1–6.

[345] Nishant Chowdhri et al. "Integrated nonlinear model predictive control for automated driving". In: *Control Engineering Practice* 106 (2021), p. 104654. ISSN: 0967-0661. DOI: https://doi.org/10.1016/j.conengprac.2020.104654.

[346] S. G. Yi et al. "Vehicle trajectory prediction for adaptive cruise control". In: *2015 IEEE Intelligent Vehicles Symposium (IV)*. 2015, pp. 59–64.

[347] Erik Hellström et al. "Look-ahead control for heavy trucks to minimize trip time and fuel consumption". In: *Control Engineering Practice* 17 (Feb. 2009), pp. 245–254. DOI: 10.1016/j.conengprac.2008.07.005.

[348] V. Turri et al. "Fuel-efficient heavy-duty vehicle platooning by look-ahead control". In: *53rd IEEE Conference on Decision and Control*. 2014, pp. 654–660.

[349] A. Alam, J. Mårtensson, and K. H. Johansson. "Look-ahead cruise control for heavy duty vehicle platooning". In: *16th International IEEE Conference on Intelligent Transportation Systems (ITSC 2013)*. 2013, pp. 928–935.

[350] V. Turri, B. Besselink, and K. H. Johansson. "Cooperative Look-Ahead Control for Fuel-Efficient and Safe Heavy-Duty Vehicle Platooning". In: *IEEE Transactions on Control Systems Technology* 25.1 (2017), pp. 12–28.

[351] U. Ozguner, K. A. Unyelioglu, and C. Hatipoglu. "An analytical study of vehicle steering control". In: *Proceedings of International Conference on Control Applications*. 1995, pp. 125–130.

[352] S. Patwardhan, Han-Shue Tan, and J. Guldner. "A general framework for automatic steering control: system analysis". In: *Proceedings of the 1997 American Control Conference (Cat. No.97CH36041)*. Vol. 3. 1997, 1598–1602 vol.3.

[353] J. Kosecka et al. "Vision-based lateral control of vehicles". In: *Proceedings of Conference on Intelligent Transportation Systems*. 1997, pp. 900–905.

[354] J. Kosecka et al. "A comparative study of vision-based lateral control strategies for autonomous highway driving". In: *Proceedings. 1998 IEEE International Conference on Robotics and Automation (Cat. No.98CH36146)*. Vol. 3. 1998, pp. 1903–1908. DOI: 10.1109/ROBOT.1998.680590.

[355] P. Hingwe and M. Tomizuka. "A variable look-ahead controller for lateral guidance of four wheeled vehicles". In: *Proceedings of the 1998 American Control Conference. ACC (IEEE Cat. No.98CH36207)*. Vol. 1. 1998, 31–35 vol.1.

[356] Chieh Chen and Han-Shue Tan. "Steering control of high speed vehicles: dynamic look ahead and yaw rate feedback". In: *Proceedings of the 37th IEEE Conference on Decision and Control (Cat. No.98CH36171)*. Vol. 1. 1998, 1025–1030 vol.1.

[357] Han-Shue Tan and Jihua Huang. "Design of a High-Performance Automatic Steering Controller for Bus Revenue Service Based on How Drivers Steer". In: *Robotics, IEEE Transactions on* 30 (Oct. 2014), pp. 1137–1147. DOI: 10.1109/TRO.2014.2331092.

[358] M. G. Skarpetis, F. N. Koumboulis, and P. Papanikolaou. "Vehicle lateral control using a robust tracking controller based on vision look ahead system". In: *2017 IEEE 21st International Conference on Intelligent Engineering Systems (INES)*. 2017, pp. 000213–000218.

[359] Myungwook Park, Sangwoo Lee, and Wooyong Han. "Development of Steering Control System for Autonomous Vehicle Using Geometry-Based Path Tracking Algorithm". In: *ETRI Journal* 37 (May 2015). DOI: 10.4218/etrij.15.2314.0123.

[360] F. Roselli et al. "$\mathcal{H}_\infty$ control with look-ahead for lane keeping in autonomous vehicles". In: *2017 IEEE Conference on Control Technology and Applications (CCTA)*. 2017, pp. 2220–2225.

[361] K. Hasegawa and E. Konaka. "Three look-ahead distance scheme for lateral control of vision-based vehicles". In: *2014 Proceedings of the SICE Annual Conference (SICE)*. 2014, pp. 660–665.

[362] S. Lee et al. "Multirate active steering control for autonomous vehicle lateral maneuvering". In: *2012 IEEE Intelligent Vehicles Symposium*. 2012, pp. 772–777.

[363] C. M. Kang, S. Lee, and C. C. Chung. "A comparative study of lane keeping system: Dynamic and kinematic models with look-ahead distance". In: *2015 IEEE Intelligent Vehicles Symposium (IV)*. 2015, pp. 1038–1043.

[364] C. M. Kang S. Lee and C. C. Chung. "Linear Parameter Varying Design for Lateral Control using Kinematics of Vehicle Motion". In: *2018 Annual American Control Conference (ACC)*. 2018, pp. 3239–3244.

[365] Yoshiaki Kuwata et al. "Motion Planning in Complex Environments Using Closed-loop Prediction". In: (Aug. 2008). DOI: 10.2514/6.2008-7166.

[366] Y. Kuwata et al. "Real-Time Motion Planning With Applications to Autonomous Urban Driving". In: *IEEE Transactions on Control Systems Technology* 17.5 (2009), pp. 1105–1118.

[367] Yun-xiao Shan et al. "CF-Pursuit: A Pursuit Method with a Clothoid Fitting and a Fuzzy Controller for Autonomous Vehicles". In: *Int J Adv Robot Syst* (Sept. 2015). DOI: 10.5772/61391.

[368] L. Chen et al. "A Robust Look-ahead Distance Tuning Strategy for the Geometric Path Tracking Controllers". In: *2018 IEEE Intelligent Vehicles Symposium (IV)*. 2018, pp. 262–267.

[369] H. Atoui et al. "Real-Time Look-Ahead Distance Optimization for Smooth and Robust Steering Control of Autonomous Vehicles". In: *2021 29th Mediterranean Conference on Control and Automation (MED)*. 2021, pp. 924–929. DOI: 10.1109/MED51440.2021.9480235.

[370] F. Gottmann, H. Wind, and O. Sawodny. "On the Influence of Rear Axle Steering and Modeling Depth on a Model Based Racing Line Generation for Autonomous Racing". In: *2018 IEEE Conference on Control Technology and Applications (CCTA)*. 2018, pp. 846–852. DOI: 10.1109/CCTA.2018.8511508.

[371] Christian Hoffmann and Herbert Werner. "Complexity of implementation and synthesis in linear parameter-varying control". In: *IFAC Proceedings Volumes* 47.3 (2014), pp. 11749–11760.

[372] D. Robert, O. Sename, and D. Simon. "A reduced polytopic LPV synthesis for a sampling varying controller: Experimentation with a T inverted pendulum". In: *2007 European Control Conference (ECC)*. 2007, pp. 4316–4323. DOI: 10.23919/ECC.2007.7068562.

[373] Corentin Briat. *Linear Parameter-Varying and Time-Delay Systems. Analysis, Observation, Filtering & Control*. Springer-Verlag, 2015.

[374] Christophe Gauthier et al. "SOME EXPERIMENTAL RESULTS OF AN $\mathcal{H}_\infty$-LPV CONTROLLER APPLIED TO A DIESEL ENGINE COMMON RAIL INJECTION SYSTEM". In: *IFAC Proceedings Volumes* 40.10 (2007), pp. 417–424.

[375] K. Berntorp and S. Di Cairano. "Tire-Stiffness and Vehicle-State Estimation Based on Noise-Adaptive Particle Filtering". In: *IEEE Transactions on Control Systems Technology* 27.3 (2019), pp. 1100–1114. DOI: 10.1109/TCST.2018.2790397.

[376] W. Wang et al. "Model reduction of LFT systems". In: *[1991] Proceedings of the 30th IEEE Conference on Decision and Control*. 1991, 1233–1238 vol.2. DOI: 10.1109/CDC.1991.261574.

[377] Zhenxing GAO and Jun FU. "Robust LPV modeling and control of aircraft flying through wind disturbance". In: *Chinese Journal of Aeronautics* 32.7 (2019), pp. 1588–1602. ISSN: 1000-9361. DOI: https://doi.org/10.1016/j.cja.2019.03.029.

[378] Béla Takarics et al. "Flight control oriented bottom-up nonlinear modeling of aeroelastic vehicles". In: *2018 IEEE Aerospace Conference*. 2018, pp. 1–10. DOI: 10.1109/AERO.2018.8396537.

[379] Rajamani Ravi, Krishan M Nagpal, and Pramod P Khargonekar. "$\mathcal{H}_\infty$ control of linear time-varying systems: A state-space approach". In: *SIAM journal on control and optimization* 29.6 (1991), pp. 1394–1413.

[380] Dimitris Kapsalis. "LPV/Gain-Scheduled Lateral Control Architectures for Autonomous Vehicles". PhD thesis. July 2022.

[381] Hussam Atoui et al. "Intelligent Control Switching for Autonomous Vehicles based on Reinforcement Learning". In: *2022 IEEE Intelligent Vehicles Symposium (IV)*. 2022, pp. 792–797. DOI: 10.1109/IV51971.2022.9827384.

[382] Bangalore Ravi Kiran et al. "Deep Reinforcement Learning for Autonomous Driving: A Survey". In: *ArXiv* abs/2002.00444 (2020).

[383] Dong Li et al. "Reinforcement Learning and Deep Learning based Lateral Control for Autonomous Driving". In: *ArXiv* abs/1810.12778 (2018).

[384] Asanka Wasala et al. "Trajectory based lateral control: A Reinforcement Learning case study". In: *Engineering Applications of Artificial Intelligence* 94 (2020), p. 103799. ISSN: 0952-1976. DOI: https://doi.org/10.1016/j.engappai.2020.103799. URL: https://www.sciencedirect.com/science/article/pii/S0952197620301858.

[385] Minghao Han et al. "Reinforcement learning control of constrained dynamic systems with uniformly ultimate boundedness stability guarantee". In: *Automatica* 129 (2021), p. 109689. ISSN: 0005-1098. DOI: https://doi.org/10.1016/j.automatica.2021.109689. URL: https://www.sciencedirect.com/science/article/pii/S0005109821002090.

[386] Felix Berkenkamp et al. "Safe Model-based Reinforcement Learning with Stability Guarantees". In: *NIPS*. 2017.

[387] M.T. Rosenstein and A.G. Barto. "Reinforcement learning with supervision by a stable controller". In: *Proceedings of the 2004 American Control Conference*. Vol. 5. 2004, 4517–4522 vol.5. DOI: 10.23919/ACC.2004.1384022.

[388] Lu Zhao et al. "Imitation of Real Lane-Change Decisions Using Reinforcement Learning". In: *IFAC-PapersOnLine* 54.2 (2021). 16th IFAC Symposium on Control in Transportation Systems CTS 2021, pp. 203–209. ISSN: 2405-8963. DOI: https://doi.org/10.1016/j.ifacol.2021.06.023. URL: https://www.sciencedirect.com/science/article/pii/S2405896321004596.

[389] Fei Ye et al. "Automated Lane Change Strategy using Proximal Policy Optimization-based Deep Reinforcement Learning". In: *2020 IEEE Intelligent Vehicles Symposium (IV)*. 2020, pp. 1746–1752. DOI: 10.1109/IV47402.2020.9304668.

[390] Pin Wang, Ching-Yao Chan, and Arnaud de La Fortelle. "A Reinforcement Learning Based Approach for Automated Lane Change Maneuvers". In: *2018 IEEE Intelligent Vehicles Symposium (IV)*. 2018, pp. 1379–1384. DOI: 10.1109/IVS.2018.8500556.

[391] Richard S Sutton and Andrew G Barto. *Reinforcement learning: An introduction*. MIT press, 2018.

[392] Ivo Grondman et al. "A Survey of Actor-Critic Reinforcement Learning: Standard and Natural Policy Gradients". In: *IEEE Transactions on Systems, Man, and Cybernetics, Part C (Applications and Reviews)* 42.6 (2012), pp. 1291–1307. DOI: 10.1109/TSMCC.2012.2218595.

Résumé

De nos jours, les systèmes deviennent de plus en plus complexes, ce qui nécessite des algorithmes de contrôle capables de prendre en compte en ligne des objectifs variables de performance et de sécurité. Le domaine des systèmes autonomes, en particulier les véhicules autonomes, est révélateur d'une telle évolution. En effet, leurs capacités de conduite ont été récemment améliorées pour une conduite hautement, voire totalement, autonome grâce à une théorie de contrôle avancée. Une voiture entièrement autonome doit effectuer plusieurs tâches dont le contrôle longitudinal, le contrôle latéral, le contrôle du châssis, etc. La présente thèse propose différentes structures de contrôle multi-objectifs visant à adapter les performances du véhicule en couvrant toute la plage de vitesse.
Cette thèse présente de nouvelles architectures de contrôle pour commuter/interpoler entre plusieurs controleurs linéaires à paramètres variants (LPV), en considérant la vitesse du véhicule comme un paramètre variable. Le schéma de commutation ou d'interpolation est réalisé sur la base du paramétrisation de Youla-Kucera (YK). L'architecture de contrôle LPV-YK peut incorporer plusieurs contrôleurs LPV ou LTI qui peuvent commuter/interpoler entre eux en garantissant la stabilité. Elle peut être utilisée pour interpoler entre différentes performances de contrôle visant à atteindre différentes spécifications en boucle fermée dans différentes situations de conduite (c'est-à-dire changement de voie, évitement d'obstacles), ou pour basculer entre des sous-ensembles de paramètres cloisonnés lorsqu'on a affaire à de grandes variations de paramètres (c'est-à-dire à des vitesses de véhicule faibles et élevées). La stabilité en boucle fermée est garantie pour tout signal d'interpolation continu/discontinu en termes d'un ensemble d'inégalités linéaires matricielles (LMI). Les structures de contrôle proposées peuvent aider les systèmes multi-variables et multi-objectifs à atteindre des performances élevées dans différentes conditions de fonctionnement et différentes situations critiques, quel que soit le taux d'interpolation. Des exemples numériques sont simulés pour montrer l'importance des méthodes proposées pour atteindre différents objectifs pour le contrôle latéral des véhicules autonomes. En outre, les différentes structures de contrôle ont été testées sur un véhicule Renault ZOE réel pour valider leurs performances réelles et les comparer aux contrôleurs LPV standard.

Mots Clés

Contrôle latéral; Contrôle LPV; Paramétrisation Youla-Kucera; Contrôle de switch; Contrôle robuste; Véhicules autonomes.

Abstract

Nowadays, systems are getting more and more complex leading to control algorithms able to consider online varying objectives for performance and safety. The field of autonomous systems, in particular autonomous vehicles, is indicative of such an evolution. Indeed, their driving capabilities have been recently improved for highly, and even fully, autonomous driving thanks to advanced control theory. A fully autonomous car needs to perform several tasks including longitudinal control, lateral control, chassis control, etc. The current thesis proposes different multi-objective control structures aiming to adapt the vehicle performance with covering the full speed range.
This thesis presents novel control architectures to switch/interpolate between multiple Linear Parameter-Varying (LPV) controllers, by considering the vehicle speed as the varying parameter. The switching or interpolation scheme is achieved based on Youla-Kucera (YK) parameterization. The LPV-YK control architecture can incorporate multiple LPV or LTI controllers which can switch/ interpolate between them with ensuring stability. It can be used to interpolate between different control performances aiming to achieve different closed-loop specifications in different driving situations (i.e. lane change, obstacle avoidance), or to switch over partitioned parameter subsets when dealing with large parameter variations (i.e. at low and high vehicle speeds). The closed-loop stability is guaranteed for any continuous/discontinuous interpolating signals in terms of a set of Linear Matrix Inequalities (LMIs). The proposed control structures can help multi-variable and multi-objective systems to achieve high performances at different operating conditions and different critical situations regardless of the interpolation rate.
Numerical examples are simulated to show the importance of the proposed methods to achieve different objectives for lateral control of autonomous vehicles. In addition, the different control structures have been tested on a real Renault ZOE vehicle to validate their real performance, and compare them with the standard LPV controllers.

Keywords

Lateral control; LPV control; Youla-Kucera parameterization; Switching control; Robust control; Autonomous vehicles.